University of Sheffield

The University of Sheffield

Faculty of Engineering

Department of Electronic & Electrical Engineering

Analysis of Battery Energy Storage for Frequency Response Services

A thesis submitted in partial fulfilment of the requirements for the degree of Doctor of Philosophy

Abdulkarim A Ahmouda
Supervisor: Prof. Dan Gladwin

May 2023

Abstract

As the use of renewable energy sources (RESs) increases worldwide, there is a rising interest in their impacts on power system operation and control. These resources are considered variable, independent, and intermittent by nature and can contribute to power quality, stability, and reliability issues. To overcome such problems, in Great Britain (GB), the National Grid Electricity System Operator (NGESO) – the primary electricity system network operator – has introduced various frequency response services to provide a real-time response to deviations in the grid frequency. Battery Energy Storage Systems (BESS) are considered a good solution to deliver such services to the grid. In this thesis, the control algorithm for a generic BESS has been implemented in Matlab Simulink to deliver frequency response services according to National Grid (NG) specifications.

Moreover, this thesis presents a sensitivity analysis of the power-to-energy ratio for Energy Storage Systems (ESS) providing frequency services with respect to availability, compliance against service terms and conditions, and lifetime. It shows that there is a significant difference between the frequency services and demonstrates that the newer dynamic containment service can be effectively delivered by a higher power-to-energy ratio ESS, offering opportunities for other technologies such as supercapacitors and flywheels. Control methodologies are investigated that exploit the delivery envelopes to manage the state of charge and improve the availability of a battery energy storage system, potentially resulting in higher revenues, increase in cycle life, and decreased penalty payments. To investigate life-time, different methods to analyse battery operation to provide degradation estimates are presented which are then informed through experimental work.

Finally, in this thesis, financial costs for using GB's electricity system have been investigated and simulated to provide a comparison between delivering different frequency services.

List of Publications

Certain aspects of the research findings delineated in this thesis have been communicated in prestigious publications of global repute. These include:

Conference Proceedings

1. **A. Abdulkarim**, D. T. Gladwin, "A sensitivity analysis on power to energy ratios for energy storage systems providing both dynamic firm and dynamic containment frequency response services in the uk ," in *IECON 2021 – 47th Annual Conference of the IEEE Industrial Electronics Society* , pp. 1-6, 2021.

2. **A. Abdulkarim**, D. T. Gladwin, "Maximizing energy availability for a Dynamic Regulation Frequency Response Service for Battery Energy Storage Systems ," in *IECON 2021 – 47th Annual Conference of the IEEE Industrial Electronics Society* , pp. 1-6, 2022.

Journal Publication

A. Ahmouda,and D. T. Gladwin, "Enhanced Dynamic Control Strategy for Stacked Dynamic Regulation Frequency Response Services in Battery Energy Storage Systems," Energies, vol. 16, no. 23, p. 7686, Nov. 2023, doi: 10.3390/en16237686.

Manuscript under Review

A. Abdulkarim, D. T. Gladwin, "Technic-economic assessment of Grid Connected Batteries providing both Dynamic Firm and Dynamic Containment Frequency Response Services in the UK," *Journal of Energy Storage*, MDPI.

Acknowledgements

I would like to express my deepest gratitude to my supervisor, Prof. Dan Gladwin, for his invaluable guidance, support, and encouragement throughout my PhD journey. His expertise, patience, and enthusiasm have been instrumental in shaping my research, and I am truly grateful for his mentorship.

I am grateful to the University of Sheffield for providing me with the resources, facilities, and opportunities that enabled me to pursue my PhD. The department of Electronic and Electrical Engineering has been instrumental in shaping my academic and professional development, and I am proud to be a part of this esteemed institution.

I would like to express my heartfelt gratitude to my wife for her constant love, unwavering support, and encouragement throughout my academic journey. Her sacrifices, patience, and understanding have been my greatest source of strength.

I am also grateful to Libyan Embassy for funding my PhD study. Their generous support has enabled me to pursue my academic and research goals and has been integral to my success.

Finally, I would like to express my sincere gratitude to all the participants who generously gave their time and expertise to contribute to my research. Their insights and perspectives have been invaluable, and I am honored to have had the opportunity to learn from them.

Thank you all for your invaluable contributions, and for making this journey an unforgettable experience.

Contents

List of Figures

List of Tables

xvii

Abbreviation

AAHEDC Assistance for Area with High Electricity Distribution Cost.

AC Alternating current.

AD Anaerobic digestion.

ANN Artificial neural network.

AR Allocation Round.

AS Ancillary services.

BEIS Business, Energy & Industrial Strategy.

BESS Battery energy storage system.

BMS In-built battery management system.

BOS Balancing of the system.

BSC Balancing and Settlement Code.

BSUoS Balancing Service Use of System.

CAES Compressed Air Energy Storage.

CC Constant current.

CCCV Constant current constant volage.

CCM Cycle Counting Method.

CFD Contract for Difference.

CHP Micro Combined heat and power.

CM Capacity Market.

CVA Central Volume Allocation.

DB Dead-band.

DC Dynamic Containment.

DC/DA Data Collection/Data Aggregation.

DER Distributed energy resources.

DFR Dynamic Frequency Response.

DG Distributed generation.

DM Dynamic Moderation.

DNO Distribution Network Operator.

DoD Deep-of- discharge.

DOLTC Decupled on-load tap changers.

DR Dynmaic Regulation.

DRES Distributed renewable energy sources.

DR-HF Dynamic Regulation High Frequency Response.

DR-LF Dynamic Regulation Low Frequency Response.

DSO Distribution system operator.

D-STATCOM Distribution static compensators.

DUoS Distribution Use of System.

DVR Dynamic voltage restorers.

EFA electricity forward agreement.

EFCs Equivalent Full Cycles.

ES Energy storage.

ESS Energy storage system.

FFR Firm Frequency Response.

FiT Feed in Tariff.

FPF Fixed power factor.

G/D Generation/Demand split.

GB Great Britain.

GDUoS Generator Distribution Use of System.

GSP Generator Supply Point.

HFC Hydrogen fuel cells.

HH Half-hourly.

LCCC Low Carbon Contracts Company.

LOT Lithium-Titanate.

LTO Lithium Ion.

LV Low voltage.

MEC Maximum Export Capacity.

MIC Maximum Import Capacity.

MOP Meter Operator.

MOP DA/DC Meter Operator/Data Aggregation/Data Collection.

MPAN Meter Point Administration Number.

MSP Meter Supply Point.

MV Medium voltage.

NaS Sodium Sulfur.

NBP National Balancing Point.

NG National Grid.

NGESO National grid electricity system operator.

NiCd Nickel-cadmium.

NiMH Nickel-metal hydride.

NiZn Nickel-zinc.

NMC Nickel Manganese Cobalt.

NYSE: VST Vistra Energy.

O and M Operation and Maintenance.

OCL Operational Costs Levy.

OCV Open Circuit voltage.

Ofgem Office of Gas and Electricity Markets.

OLTC On-load tap changers.

$\mathbf{P}_{Base}$ Baseline Power.

PF Power factor.

PMSG Synchronous generators with permanent magnets.

PSB Polysulfide–bromide battery.

PSH Pumped-storage hydro.

PV Photovoltaic.

PV RR photovoltaic Ramp Rate.

$\mathbf{R}_{dc}$ DC resistance.

RES Renewable energy resources.

RESU Residential Energy Storage Unit.

RO Renewable Obligation.

ROCs Renewable Obligation Certificates.

SBP System buys price.

SMES Superconducting magnetic energy storage.

SNaPS System Needs and Product Strategy.

SOC State-of-charge.

SOH State-of-Health.

SP Settlement Period.

SPM Service performance measurement.

SSP System sell price.

STOR Short-Term Operating Reserve.

SVA Supplier Volume Allocation.

TL Transmission Loss.

TNUoS Transmission Network Use of System.

TNUoS EET Transmission Network Use of System-Embedded Export Tariff.

UPS Uninterruptible power supply.

VAR Reactive power.

VRB Vanadium Redox Flow Battery.

VRES Variable renewable electricity system.

VRFB vanadium redox flow battery.

VSG Virtual Synchronous Generator (VSG).

VSM Virtual synchronous machine.

VUF Voltage unbalance factor.

WESS Willenhall Energy Storage System.

ZBFB Zinc–bromine redox flow battery.

Nomenclature

C	Rated capacity (the battery capacity at the normal condition)	Wh
C_{actual}	Battery actual capacity	Ah
CCM	Cycle counting method	Cycle
CF	Capacity Factor	(%)
C_r	Rated capacity	Wh
C_{rate}	The rate of charge/discharge as a ratio of its capacity	C
DB	Dead-band frequency	Hz
E	Performance score	number
EFCs	Equivalent Full Cycles	Cycle
e_m	calculated error	number
es_m	Scaled error	number
E_t	Stored energy in the battery at that hour (t)	kWh
f	Grid frequency	Hz
i	Charge and discharge current	mA
ILR	Interim Levy Rate	£/MWh
K_e	Payment adjustment	number
K_j	factor for each settlement period	number
MAPE	Mean Absolute Percent Error	(%)
NPV	Net Present Value	£
P_{Base}	Baseline Power	kW
P_{BESS}	Battery Energy Storage System Power	kW
$P_{contract}$	Contracted quantity that the provider is contracted to deliver	MW
P_{DC}	Dynamic Containment Frequency Response Power	kW
P_{Demand}	Demand power	kW
P_{DFR}	Dynamic Frequency Response Power	kW
P_{DR}	Dynamic Regulation Frequency Response Power	kW
P_{DR}	Change of Dynamic Regulation power	kW
$\Delta P_{(DR-HF)}$	Change in the power of Dynamic Regulation High Frequency Response	(%)
$\Delta P_{(DR-LF)}$	Change in the power of Dynamic Regulation Low Frequency Response	(%)
$P_{DR(lower)}$	Lower bounds of Dynamic Regulation Frequency Response Power	kW
$P_{DR(upper)}$	Upper bounds of Dynamic Regulation Frequency Response Power	kW
P_t	Battery power for charging or discharging at a specific hour (t)	kW
Q	Reactive power	VAR

Q_{max}	Maximum charge available of the battery	AH
RMSE	Root Mean Square Error	(%)
ΔSOC	Change in state of charge	(%)
SOC_{end}	The last value of state of charge	(%)
SOC_{chg}	Sum of SOC up index	(%)
SOC_{dischg}	Sum of SOC lower index	(%)
SOC_{high}	High limit of Baseline power SOC setpoints	(%)
SOC_{high}	High limit of Dynamic control SOC setpoints	(%)
SOC_{high}	High operation limit of state of charge	(%)
SOC_{init}	Initial state of charge	(%)
SOC_{low}	Low limit of Baseline power SOC	(%)
SOC_{low}	Low limit of Dynamic control SOC setpoints	(%)
SOC_{low}	Low operation limit of state of charge	(%)
SOC_{out}	Current state of charge	(%)
SOC_{start}	Starting value of state of charge	(%)
SOC_{t}	The present SOC	(%)
SOC_{t-1}	The previous SOC at (t-1)	(%)
SOH	State-of-Health	(%)
OCL	Operational Costs Levy	£/MWh
η_D	Battery discharge efficiency	(%)
η_C	Battery charge efficiency	(%)
TLF	Transmission Loss Factor	number
TLM	Transmission Loss Multiplier	number

Chapter 1

General Introduction

As the global demand for renewable energy sources continues to rise, the integration of these resources into existing power systems presents new challenges. The inherent variability and intermittency of renewable energy pose significant issues for power quality, stability, and reliability. To address these challenges, the National Grid Electricity System Operator (NGESO) in Great Britain has introduced various frequency response services.

This thesis focuses on the crucial role of Battery Energy Storage Systems (BESS) in delivering frequency response services to the grid. The objective is to understand, optimize, and model BESS performance for services such as Dynamic Frequency Response (DFR), Dynamic Containment (DC), and Dynamic Regulation (DR). The research aims to bridge existing knowledge gaps, exploring the complexities that arise with the increasing penetration of renewable sources and developing effective strategies to enhance the UK grid's adaptability.

1.1 Motivations and Challenges

Motivations

1. Renewable Energy Integration: The global shift towards renewable energy necessitates innovative solutions for the integration of intermittent sources, driving the need for effective energy storage systems.

2. Frequency Response Demands: The dynamic nature of renewable energy generation introduces challenges in maintaining grid stability, making frequency response services paramount for grid operators.

3. Optimizing Power-to-Energy Ratio: The power-to-energy ratio is a key determinant in the performance of ESS, and optimizing this ratio is crucial for ensuring consistent and reliable service delivery.

4. Optimizing BESS Performance: Control methodologies are investigated to optimize the performance of BESS, managing SOC and enhancing availability. This optimization is expected to result in higher revenues, increased cycle life, and reduced penalty payments.

1

5. Battery Operation Analysis: The thesis delves into different methods to analyze battery operation and provides degradation estimates. Experimental work informs these estimates, contributing to a comprehensive investigation into the lifetime of batteries.

6. Techno-Economic Evaluation: The economic viability of grid-connected batteries providing services like DFR, DC, and DR is a critical aspect in the transition to sustainable energy solutions.

Challenges

1. Availability and Compliance: Ensuring ESS availability and compliance with service terms and conditions, particularly in energy-limited assets, poses a challenge that requires careful analysis and optimization.

2. Dynamic Control for Frequency Response: Developing a dynamic control algorithm for the newly introduced DR service involves addressing the complexities of managing high and low-frequency events in a stacked configuration.

3. Techno-Economic Decision-Making: Conducting a comprehensive techno-economic assessment involves navigating the intricate balance between different C-rates, SOC management, and revenue considerations.

4. Battery Degradation and Lifetime Estimation: Analyzing battery operation and providing accurate degradation estimates for different cycling scenarios involve challenges in experimental setup, data analysis, and extrapolation of results to predict long-term battery lifetime.

This thesis endeavors to contribute novel insights, methodologies, and solutions to these motivations and challenges, aiming to advance the effective utilization of grid-connected battery energy storage in shaping the future of sustainable energy systems.

Research Gaps

Despite the growing interest in utilizing BESS for frequency regulation in the context of renewable energy integration, several research gaps persist. Firstly, there is a need for a comprehensive understanding of the key challenges and new complexities arising with the increasing penetration of renewable sources. Bridging this knowledge gap is crucial for developing effective strategies to enhance the grid's ability to handle variability and intermittency.

Another research gap lies in the optimization of BESS for frequency regulation. While the thesis recognizes the necessity to delve into the intricacies of sizing, classification, and specification of different ESS to determine the most suitable solutions for mitigating challenges associated with RES integration, specific methodologies for optimal sizing and deployment require further exploration.

Additionally, a critical research gap involves the accurate modelling of battery behavior and predicting its lifetime in the context of frequency regulation services. The thesis aims to contribute to addressing these research gaps by providing insights into battery degradation, life cycle analysis, and proposing methodologies for predicting and mitigating potential issues associated with BESS deployment in frequency regulation. Furthermore, there is a need to explore the nuances of sensitivity analysis on the power-to-energy ratio, dynamic control algorithms for DR, and techno-economic assessments for grid-connected ESS providing frequency response services, which are integral components in achieving an effective and efficient integration of BESS into power systems. Filling these research gaps will not only advance the understanding of BESS performance but also guide the development of robust strategies for optimal BESS deployment in frequency regulation services

1.2   Thesis Organizations

Some of the work presented in this thesis, which can be found in Chapters 4, 5, and 6, has been published in two conference papers and one journal article. The thesis is organized into different chapters, each of which is summarized below, along with the objectives of the thesis. **Chapter 1** outlines the motivations and challenges of the thesis along with the research gaps.

Chapter 2 presents an overview of the key issues and new challenges related to frequency regulation concerning the integration of renewable energy units into power systems. Some suggested solutions are also presented. Previous studies related to the sizing of BESS are discussed. The classification and specification of different ESS that can be adopted as an optimal solution to mitigate the integration of Renewable Energy Sources (RES) issues are presented. BESS is studied in terms of battery types, battery characteristics (such as nameplate capacity, calendar life, and cycle life), BESS parts, SOH, SOC, and DoD. Battery modeling is also investigated with the advantages and disadvantages presented. The lifetime analysis of a BESS operating in frequency regulation is presented and finally, three different cycle counting methods and battery degradation methodologies are introduced and discussed.

Chapter 3 introduces the BESS model developed in MATLAB/ Simulink using the 'Bucket Model' principle. The model simplifies the representation of any ESS by using an integrator block to calculate energy at each time step. The model includes sub-blocks such as efficiencies, SOC management systems, control systems, and analysis blocks. The proposed blocks are the BESS Block, Application Block, Control Block, and Metrics Block. The control algorithm for each frequency response service (DFR, DC, and DR) that allows BESS to deliver dynamic power in response to the change in the real frequency events according to NG specifications is also presented. The simulation results for BESS used to deliver the frequency response services are presented.

The BESS model was validated against a 2MW/0.986MWh battery called the Willenhall Energy Storage System (WESS) operated by the University of Sheffield using two different error calculations, including Root Mean Square Error (RMSE) and Mean Absolute Percent Error (MAPE) in order to assess the accuracy of the simulation models delivered frequency response such as DFR, DC, and DR services.

Chapter 4 begins by giving an overview of both DC and DFR services which covers; service specification, control service, and service envelop with the simulation results of both services delivered by BESS for a specific time. It then introduces a sensitivity analysis for the power to energy ratio for ESS providing DFR & DC services in respect to availability, compliance against the service terms and conditions, and the required equivalent full cycles. Moreover, this chapter introduces a baseline power (P_{Base}) technique using SOC target management in order to assess DC service in terms of availability, and non-compliance.

In this chapter, both frequency response algorithms of DFR & DC services that have been developed in the Chapter 3 are simulated to produce energy throughput over a period of time using real frequency data and then use this to calculate the number of Equivalent Full Cycles (EFCs). The analysis of the battery behaviour is further extended to investigate micro-cycles using CCM. Using these outputs the Miner's Rule life prediction method is implemented for degradation estimation and lifetime analysis.

Finally, 8 battery cells are cycled under lab-conditions to effectively deliver the DFR and DC services to measure the level of degradation rate that these specific cycling profiles cause.

Chapter 5 begins with describing the dynamic regulation (DR) service and outlining the service specification, and shows the service envelope for dynamic regulation high (DR-HF) and dynamic regulation low (DR-LF) followed by the simulation results for both services. DR services (DR-HF & DR-LF) are simulated for six electricity forward agreement (EFA) blocks based on two different scenarios (S1 & S2), S1 is considered without applying dynamic control while S2 with implementing dynamic control which comprises of a fast and slow response, and the obtained results show how the dynamic control is used to improve the availability of a battery energy storage system, potentially resulting in higher revenues and a reduction in the number equivalent full cycles.

This chapter extends to show how dynamic control can be exploited to improve availability while avoiding a penalty payment in additon to minimising the number of cycles, this has also been carried out by delivering both services (DR-HF & DR-LF) in a stacked bid.

Finally, in this chapter, the two-cycle counting method (EFCs & CCM) that has been discussed in Chapter 4 have been implemented here to deliver DR service (DR-HF & DR-LF) for a full month (Jan-2019), and the whole year (2019) in order to compare between delivering a DR service without applying dynamic control against with dynamic control.

Chapter 6 gives a comprehensive breakdown of the costs involved in operating a

battery asset with respect to the electricity network charges. The three services (DFR, DC, and DR) delivered by BESS with different C-rates are analyzed and discussed. This chapter presents the analysis and discussion of revenue vs C-rates as well as revenue vs SOC management then finally, there are different scenarios represented by a BESS used to deliver DFR, DC & DR for 15 years based on battery lifetime and they have been assessed based a financial method called net present value (NPV) in order to assess which scenario is more profitable than the other.

Chapter 7 presents several conclusions and summarizes the contributions of this thesis to the management of large-scale grid-connected battery energy storage systems. Additionally, it outlines potential areas for future research that could build on the work presented in this thesis.

1.3   Thesis Contributions

The main contributions of this thesis are as follows;

1. Introduction of a sensitivity analysis on the power to energy ratio for ESS providing DFR and DC services on the GB electricity network. This analysis assesses how the power to energy ratio affects service performance, taking into account the availability, compliance against service terms and conditions, and equivalent cycles. For energy-limited assets such as ESS, the ratio of power to energy has a significant impact on its ability to deliver the service 100% of the time. Furthermore, a DC service model has been developed by implementing a baseline power that is used for SOC management in each (HH) period. This allows for higher C-rates to be utilized while improving availability and remaining compliant with sustained delivery requirements which is important to the electricity system operator, albeit at reduced revenue for the asset owner.

2. Presents a dynamic control algorithm for the newly introduced DR frequency response service for the GB electrical grid. This algorithm has been applied to DR-HF or DR-LF and then developed to manage the SOC of a stacked DR-HF and DR-LF contract, where the ESS responds to both high and low frequency events in the same EFA block. The aim of this control is to improve the availability of a battery energy storage system, potentially resulting in higher revenues and a reduction in the number of equivalent full cycles.

3. This thesis offers a techno-economic assessment of grid-connected batteries that provide DFR, DC, and DR services with repspect to the electricy use of system charges. The NPV financial method has been implemented to assess different scenarios, including C-rate versus revenue and SOC management versus revenue, to determine which is more profitable. This assessment enables the selection of the optimum battery size to deliver such frequency response services.

4. This thesis introduces two different cycle methods, CCM & EFCs and their improvement by considering the effects of C-rate and SOC on battery lifetime when delivering DFR, DC, and DR services. This will aid to predict the battery degradation and its lifetime.

Chapter 2

Literature Review

2.1   Grid Balancing

The heightened integration of variable RES, such as wind and solar, into the power grid through distributed generation (DG) has spurred global initiatives aimed at reducing greenhouse gas emissions. These resources exhibit variability, independent control, and inherent intermittency, impacting power quality, stability, and reliability [1]. Consequently, the growing penetration of RES into the power grid introduces greater complexity in the task of balancing demand and supply [2], [3], [4]. The main reason that has led to the photovoltaic (PV) and wind generation being described as intermittent source, is the lack of its inertia since power electronic-based inverters do not have any physical rotating mass, this will have a negative impact on the overall inertial response of a synchronous power system [5].

In the context of PV energy systems, the unidirectional power flow of distribution networks represents a significant obstacle to achieving higher levels of PV penetration. As noted in [6], the increased use of PV in the grid will present even greater technical challenges in the future. When the level of PV penetration rises, several issues may arise, such as abrupt changes in cloud movement or an anticipated solar eclipse, resulting in rapid fluctuations in PV output that can exceed 60% within seconds and up to 63% of total capacity within a minute. These fluctuations can have a profound impact on grid power, particularly when PV penetration levels are high (around 50%). To address these impending challenges, novel control strategies must be developed, and advances must be made in weather forecasting to enable the activation of storage facilities and other energy generation sources to mitigate the effects of abrupt PV output ramping. The integration of high levels of PV generation with power grids gives rise to various technical challenges, including reverse power flow, voltage fluctuations, power quality issues, dynamic stability, and big data management, which are mainly attributed to the intermittent nature of solar energy and the influence of power electronic-based smart inverters on the smart grid architecture [7]. The penetration of Distribution Renewable Energy Sources (DRES) at low voltage networks (LV) leads to emerging voltage unbalance due to increasing the number of the (mainly) single-phase connected DRES. Furthermore, the distribution system operator will face challenges in identifying

the locations associated with DRES and their connected phases. This complication poses a barrier to implementing a centralized solution [6]. Moreover, overvoltages and voltage unbalance are the most common problems that relate to power quality issues. The overvoltage problems are related to the hosting capacity of the feeders and occur when high injection and low demand are present in the grid. On the other hand, voltage unbalance is caused by asymmetrical RES [7]. To mitigate these problems, with respect of energy-based electricity markets, ancillary services (AS) are needed to grant the secure operation of the power system. Ancillary services refer to critical support functions that the transmission or distribution system operator is responsible for providing to maintain the reliability, stability, and quality of power transmission or distribution systems. These services are essential for ensuring the proper functioning of the grid and mitigating the effects of disturbances or faults that could compromise system integrity [8]. The ancillary services include; active power reserves, frequency and voltage regulation, reactive power control, black start capability, and islanding. Table A1 in Appendix A gives a list of the issues with some of the suggested solutions to improve the inverter of RES to allow an increase in the penetration level of RES to the grid.

Additionally, to mitigate these problems, excess energy should be stored when generation exceeds demand and then this stored energy can be used when demand exceeds supply such as at peak times [9]. ESS together with DER is widely regarded as a good solution to tackle such problems [10], [11]. The stored energy can be used to improve power quality as well as to achieve better grid performance. Moreover, energy storage can be used to mitigate energy security issues that result from intermittent renewable power. This will lead to a better contribution in the prediction response of such resources, while at the same time providing additional flexibility in the energy system [12]. Integration of ESS with the grid will enable the large-scale expansion of RES and lead to a faster transition to a low-carbon future energy system [13]. There are many features of ESS that relate to its electrical capacity, efficiency, charge/discharge behaviour, lifetime, cost, and environmental/location issues. Some of these characteristics are intimately related to each other [2]. Energy storage can be provided by using different technologies which include; battery, flywheel, pumped-storage hydropower, supercapacitor, compressed air, Hydrogen, and thermal (including molten salt). The unique characteristics of various ESS stem from their distinct underlying technologies and operational principles. Consequently, the operational capabilities of these systems can vary significantly, with certain methods of storage being better suited for addressing long-term, annual fluctuations in energy demand, while others are more suited for meeting short-term, high peak power requirements [14], [13]. In [15], compared to other ESS, BESS have been successfully demonstrated in microgrid applications and at the grid level for managing grid frequency. BESS has several advantages, including high energy efficiency, good energy density, a high capability of charging/discharging rate, faster

response time compared to conventional energy generation sources, low self-discharge rates, and low maintenance. Moreover, in recent years, the cost of batteries has been decreasing, leading to increased profitability for large-scale grid applications. In the UK, the NGESO, the primary electrical system network operator for the GB electrical grid, has introduced various frequency response services to provide a real-time response to deviations in grid frequency.

In this thesis, three of the services will be considered DFR, DC, and DR. BESS are considered suitable candidates for delivering such services to the grid, due to their capability of importing/exporting and responding quickly. [16] states that BESS can provide (AS) related to the balancing of demand and supply, including fast frequency response services, voltage support, and peak power lopping. According to [17], there are two types of BESS applications: Energy applications and Power applications. Energy applications are defined as storage used to supply electricity for long time periods (hours), such as energy arbitrage, support for renewable energy curtailment, load shifting, and peak load. On the other hand, power applications are defined as storage used to supply electricity for a short time period (seconds, minutes) to ancillary services such as frequency and voltage regulation. [18], [19], [20] report that in the UK and some countries around the world, including the US, China, Japan, and the EU, there are numerous BESS projects implemented for various ancillary services, energy supply, and load shifting. However, their power rating and energy rating are considered very low, ranging from 0.5MW to 50MW for power rating and from 0.5MWh to 50MWh for energy rating. In Australia, BESS with a power-to-energy ratio of 100 MW/129.MWh has been built by Tesla to prevent grid blackouts caused by renewable intermittency. [21] reports that, the Moss Landing Energy Storage Facility, recognized as the globe's most extensive lithium-ion battery energy storage system, has undergone an expansion, now reaching a capacity of 750 MW/3,000 MWh. Situated in Monterey County, California, Moss Landing occupies the site of a gas-powered plant and is under the ownership of Vistra Energy (NYSE: VST), a Texas-based retail electricity and power generation company. Vistra, which holds the second-highest energy storage capacity in the United States, recently announced the successful completion of Moss Landing's Phase III expansion, adding 350MW/1,400MWh. This expansion elevates the total capacity of the battery storage system to 750 MW/3,000 MWh, making it the largest of its kind globally.

There are numerous studies on BESS for energy applications that can be found in the literature. These studies relate to energy arbitrage, peak shaving, and peak load management. However, they are generally limited to small-scale BESS (ranging from kW to MW) and focus on technical suitability instead of economic viability. For instance, in [22], a 1 MW/1 MWh lithium-titanate BESS has been used with battery energy management strategies for GB firm frequency response services and energy arbitrage.

Additionally, a 2 kW/30 kWh Vanadium Redox Flow Battery (VRB) has been used as an energy storage solution for small grids and stand-alone PV systems [23]. Another study proposed an ideal operating plan for a local power grid that utilizes wind, solar, and hydropower systems, where a 6 MWh BESS controls peak demand [24].

There are only a few studies that have focused on selecting the optimum size of energy storage. For instance, in [25], the authors implemented an empirical model called a Virtual Synchronous Generator (VSG) to size a BESS to overcome the lowered inertia that might be caused by integrating renewable energy resources into the grid, as well as for damping control. The emulated inertia was achieved by adding an ESS to the PV Plant through simulation and the area under the power swing curve. The obtained results show that it is possible to achieve a high level of renewable energy integration into the grid with an appropriately sized BESS with respect to power and energy to meet the system target. In their research published in [26], the authors conducted a systematic study on the impact of ramp rate control for PV strings and inverter size on the sizing of an ESS. They based their study on measurements of a PV string with 23 PV modules' current-voltage curves taken over 38 days. During this time, they increased the DC/AC power ratio from 1.0 to 2.0 and changed the PV ramp rate limit from 1% to 20%/min concerning the nominal grid connection power. The test always began by measuring the power and energy capacities that PV power variability imposed on the ESS. This was achieved by calculating the size of the ESS to comply with the ramp rate limit group of PV. The results obtained showed that while this sizing method was not economically viable, it could still be applicable if the network operator set severe ramp rate limitations. Additionally, both inverter sizing and ramp rate limit were considered important factors in ESS sizing for PV RR control. The required power capacity of the ESS could be reduced through power curtailment, which helped smooth the fastest upward power ramps.

2.2 Energy Storage (ES) applications

Within this section, the investigation focused on delineating the diverse classifications of ESs and elucidating their operational characteristics. Each type's distinct advantages and disadvantages were thoughtfully and critically examined in the subsequent sections that follow.

2.2.1 Battery Energy Storage System (BESS)

A BESSs refer to a type of rechargeable electrochemical system designed for energy storage purposes. BESSs work by delivering chemical energy in the form of electric energy generated from electrochemical reactions. Typically, a battery comprises one or more cells that can be interconnected in series, parallel, or both, depending on the intended output voltage and capacity [27]. A battery cell is composed of four main parts, namely the anode, cathode, electrolyte, and separator. The anode is a negatively charged electrode

10

that supplies electrons to the load and is oxidized during the electrochemical reaction. On the other hand, the cathode is a positively charged electrode that accepts electrons and is reduced during the reaction. The electrolyte serves as a medium that enables the transfer of electrons between the anode and cathode, while the separator is placed between the positive and negative electrodes. When a load is connected to the cell's terminal, the reactions between the two electrodes immersed in an electrolyte occur. These reactions can be initiated by setting up the electrodes in a basic cell, and they facilitate the transfer of electrons from one electrode to the other through an external electric circuit/load [28].

2.2.2 Battery Terminologies

Response Time

It is defined as the time that a storage system needs to transition from standby mode to full output. This performance criterion is a crucial gauge of how flexible storage is as a grid resource when compared to alternatives. The majority of storage systems respond quickly, usually in less than a minute. In comparison to other energy storage systems such as; compressed air, pumped hydroelectric storage, and other energy storage systems, BESS offers the quickest response time [29].

Energy Density

Energy density is defined as the quantity of energy that can be held in a given amount of area, mass, or volume. It is important to consider such a criterion, especially in applications where the area is a limiting factor, such as in an urban substation which might be difficult for the energy to be stored because of a limiting constraint for the space of the storage site.

Power Density

Power density describes how much power can be delivered for a specific area, mass, or volume. Additionally, power density varies greatly among various types of storage, much like energy density does. Once more, power density is crucial if area, space, or weight are constrained.

Nameplate capacity

The nameplate capacity of a battery or battery bank refers to its highest chemical potential. It is often measured in amp-hours (Ah). When determining battery capacity using the Ah nomenclature, the voltage of the system must always be taken into consideration. By way of illustration, a 500 Ah battery bank string at 24 V will have a capacity of 12 kWh, whereas a 500 Ah battery bank string at 48 V will have a capacity of 24 kWh [30].

Calendar Life and Cycle Life

The term "calendar life" refers to the duration during which a battery can be kept in storage without being used or with minimal use while maintaining a capacity level above 80% of its original capacity. Cycle life refers to how many times a battery will be charged and discharged throughout its lifespan. Cycle life is inversely correlated with the depth of discharge (DoD) of the battery since the number of predicted cycles typically declines fairly linearly as DoD rises. Even when End of Life (EoL) is reached—batteries that have reached the end of their usefulness and/or lifespan and no longer operate at sufficient capacity—70%−80%, primarily for EV batteries, the battery is frequently still functional. However, this is not always the case or explicitly stated by the manufacturer. When choosing a battery, it is critical to understand cycle life as it relates to battery chemistry. In general, lead-acid batteries have rated cycle lives of 500−1000 cycles, with advanced carbon lead-acid products increasing the limit to 5,500 cycles. In contrast, lithium-ion technology has cycle lives ranging between 3,000 and 10,000 cycles [30].

Depth of Discharge

The DoD is defined as the percentage of the battery that has been discharged compared to its total capacity. For instance, if we have a battery type such as LG Chem's Residential Energy Storage Unit (RESU) batteries and it holds 9.3 kWh of electricity and is discharged to 8.8 kWh, then DoD is roughly 95%. According to [30] the percentage of a battery's nameplate being used is known as the DoD. For example, consider a battery bank with a capacity of 10 kWh, discharged at a DoD of 20%. This means that only 2 kWh will be utilized for its available energy storage. It is crucial to select an appropriate DoD level for each specific use case. To illustrate, if we take the previously mentioned battery bank and aim to design a battery backup solution, the choice of DoD becomes pivotal. If the battery is utilized only 40 times per year, we might observe a 10-year lifespan at 80% DoD (400 cycles/10 years = 40 cycles/year). Conversely, in an off-grid scenario where the battery undergoes daily cycling, the system's lifespan at the same DoD would be considerably shorter, approximately one year [31]. Figure 2.1 is used herein to define the DoD bases on SOC. As we can see, $SOC_{initial} = 100\%$, and when a battery discharged to 80% ($\Delta SOC = -20\%$) then DoD = 20%. If the battery discharged to 40% ($\Delta SOC = -60\%$) then DoD = 60%. In case of recharged the battery from 40% to 100% ($\Delta SOC = 60\%$) then DoD = 0%.
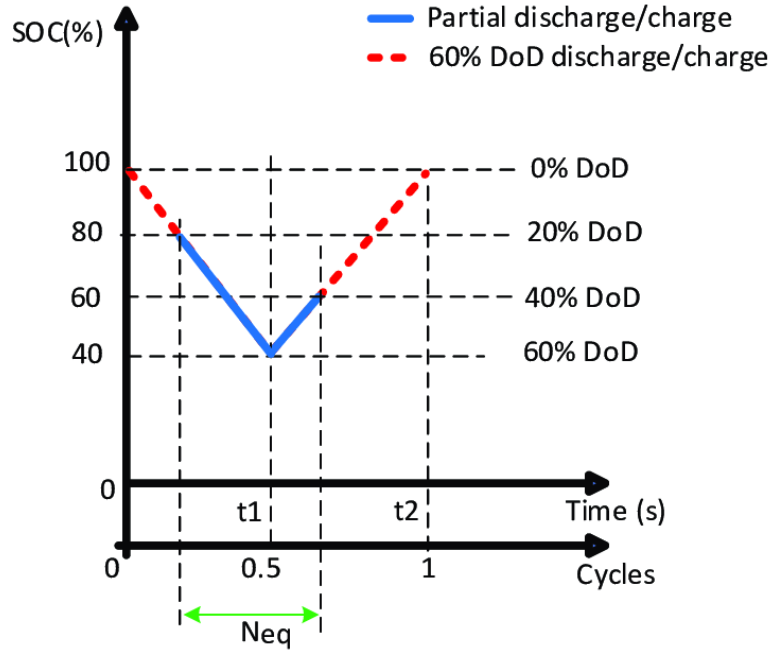
Figure. 2.1 Equivalent number of cycle concept [31]

State-of-Health (SOH)

SOH is described as the proportion between the maximum battery charge to its rated capacity. The SOH can be calculated using;

$$SOH = \frac{Q_{max}}{C_r} \times 100 \tag{2.1}$$

Where; Q_{max} is the maximum charge available of the battery measured by AH, and C_r is a rated capacity. This formula provides a numerical representation indicating the health of the battery, offering insights into its current state in relation to its designated capacity. Beyond capacity, which serves as a primary indicator, several other metrics contribute to evaluating the overall health of a battery. These additional indicators include remaining cycle life, impedance or conductance, internal resistance, self-discharge, charge acceptance, and discharge capabilities. Therefore, SOH offers a comprehensive assessment of a battery's condition by considering various factors beyond mere capacity, providing a more nuanced understanding of its overall performance and longevity.

Ambient temperature

The ambient temperature plays a crucial role in influencing battery performance. This influence is temperature-dependent and affects various aspects of batteries, including their performance, lifespan, and safety, with a specific focus on distinguishing between high and cold temperatures. In elevated temperatures, the acceleration of chemical reactions within batteries results in improved performance and increased storage capacity. However, this advantage is counterbalanced by substantial lifecycle degradation. [32]

13

reported a notable 20% rise in storage capacity at 45C° for lithium-ion batteries, yet charging at this temperature induces more than double the degradation observed at 25C°, signalling potential enduring issues. Conversely, cold temperatures elevate internal resistance, complicating the charging process and diminishing capacity, particularly noticeable in lead-acid batteries, which may provide only half their nominal capacity at ∼ -17.78C°. Each battery type has its defined operating temperature ranges, and straying from these ranges can reduce charge acceptance and introduce safety concerns, underscoring the critical importance of thoughtful temperature management for maintaining optimal battery health and performance.

Energy Retention or Standby Losses

The amount of time that a storage system can retain its charge is called energy retention time. The idea of energy retention is crucial since some storage systems have the propensity to self-discharge or lose energy while not in use [29].

2.2.3   Battery types

Large-scale ESS utilize a variety of battery types, each with its own distinct characteristics. This section explores the attributes of batteries commonly employed in large-scale BESS projects, including Lead-acid, nickel metal hydride (NiMH), nickel-zinc (NiZn), nickel-metal hydride (NiMH), lithium-ion (Li-ion), Solid State Batteries, Metal air and flow batteries, among others. The discourse not only covers the technical aspects but also delves into the practical applications associated with these battery technologies. The characteristics of these battery types are detailed in the following subsections:

A. Lead-acid

In respect of ESS, Lead-acid batteries were the first battery technology to be used. This type of battery is considered a rechargeable battery and is based on chemical reactions that involve lead dioxide which forms the positive electrode, the sponge lead is responsible for forming the negative electrode, and sulphuric acid which acts as the electrolyte [33]. [34] reports that, in the discharge phase, the negative plate undergoes a process where lead dissolves into the electrolyte, forming lead sulfate and leaving two electrons. These electrons then travel through the external circuit to the positive plate. Subsequently, the lead in the positive plate also dissolves into the electrolyte, resulting in lead sulfate formation. As a consequence, the electrolyte experiences a reduction in dissolved sulfuric acid content, predominantly turning into water.

As a battery discharges, the lead plates become more chemically similar, leading to a weakening of the acid and a subsequent voltage drop. Eventually, the battery becomes so discharged that it loses its capacity to deliver a useful voltage. Nevertheless, the

battery can be recharged by supplying it with electrical current, reinstating the chemical distinction between the plates, and restoring the battery to its full operational power.

The most significant negative factors of lead-acid batteries include; the relatively low cycle life and battery operational lifetime. The lifetimes of these batteries are very short, between $500-1000$ charge/discharge cycles or $5-15$ years of operation. Both DoD and temperature will have a negative effect on the life of these types of batteries. At the fully discharged stage, these batteries suffer from damage to the electrodes, thus reducing lifetime [35]. The energy density of lead-acid is considered very low ranging from 30 Wh/kg$-$45Wh/kg, with a power density of around 180 W/kg. The main advantages of these batteries include; the required maintenance is at a relatively low level and the batteries are easy to install [36]. Moreover, in this type of battery, the self-discharge rates are very low ($< 0.3\%$), which makes them more suitable for long-term storage applications. However, cost low energy density and short life cycles have made lead-acid batteries not popular for grid storage. These batteries are commonly used for electric cars, backup power systems, and renewable energy storage [37].

B. Nickel-based batteries

The category of nickel-based batteries includes three different types: nickel-cadmium (NiCd), nickel-metal hydride (NiMH), and nickel-zinc (NiZn) batteries. These batteries all share the same positive electrode material, which is nickel hydroxide. The electrolyte used is an aqueous solution of potassium hydroxide with some lithium hydroxide. However, the negative electrode varies depending on the type of battery; the NiCd type uses cadmium hydroxide, the NiMH uses a metal alloy, and the NiZn uses zinc hydroxide [38]. Compared to lead-acid batteries, Nickel-based batteries have a higher typical maximum energy density, ranging from 50 Wh/kg for the NiCd to 80 Wh/kg for the NiMH and 60 Wh/kg for the NiZn. The operational life and cycle life of NiCd batteries are considered high compared to lead-acid batteries, with the range of deep discharge levels and typical lifetimes varying from 1500 cycles for the pocket plate vented type to 3000 cycles for the sinter vented type [37]. However, for industrial use or supporting renewable energy power systems, NiCd and other types of nickel-based batteries have some disadvantages over lead-acid batteries. The cost of the NiCd battery is high, up to 10 times more than lead-acid batteries, and different types of Nickel-based batteries have lower energy efficiency than lead-acid batteries. NiMH batteries have an energy efficiency ranging from $65\%-70\%$, while NiZn batteries have 80% efficiency. The energy efficiency of NiCd batteries depends on the technology used during manufacture but is generally limited to $60\%-83\%$. Additionally, advanced NiCd batteries have high self-discharge rates that exceed 10% of the rated capacity per month. Despite these limitations, NiCd batteries are still used for industrial UPS applications such as large energy storage for renewable energy systems (RES) [35].

C. Lithium-based battery

The early 1990s saw the production of the lithium-ion battery by Sony. Initially, the use of this type of battery was limited to small-scale consumer devices such as cell phones. However, in recent times, it has been further developed and utilized for larger-scale battery storage and electric vehicles [37]. The cathode of the lithium-ion battery is composed of lithium metal oxide, while the anode is made of graphitic carbon with a layered structure. The electrolyte in the lithium-ion battery consists of lithium salts that are melted in organic carbonates. During the charging process of the battery, the lithium atoms located in the cathode become ions and are carried by the electrolyte to the carbon anode, where they combine with external electrons and are deposited between carbon layers as lithium atoms. The reverse process occurs during the discharge stage [35]. There are two main types of lithium technology batteries, namely lithium-ion and lithium-polymer cells. Lithium technology batteries have numerous advantages over NiCd and lead-acid batteries, including higher energy density and energy efficiency, low maintenance requirements, low self-discharge rate, which is approximately 1.5% per month, and a long battery lifetime that can exceed 1500 cycles. The energy densities of the lithium-ion battery ranged from 200 Wh/kg$-$300 Wh/kg, and energy efficiencies ranged from 90%$-$100% [39]. In terms of power density, lithium-ion cells have a range of 500W/kg$-$2000W/kg, while lithium-polymer cells range from 50W/kg$-$250W/kg. However, high temperatures can accelerate the aging of lithium-ion batteries, and deep discharges can significantly reduce their lifetime. Therefore, it is necessary to use a protection circuit during the charge and discharge stages to prevent the peak voltage of each cell from exceeding the limit and to prevent the cell voltage from dropping too low [40]. According to [41], the cost of a lithium-ion battery pack is forecasted to reach £152/kWh in 2023, up from £141/kWh the previous year, with an assumed cycle life ranging between 5$-$15 years. Bloomberg New Energy Finance predicts that the cost of lithium-ion batteries will drop to less than £100/kWh by 2025. Currently, lithium-ion batteries are the most widely used battery storage option, accounting for more than 90% of the global grid battery storage market and providing ancillary services. To make lithium-ion batteries more competitive for long-term storage, improvements such as the use of silicon instead of graphite to increase the battery's power capacity have been added. Lithium-ion batteries are also being used for rural electrification in developing countries. These batteries have been integrated with solar panels to provide a limited amount of electricity to charge cell phones, run appliances, and light buildings in rural communities [37].

D. Solid State Batteries

Solid-state batteries are a type of battery that use solid electrolytes, which offer various advantages over lithium-ion batteries, particularly in large-scale grid applications. These

advantages include higher energy densities, lower risk of fires compared to liquid electrolytes, and increased safety due to their smaller size. However, solid-state batteries are costlier than lithium-ion batteries because they are not as widely developed. Despite this, the production of lithium-ion batteries is rapidly increasing, leading to economies of scale that solid-state batteries may struggle to compete with in the future [33].

E. Metal air

Metal-air batteries, such as lithium-air, zinc-air, magnesium-air, and aluminum-air batteries are effectively utilized in different fields, especially in power supply applications. These batteries utilize atmospheric oxygen as a key reactant, thereby reducing overall battery weight and maximizing space for energy storage [42]. Among the various metal-air batteries, lithium-air stands out with the highest theoretical energy density, reaching levels comparable to gasoline engines at 13000 Wh/kg. This superior energy density positions lithium-air batteries as a notable choice compared to other rechargeable battery technologies [43]. According to [44], metal-air batteries, in general, offer significant advantages due to their high volumetric and gravimetric energy density, along with extended lifespans. Specifically, lithium-air batteries show potential applications in various technologies, including electric vehicles, plug-in hybrid electric vehicles, robots, and electric power storage systems. However, it's worth noting that current commercial lithium-air batteries face challenges, lacking the practical energy density required for high-power consumption devices and exhibiting a limited life cycle. Notably, lithium-air batteries differ from other metal-air batteries, such as zinc-air, aluminum-air, and magnesium-air batteries, as they are not moisture-stable in atmospheric conditions. This distinction contributes to higher manufacturing costs and complexity. Despite these hurdles, the reversibility of lithium-air batteries surpasses that of zinc-air and magnesium-air batteries, though it's important to mention that aluminum-air batteries are not rechargeable.

F. Flow batteries

Flow batteries represent a specific battery type comprising two separate electrolyte reservoirs that necessitate a pump for circulation. The electrochemical cell within the battery involves a cathode, an anode, and a membrane separator. As electrolytes flow, chemical energy converts to electricity within the electrochemical cell. Each electrolyte is stored in a large external tank, determining the battery's energy density by tank size and electrolyte quantity. Flow batteries, also termed redox flow batteries, derive their name from oxidation and reduction reactions between electrolytes [45]. In conventional flow battery systems, two liquid electrolytes, often with metals like vanadium or iron, undergo electrochemical reductions and oxidations during charging and discharging. Housed in sizable tanks resembling shipping containers, these electrolytes generate electricity when

pumped over electrodes separated by an ion-exchange membrane. During charging, ions move through the battery's membrane from one electrolyte to reach the second [46].

[47] reports that, numerous flow batteries are deployed commercially, predominantly employing vanadium-saturated electrolytes, typically a mix of vanadium sulfate and sulfuric acid. This choice is due to vanadium's ability to achieve the highest energy density while ensuring prolonged battery life. Projections for 2030 indicate flow batteries could store around 61 MWh annually, contributing to producers' annual sales surpassing £22 billion. A drawback of vanadium flow batteries is their lower energy density compared to lithium-ion batteries, approximately 30 W h/L, but higher than iron-chromium flow batteries, constituting roughly 10% of lithium-ion energy density. A notable advantage is stability, with vanadium flow batteries recognized for having the longest lifetimes among battery types, enduring over 20,000 charge-and-discharge cycles, equivalent to 15–25 years, with minimal performance degradation.

Flow batteries boast an efficiency of nearly 85%, offering advantages like tolerance to overcharging, low maintenance costs, and unaffected life cycles. However, they are unsuitable for small-scale energy storage, necessitating sensors, pumps, power management, and secondary containment [37].

2.2.4 Other Energy Storage Applications

Supercapacitor Storage Technology

The supercapacitor, also known as the ultracapacitor, is comprised of activated capacitors with remarkably high surface areas. Unlike traditional capacitors, the supercapacitor features a molecule-thin layer of electrolyte that acts as a separator for the charge. Its defining characteristic is its ability to provide high capacitance in a compact form. The supercapacitor functions by separating charges at an electric interface that is measured in nanometres, compared to polymer film capacitors that are measured in micrometres. During the charging process, the charged ions present in the electrolyte move towards the electrodes of opposite polarity, resulting from the electric field created by the applied voltage [28]. The supercapacitor and the battery differ in how they store energy; the former utilizes static charge, while the latter uses an electrochemical process. Due to the lack of any chemical reactions, the supercapacitor experiences minimal degradation in cases of deep discharge or overcharge, leading to a long cycle life of hundreds of thousands of cycles. At 100% depth of discharge, the supercapacitor can achieve a cycle life of more than 500,000 cycles, providing up to 12 years of operational life. Although the supercapacitor and capacitor share certain characteristics, such as high power density, which is around 10,000W/kg, and efficiency approaching 98%, they are not identical [40]. The supercapacitor technology allows for quick and efficient charge and discharge processes, as it directly stores electrical energy. However, its energy density is relatively low. The cost of the supercapacitor per unit of energy is also high, estimated

at around £20,000/kWh, in addition to a high energy dissipation rate of $5-40\%$ per day [37]. To overcome these limitations, a hybrid approach combining supercapacitors with other high-energy density storage systems such as batteries could provide advantages for various applications, from large-scale grid systems to portable devices and electric vehicles. Supercapacitors are often used for power factor correction, voltage and VAR support, and harmonic protection, rather than energy storage in power systems [46].

Flywheel storage

A flywheel is a device consisting of a mass that rotates around an axis, designed to store energy in the form of kinetic energy. To set the flywheel in motion, energy is required to accelerate it. This energy is supplied by an electric motor within the electrical system. During the initial stages of rotation, the flywheel serves as a mechanical battery that stores a specific amount of energy, which is determined by its moment of inertia and rotational velocity. The more rapidly the flywheel rotates, the greater the amount of energy stored. To release stored energy, the flywheel must be slowed down using a decelerating torque. The kinetic energy released is then returned to the electric motor, which functions as a generator [28]. The flywheel energy system offers several benefits, such as rapid charge and discharge rates over numerous flywheel cycles. In addition, it has a high cycling capacity that is not dependent on the rate of charge or discharge. The system also has a long lifespan, lasting approximately $15-20$ years, with a cycle life of $10,000-100,000$ cycles. Furthermore, it has a high-efficiency rate, typically ranging from $90\%-95\%$ [40]. In addition, high specific energy for the typical state-of-the-art composite rotors that reach up to 100 Wh/kg, with high specific power. However, in terms of capital cost for flywheels it is considered very high ranging from £1000/kWh$-$£5000/kWh, also, the range of self-discharge rate for standard flywheels is between 55%/day-100%/day [46]. Advanced flywheels utilise magnetic bearings and vacuum containment to significantly minimise energy losses. Although flywheels have low energy densities and high discharge rates, making them unsuitable for long-term energy storage, they can effectively provide quick response power to accommodate fluctuating power demands [48]. In addition, the maintenance expenses associated with flywheels are minimal, and they are deemed eco-friendly because they do not produce any greenhouse gases or hazardous substances during operation [49]. Flywheels have recently started to be incorporated into variable renewable energy systems (VRES). For instance, a 5 kWh/200 kW flywheel was employed in a wind-hydrogen system to stabilize the power supply for 10 households in Utsira, Norway. Urenco Power Technologies has also installed some flywheels to regulate the output of wind turbines and stabilise the power supply to a small island. Flywheels are expected to help mitigate the impact of cloud cover on solar photovoltaic systems by preventing voltage fluctuations and acting as energy buffers to counteract wind power surges, according to [50]. To enable better integration of VRES, it is recommended to combine flywheels with other devices such as pumped

hydro storage, hydrogen, or diesel to overcome the limitations of each technology [40].

Pumped-storage hydro (PSH)

PSH is a type of energy storage technology that uses gravity to produce electricity on a large scale. Initially, the process involves pumping water to a higher elevation to store it using low-cost energy. Later, when there is a power demand, the water is released back into the lower pool and used to generate electricity using turbines. Some recent advancements have been made in PSH technology, including adjustable speeds that allow for better responsiveness when there is an imbalance between energy supply and generation. The technology also now allows for closed-loop systems to be used [37]. In terms of cost, PSH is considered a relatively inexpensive energy storage option compared to other types, particularly for large-capacity storage. The installation cost for PSH, according to the Electric Power Research Institute, ranges from £1,700/kW to £5,100/kW, while the cost for lithium-ion batteries falls between £2,500/kW and £3,900/kW. PSH also has an energy efficiency of more than 80% throughout its full cycle and can provide electricity for up to 10 hours, which is longer than the almost 6 hours provided by lithium-ion batteries. However, PSH projects require significant long-term investment due to the permitting process and construction activities, which can take 3 to 5 years. This delay may deter investors who prefer short-term investments, particularly in a rapidly changing market [40].

Compressed Air Energy Storage (CAES)

Compressed air energy storage (CAES) is a form of energy storage that involves pumping air into an underground hole, typically a salt cavern, during periods of low electricity demand when energy is less expensive. When electricity is needed, stored air is released from the underground cavern and brought back to the facility, and the resulting expansion is used to turn an electricity generator [51]. However, the utilization of CAES technology can lead to a threefold increase in the energy output of facilities that solely rely on natural gas. If the heat generated by air pressure is conserved, CAES has the potential to achieve energy efficiency of up to 70%, otherwise, it ranges between 42%-55%. At present, there exist only two CAES facilities that are operational - one in Huntorf, Germany, and another in McIntosh, Alabama [52]. The McIntosh plant, established in 1991, has an energy storage capacity of 110 MWh. Moreover, a 317 MWh CAES plant is presently being built in Anderson County, Texas [40]. CAES systems are typically limited to large-scale applications and have the highest capacity among energy storage options, except for hydro pump systems. With a capacity range of $50 MWh - 300$ MWh and the potential for storage periods exceeding one year, CAES systems have minimal losses during storage. Compared to conventional combustion turbine peaking plants, CAES has a fast start-up time, providing emergency start-up times of $9 - 12$ minutes under normal conditions. Although the installation cost of CAES can be significant if a natural

geological formation is not used, greenhouse gas emissions are lower than in traditional gas plants. However, the reliance on geological structures is a significant challenge due to the limited availability of underground caverns. Nonetheless, CAES can provide a significant energy storage capacity with extended time periods if installed in suitable locations [28].

Thermal (including Molten Salt)

This form of energy storage uses a heating or cooling medium to store energy. The procedure involves heating various materials, such as rocks, water, or salts, and enclosing them in isolated environments. To generate energy, cold water is pumped onto hot rocks, salts, or hot water, which produces steam in the form of thermal energy that is utilised to rotate turbines [37]. Thermal energy storage has two primary applications: generating electricity and regulating the temperature of buildings. As stated by [46], thermal energy may be utilized to create ice overnight, which can then be employed to cool a building during the day. [53] reporters that, the thermal energy storage exhibits a relatively modest overall cycle efficiency, ranging from 30%−50%. However, it boasts significant advantages such as a high energy density and minimal daily self-discharge. Notably, this technology is environmentally friendly, and its initial capital cost for project initiation is relatively economical. These features render thermal energy storage suitable for large-scale energy storage systems.

Hydrogen fuel cell (HFC)

Hydrogen fuel cells (HFC) are gaining heightened attention as a chemical energy storage solution for power systems. The fundamental components of HFC include hydrogen and oxygen, with their chemical interplay resulting in the generation of both electricity and water [54]. To store energy, the process can be reversed using electrolysis of water, producing oxygen and hydrogen.

Consequently, hydrogen produced during times of low electricity demand can be utilized to generate electricity when needed. Typically, hydrogen is produced in one location and utilised in another. There are alternative methods for producing hydrogen, such as reforming biogas, ethanol, or hydrocarbons, which are cheaper but emit carbon pollution.

This form of energy storage boasts several advantages, including reliability, large-scale power support, silent operation with no moving parts, satisfiable storage capacity, high energy density (0.6−1.2 kWh/kg), simple construction, and zero emissions when running on pure hydrogen, producing only water as a byproduct, according to [37]. The high cost of hydrogen fuel cells, which require the use of expensive platinum, and the low efficiency ranging from 20%−50%, are significant drawbacks [46].

There are different technologies to store energy, each with its strengths and

weaknesses. Table 2.1 compares a list of the storage technologies that are being used or have the protentional for grid-scale storage.

Table. 2.1 Some properties of Energy Storage System of Grid Applications [33], [54], [55]

ESS	Power Rating (MW)	Discharge time	lifetime (years)	Energy density (Wh/Kg)	Efficiency (%)	Cost (£/kWh)
Pumped hydro	100–5000	1–24h+	40–60	0.2–2	70–85	5–100
Compressed air	5–300	1–24h+	20–40	2–6	41–75	2–50
Molten salt (thermal)	150	Hours	30	80–250	80–90	25–70
Li-ion battery	100	1min–8h	≤ 15	200–300	85–98	132
Lead-acid battery	0–20	Secs−hrs	5–15	30–50	75–90	200–400
Flow battery	100	Hours	≤ 20	20–70	75–80	150–1000
Hydrogen fuel cell	100	mins–week	5–30	800–10,000	20–50	160
Flywheel	20	secs–mins	10–20	5–30	80–90	1000–5000
Supercapacitor	Up to 10,000 W, Specific power (W/kg)	Discharge from 100% to 50% in 30 to 40 days	≤ 20	1–15	95–98	300–2000

Figure 2.2 displays a comparison of energy density and power density for various ES technologies. When considering a specific amount of energy, the greater the power and energy densities are, the less space the energy storage system will require.
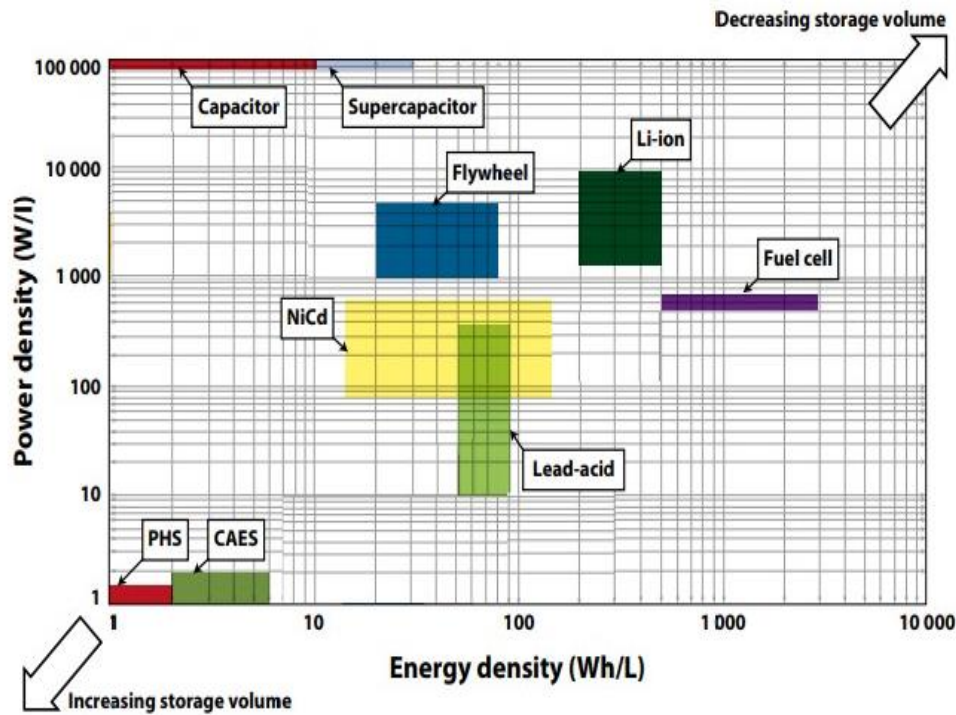
Figure. 2.2 A comparison between the power density and energy density of various energy storage technologies, adopted from [56].

The diagram presented in Figure 2.2 depicts various ESS technologies based on their energy density and power density. The compact EES tech- nologies that are best suited for applications with limited space requirements are positioned in the upper right corner, while the larger EES systems that require significant volume are located in the lower left corner. It is evident from the diagram that most batteries, fuel cells, and flywheels have moderate energy and power densities. The PHS and CAES have lower densities, making them more suitable for stationary EES and necessitating large reservoirs for grid-scale applications. Supercapacitors and capacitors have very high power densities but low energy densities. Flow batteries, in general, have lower densities than conventional batteries. Lithium-ion batteries, on the other hand, have high energy and power densities, making them widely used in portable devices and demonstrating significant potential in transportation, small-scale as well as large-scale ESS applications, Currently, some large-scale battery storage systems, the largest 750 MW/3,000 MWh. Moss Landing is in Monterey County, California [21].

2.2.5 ESS and Grid support services provided by the Transmission or Distribution system

Peak shaving

Peak shaving involves minimizing electrical power consumption during periods of heightened demand. This strategy can be executed by either powering down equipment

or implementing energy storage solutions, such as on-site battery storage systems. The goal is to eliminate momentary spikes in demand and decrease the overall costs associated with electricity usage. ESS, such as batteries or pumped hydro storage, can be used for peak shaving by storing energy during off-peak periods and discharging it during periods of high electricity demand. This helps reduce the reliance on expensive peak electricity generation, providing economic benefits to both utilities and consumers. [56].

Load Levelling

Load levelling is a strategy that involves storing power during periods of low demand and releasing it when demand peaks. This process, particularly crucial during high-demand periods, allows the ESS to supply power, thereby reducing the load on less cost-effective peak-generating facilities. The significance of load levelling lies in its ability to defer investments in grid upgrades or the creation of new generating capacity. The versatility of load levelling extends to both conventional batteries and flow batteries, which find applications not only in load levelling but also in peak shaving, load following, and time shifting. To gain a competitive edge, a crucial requirement is an overall reduction in costs and an improvement in cycle times. [57].

Energy Arbitrage

ESS has the potential to help manage energy costs by shifting electricity consumption from periods of high to low cost. They can also facilitate the shift of solar production from peak midday hours to evening hours. This is known as energy arbitrage, where the idea is to charge the ESS when electricity prices are low, and discharge when prices are high, to maximize savings. Energy arbitrage can also be combined with ESS applications to further optimise energy management. In general, savings from energy arbitrage are reflected as a direct reduction in energy costs on the monthly utility bill [58].

Ancillary Services/frequency regulation

ESS can serve as a valuable resource in maintaining voltage and frequency stability on the utility grid. It can absorb power from the grid when the frequency goes above a predefined upper frequency threshold, while it releases the active power to the grid when the frequency falls below a predefined lower frequency threshold. In certain markets, private entities can participate in the ancillary service market by submitting bids to provide services like frequency regulation to the independent system operator. Upon successful acceptance of their bid and provision of the service when called upon, these entities receive payment for their services. However, the regulations surrounding participation in the markets of ancillary services are complex and vary regionally, and the market is constantly evolving. Nonetheless, this can be a substantial revenue source for batteries, especially in large-scale utility systems [58].

Voltage Support

Ensuring proper voltage control is a critical element in any electrical energy system. In the context of transmission, this is typically regulated by power generators, while for distribution, reactive power is supplied by various assets. An additional consideration is that energy storage systems can also contribute to providing this service. When an energy storage system engages in voltage control, it falls under the category of a"power quality" application. This classification is due to its substantial improvement in the quality of service provided by the distribution system operator [59].

Black Start

A black start involves the restoration of an electric power station or a segment of an electric grid to functionality without depending on the external power transmission network, particularly after a complete or partial shutdown [60].

The service requires the provider to initiate the primary generator(s) to energise specific portions of the National Transmission System and distribution network. Activation of this service is directed by National Grid and follows a site-specific restoration plan. The Black Start generator might also be tasked with supplying start-up power to other power stations during the reactivation process of the system [61].

When a blackout occurs on a network, the resulting inconvenience can be minimised for affected users by using an energy storage system. Such a system can provide enough power to mitigate the impact of the blackout. In addition, an energy storage system can also be employed in the event of a complete blackout to assist with the restart of the entire electrical system. Recent scholarly works have highlighted BESS as an optimal and widely recognised solution for black start applications in power grids, due to its voltage source converter-based functionalities for active and reactive power regulation [59].

2.2.6 BESS compound system

BESS consists of a combination of hardware components and low- and high-level software. The main parts of BESS are shown in Figure 2.3 and explained below.
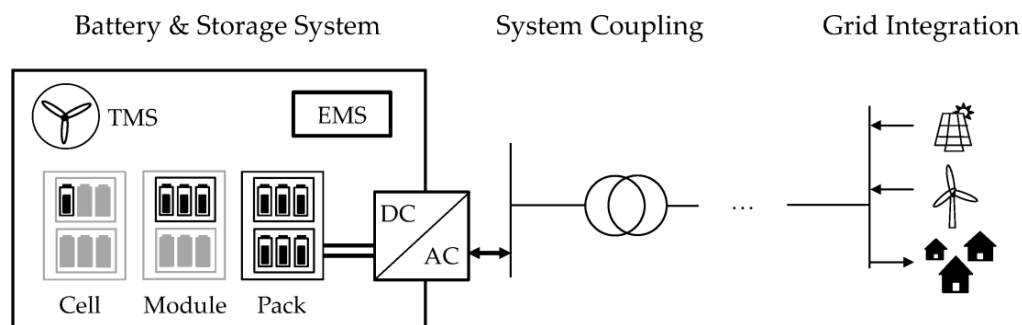
Figure. 2.3 Formalized Schematic Diagram depicting BESS, Power System Coupling, and Grid Interface Components [62].

1. **Battery System**. Battery systems comprise discrete battery cells that convert chemical energy into electrical energy. These cells are assembled into modules, which in turn are configured into battery packs.

2. **Battery Management System (BMS)** serve as electronic control circuits designed to monitor and regulate the charging and discharging activities of batteries. These systems are tasked with overseeing a range of battery characteristics, including the identification of battery types, monitoring voltages, temperatures, capacities, SOC, power consumption, remaining operating time, charging cycles, and additional relevant parameters. The primary role of battery management systems is to maximise efficient utilisation of the remaining energy within a battery. To prevent battery overload, BMS systems safeguard against deep discharge and over-voltage, conditions that can arise from excessively rapid charging or extremely high discharge currents. In situations involving multi-cell batteries, the battery management system additionally performs cell balancing, ensuring that various battery cells adhere to consistent charging and discharging criteria [63].

3. **An inverter or power conversion device (PCS)** is used to convert the direct current (DC) generated by batteries into alternating current (AC) and then supplied to the grid. Bi-directional inverters can be utilised in BESS to allow both charging and discharging.

4. **Energy Management System (EMS)**. The energy flow of a battery storage system must be monitored and managed by an energy management system (EMS). Furthermore, EMS is required to coordinate the work of BMS, PCS, and other BESS components. EMS can effectively manage the system's power resources by gathering and analysing energy data.
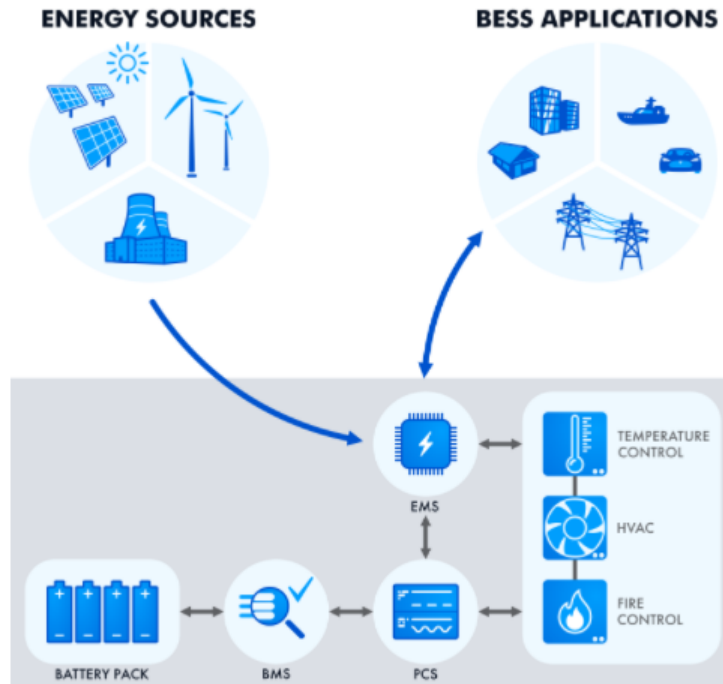
Figure. 2.4 Battery energy storage system architecture [64].

Figure 2.4 shows the BESS architecture, according to [64], a BESS, depending on its operational requirements and functionality, can encompass various safety mechanisms such as a fire suppression system, smoke detector, temperature regulation system, ventilation, cooling, heating, and air conditioning systems. These safety mechanisms are equipped with their own monitoring and control modules, which ensure the safe and secure operation of the BESS. They supervise the system's variables and promptly respond to emergency situations to ensure the safety of the BESS.

2.2.7   SOC Estimation

The proportion of total energy that a fully charged battery can store is referred to as the state of charge (SOC), which varies with the charging and discharging cycles. Accurately estimating the SOC is crucial for developing effective battery models and control algorithms, with Open-circuit voltage (OCV) measurement and current integration (coulomb counting) being popular methods for estimating SOC. However, for modern battery chemistries with flat OCV-SOC discharge signatures, alternative approaches, such as Kalman filtering, are required. In this regard, this thesis adopts the Coulomb counting method, which involves measuring the discharging current of the battery and integrating it over time to estimate the SOC [65]. The Coulomb counting method is used to estimate SOC_t using Eq.2.2 as calculated in [66].

$$SOC_t = SOC_{t-1} - \frac{1}{C} \int_0^t i \, dt \qquad (2.2)$$

27

Where SOC_{t-1} is the initial SOC at (t-1), SOC_t is the present SOC, (C) represents the rated capacity (the battery capacity at the normal condition), and (i) represents the charge and discharge current.

Table 2.2 gives a summary of the comparison between the SOC estimation methods.

Table. 2.2 Pros and Cons of SOC estimation methods [66], [67], [68], [69], [70], [71], [72]

Method	Summarized Features	Pros	Cons
Coulomb counting	Determines the number of charges injected or pumped out of a battery.	Simple and easily implementable, with direct SOC calculation.	The accuracy decreases over time due to the accumulation of errors in the current measurement. Accurate initial SOC measurement is needed.
Open circuit voltage (OCV)	OCV-SOC look-up table	Provides reasonably accurate SOC estimation under steady-state conditions. Easy to implement with a small amount of computation.	The accuracy is highly dependent on the battery type, temperature, and age. Only suitable for very high and very low SOC.
Impedance	Impedance of the battery (RC combination)	Accurate, useful for providing additional information about SOH.	Accuracy can be affected by temperature and load.
Discharge	Discharge and measure time to a specific threshold	Easy to implement and most accurate.	Time-consuming, not suitable for real-time SOC estimation, and only used offline.
Kalman filter	Extracts accurate information from noisy or inaccurate data.	Accurate and dynamic.	Highly independent of model accuracy, large computing requirement, and easily affected by temperature.
DC resistance	R_{dc}	Simple	Not accuracy and affected by temperature.
Fuzzy Logic		Online	Not accurate, high cost to implement.
Artificial neural network (ANN)	Adaptive ANN system	Can be used for all types of batteries.	Large amount of data required.

2.3   Battery Modelling

2.3.1   Types of Battery Modelling

The determination of battery parameters plays a pivotal role in battery modelling. Various methodologies, such as electrochemical, mathematical, circuit-oriented, and data-driven approaches, are employed to extract these parameters. Figure 2.5 illustrates the categorization of battery models; for more details, see the references attached in the figure.
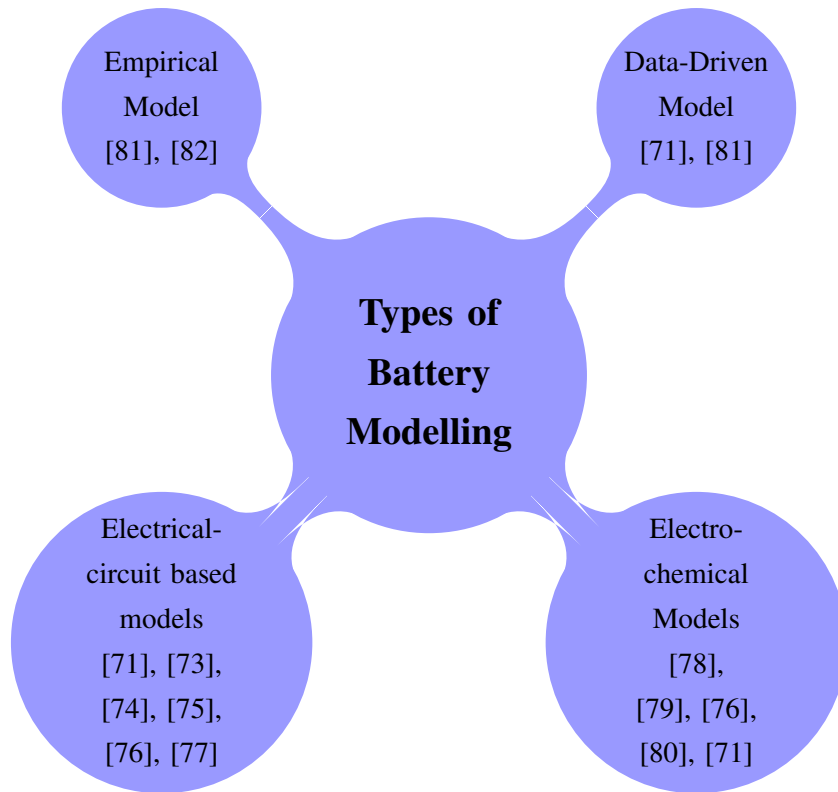
Figure. 2.5 Classifications of Battery Models.

The advantages and disadvantages of the above-classified battery model are summarized in Table 2.3.

Table. 2.3 Pros and cons of the battery modeling methods [72], [81], [82]

Battery Modelling Methods	Pros	Cons
Electrical-circuit based models	Simple and easy to use, relatively fast to develop and calibrate, can be useful for predicting battery behaviour under different operating conditions, and it's used widely in SOC estimation.	May require extensive calibration to achieve high accuracy, a complex parameter identification process, and it may not provide as much insight into the underlying physics of the battery as other types of models.
Empirical Model	Simple expression, They can provide accurate predictions for short-term battery behavior, and computational efficiency	limited ability to describe the terminal voltage, and it's specific to a particular battery type and may not be easily transferable to other batteries.
Electro-chemical Models	Can provide detailed insight into the underlying chemical reactions and processes occurring in the battery, high accuracy, and predictive capability when properly calibrated, and it can be used to explore the effects of changes to the battery design or operating conditions on battery performance.	Often require a high level of expertise and computational resources to develop and use, can be time-consuming and expensive to calibrate, may be limited in their applicability to specific battery chemistries and operating conditions, and Require prior knowledge of the battery.
Data-Driven Model	It's useful when experimental data is accessible, it can be utilized to predict various battery types and operating conditions after being trained, it's comparatively faster and less computationally demanding, while still providing high-precision voltage calculations, and it doesn't require prior knowledge of the battery.	May not provide as much insight into the underlying physics of the battery as other types of models, may be limited by the quality and quantity of available data, may not be able to predict the effects of changes to the battery design or operating conditions as accurately as other types of models.

In this thesis, the BESS model was developed in MATLAB/Simulation using the 'Bucket Model' based on a method shown in [83], [84]. This method was mainly carried out to facilitate and simplify the representation of any ESS, which could be achieved by using an integrator block where the energy can be calculated at each time step by adding

or subtracting it from the integrator (the 'bucket').

2.3.2   Lifetime Analyses of BESS Operating Frequency Regulation

In essence, battery life can be divided into two categories: calendar life and cycle life. Calendar life pertains to the deterioration of the battery that occurs during storage without any cycling, whereas cycle life relates to the degradation resulting from charge and discharge cycles, which corresponds to the battery's cycling within a vehicle.

Various factors, including C-rate (the rate of charge/discharge as a ratio of its capacity), temperature, accumulated ampere-hour throughput, SOC range, and DoD range, impact battery aging. It is crucial to comprehend the effects of these factors on battery aging to prolong battery life by optimizing its operating conditions [85]. For actual EVs, batteries may charge and discharge while driving or at charging stations. While parked, the battery may be idle. Therefore, both calendar life and cycle life must be taken into account. Studies have shown that charging and discharging at high rates accelerate battery aging [86] Additionally, the DoD is another factor that affects aging, with greater DoD resulting in increased aging [87], [88]. Many studies have concluded that high temperatures have a detrimental effect on battery aging [89], [90], [91], [92], [93]. The author of [94] found that C-rates exceeding 3C are considered high for the tested cell, and if used for longer than a few seconds, will rapidly deteriorate the cell. In [95], the degradation of commercial lithium-ion cells was investigated in terms of chemistry and cycling conditions over several years, by varying C-rate, DoD, and environmental temperature. The results showed that cell degradation was greatly influenced by the range of cycling conditions, even when operated within the manufacturer's specifications. Time to reach 80% capacity varied by thousands of hours and cycle counts among cells of each chemistry.

The study conducted in [96] examined the long-term impact of C-rate and cut-off voltages on capacity degradation and resistance increase. The findings revealed the existence of critical values for charging stress, beyond which battery degradation speeds are greatly accelerated. Incremental capacity analysis was employed to investigate the various aging mechanisms at different charging currents and cutoff voltages. The results suggested that reducing the charging current and cut-off voltage can slow down battery degradation when the battery has degraded to a certain extent. The cost of operating a battery is mainly due to the degradation effect of repeated charging and discharging [97]. When the capacity of battery cells falls below a certain minimum threshold (e.g., 80% of the original capacity) [98], they reach their end-of-life (EoL) and can no longer perform as expected. As a result, the predominant operating cost of batteries is the cost of cell replacement, which is high due to the high manufacturing prices of most electrochemical battery cells [99].

2.4 Reviewing Cycle Counting Methods and Battery Degradation

2.4.1 Rainflow cycle counting algorithm

Cycle counting refers to the process of dividing a strain/time history into smaller cycles, as described by previous studies [100], [101], [102]. The Rainflow algorithm is commonly employed to count cycles when assessing fatigue data. In the context of battery life evaluation, this algorithm is applied to a time series of a battery's SOC, which allows for the determination of the magnitude of all cycles contained within the series.
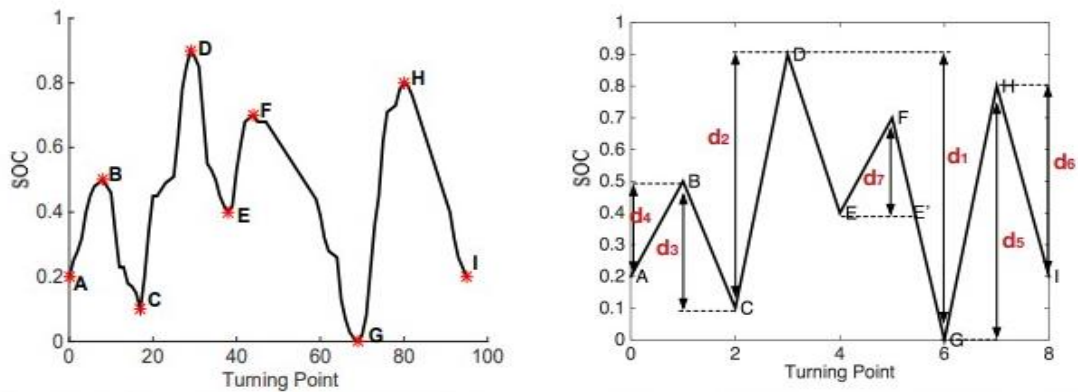
(a) Battery SOC time history. Red stars mark the local maximum and local minimum points **(b)** Rainflow cycle counting results, based on extracted local maximum and minimum points

Figure. 2.6 Rainflow cycle counting algorithm procedures [100].

Table. 2.4 The Rainflow cycle counting analysis was performed on the SOC profile presented in Figure 2.6a. The calculation of the "SOC range" was based on the absolute difference between the starting and ending SOC values of each cycle [100]

Path	A-B	B-C	C-D	D-G	E-F-E'	G-H	H-I
SOC range	0.3	0.4	0.8	0.9	0.3	0.8	0.6
Cycle	half	half	half	half	half	half	half

The application of the rainflow algorithm to count cycles in a battery's state of charge (SOC) profile is illustrated in Figure 2.6, and the resulting cycle analysis data is presented in Table 2.4. Algorithm 1, which is detailed in the paper by [103], was employed to perform the standard procedures of the rainflow algorithm. The SoC profile was analyzed by first identifying all local extreme points and arranging them, as shown in Figure 2.6b. The deepest half cycle, D-G, was then identified, followed by the identification of half cycles before D (C-D(d2), B-C(d3), A-B(d4)) and after G (G-H(d5) and H-I(d6)). The remaining full cycle, E-F-E', with a depth of d7, was counted, which could also be viewed as a combination of one charging half cycle and one discharging half cycle with equal depth. The cycle depths identified by the rainflow algorithm were recorded as [d1, d2, ..., dN].

2.4.2 Fast Cycle Counting Method (CCM)

This method is used to calculate micro charge/discharge full cycles based on the SOC profile [104]. Figure 2.7 illustrates the flowchart of CCM implemented in MATLAB/Simulink.
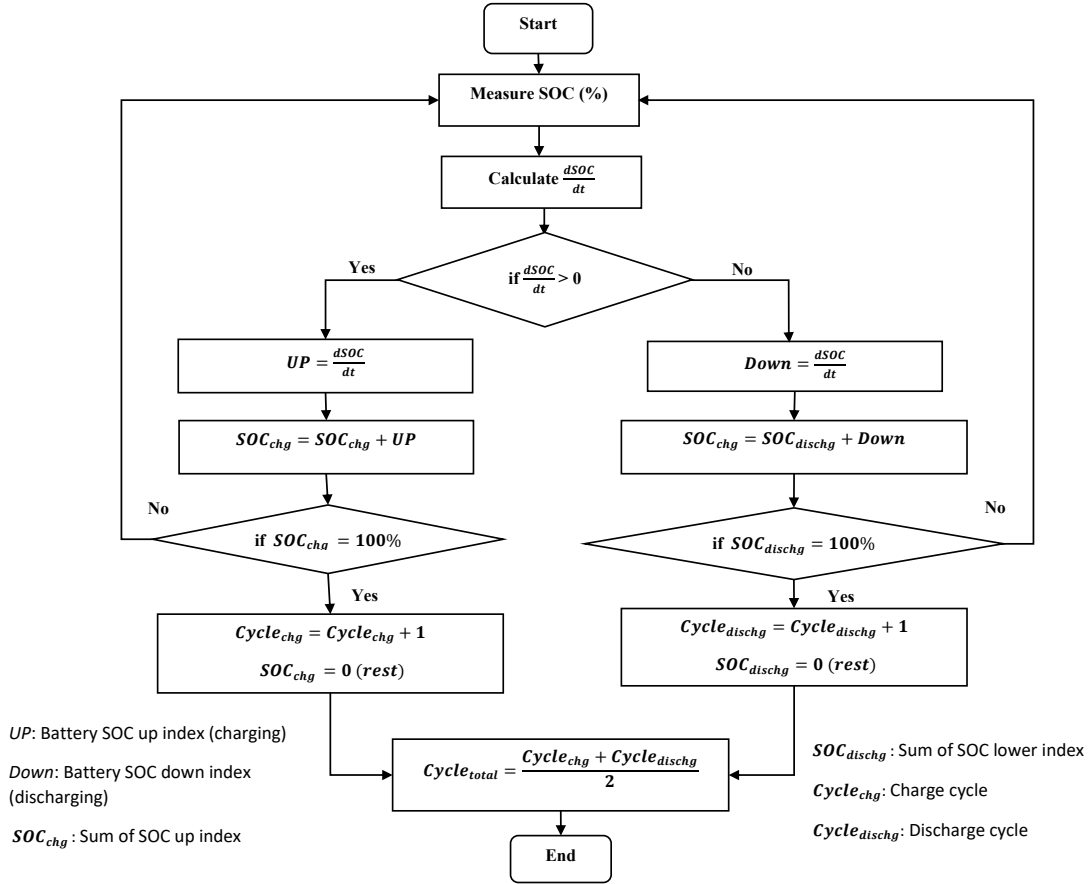
Figure. 2.7 Flow chart of the proposed cycle counting method (CCM) for a grid-tied BESS subjected to micro charge/discharge cycles.

The number of partial charge/discharge cycles can be calculated using CCM as shown in Figure 2.7 with steps summarized below;

1. The algorithm starts by detecting SOC every second and then calculates ΔSOC.

2. In this step, the sign of obtained ΔSOC each second will be monitored, so if ΔSOC >0, then the positive index (UP) will be summed up until reaches 100% which represents half-cycle (half-charge cycle).

3. In the third step, the same scenario as step two will be applied for ΔSOC when it is <0, then the negative index (Down) will be summed up until reaches 100% which represents half-cycle (half-discharge cycle).

4. In the last step, the total number of charge/discharge full cycles will be obtained by taking the sum of both micro charge and discharge and then dividing by two.

2.4.3 Number of Equivalent Full Cycles (EFCs)

In this thesis, a method is used to calculate the number of Equivalent Full Cycles (EFCs) required to deliver a service over a time period. This is particularly important for a BESS as the system will degrade (reduced capacity for example) with increased cycles, [105] states that in commercial documents, such as warranties, an EFCs is calculated using energy throughput as shown in eq.2.3;

$$EFCs = \frac{Total\ of\ Export\ and\ Import\ Energy\ of\ ESS}{Total\ Energy\ throughput\ by\ Capacity}/2 \qquad (2.3)$$

In this thesis, both CCM & EFCs will be considered to calculate the number of cycles for BESS used to deliver frequency response services such as DFR, DC, and DR services over a period of time (Month, and Year).

2.4.4 Battery Degradation Analyses Methodology

Battery degradation is a natural process that occurs over time and results in a reduction in the battery's ability to hold a charge and deliver power. There are several contributing factors to battery degradation, including; DoD, operational temperature, cycle life, SOC, and C-rate. In this thesis, the two degradation factors have been considered for lifetime analysis which includes C-rate and SOC. As discussed in the introduction, battery degradation analysis has been carried out using the two different cycle methodologies which include; CCM and EFCs, Once the number of cycles obtained by using such methods then compared with the cycling capacity curves of the various batteries using;

$$Battery\ Degradation\ (\%) = \frac{Total\ number\ of\ cycles}{Maximum\ number\ of\ cycles} \times 100 \qquad (2.4)$$

2.4.5 Ancillary (Balancing) Services

The provision of Ancillary (Balancing) Services involves NGESO compensating participants for the ability to purchase energy at a prearranged rate, which assists National Grid in fulfilling its responsibility of maintaining network stability. According to [106] participants may be requested to supply power or load-management capacity outside of emergency situations. In the UK, balancing services that the ESO uses are include;

- Existing services: demand flexibility service, frequency response, reserve services, local constraint market, system security services, reactive power services, trading, and electricity system restoration standards.

- Future services: Future frequency response products, future of reserve services, future of reactive power, stability market.

Reserve services

During specific periods throughout the day, there is a necessity for additional power resources, either through augmented generation or demand reduction. This capability is crucial for effectively handling electricity demand that exceeds initial forecasts for the transmission system in Britain. The supplementary power sources at NGESO disposal are referred to as 'reserve services'.

Various sources require different preparation times to be ready to provide the required service. These reserve services are categorised on the basis of their respective timescales, prioritising the shortest timescales first. They include balancing reserve, fast reserve, Super SEL, quick reserve, BM start-up, short-term operating reserve (STOR), and slow reserve [106].

Short-Term Operating Reserve (STOR)

(STOR) is a contractual arrangement between NGESO and energy providers that focuses on delivering supplementary power in a short time frame of less than 4 hours. According to [107] The STOR procurement process involves a daily pay-as-clear auction system, with contracts that span a single day. This auction concludes at 05:00, determining the delivery for the subsequent service day within the 05:00 - 05:00 time frame, covering the Firm or 'Committed Windows'. Providers must submit their availability, proposed prices, and MW offerings before the auction. STOR units must exhibit the ability to:

- Provide a minimum of 3 MW, either through generation or consistent demand reduction, which can be aggregated from multiple sites.

- Respond to instructions within a maximum time frame of 20 minutes. Sustain the response for a minimum of two hours.

- Be prepared to respond again after a recovery period not exceeding 1200 minutes.

The available capacity is specified for various windows depending on the season, day of the week, and time of day. Generators or consumers can submit bids at different prices, ensuring varying levels of availability for different windows. The proposals must be formulated on Friday before the delivery week. Providers receive payment for both availability and utilisation, with STOR contract prices showing notable volatility ranging from £1.50 to £22.50/MW/hour for availability payments and from £63.00 to £220/MWh for utilization charges [108].

Fast Reserve

For conventional energy generators, a high ramp rate is available, which requires a minimum capacity of 25 MW and must be provided for up to 15 minutes. The unit must

be able to generate electricity in 2 minutes and achieve a ramp rate greater than 25MW per minute, which is easily achievable for the BESS. NGESO is currently not offering this firm service but instead is offering an optional service. Providers of the optional service receive an Enhanced Rate Availability Fee (£/h) and a Utilization fee (£/MWh) for the energy supplied [109], [110].

Frequency response services

The obligation of the National Grid (NG) involves maintaining the frequency of the system at 50Hz with a variation of plus or minus 1%, ensuring preparedness for all plausible circumstances that may cause frequency fluctuations. To achieve this, NG procures different types of frequency response services, classified into Dynamic Frequency Response and Static Frequency Response, as detailed in a referenced source [111].

Dynamic Frequency Response encompasses three services:

- Primary Response: The frequency of the system during an event is sustained for 10 seconds and is sustainable for an additional 20 seconds.

- Secondary Response: Provided within 30 seconds of an event, with sustainability for an extra 30 minutes.

- High-Frequency Response: Offered within 10 seconds of an event and is sustainable indefinitely.

In contrast, Static Frequency Response is a non-dynamic service activated at a defined frequency deviation. The response is initiated in 30 seconds and remains effective until 30 minutes after reaching the frequency trigger.

As per NGESO, the new suite of Dynamic Response Services, including DC, Dynamic Moderation (DM), and DR, contributes collectively to maintaining system frequency within the stipulated license obligations of 50Hz plus or minus 1%. DM responds rapidly in pre-fault situations during particularly volatile periods, DR functions as a slower pre-fault service, and DC serves as a post-fault service, altogether ensuring effective control of system frequency.

As stated by NGESO, the conventional method for balancing grid frequency in real-time is Firm Frequency Response (FFR).

The procurement of static FFR will persist until it is substituted with a forthcoming enduring static solution. Simultaneously, Dynamic FFR is gradually being phased out during the FY23/24 period, with the introduction of emerging dynamic response services (DC, DM, DR) designed to fulfill this role.

Summary

A brief summary of this chapter:

- Provides an overview of key issues and challenges related to frequency regulation.

- Discusses previous studies on the sizing of BESS.

- Explore different energy storage systems and their specifications. A lithium-ion battery will be adopted for this research.

- Reviews SOC estimation methods with pros and cons. This thesis adopts the Coulomb counting method.

- Investigate battery modelling, advantages, disadvantages, and lifetime analysis. The BESS model was developed in MATLAB/Simulink using the 'Bucket Model,' which will be discussed in Chapter 3. With regard to factors that affect battery lifetime aging, two considerations are made in this thesis: C-rate and SOC.

- Reviews Cycle Counting Methods and Battery Degradation. In this thesis, both CCM and EFCs will be considered to calculate the number of cycles for BESS used to deliver frequency response services. Presents Battery Degradation Analysis Methodology.

- Reviews Ancillary (Balancing) Services. In this thesis, three frequency response services which include; DFR, DC, and DR will be considered and delivered by BESS.

The following chapter will introduce the BESS model developed in MATLAB/Simulink using the 'Bucket Model' principle. Validate the model against the Willenhall Energy Storage System (WESS) using different error calculation methods. Present control algorithms for various frequency response services and simulation results.

Chapter 3

Battery and Frequency Response Services Models

3.1 Introduction

In this chapter, the BESS model was developed in MATLAB / simulation using the 'Bucket Model' principle. This method was carried out mainly to facilitate and simplify the representation of any ESS, which could be achieved by using an integrator block where the energy can be calculated at each time step by adding or subtracting it from the integrator (the 'bucket'). In addition to that, many sub-blocks have been built around the battery bucket model, including efficiencies, SOC management systems, control systems, and analysis blocks such as availability, non-compliance, error calculation, and cycle counts.

The proposed blocks are intended to be the BESS Block, Application Block, Control Block, and Metrics Block. In addition, each frequency response service was discussed in terms of the implementation of the block diagram, specifications, control algorithm, and service parameters. In this thesis, the BESS model has been validated against a 2MW/986kWh battery called the Willenhall Energy Storage System (WESS), which has been built and operated by the University of Sheffield. The validation was carried out using two different error calculation methods, including Root Mean Square Error (RMSE) and Mean Absolute Percent Error (MAPE).

3.2 BESS Block
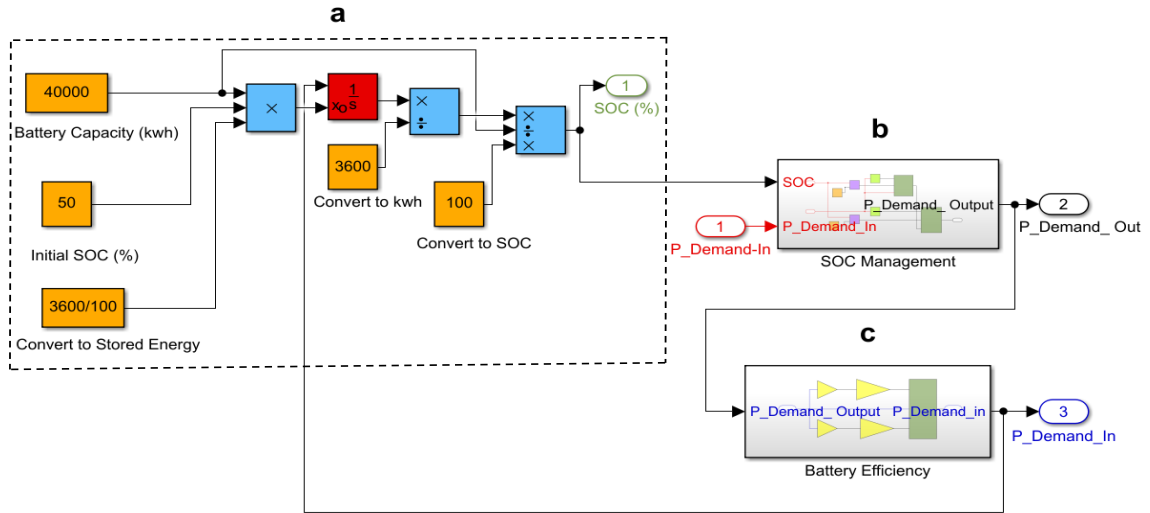
Figure. 3.1 An Outline of the BESS Module in the Matlab/Simulink Model.

Figure 3.1 gives an overview of the BESS block, which is divided into three parts. Part-a is about the battery itself, connected in a closed loop with two subsystems named (b, c).

Part-a

This part represents the integrator block with inputs of battery capacity (kWh) and charge/discharge powers received from the inverter, shown in Part-c, and the output is the SOC of the battery (

$$SOC_{out} = SOC_{init} + \frac{\int_0^t P_{BESS}\, dt}{3600.Q} \tag{3.1}$$

Where SOC_{init}, Q and P_{BESS} represent initial SOC, Watt-hour capacity, and instantaneous P_{BESS}, respectively.

Part-b
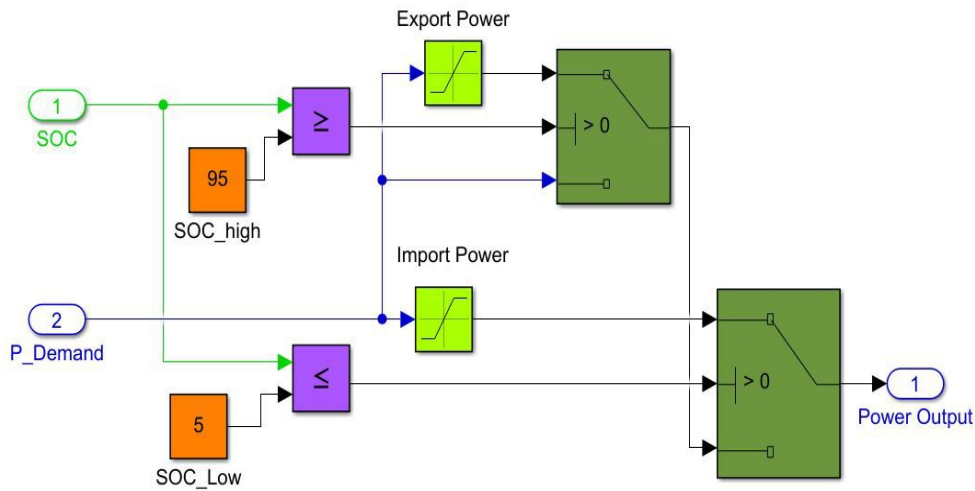
Figure. 3.2 P_{Demand_Output} Calculation based on SOC limits (high & low).

The P_{Demand_input} is the output of the inverter, which is directly connected to the control block shown in Subsection 3.3.2 (Figure 3.5). The SOC is fed from Part-a, and the SOC limits include SOC$_{low}$=5%, and SOC$_{high}$=95%. Therefore, if the battery SOC reaches the upper or lower limit, it stops importing or exporting.

Part-c

This part shows how the stored energy in the BESS has been calculated using a switch, where the input is the P_{Demand_Output} calculated in Part-b, multiplied by the charge/discharge efficiency. The output is P_{Demand_input}, which is then connected as an input to the integrator block shown in Part-a.
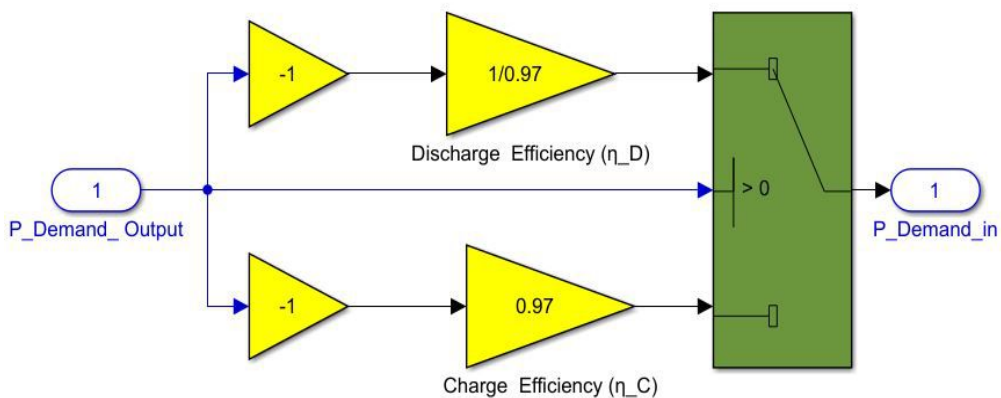
Figure. 3.3 Implementing Stored Energy Calculation in BESS.

Figure 3.3 shows the implementation of the calculation of Stored Energy in the BESS

as in [22] and expressed in the following equations;

$$E_t = -\int_0^t \frac{P_t}{\eta_D}.dt \qquad (3.2)$$

$$E_t = -\int_0^t P_t.\eta_C.dt \qquad (3.3)$$

Where η_D, η_C, P_t, and E_t refer to the battery discharge efficiency, battery charge efficiency, battery power for charging or discharging at a specific hour (t), and stored energy in the battery at that hour (t). It's important to note that if $P_t>0$ is positive, indicating that the system is exporting or discharging, eq.3.2 can be used, whereas if P_t is negative, indicating that the system is importing or charging, eq.3.3 can be used.

3.3 Dynamic Frequency Response (DFR)

Dynamic frequency response is a continuously provided service used to manage second-by-second frequency deviations on the grid. [22] reports that the specification for DFR service is currently a 15 mHz DB around 50Hz and then a linear response to ±0.5Hz up to contracted power as shown in Figure 3.4. The high level of a block diagram of the DFR service model is presented in 3.5 .

3.3.1 DFR Service Envelope
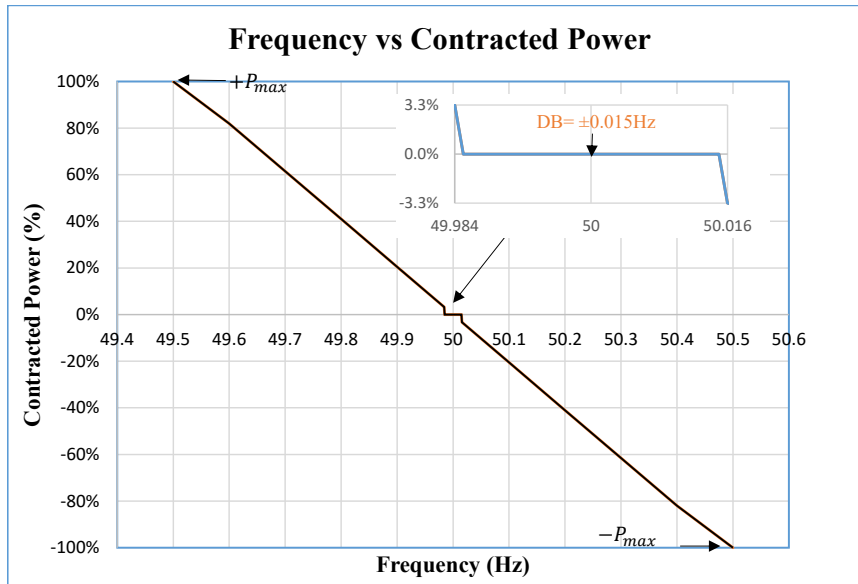
Figure. 3.4 Power vs frequency for DFR service.

Figure 3.4 illustrates the relationship between demand power and the frequency data for DFR service. The DB of this service is the same as DC (±0.015Hz), as well as the control and modelling. However, the power setpoint (power calculation) is different and

it is based on differing service specifications. The DFR service has been shown in Table 3.1, and the implemented BESS power management strategy for the DFR service is shown in Figure 3.7.

3.3.2 Dynamic Frequency Response Model (DFR)
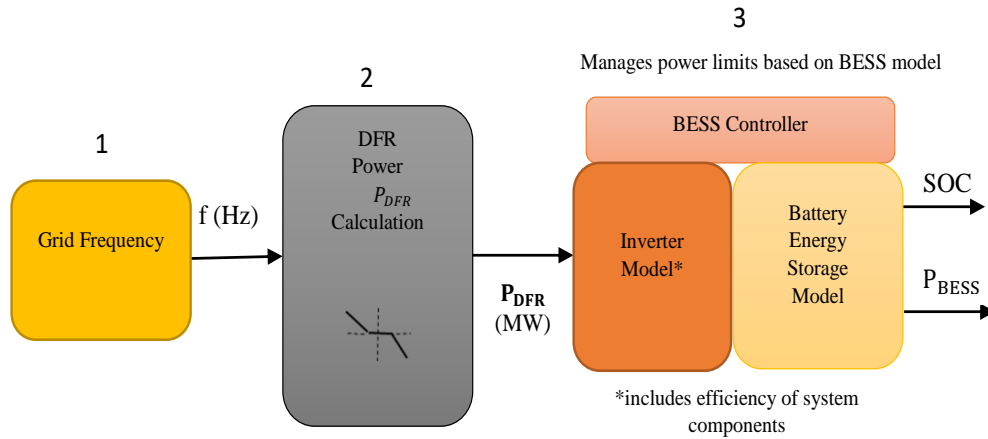
Figure. 3.5 The High Level of Block Diagram of DFR service model.

Figure 3.5 shows the high level of a block diagram of the DFR service model which is described below;

Block-1

This block represents the real-time grid frequency (f) with a unit (Hz) that changes second by second and has been obtained from the national grid (NG) [112].

Block-2
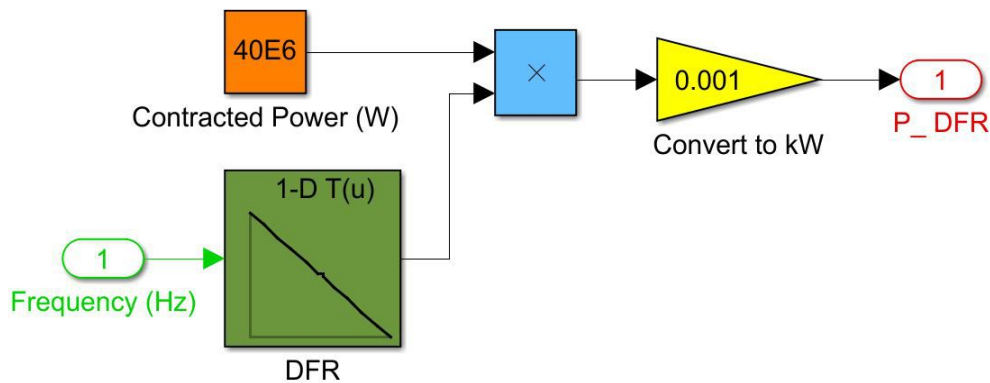
Figure. 3.6 Implementation of P_{DFR} calculation.

Figure 3.6 represents the application block that has been modified for use in simulating various applications such as DFR, DC, and DR services. This block is used to generate a

power-request signal to the BESS in accordance with NG specifications.

As we can see, the input of the lookup table is a frequency datum (f), which is defined in Block-1, and the output represents the contracted power (P_{DFR}), which is set at 40 MW in this case. The calculation of P_{DFR} is demonstrated in Table 3.1, where the required P_{DFR} envelope is calculated as a function of the desired limits according to NG specifications. The obtained P_{DFR} is measured in watts (W) and then converted to kilowatts (kW). It is also possible to convert the power unit to per unit (p.u), so 40 MW is equal to 1 p.u.

Figure 3.7 and Table 3.1 illustrate the algorithm for the proposed model, which starts by detecting the position of the measured frequency about the zones bounded by frequency values 'A' to 'R', as shown in Table 3.1. This step can be achieved by the P_{DFR} Calculation block. According to NG specifications, the output power must remain within this envelope at all times. If the power is provided outside this envelope, it will result in a reduction in the service performance measurement (SPM) and income revenue. In the DB, the required $P_{DFR} = 0$.
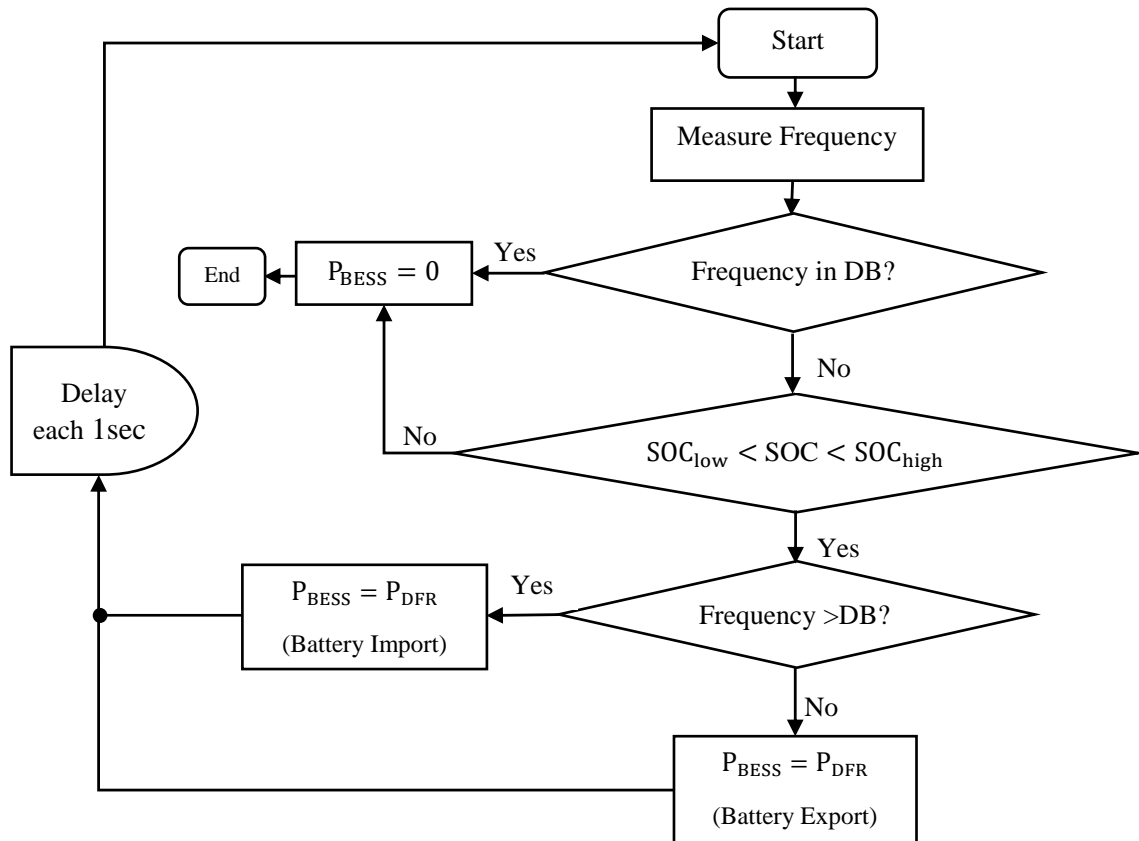
Figure. 3.7 Implemented BESS power management strategy for DFR service model.

Table. 3.1 P_{DFR} & Frequency setpoints and calculation in the control algorithm

Freq. Hz	Contracted Power, (p.u)	P_{DFR}, (p.u)
A=49.5	$a = 1$	$P_{DFR} = a$
B=49.6	$b = 0.8$	$P_{DFR} = [(\frac{(B-f)}{(B-A)}) \times (a - b) + b]$
C=49.7	$c = 0.6$	$P_{DFR} = [(\frac{(C-f)}{(C-B)}) \times (b - c) + c]$
D=49.8	$d = 0.4$	$P_{DFR} = [(\frac{(D-f)}{(D-C)}) \times (c - d) + d]$
E=49.9	$e = 0.2$	$P_{DFR} = [(\frac{(E-f)}{(E-D)}) \times (d - e) + e]$
F=49.984	$f = 0.033$	$P_{DFR} = [(\frac{(F-f)}{(F-E)}) \times (e - f) + f]$
G=49.985	$g = 0$	$P_{DFR} = 0$
H=50	$h = 0$	$P_{DFR} = 0$
J=50.015	$j = 0$	$P_{DFR} = 0$
K=50.016	$k = -0.033$	$P_{DFR} = [(\frac{(K-f)}{(K-J)}) \times (j - k) + k]$
L=50.1	$l = -0.2$	$P_{DFR} = [(\frac{(L-f)}{(L-K)}) \times (k - l) + l]$
M=50.2	$m = -0.4$	$P_{DFR} = [(\frac{(M-f)}{(M-L)}) \times (l - m) + m]$
N=50.3	$n = -0.6$	$P_{DFR} = [(\frac{(N-f)}{(N-M)}) \times (m - n) + n]$
P=50.4	$p = -0.8$	$P_{DFR} = [(\frac{(P-f)}{(P-N)}) \times (n - p) + p]$
R=50.5	$r = -1$	$P_{DFR} = r$

DFR Model Parameters

The parameters that have been considered to implement the DFR model in MATLAB/Simulink are shown in Table 3.2.

Table. 3.2 DFR Model Parameters

Parameters	Values
Nominal Grid Frequency	50Hz
DeadBand (DB)	±0.015
Battery initial (SOC_{init})	50%
Battery charge/discharge Efficiency	97% [113], [68]
Inverter Efficiency	97% [113], [68]
Battery Power/ Energy	40MW/40MWh

Simulation Results of BESS delivering DFR service Model
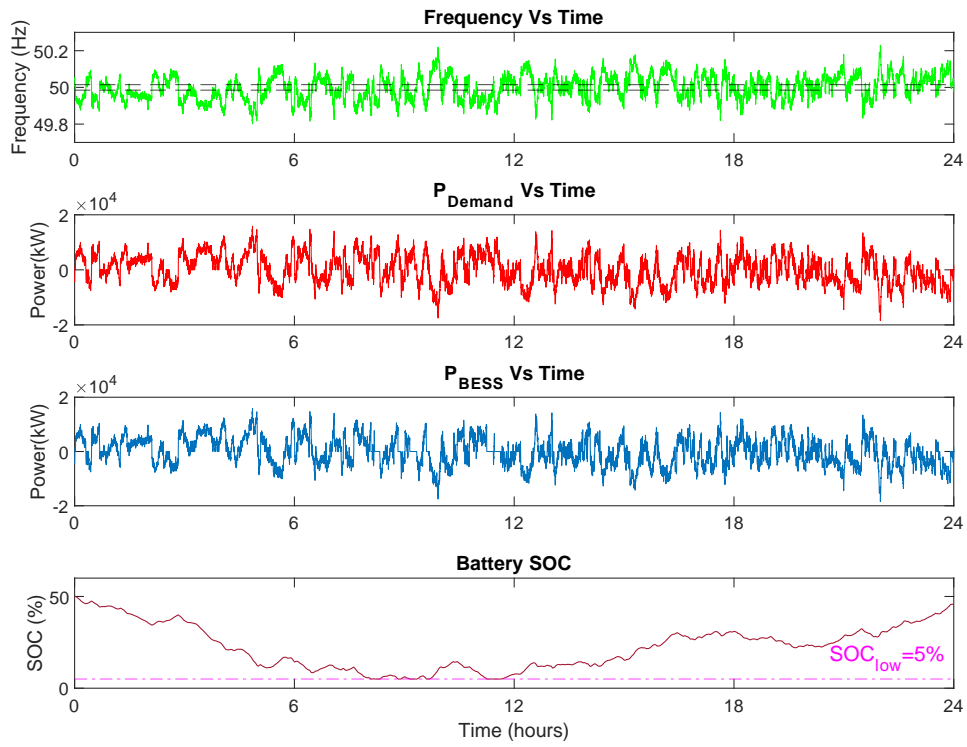
Figure. 3.8 Simulation Results of BESS delivering DFR service Model for the first day of Jun-2019 frequency data.
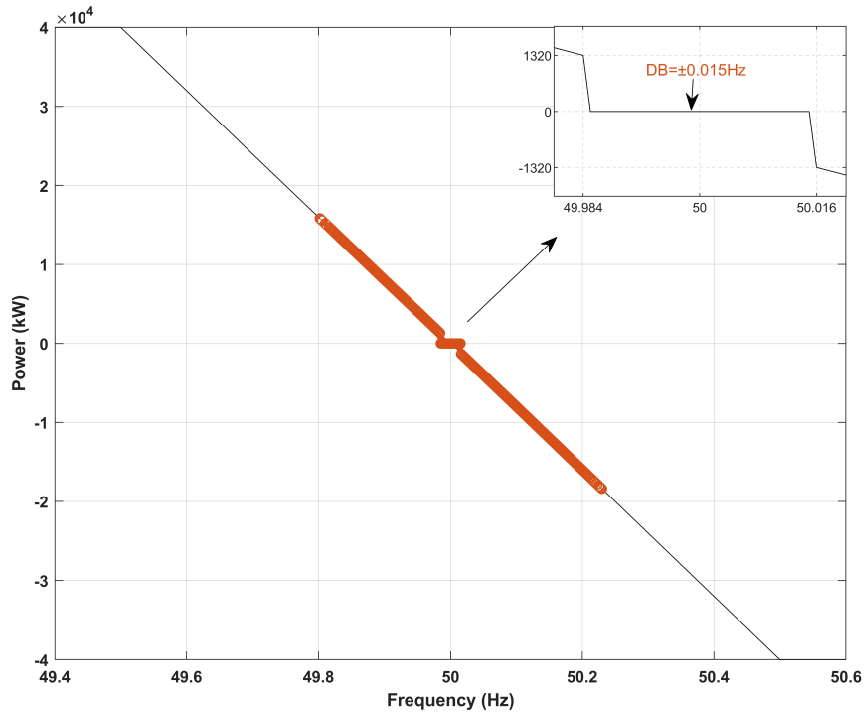
Figure. 3.9 Power vs frequency plot of measured DFR algorithm for the first day of Jun-2019 frequency data.

Figure 3.8, and Figure 3.9 illustrate the simulation results of BESS used to deliver DFR service for the first day of Jun-2019, and it a clear that P_{Demand} changes proportionally with the change in the frequency data, SOC increases (charge) when battery import power from the NG while SOC decreases (discharge) when battery export power to the NG and its limits were not breached. Moreover, P_{BESS} has been delivered according to the required service envelope in the NG specification as shown in Figure 3.4.

3.4 Dynamic Containment (DC)

Dynamic Containment is a service that rapidly responds to frequency changes, ensuring that the frequency remains within the mandated range of 50±0.5Hz in the event of an unexpected increase or decrease in demand or generation. This service is highly responsive and provides a proportional response to any frequency deviation. It is specifically intended for use after a fault has occurred and is deployed to address the need for faster-acting frequency response by the National Grid [114].

3.4.1 Dynamic Containment (DC) Control

To adhere to the NGET specifications outlined in Table 3.3, a response time is mandated to be no faster than 500ms but no later than 1 second. In this thesis, it is considered 1s. The ESS is required to continuously respond to frequency deviations from the grid by adjusting import/export power. In this service, the DB is defined as the area limited by the frequency band ± 0.015 Hz. In the DB, there is no requirement to import/export power, but there is also no opportunity to charge/discharge the ESS to manage its SOC. The high level of a block diagram of the DC service model is illustrated in Figure 3.11.

47

3.4.2 DC Service Specification

<p align="center">Table. 3.3 DC service specification model   [114]</p>

Parameter	Detail
Deadband (delivery %)	±0.015Hz (%)
Initial linear range (delivery %)	From 0.015Hz to 0.2Hz(to max of 5% at 0.2Hz)
Knee point	±0.2Hz
Second linear range (delivery %)	From 0.2Hz to 0.5Hz (to max of 100% at 0.5Hz)
Full delivery point	±0.5Hz
Speed of response	Full delivery of the required quantity (MW) in 1s (but not faster than 0.5s)

3.4.3 DC Service Envelope
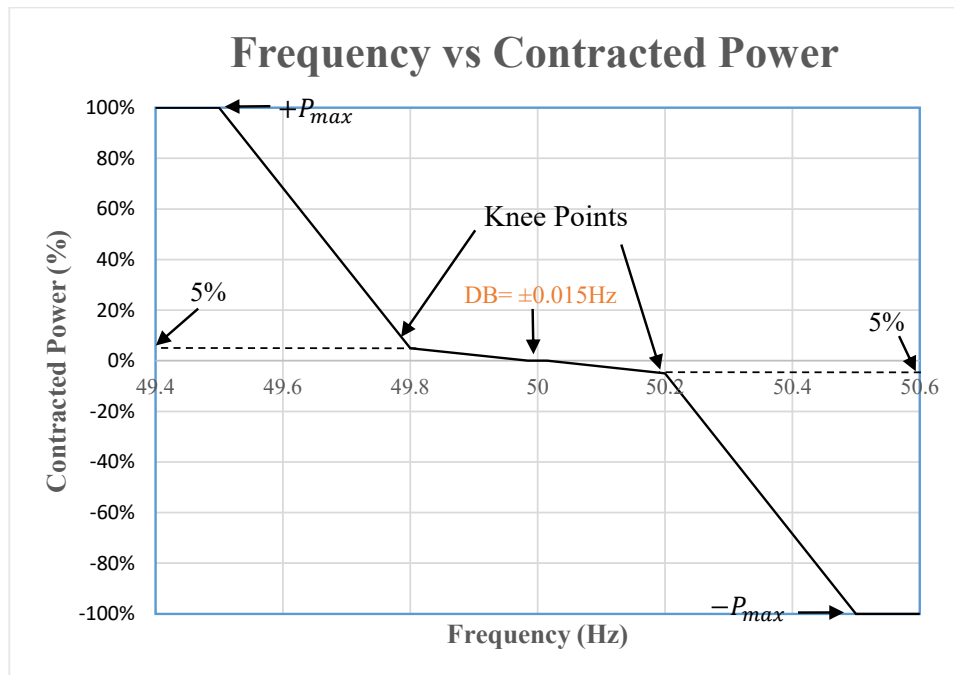
<p align="center">Figure. 3.10 Power vs frequency for DC service / 40MW profile.</p>

Figure 3.10 shows that the DC power output is responding proportionally to the change of frequency according to service specification. The power setpoints (P_{DC}) are calculated using a proper equation as shown in the last column of Table 3.4, and the BESS power management strategy implemented for DC service is as DFR service.

3.4.4 Dynamic Containment Frequency Response Service Model (DC)
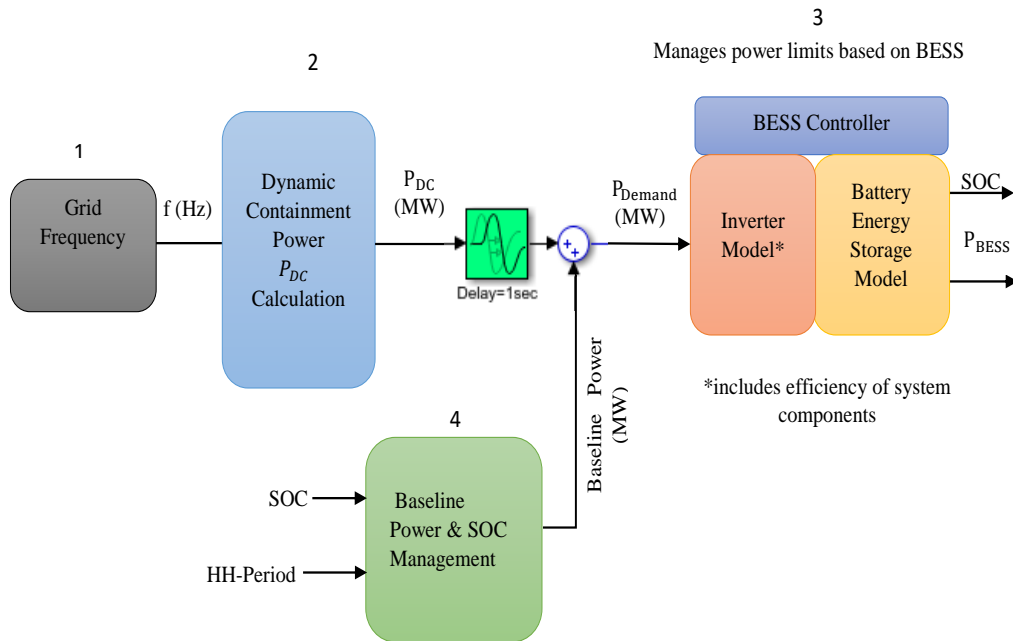
Figure. 3.11 The High Level of Block Diagram of DC service model.

Block-1

This block is described in Subsubsection 3.3.2as being used here as input to block-2.

Block-2

In this block (application block), the P_{DC} is calculated using the same method as discussed in Subsubsection 3.3.2 (Block-2), the only difference is that the DC service specifications as illustrated in Table 3.3, Subsubsection 3.4.2. The calculation P_{DC} is shown in the last column of Table 3.4. In the regard to implementation of the BESS power management strategy for DC service without submitting a baseline power has been applied as shown in Figure 3.7, Subsubsection 3.3.2.

Table. 3.4 P_{DC} & frequency set-points and calculation in the control algorithm [115]

Freq. Hz	Contracted Power, (p.u)	P_{DC}, (p.u)
A=49.5	$a = 1$	$P_{DC} = a$
B=49.8	$b = 0.05$	$P_{DC} = [(\frac{(B-f)}{(B-A)}) \times (a - b) + b]$
C=49.985	$c = 0$	$P_{DC} = 0$
D=50	$d = 0$	$P_{DC} = 0$
E=50.015	$e = 0$	$P_{DC} = 0$
F=50.2	$f = -0.05$	$P_{DC} = [(\frac{(G-f)}{(G-F)}) \times (f - g) + g]$
G=50.5	$g = -1$	$P_{DC} = g$

Block-3

This block is about the BESS block which has been discussed in Section 3.2 part-(a,b,c).

Block-4

This block represents a baseline power control algorithm that has been implemented in MATLAB / Simulink to manage SOC using baseline power for charge and discharge purposes. Figure 3.12 illustrates the baseline power management strategy implemented for the DC service model.
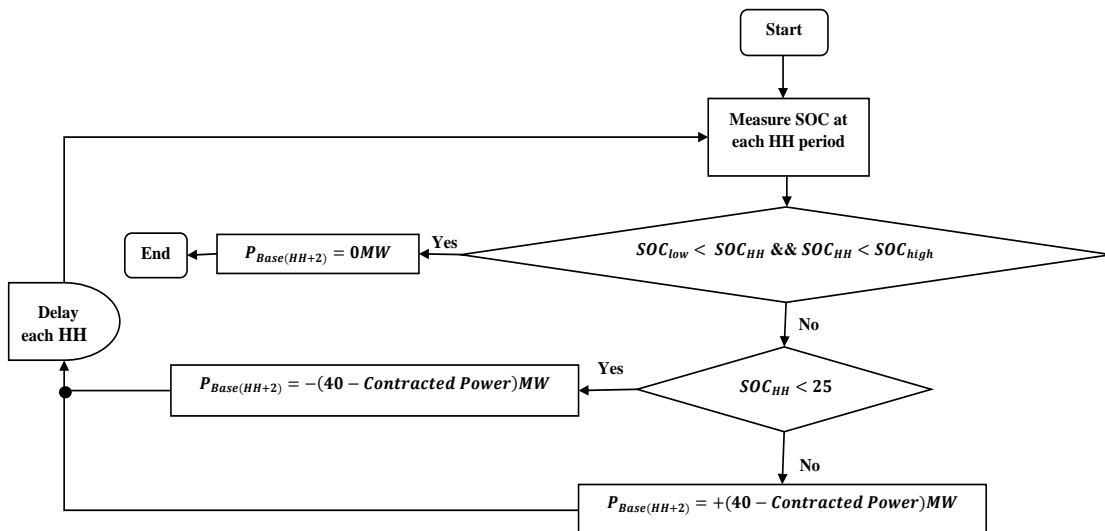
Figure. 3.12 Implemented a baseline power P_{Base} management strategy for DC service model, BESS with 40MW profile.

The inputs are battery SOC and the settlement period (HH), whereas, the output is the baseline power (P_{Base} (MW)) which will be added to P_{DC} to get P_{Demand} that will

feed to the battery throughout the inverter as shown in the block-3. According to the service specification for DC, a baseline power can be submitted to NGESO 1 hour before delivery, this baseline can be used to charge/discharge the ESS. However, this baseline is not accounted for in the contracted service power i.e. the baseline plus the contracted service power cannot exceed the power capacity of the asset [116]. For example, a 40MW ESS cannot provide a service contract power of 40MW and then utilize a baseline power of 1MW. To be able to use a 1MW baseline a reduced maximum service power of 39MW should be contracted.

DC Model Parameters

Table 3.5 presents the parameters that have been used to implement the DC service model in MATLAB/Simulink.

Table. 3.5 DC Model Parameters

Parameters	Values
Nominal Grid Frequency	50Hz
DeadBand (DB)	± 0.015Hz
Battery initial (SOC_{init})	50%
Battery charge/discharge Efficiency	97%
Inverter Efficiency	97%
Battery Power/ Energy	40MW/40MWh
Baseline power SOC setpoints (SOC_{low} & SOC_{high})	25% - 75%

Simulation Results of BESS delivering DC service Model
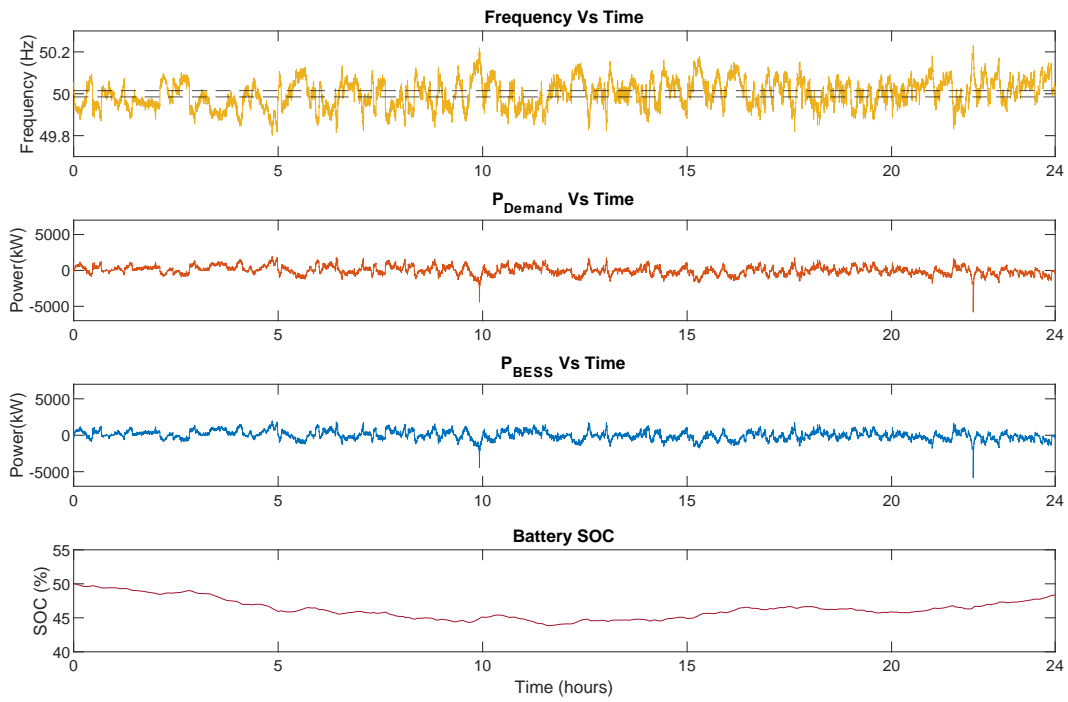
Figure. 3.13 Simulation Results of BESS delivering DC service Model without submitting a baseline Power for the first day of Jun-2019 frequency data.
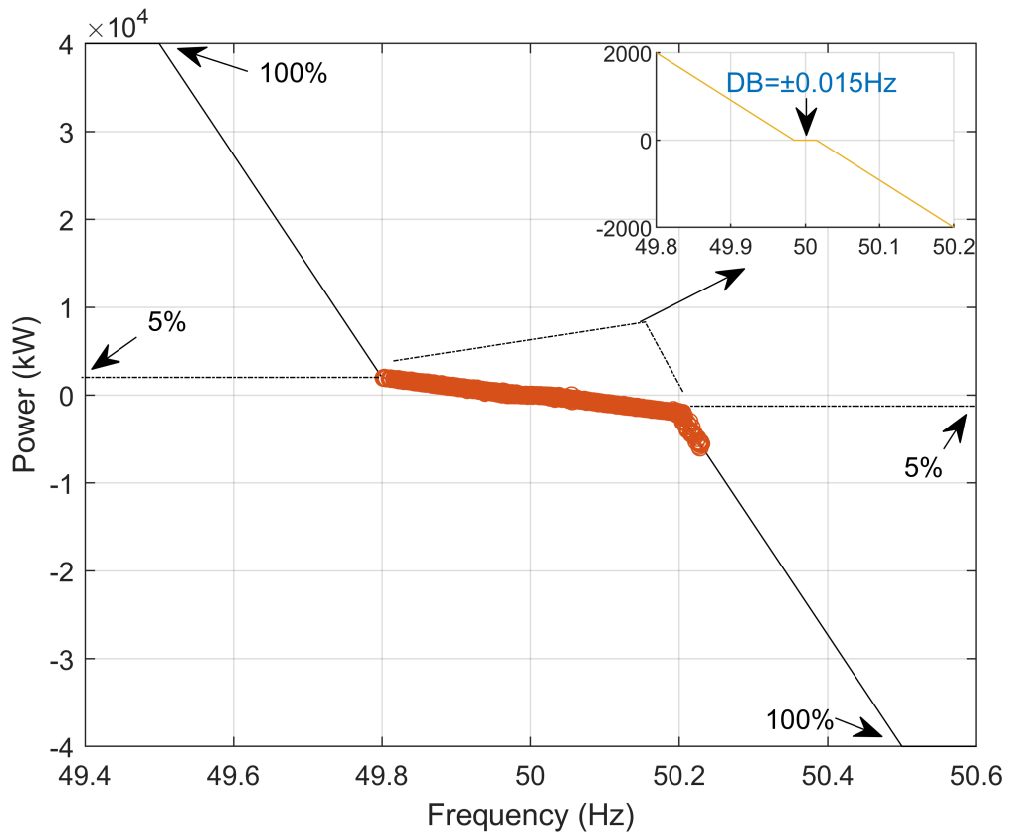
Figure. 3.14 Power vs frequency plot of measured DC algorithm for the first day of Jun-2019 frequency data.

Figure 3.13, and Figure 3.14 show the simulation results for BESS used to deliver the DC service without submitting a baseline power for the first day of Jun-2019, and it can be observed that P_{Demand} changes proportionally with the change in the frequency date and P_{BESS} was delivered according to the DC service envelope mentioned in the NG specification.

3.5 Dynamic Regulation Frequency Response Service (DR)

DR is considered a pre-fault service that is designed to slowly correct continuous but small deviations in frequency. The DR contains two service conditions; Dynamic Regulation High Frequency Response (DR-HF) and Dynamic Regulation Low Frequency Response (DR-LF). Such a service aims to continuously regulate the frequency around the target of 50Hz [117]. To comply with the NGESO specifications as shown in Table 3.6, an ESS must continuously respond to the deviation in frequency from the grid by increasing or decreasing the import/export power. In this service, the deadband (DB) is considered as the area that is limited by frequency band ±0.015Hz. For both DR-LF and DR-HF, there is no requirement to import/export power in the DB, but there is also no opportunity to charge/discharge the ESS to manage its SOC. From the edge of the DB to -0.2Hz for DR-LF or +0.2Hz for DR-HF, the demand for DR power (P_{DR}) increases linearly to (100%) of the contracted quantity. According to NGESO specifications, the actual BESS power (P_{BESS}) needs to start responding to changes in P_{DR} in 2 seconds and must deliver the full P_{DR} no later than 10 seconds [117].

3.5.1 DR Service Specification

Table. 3.6 Service specification of DR service model [117]

Parameter	Detail
Deadband (delivery %)	±0.015Hz (%)
Delivery range	±0.015Hz to ±0.2 Hz
Initial linear range (delivery %)	±0.015Hz to ±0.2 Hz (100% at ±0.2Hz)
Full delivery point	±0.2Hz
Max time to full delivery	10s
Ramp time	8s
Max ramp start	2s
Delivery duration	1h

3.5.2   DR Service Envelope
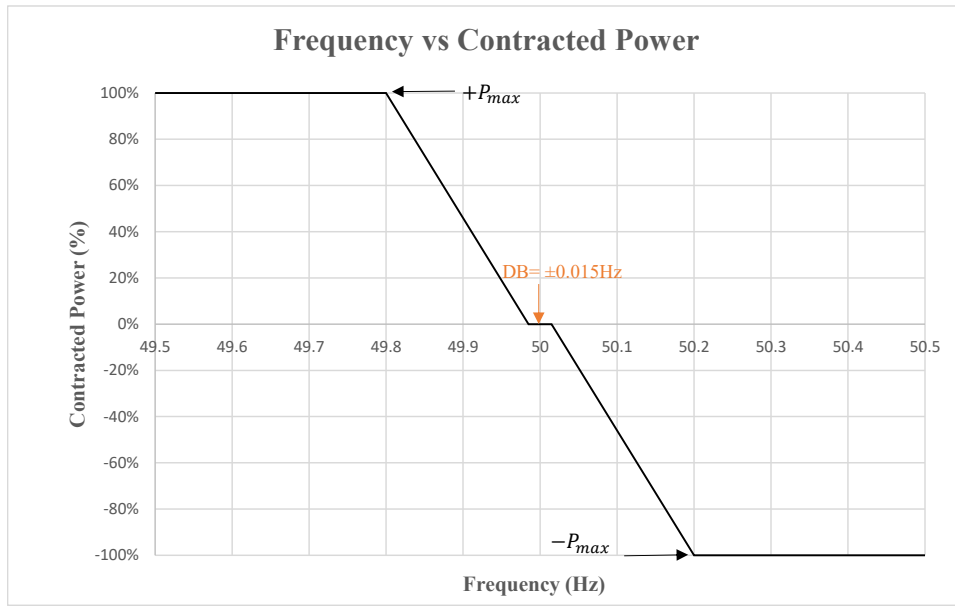
Figure. 3.15 Power vs frequency for DR-HF & DR-LF service.

Figure 3.15 illustrates the relationship between the frequency data obtained from NG and P_{DR} for stacked DR-LF and DR-HF. In this service, the assets must respond to both low- and high-frequency events by exporting and importing power.

3.5.3   Dynamic Regulation Frequency Response Service Model (DR)
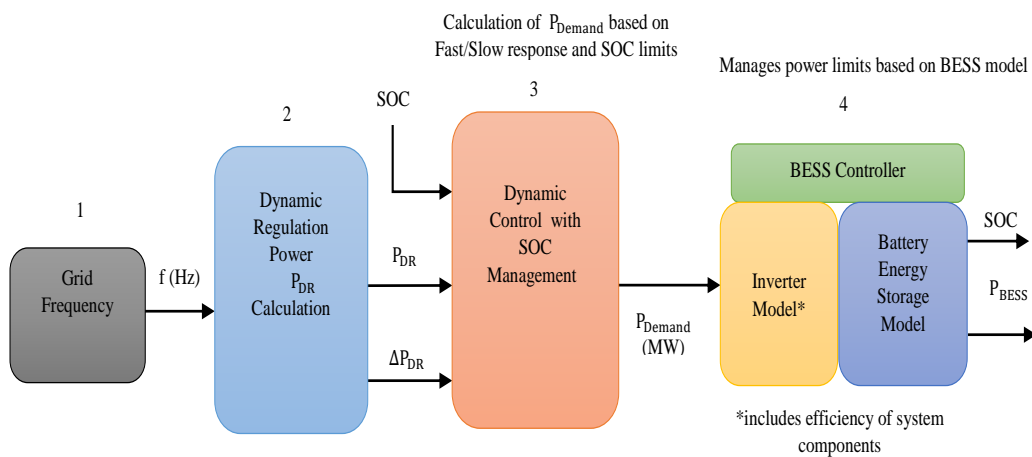
Figure. 3.16 The High Level of Block Diagram of DR service model.

Block-1

This block is described in Section 3.1 as being used here as input to block-2.

Block-2

In this block (application block), P_{DR} is calculated using the same method as discussed in Subsubsections 3.3.2 and 3.4.4 (Block-2), the only difference is the DR service specification, which will be shown in 3.6. The P_{DR} calculation is shown in the last column of Table 3.7. In the regard to implementation of the BESS power management strategy for DR service without implementing a dynamic control has been applied as shown in Subsubsection 3.3.2, Figure 3.7.

Table. 3.7 P_{DR} & frequency setpoints and calculation in the control algorithm

Freq. Hz	Contracted Power, (p.u)	P_{DR}, (p.u)
J=49.5	$j = 1$	$P_{DR} = j$
K=49.8	$k = 1$	$P_{DR} = k$
L=49.985	$l = 0$	$P_{DR} = [(\frac{(L-f)}{(L-K)}) \times (k - l) + l]$
M=50	$m = 0$	$P_{DR} = 0$
N=50.015	$n = 0$	$P_{DR} = [(\frac{(O-f)}{(O-N)}) \times (n - o) + o]$
O=50.2	$o = -1$	$P_{DR} = o$
P=50.5	$p = -1$	$P_{DR} = p$

Block-3

This block represents the dynamic control with SOC management, where the three inputs are included; SOC which is obtained from Section 3.2 (BESS bock), power calculations $P_{DR(LF\,or\,HF)}$ or for both services, and $\Delta P_{DR(LF\,or\,HF)}$ or for both services, while the output is the required P_{Demand} which is connected to the BESS block through the inverter as illustrated in Figure 3.3. Figure 3.17 and Figure 3.18 show the implementation of dynamic control of the DR service model.
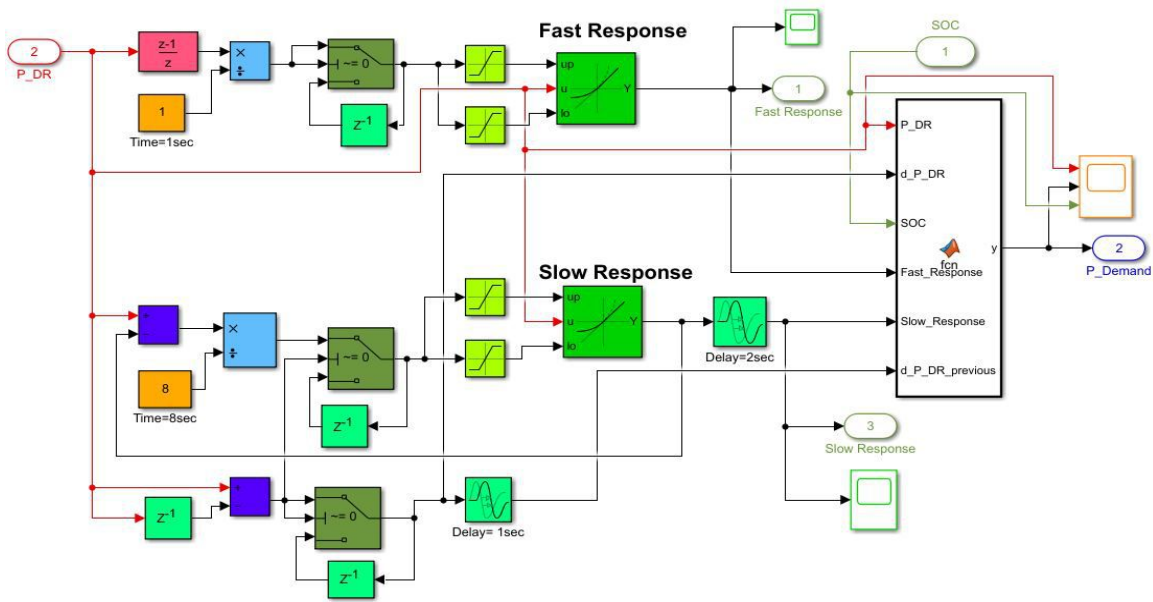
Figure. 3.17 Dynamic control of DR service model.
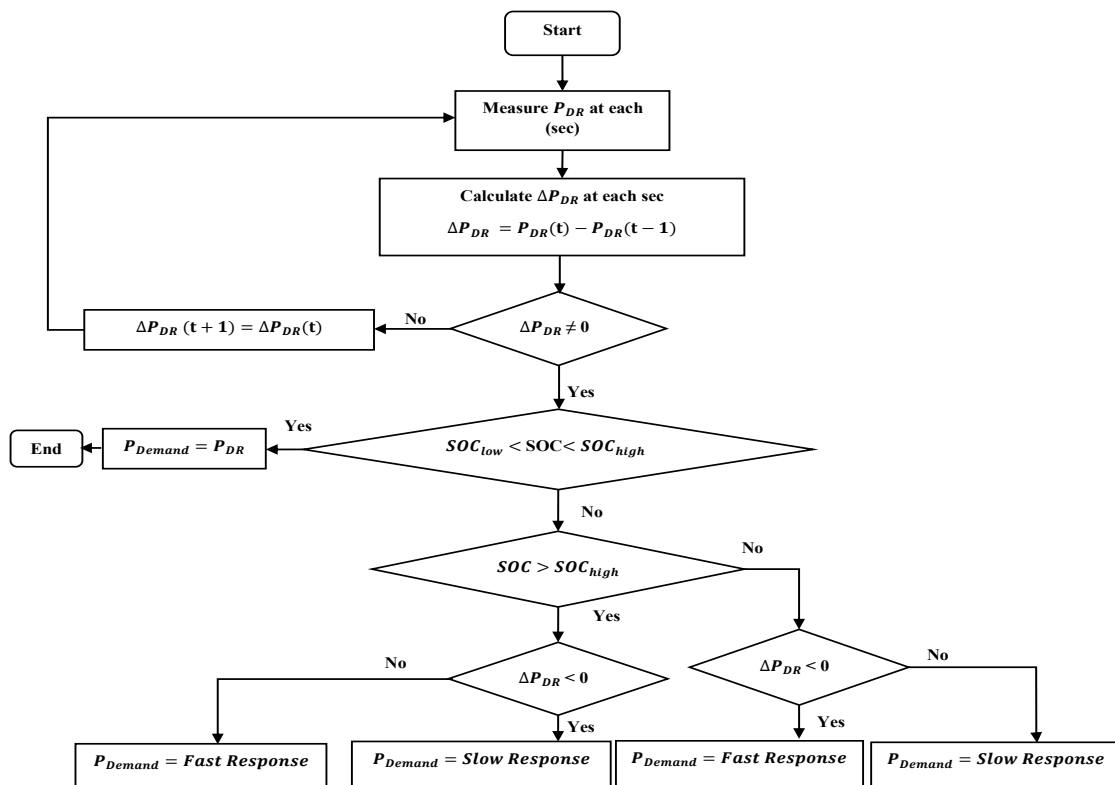
Figure. 3.18 Flow diagram of Dynamic Control Model.

As we can see from both figures 3.17 and Figure 3.18, the logarithm starts to measure P_{DR} each second and then calculates the ΔP_{DR} and this will be based on the desired SOC limitations. So, if ΔP_{DR} equal to zero then the current ΔP_{DR} will be equal to the previous ΔP_{DR}. Whereas, if ΔP_{DR} is negative or positive and SOC is in between the agreed limits, then P_{Demand} will equal the contracted power (P_{DR}). However, if the SOC is greater than the SOC$_{high}$ and ΔP_{DR} less than zero, then the slow response will be

implemented, while if ΔP_{DR} greater than zero then the fast response will be implemented and vice versa in the case where the SOC is less than SOC$_{low}$. Figure 3.18 shows how slow and fast responses have been implemented in MATLAB/Simulink. In the case of fast response, the Rate limiter dynamic block has been used to ramp P_{DR} 100%, whereas, in the case of slow response, the Rate limiter dynamic block is used to ramp P_{DR} for 12.5/p.u/sec (ramp for 8 sec) then used delay for 2 sec then full P_{Demand} will be delivered within 10 sec [117].

Block-4

This is about the BESS block which has been discussed in section 3.2 part-(a,b,c).

DR Model Parameters

Table 3.8 shows the parameters that have been used to implement the DR service with and without dynamic control in MATLAB/Simulink.

Table. 3.8 DR Model Parameters

Parameters	Values
Nominal Grid Frequency	50Hz
DeadBand (DB)	± 0.015
Battery initial (SOC$_{init}$)	50%
Battery charge/discharge Efficiency	97%
Inverter Efficiency	97%
Battery Power/ Energy	40MW/40MWh
Dynamic control SOC set-points (SOC$_{low}$ & SOC$_{high}$)	40% - 45%

Simulation Results of BESS delivering DR service Model without applying Dynamic Control for the first day of Jun-2019 frequency data
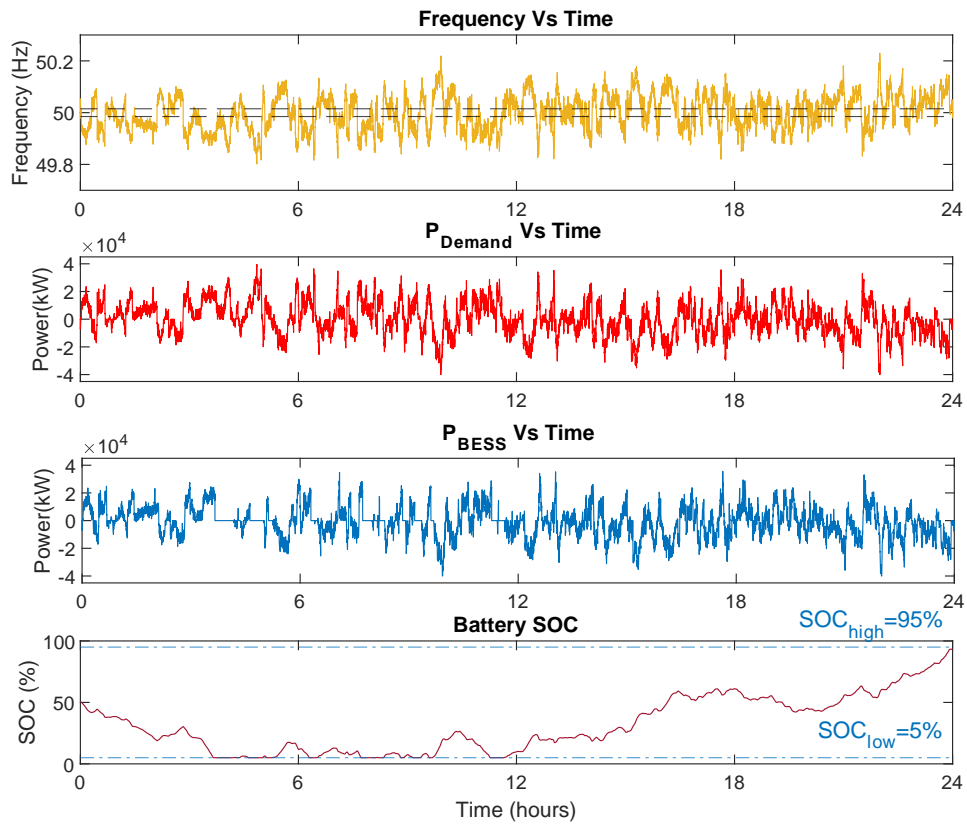
Figure. 3.19 Simulation Results of BESS delivering DR service Model without applying Dynamic Control for the first day of Jun-2019 Frequency Data.
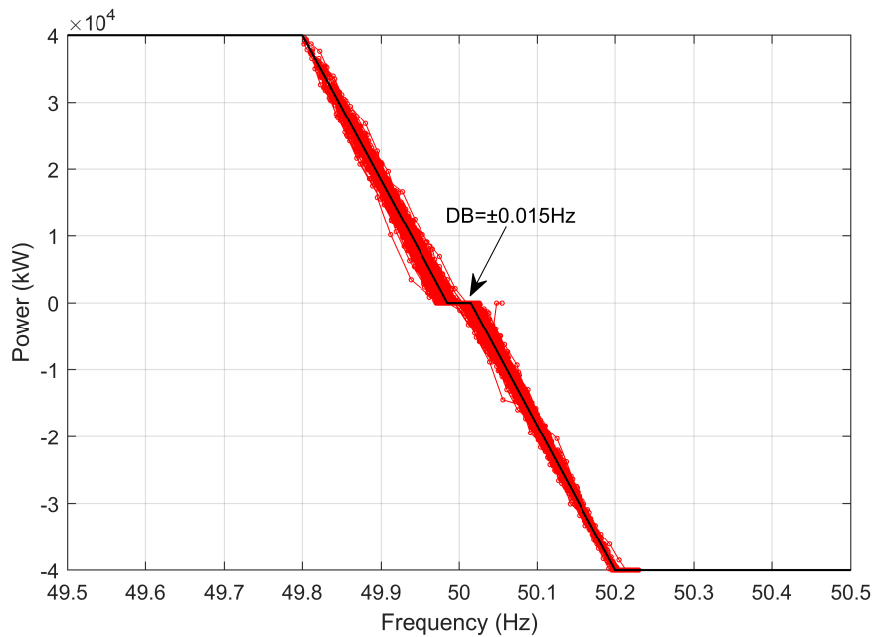
Figure. 3.20 Power vs frequency plot of measured DR algorithm without implementing a dynamic control for the first day of Jun-2019 frequency data.

Figure 3.19 and Figure 3.20 show the simulation results of BESS used to deliver DR service without implementing dynamic control for the first day of Jun-2019, and it can be noticed that the P_{Demand} varies proportionally with changes in the frequency data, while the P_{BESS} adheres to the DR service envelope specified by the NG. However, there are data points outside of this line due to the ramp rate, as it takes time for the power to return to the main envelope.

To provide further clarity, the power ramp rate describes the rate of change in power output over time. When the system experiences a rapid change in frequency, there can be a temporary power imbalance that causes power output to deviate from the main envelope. This is because the battery system takes time to respond and adjust its output to match the new frequency data. Therefore, data points outside of the main envelope can be attributed to the ramp rate of the battery system and the temporary power imbalance that occurs during a rapid frequency change.

Analysis of DFR vs DC vs DR service model

Table. 3.9 Simulation results of DFR vs DC vs DR service model without applying a SOC management for Jun-2019 frequency data/ 40MW profile

Services	Total Import Energy (MWh)	Total Export Energy (MWh)	Av.g Import Power (kW)	Avg. Export Power (kW)	Peak Export Power (kW)	Peak Import Power (kW)	Av.g SOC (%)
DFR	-52.25	47.79	-2,178.43	1,992.66	15,840	-18,400	22.33
DC	-5.36	5.39	-223.54	224.22	2,000	-5,990	46.27
DR	-106.72	78.13	-4,449.08	3,257.18	35,675.68	-40,000	31.34

3.6   Willenhall Energy Storage System (WESS)

WESS, located at Willenhall in the West Midlands, is the largest grid-tied Lithium-Titanate (LOT) system in the UK, with a capacity of 2MW/986kWh [118]. The University of Sheffield commissioned the WESS in 2015, and it consists of a Toshiba LTO battery connected to the grid through an 11kV feed located at the Willenhall Primary Substation in the UK. The decision to use LOT technology in the WESS was based on several factors, including its long cycle life, high capability of fast charge and discharge (over 10,000 charge-discharge cycles), and its operational safety and reliability, particularly in terms of low risk of fire, a hazard associated with conventional lithium-ion batteries. When high performance and extended life are required, the ESS based on Toshiba's SCiB™ is an excellent option, particularly for the supply of efficient and effective frequency regulation [119]. Figure 3.21 shows block diagram (a) and photo (b) of the WESS.
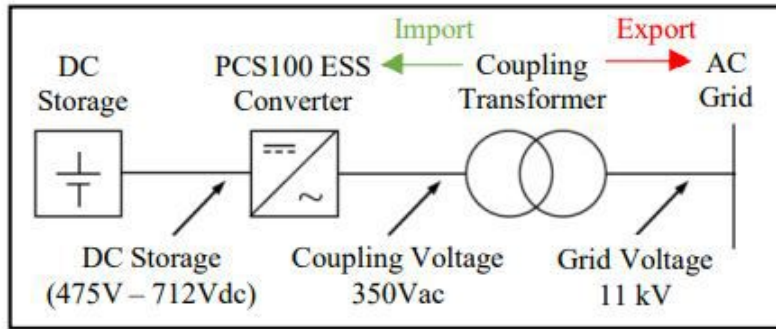
Figure. 3.21 Block diagram (a) and photo (b) of 2MW/986kWh WESS plant.

The battery storage system of the WESS consists of 40 racks connected in parallel, with each rack consisting of 22 series-connected battery modules. Each battery module comprises 24 battery cells arranged in a 2P12S configuration, resulting in a total of 21,120 cells in the DC battery, with a maximum capacity of approximately 986kWh. As depicted in Figure 3.21(a), the WESS is composed of a battery with a maximum capacity of almost 986kWh, which is connected to a PCS100 ESS Converter with a capacity of 2MW that controls the active and reactive power based on the system's requirements. The converter is then connected to a 2.1 MVA transformer that transfers power from the converter to the 11kV AC grid [120]. To facilitate communication and control between the storage and converter systems, a customized control technology, known as a bespoke control system, was developed by the University of Sheffield.

3.6.1 Validation of model against the operation of Willenhall.

WESS has been widely used for various research purposes, such as assessing frequency response services [121] provided by NGESO, model validation, SOC & SOH management, round trip energy efficiency, arbitrage, and triad avoidance. Several research papers have utilized WESS in these areas, including those represented in [122], [123], [124], [125], [126]. In this thesis, the model validation was carried out using

60

two different error calculation methods which include; Root Mean Square Error (RMSE) and Mean Absolute Percent Error (MAPE) [127]. These error methods are considered accurate when they have been used to measure modeling errors for a variety of different applications. According to [128], [129], [130], [127] these approaches have been used to compare battery metrics such as state of charge (SOC). [124] reports that for comparison of SOC using the RMSE if the value of RMSE is between 0.50% to 2.00% then the measured SOC is considered accurate. In this thesis, to enhance the model's accuracy, two validation exercises have been considered and each one has been carried out based on a different sample of SOC profiles that were provided by WESS. The SOC used here is called 'BMS' and represents the in-built battery management system reading offered by Toshiba. To improve the model's accuracy compared to the real data that are obtained from WESS, three parameters have been taken place and they include, charge efficiency, discharge efficiency, and power losses. The power losses were represented by a constant block connected to the integrator which is shown in Figure 3.1 and each time step the power losses will be subtracted from the output power $P_{Demand} - in$ which is coming from the inverter efficiency as illustrated in Figure 3.1. In addition to that, in the model, battery size has been set to 986kWh, and SOC_{init} has been set to match SOC_{init} of WESS. The two verification exercises are explained as follows;

Verification 1

In this exercise, a real power profile derived from the WESS during the same time as the SOC is presented in Figure 3.22. This profile was used as an input to the inverter block, which is in turn connected to the battery model as illustrated in Figure 3.5. The SOC obtained from the model was then compared to the SOC offered by WESS, using both RMSE and MAPE methods, as depicted in Figure 3.23. The parameters utilized in this exercise are presented in the first column of Table 3.10, and the first row indicates five steps of changes in these parameters to minimize the values of RMSE and MAPE. The results obtained are displayed in Figure 3.22.
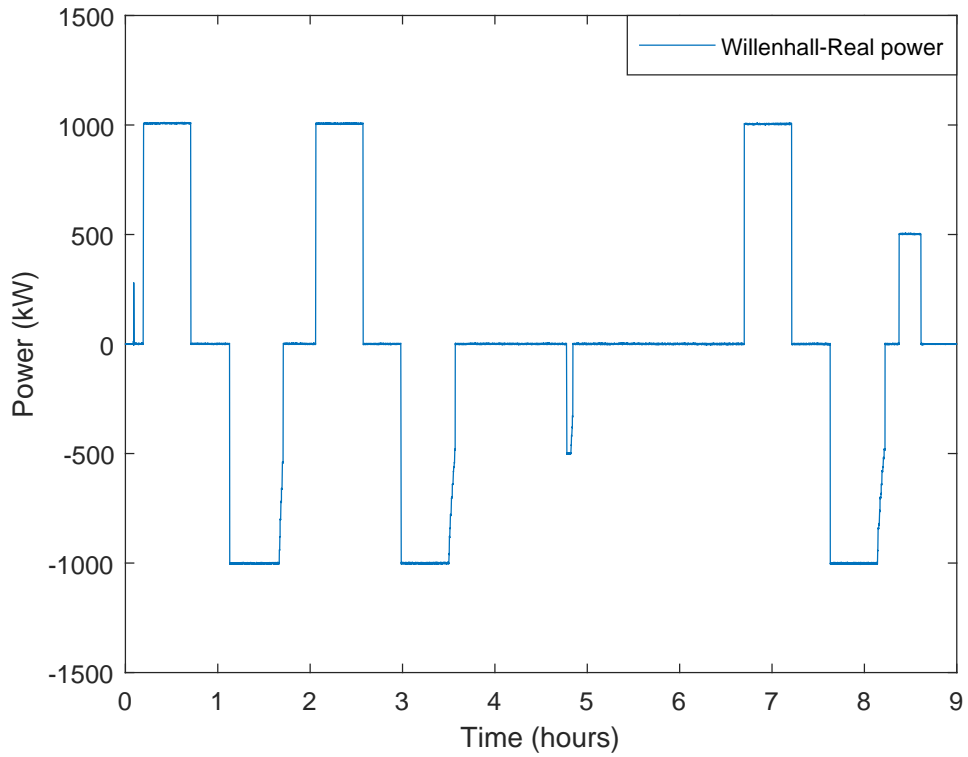
Figure. 3.22 WESS-Real power profile used to assess the performance of the MATLAB/Simulink model for 30/08/2022.

Table. 3.10 Parameter values are used to improve the accuracy of the model by minimizing both RMSE & MAPE for the model validation.

	Sim1	Sim2	Sim3	Sim4	Sim5
Charge Efficiency (%)	97	99.1	98.7	98.7	99.1
Discharge Efficiency (%)	97	98.7	99.1	99.1	98.7
Power losses (kW)	8	10	8	7	8
RMSE (%)	2.73	1.81	1.7	1.67	1.61
MAPE (%)	6.05	4.32	4.28	4.30	4.26
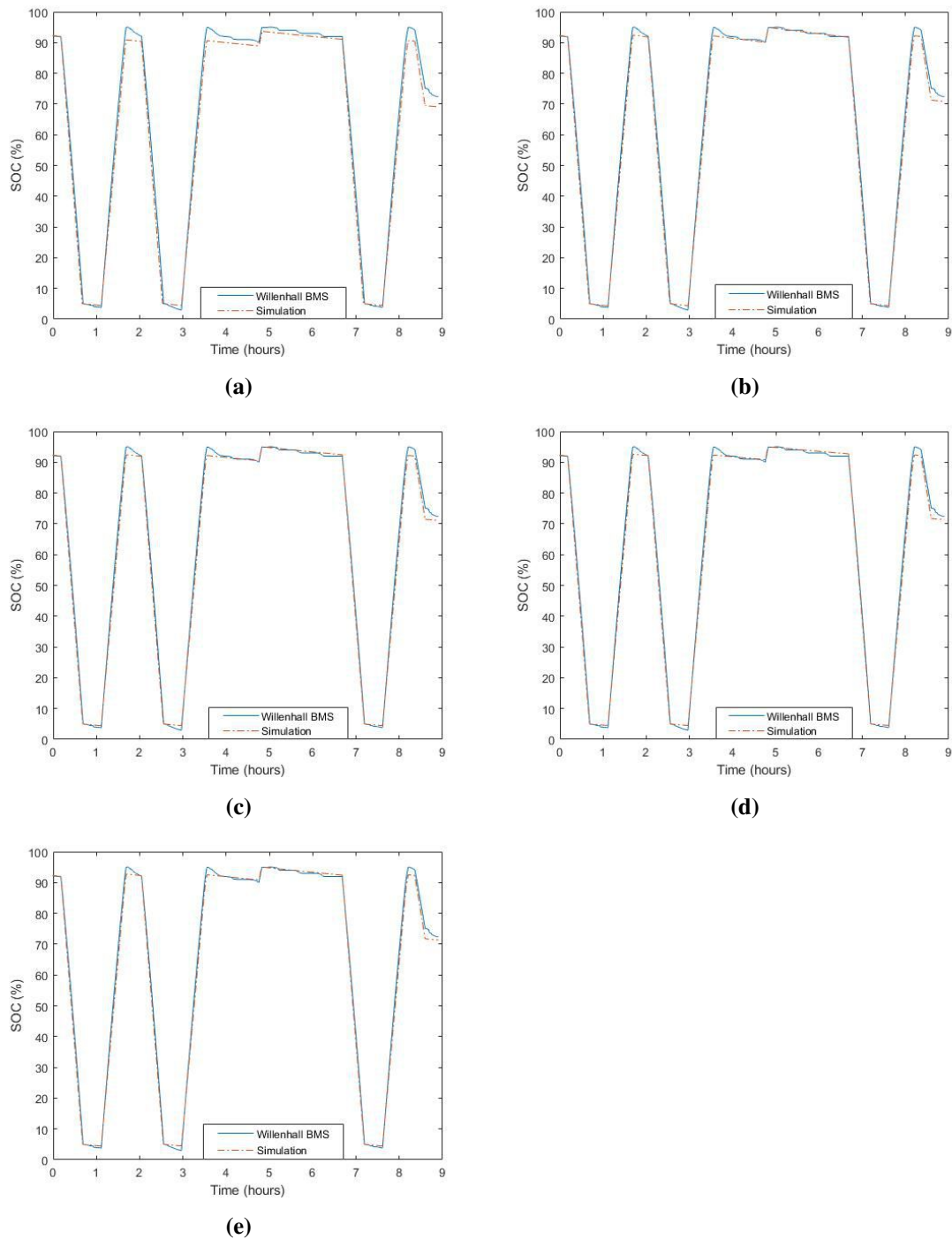
Figure. 3.23 SOC profiles for Verification 1 as the variables are modified in accordance with Table 3.10. The SOC profiles are divided into five sets, including (a) Set 1, (b) Set 2, (c) Set 3, (d) Set 4, and (e) Set 5.

Figure 3.23 illustrates a comparison between the simulated SOC results from the generic BESS model and the experimental SOC results from the last day of Aug-2022, which lasted approximately 9 hours. Table 3.10 displays the parameters used in this comparison, with the first row showing a five-step alteration in the parameters to minimize the values of RMSE & MAPE. Based on both Figure 3.23 and Table 3.10, it is evident that set (a) has the highest values of both RMSE & MAPE, which are 2.73% and 6.05%,

respectively, while set (e) has the lowest values of 1.61% and 4.26%, respectively. This suggests that sets (e) are more accurate than sets (a) to (d). Nevertheless, there is still a slight variation between the SOC obtained from the simulation and the WESS SOC. This discrepancy is due to differences in the settings of SOC limitations, as the model sets SOC_{low}=5% and SOC_{high}=95%, while WESS sets SOC_{low}=0% and SOC_{high}=100%. Additionally, the injected power profile (WESS real power) was not provided at every second.

Verification 2

In this exercise, another sample of SOC provided by WESS was used to validate the model. The real power data was extracted from WESS for an almost 26-hour period, along with the corresponding SOC periods as shown in Figure 3.24 and Figure 3.25. The parameters used in this exercise are presented in the first column of Table 3.11, and the first row indicates five steps for changing these parameters in order to minimize the values of RMSE and MAPE. The obtained results are presented in Figure 3.25.
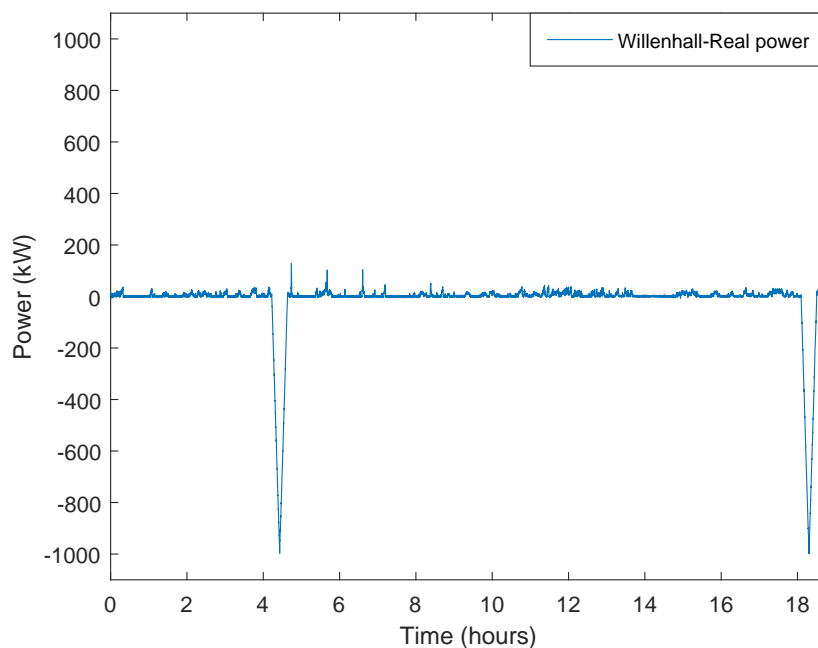
Figure. 3.24 WESS-Real power profile used to assess the performance of the MATLAB/Simulink model for a period (from 15/08/2022 to 16/08/2022).

Table. 3.11 Parameter values as varied to incrementally improve both RMSE & MAPE for the model validation

	Sim1	Sim2	Sim3	Sim4	Sim5
Charge Efficiency (%)	97	97	99.1	98.7	97
Discharge Efficiency (%)	97	97	98.7	99.1	97
Power losses (kW)	7	9	8.3	8.3	8.3
RMSE (%)	2.21	1.57	0.82	0.78	0.68
MAPE (%)	4.19	2.75	1.49	1.45	1.07
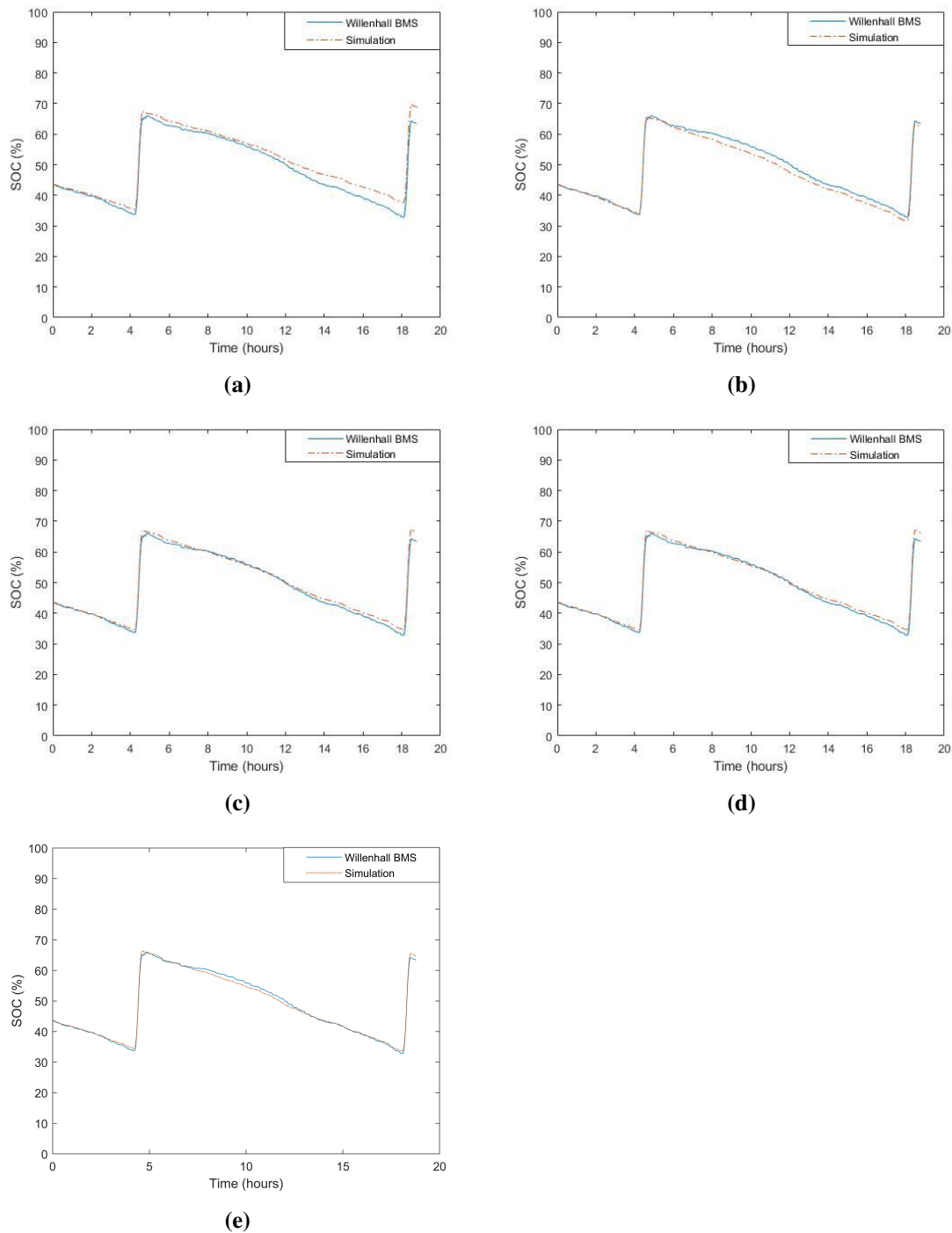
Figure. 3.25 SOC profiles for Verification 1 as the variables are modified in accordance with Table 3.11. The SOC profiles are divided into five sets, including (a) Set 1, (b) Set 2, (c) Set 3, (d) Set 4, and (e) Set 5

Figure 3.25 illustrates the SOC profiles for the first 18.77 hours of August 15, 2022, which were obtained from WESS BMS, and the simulation results for the model during this period. This figure contains five sub-figures, labeled above, where the SOC model was modified according to Table 3.11.

From both Figure 3.25 and Table 3.11, it is evident that the highest values of both RMSE and MAPE occurred in set (a), with values of 2.21% and 4.19%, respectively. The

lowest values were found in the set (e), with values of 0.68% and 1.07%, respectively. This indicates that set (e) is the most accurate value compared to all sets from (a) to (d). Therefore, when comparing validation 1 and validation 2, the lowest values for both RMSE and MAPE were found in validation 2. This was due to the SOC model hitting its limits, which are different compared to the WESS SOC, as discussed in Validation 1.

Summary

A brief summary of this chapter:

- The BESS model was developed using MATLAB/Simulink, and each sub-block was explained in terms of its construction. The model was designed to allow for rapid modifications and rearrangement to simulate other ESS applications such as flywheel, supercapacitor, etc.

- Simulation results confirm the successful delivery of frequency response services (DFR, DC & DR) in compliance with NG specifications.

- The DC service is less demanding, exhibiting significantly lower average power and energy throughput compared to DFR and DR.

- Among the services, the DR service reaches the maximum peak import power, while the DC service shows the highest average SOC.

- The model was experimentally verified against 2MW/986kWh (WESS), and based on two verification exercises, the results showed that the model presented in this thesis achieved an RMSE value of 1.61% and MAPE value of 4.26% for verification 1, while in verification 2, the model achieved an RMSE value of 0.68% and MAPE value of 1.07%. Therefore, based on these values, the model is considered accurate.

In the next chapter, a sensitivity analysis of power-to-energy ratios for ESS used to deliver DFR & DC services on the GB will be presented and discussed in detail. Lifetime analysis will be carried out based on two proposed cycle counting methods, including EFCs and CCM, which will be examined and discussed in detail using BESS to deliver DFR & DC services. Additionally, experimental degradation of DFR and DC will be carried out using 8 battery cells to deliver such services under different temperatures to assess battery capacity.

Chapter 4

Sensitivity Analysis of Power-to-Energy Ratios and Battery Lifetime for Dynamic Frequency Response Services in UK Energy Storage Systems

4.1 Introduction

In this chapter, a sensitivity analysis was carried out on the power-to-energy ratio for ESS providing frequency response services on the GB electricity network. Two services are considered; DFR and DC, with the latter being a new service introduced in Oct 2020 by the Electricity System Operator. Each service proportionally responds in power to changes in grid frequency with each service differing in the response envelope. Whilst these services are based on power, for energy-limited assets such as ESS, the ratio of power to energy has an effect on its ability to deliver the service 100% of the time. In this chapter, the availability, compliance against service terms and conditions, and equivalent cycles are considered showing that there is a significant difference between the two services. Currently, these services are delivered by battery ESS, however, it is demonstrated that the newer dynamic containment service can be effectively delivered by a higher power-to-energy ratio ESS and therefore offers opportunities for other technologies such as supercapacitors and flywheels. Moreover, two proposed counting methods which include; EFCs and CCM have been presented and discussed in detail using BESS to deliver DFR & DC service for a certain time period (Jan-2019, and the full year of 2019). Finally, experimental degradation of DFR and DC has been carried out using 8 battery cells to deliver such services under different temperatures to assess battery capacity.

4.2 Simulation Results

A. Simulation result of DC Service
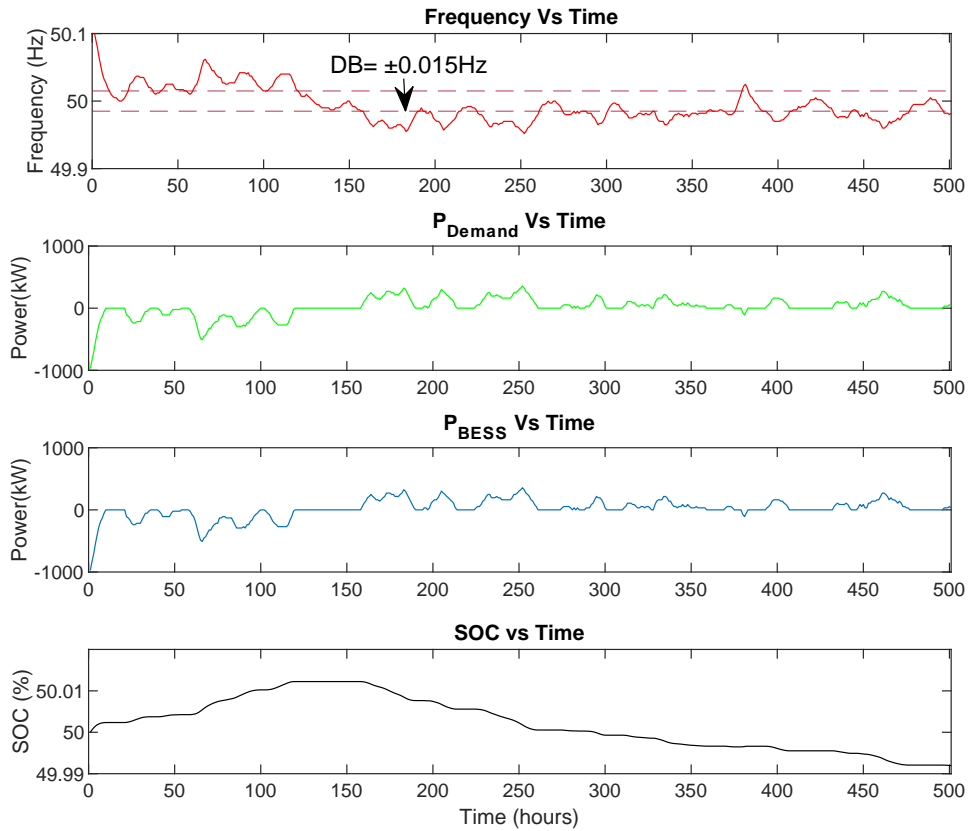
Figure. 4.1 Simulation result for BESS used to deliver **DC service** for 500s of the first day of Jan-2018 (40MW/40MWh BESS).

Figure 4.1 illustrates the relationship between frequency, P_{Demand}, P_{BESS}, and BESS SOC based on simulation results of DC service that is delivered by a 40MW/40MWh BESS for the full month of Jan-2018. It is shown that the BESS delivers continuous import/export power as per the DC service envelope which is calculated as seen in Chapter 3, Section 3.4.4, Table 3.4 and shown in Figure 3.10. The SOC increases when the BESS imports power from the grid, which means that the BESS has been charged, while the SOC decreases when the BESS exports power to the grid, which means that the BESS has been discharged.

B. Simulation result of DFR Service
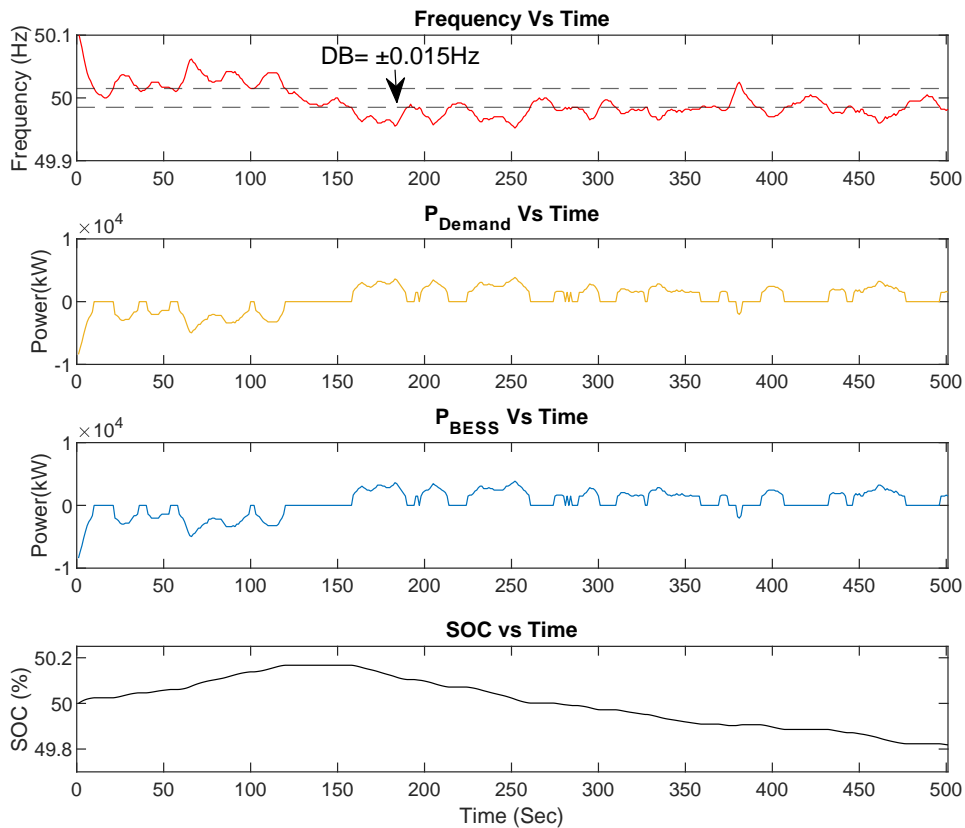
Figure. 4.2 Simulation results for BESS used to deliver **DFR service** for 500s of the first day of Jan-2018 frequency data, (40MW/40MWh BESS).

Figure 4.2 shows the relationship between frequency data, P_{Demand}, P_{BESS}, and BESS SOC for DFR service. From the above figure, it can be seen that BESS has delivered the DFR service envelope which is calculated as seen in Chapter 3, Section 3.3.2, Table 3.1 and shown in Figure 3.4 which complied with the required specifications. From the above figures and comparing the obtained results from DFR and DC, it can be noticed that, for DFR, both P_{Demand}, and P_{BESS} are almost 10 times higher than DC service, and this has led to increase in SOC values (charge/discharge) compared to DC service.

4.3 Analysis of DFR vs DC

Table. 4.1 Analysis of DFR vs DC for the full month of Jan-2018

Contracted Service Power	Total Import Energy	Total Export Energy	Avg. Import Power	Avg. Export power	Services
pu	34.27	34.54	0.046	0.046	DFR
	3.55	3.97	0.0048	0.0053	DC

Table 4.1 illustrates the simulation results of an ESS that has delivered both services (DFR & DC) for the full month of Jan-2018, and it is clear that a higher (import/export) average power and total (import/export) energy is required for delivery of DFR compared with DC services.

4.3.1 BESS Availability

In this thesis, the availability of the BESS is defined as the percentage of time that it can deliver P_{Demand} it is considered unavailable when the SOC is at its limit and therefore unable to deliver P_{Demand}. The availability of BESS can be calculated using;

$$Availability = (1 - \frac{(Non - available\,BESS\,time)}{(Total\,simulation\,time)}) \times 100 \qquad (4.1)$$

In the results 'avg. Availability' is presented, this is the average value of the BESS Availability for each month and does include the BESS being available when the P_{Demand} = 0.

4.3.2 C-rate of BESS

The C-rate (ratio of power to energy) of the ESS is calculated based on this equation;

$$C_{rate} = \frac{Power(MW)}{Capacity(MWh)} \qquad (4.2)$$

In this section, the C-rate is varied in order to consider different ESS types. The maximum demand power was fixed at 40MW, and the ESS energy capacity was varied from 400kWh to 800MWh.

Analysis of C-rate vs Availability vs EFCs

In this section, the analysis findings of average Availability, vs EFCs for BESS with different C-rates used to deliver DFR & DC separately for Jan-2018 frequency data, are shown in Table 4.2, and Figure 4.3, the EFCs are calculated using eq.2.3, Subsubsection 2.4.3, Chapter 2.

Table. 4.2 Simulation results of DFR & DC models for Jan-2018, sensitivity analysis for different C-rate vs availability vs EFCs (cycles)

C-Rate (C)	DFR		DC	
	Avg.Availability (%)	EFCs (cycles)	Avg.Availability (%)	EFCs (cycles)
100	42.39	924	71.27	239
50	51.19	694	79.36	139
20	63.87	410	87.60	64
5	79.81	141	96.33	18
4	81.96	117	96.85	14
3	84.52	92	97.95	11
2	88.22	65	99.1	7
1.5	91.22	50	99.45	6
1	93.42	34	99.88	4
0.5	95.05	17	100	2
0.25	97.11	8	100	1
0.1	99.51	3	100	0.4
0.05	100	2	100	0.2
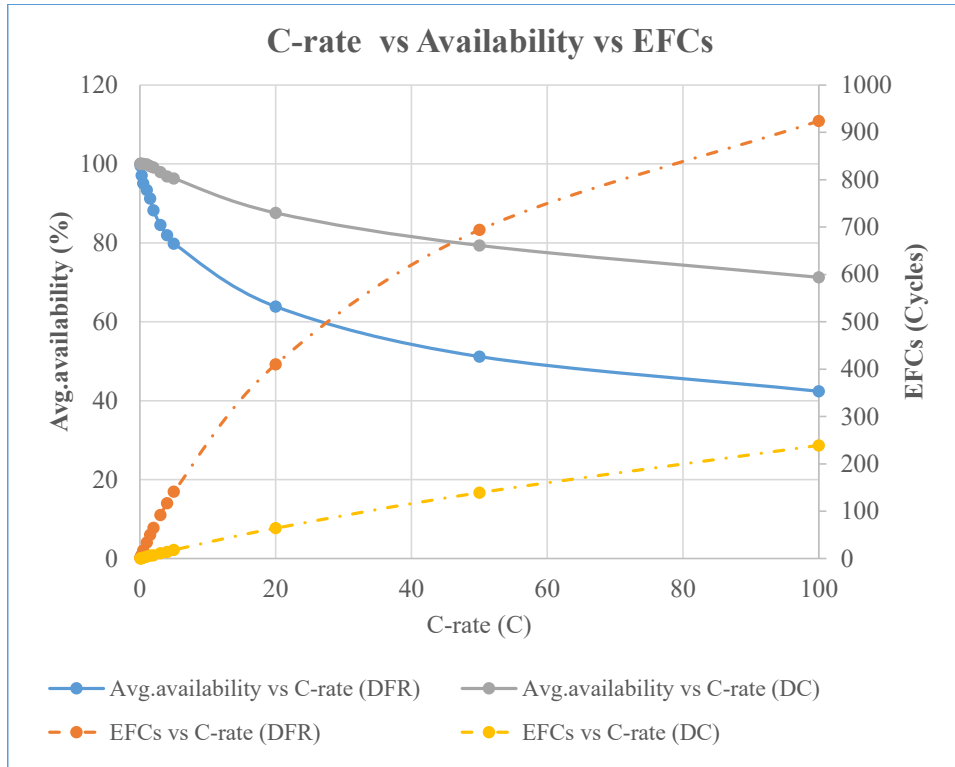
Figure. 4.3 Simulation results for both DFR &DC services for Jan-2018, C-rate vs Availability vs EFCs.

Table 4.2, and Figure 4.3, illustrate the relationship between availability, and EFCs for ESS with different C-rates whilst delivering DC or DFR services. As we can see, in both services when the C-rate increases then the number of EFCs will be increased and vice versa. For the DFR service, at 100C, the maximum number of EFCs is 924, compared to 239 cycles for the DC service. It can be seen that, in both services when the C-rate of ESS is decreasing the availability increases and vice versa. The non-linear relationship for DFR relates to the decreasing availability of the ESS as the C-rate increases, i.e. it cannot deliver power and therefore not cycle. For the DFR services, at 0.05C with a capacity of 800MWh, the availability of the ESS reaches 100% while, by increasing the C-rate up to 100C, the average availability of the ESS dropped to 42.39%. However, for DC when the C-rate of ESS has reached 100C, the average of ESS availability remains high at 71.27%. This shows that for DC, higher C-rate technologies could deliver the service whilst maintaining high availability. Both of these services are commonly delivered by 1C-rated batteries. Although there are high C-rate (>100C) batteries in development they are not commercially available at scale [131]. Therefore, for a C-rate greater than 10C then other technologies such as supercapacitor or flywheels could be utilised.

4.3.3   Noncompliance

In this section, we consider compliance against the terms and conditions of a contracted service whereby an asset must be able to sustain a power delivery at its Maximum

Export/Import Limit (MEL/MIL) for 15 minutes. We, therefore, consider compliance to be the capability of an ESS to sustain 15 minutes of the operation time which will be constrained by its current SOC and C-rate. For example, a 1C ESS will not be able to export at its MEL for 15 minutes if the SOC is lower than 25% and for import at its MIL above 75%. For the purposes of this work, we refer to the time when the SOC enters these ranges, and not already delivering sustained power, as a non-compliant period. As with availability, the total non-compliant time can be calculated as a percentage of the total simulation time. The simulation results for both DC & DFR services for the whole of Jan-2018, non-compliance vs C-rate are shown in Table 4.3, and Figure 4.4.

Table. 4.3 Simulation result of both DFR & DC Service for the full month of Jan-2018, Avg.Non-compliance vs C-rate

	DFR	DC
C-Rate (C)	**Avg. Non-compliance (%)**	**Avg. Non-compliance (%)**
2	100	100
1.5	73.62	67.41
1	48.82	9.50
0.5	32.79	0
0.25	13.21	0
0.05	0	0
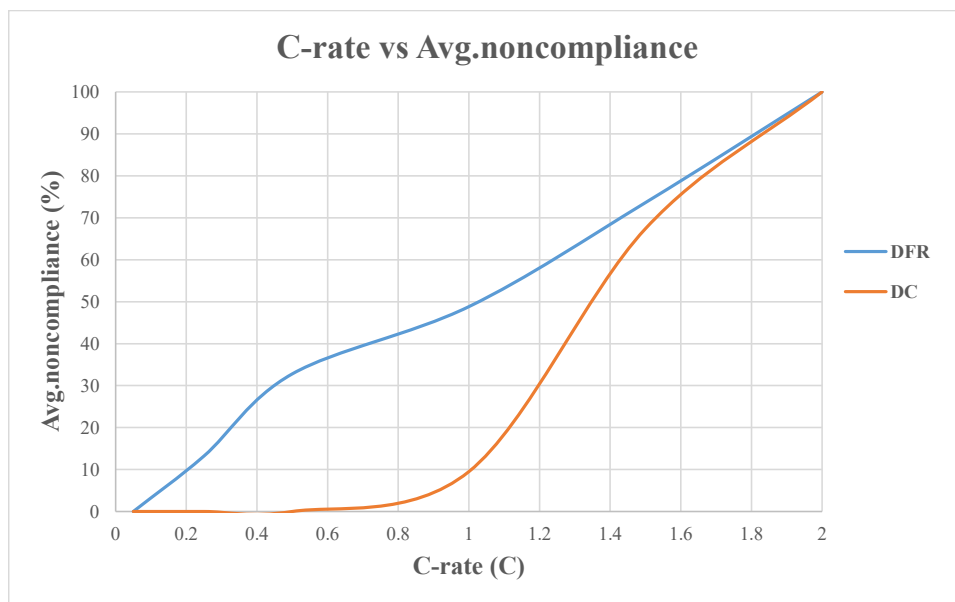
Figure. 4.4 Simulation results for both DFR & DC service for Jan-2018, C-rate vs Avg.Non-compliance

Table 4.3, and Figure 4.4 show the simulation results for average non-compliance against varying C-rates for both services. It can be seen that, in both services, the average non-compliance is increased when increasing the C-rate of the ESS and vice versa. In

both services (DC & DFR), a 2C ESS will have 100% of average non-compliance. From 0.05C to 1.5C, the average non-compliance of DFR service is higher than DC service. It is clear that for the DC service, specifically from 0.05C to 0.5C, the ESS is 100%. Whereas, in DFR service, at the same C-rate the ESS only achieves 100% compliance at a C-rate of 0.05C. This result is due to there being no SOC management, ESS assets delivering the services 24/7 to maximise revenue (service is paid £/MW/hour) and the MEL/MIL power rating is equal to that of the physical asset.

4.3.4 Baseline Power vs Availability vs Non-compliance

The control algorithm of a baseline power (P_{Base}) has been implemented in MATLAB/ Simulink as explained in Chapter3, Subsubsection 3.4.4, block 4. In this section, a baseline power is used to charge (SOC always decreasing) the ESS when the SOC falls below a defined threshold, this limit will depend on the ESS C-rate which in the example below is 1.5C, with a SOC lower charge threshold of 37.5% (15 min at MEL).

Table. 4.4 Simulation results of DC Service for the full month of Jan-2018, sensitivity analysis for 1.5C, P_{Base} vs Avg.availability vs Avg.non-compliance

Contracted Service Power (MW)	Max-Baseline Power (MW)	Avg. Availability (%)	Avg. Non-compliance (%)
40	0	99.44	67.41
39	±1	100	1.87
38	±2	100	1.18
37	±3	100	0.65
36	±4	100	0.41
35	±5	100	0.40

Table 4.4 shows the calculation of the availability and non-compliance for varying baseline charging powers for a 1.5C ESS. Note that the minimum unit of contracted power is 1MW so only integers of power are investigated. It can be seen that the average non-compliance decreases with increasing baseline power for SOC management, as would be expected. A significant improvement in availability and compliance is achieved with just 1MW of baseline power with very limited benefit beyond this. However, this 'reserving' of power for SOC management results in a lower revenue (£/MW/hour) due to the required reduction in the contracted service power.

4.4 Battery ageing and DFR & DC frequency response Services

In this section, two different types of cycle counting methodologies have been taken into account which include; CCM with algorithm shown in Subsubsection 2.4.2, Chapter

2, and EFCs which is explained and calculated using eq.2.3 in Subsubsection 2.4.3, Chapter 2. These methods are presented by considering the effects of C-rate and SOC on the battery lifetime for BESS used to deliver DFR & DC service for Jan-2019 and the whole year of 2019. The process starts by implementing these methodologies in MATLAB/Simulink to count the generic number of cycles, then these methods are improved by considering the effects of only C-rate and then the effects of SOC with C-rate on the battery lifetime. Finally, the number of cycles versus recovery discharge capacity for the Toshiba SCiB LTO battery is shown in Figure 4.5, the extracted number of cycles at each C-rate is illustrated in Figure 4.6, and for both C-rate and SOC the extracted number of cycles is presented in Table 4.5 and used for battery lifetime analysis.
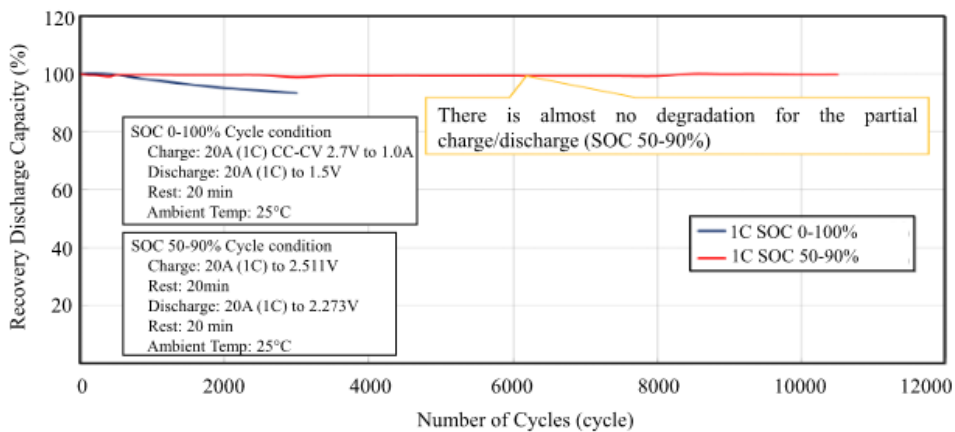
Figure. 4.5 Characteristics of Cycle Performance in Toshiba SCiB LTO Battery Cells [132]

Figure 4.5 depicts the charge/discharge life cycle of the LTO battery across varying limits of state of charge (SOC) range, namely (50-90%) and (0-100%) at 1C. The figure demonstrates that utilizing the battery within the limited SOC range of (50-90%) can result in, no degradation cycle life or an outstandingly long cycle life. Conversely, employing the battery at the full SOC range of (0-100%) leads to fast degradation and reduced cycle life compared to the SOC range of (50-90%). Therefore, it can be inferred that the highest SOC range results in the lowest cycle life.

In this thesis, when it comes to calculating LTO battery degradation, the battery life is assumed to be 12,000 cycles and it will be considered the same for each C-rates and named by (**Data1**) while calculating LTO battery degradation based on different C-rates is named by (**Data2**) and presented in Figure 4.6, and for considered both different C-rates and grouped SOC levels is shown in Table 4.5.
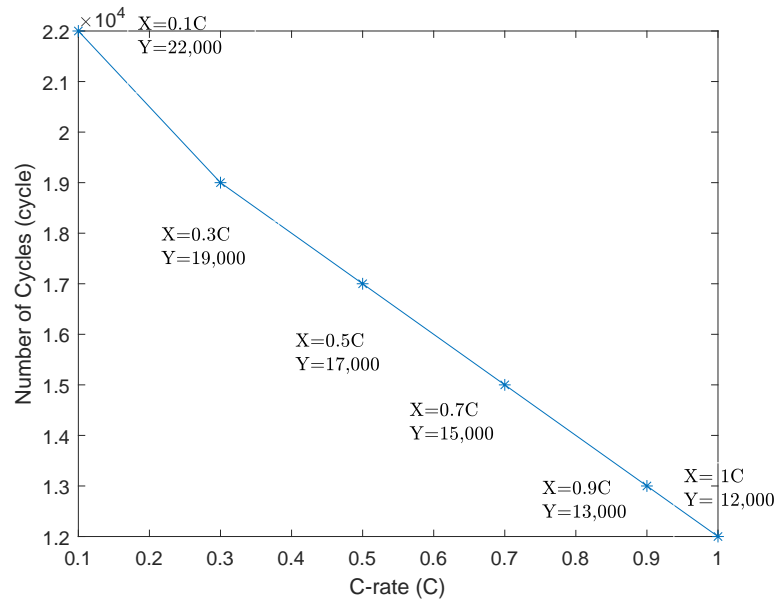
Figure. 4.6 Relationship between C-rate and Cycle Life of LTO Batteries: Analysis for Use in this thesis, (**Data2**).

Figure 4.6 illustrates the assumed number of cycles for each C-rate for the LTO battery which is named by (**Data2**). The assumption is that the number of cycles is varied for each C-rate; the higher the C-rate, the lower the number of cycles, and vice versa. In this thesis, the C-rate is grouped as (0.1C, 0.3C, and 0.5C), so the extracted number of cycles for each such C-rate is shown in Figure 4.6 and equal to 22,000, 19,000, and 17,000 cycles, respectively.

Table. 4.5 The assumed cycles data for LTO battery with different C-rates and grouped of SOC

		C-rate (C)						
		0.1	0.2	0.3	0.5	0.7	0.9	1
SOC(%)	10	26,500	24,500	23,500	21,500	19,500	17,500	16,500
	20	26,000	24,000	23,000	21,000	19,000	17,000	16,000
	30	25,500	23,500	22,500	20,500	18,500	16,500	15,500
	40	25,000	23,000	22,000	20,000	18,000	16,000	15,000
	50	24,500	22,500	21,500	19,500	17,500	15,500	14,500
	60	24,000	22,000	21,000	19,000	17,000	15,000	14,000
	70	23,500	21,500	20,500	18,500	16,500	14,500	13,500
	80	23,000	21,000	20,000	18,000	16,000	14,000	13,000
	90	22,500	20,500	19,500	17,500	15,500	13,500	12,500
	100	22,000	20,000	19,000	17,000	15,000	13,000	12,000

Table 4.5 shows the extracted number of cycles for the LTO battery at each C-rate (0.1C, 0.3C, and 0.5C) with a different SOC grouped by 10% will be used in this thesis as highlighted in a grey colour and named by (Data2), the highest C-rate with the greatest SOC, the lowest number of cycles and vice versa.

4.5 Number of Equivalent Full Cycle Method (EFCs)

In this section, the EFCs is calculated using eq.2.3 and explained in Subsubsection 2.4.3, Chapter 2. This method is used herein to demonstrate the subjected number of full cycles for BESS used to deliver DFR & DC services using real grid frequency data for the full month of Jan-2019, and the whole year-2019 [114].

4.5.1 Simulation Results of DFR Service Model for Jan-2019 Frequency data
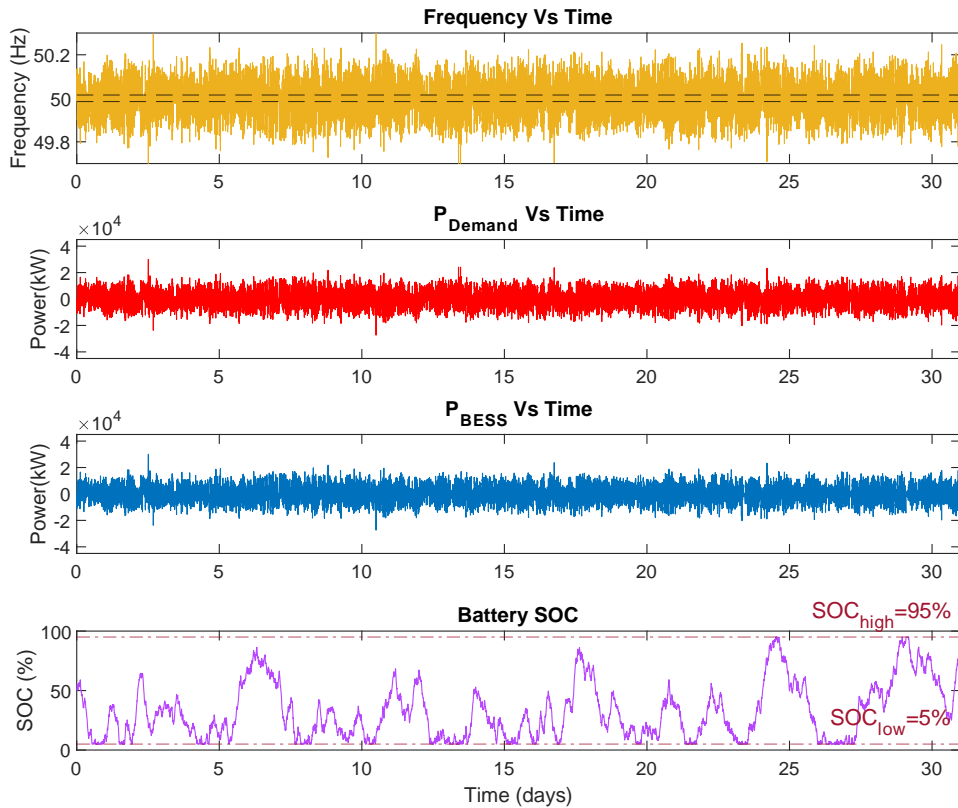
Figure. 4.7 Simulation results of DFR service for the whole of Jan-2019 frequency data.

4.5.2 Simulation results of DC service model without submitting a P_{Base} for the whole of Jan-2019 frequency data
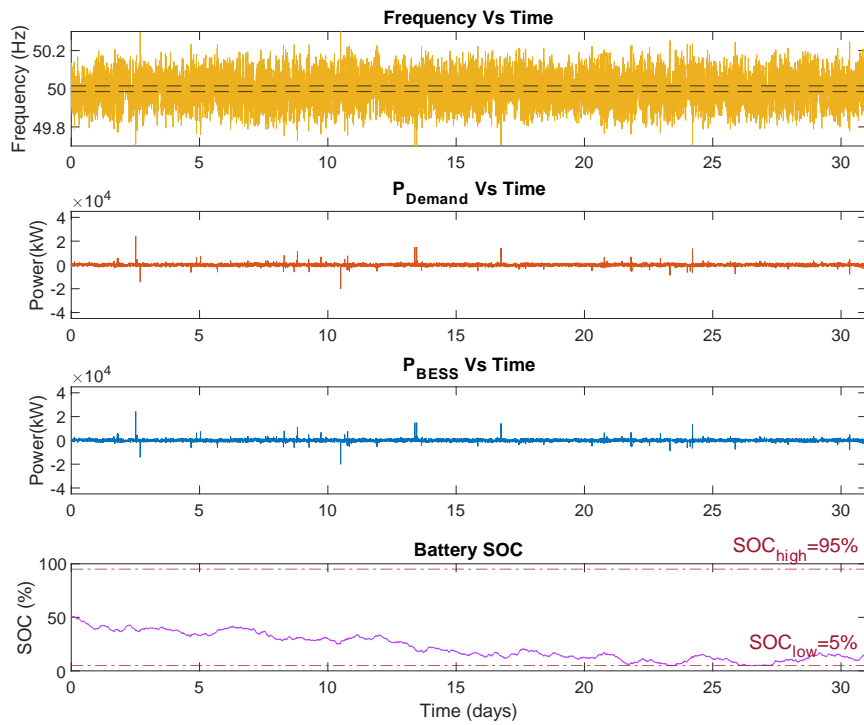
Figure. 4.8 Simulation Results of DC Service without Submitting a P_{Base} for Jan-2019 frequency data.
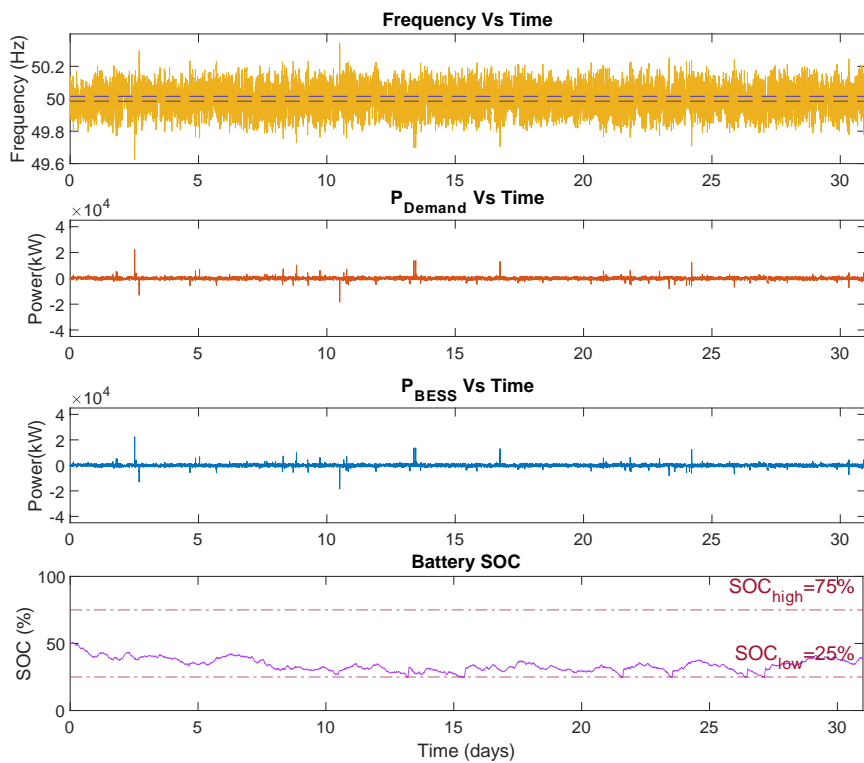
Figure. 4.9 Simulation results of BESS used to deliver DC service with submitting a $P_{Base}(\pm 3MW)$ for Jan-2019.

Figure 4.8, and Figure 4.9 present the simulation results for BESS used to deliver DC service without P_{Base}, and with submitting $\pm3MW$ P_{Base} for Jan-2019, and it can be seen that these figures show the difference between using P_{Base} and that comparing the SOC shows that the P_{Base} doesn't hit the SOC$_{lower}$ limit, and this is because of the P_{Base} is used to keep battery SOC in between the desired limits (25% to 75%) while increasing the battery availability.

In this thesis, once the total energy throughput is obtained from the simulation results of BESS-delivered DFR & DC services then using eq.2.3 in Subsubsection 2.4.3, Chapter 2 in order to calculate the generic number of cycles, then use the manufacturer cycling (12,000 cycles for LTO battery) and use eq.2.4, to calculate the battery degradation rate with the results shown in Table 4.6.

Table. 4.6 The findings regarding the number of full cycles achieved by EFCs and the degradation rate were obtained using the Miner Rule's Method for an LTO battery that had undergone 12,000 cycles(manufacturer cycling) used to deliver DFR & DC service for the **whole year of 2019** frequency data, 40MWh profile

Services	Baseline Power (MW)	Total Import Energy (MWh)	Total Export Energy (MWh)	Total no of Cycles (cycle)	LTO battery degradation (%)
DFR	0	-17,789.19	15,807.78	419.96	3.499
DC	0	-1,846.95	1,820.42	45.84	0.382
	±1	-1,927.28	1,798.04	46.57	0.388
	±2	-1,906.14	1,772.48	45.98	0.383
	±3	-1,862.37	1,730.28	44.92	0.374

4.5.3 The effects of C-rate on battery Degradation

In this section, the EFCs counting method that is calculated using eq.2.3 which is shown in Subsubsection 2.4.3, Chapter 2 has been improved by considering the effects of C-rate on the battery lifetime analysis.
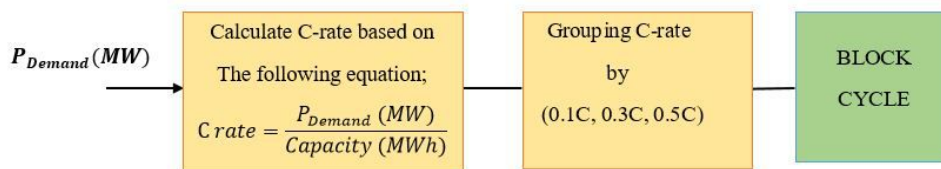
Figure. 4.10 Scheme of EFCs considering battery C-rate.

Figure 4.10 represents the scheme of EFCs counting methods that are used to calculate a number of equivalent full cycles that have been obtained by grouping different C-rates as (0.1C, 0.3C, 0.5C). The C-rate is calculated based on P_{Demand} that is obtained from the simulation frequency response service over a period of time and then divided by the battery size which is herein (40MW) using the equation shown in the first block of Figure

4.10. In the next step, the obtained C-rate is measured second by second grouped by (0.1C, 0.3C, 0.5C) in order to calculate the number of equivalent full cycles at each range of C-rate. In the last step, the approximated number of cycles which are represented by the last block in Figure 4.10 called (BLOCK CYCLE) is calculated using eq.2.3 which is shown in Subsubsection 2.4.3, Chapter 2. To calculate the battery degradation rate by considering the only effect of C-rate on the battery lifetime use the following equation;

$$\text{Battery Degradation at each C}_{rate} \ (\%) = \frac{\text{Number of cycles at each C}_{rate}}{\text{Maximum Number of cycles}} \times 100 \quad (4.3)$$

Simulation results of the EFCs with the effects of C-rate on Battery Lifetime used to deliver both DFR & DC services for Jan-2019 frequency data

In this section, the proposed EFCs counting method was used to quantify the number of full cycles for BESS with different C-rate values used to deliver DFR and DC services separately for Jan-2019. To calculate LTO battery degradation, the assumed number of cycles for each C-rate has been used as (Data1) which about the number of cycles is constant for each C-rate, and (Data2) which is presented in Figure 4.6, then used eq.(4.3). The obtained results are shown below in Tables [4.8 - 4.12].

Table. 4.7 The number of cycles and degradation results obtained from the EFCs counting method based on different C-rates for BESS used to deliver DFR service for Jan-2019 frequency data

C-rate	Total Import Energy (MWh)	Total Export Energy (MWh)	No of Cycles (cycle)	LTO battery degradation (%)
C≤ 0.1	-154.78	121.21	3.449	0.0157
0.1C< C ≤ 0.3C	-729.29	657.49	17.335	0.0912
0.3C<C ≤ 0.5C	-65.59	71.69	1.716	0.0101

Table. 4.8 The number of cycles and degradation results obtained from the EFCs counting method based on different C-rates for BESS used to deliver DC service without submitting P_{Base} for Jan-2019 frequency data

C-rate	Total Import Energy (MWh)	Total Export Energy (MWh)	No of Cycles (cycle)	LTO battery degradation (%)
C≤ 0.1	-94.88	99.10	2.42479	0.01102
0.1C< C ≤ 0.3C	-1.03	1.29	0.02916	0.000153
0.3C< C ≤ 0.5C	-0.84	0.49	0.01673	0.000098

Table. 4.9 The number of cycles and degradation results obtained from the EFCs counting method based on different C-rates for BESS used to deliver DC service with submitting a $P_{Base}(\pm$ 1MW) for Jan-2019 frequency data

C-rate	Total Import Energy (MWh)	Total Export Energy (MWh)	No of Cycles (cycle)	LTO battery degradation (%)
C$\leq$ 0.1	-104.99	100.54	2.56913	0.011678
0.1C< C $\leq$ 0.3C	-1.03	1.24	0.028375	0.00015
0.3C<C $\leq$ 0.5C	-0.78	0.47	0.015625	0.0.000092

Table. 4.10 The number of cycles and degradation results obtained from the EFCs counting method based on different C-rates for BESS used to deliver DC service with submitting a $P_{Base}(\pm$ 2MW) for Jan-2019 frequency data

C-rate	Total Import Energy (MWh)	Total Export Energy (MWh)	No of Cycles (cycle)	LTO battery degradation (%)
C$\leq$ 0.1	-104.27	99.60	2.5485	0.011584
0.1C< C $\leq$ 0.3C	-0.95	1.25	0.0275	0.000145
0.3C<C $\leq$ 0.5C	-0.74	0.42	0.0145	0.000085

Table. 4.11 The number of cycles and degradation results obtained from the EFCs counting method based on different C-rates for BESS used to deliver DC service with submitting a P_{Base} ($\pm$ 3MW) for Jan-2019 frequency data

C-rate	Total Import Energy (MWh)	Total Export Energy (MWh)	No of Cycles (cycle)	LTO battery degradation (%)
C$\leq$ 0.1	-101.84	96.75	2.30975	0.010498
0.1C< C $\leq$ 0.3C	-1.26	1.24	0.03125	0.000165
0.3C<C $\leq$ 0.5C	-0.69	0.36	0.013125	0.000077

From Table 4.7, it can be seen that the highest number of cycles that are obtained from applied EFCs on BESS used to deliver DFR service with only considered C-rate was ~17.335 cycles and occurred at 0.1<C≤0.3, with a degradation rate equates to almost 0.091%, while the lowest number of cycles was almost 1.716 cycles at C-rate ranged (0.3<C≤0.5) with a lower degradation rate equates to approximately 0.0101%. This means that BESS used to deliver the DFR service operates mainly between 0.1C and 0.3C, and rarely operates at 0.3<C≤0.5. Therefore, BESS spends most of its time operating in the C-rate range (0.1<C≤0.3), however, the degradation rates should be considered at this region.

Table 4.8, Table 4.9, Table 4.10, and Table 4.11 illustrate the number of cycles and

degradation rates obtained from implementing EFCs counting method for BESS used to deliver DC service with and without submitting a different P_{Base} values for the whole of Jan-2019 with only considering the effects of C-rate on the battery lifetime. It is clear that, at 0.1C or less, the EFCs of BESS used to deliver DC service with and without submitting a P_{Base} was the highest value compared to other C-rate ranges, the value for DC without a baseline power was almost 2.425 cycles with a degradation rate equate to $\sim$0.01102% while the number of cycles for DC service with submitting a different baseline power for charge/ discharge purposes which include; ($\pm$1MW, $\pm$2MW, $\pm$3MW) was almost 2.569, 2.549, and 2.309cycles, with the degradation rate equates to 0.011678%, 0.011584%, and 0.010498%, respectively. Whereas, the lowest values of EFCs for all DC cases were in the C-rate region between 0.3C to 0.5C and they are 0.017, 0.016, 0.015, and 0.013 respectively, with a very small degradation rate almost equates to almost zero. This means that BESS spends most of its time operating at C$\leq$0.1, and rarely operates at 0.3$<$C$\leq$0.5. The main reason behind the EFCs for BESS with C$\leq$0.1 used to deliver DC service without submitting a baseline power is slightly lowest compared to DC with submitting a P_{Base} ($\pm$1MW, $\pm$2MW) is because the baseline power is used to charge/ discharge the battery when SOC falls below or exceeds the agreed limits; (SOC$_{lower}$=25, & SOC$_{upper}$=75%), respectively, and this has led to an increase in the energy throughput which will increase the value of EFCs. However, at the same C-rate, the EFCs for BESS used to deliver DC service by submitting a P_{Base} ($\pm$3MW) was the lowest value compared to all cases and this is because of the contracted power and energy throughput are significantly decreased compared to other cases of DC service which made the EFCs with the less value, therefore, the less value of P_{Base} the more energy throughput as well as more EFCs and vice versa. In contrast, at C-rate ranges (0.1$<$C$\leq$0.3), the EFCs of BESS used to deliver DC service without submitting a baseline power was slightly higher compared to DC with submitting a baseline power.

4.5.4 The effects of both C-rate & SOC on battery Degradation

In this section, the proposed EFCs counting method has improved by considering the effects of both C-rate & SOC on battery lifetime. The scheme of such a method is shown in Figure 4.11.
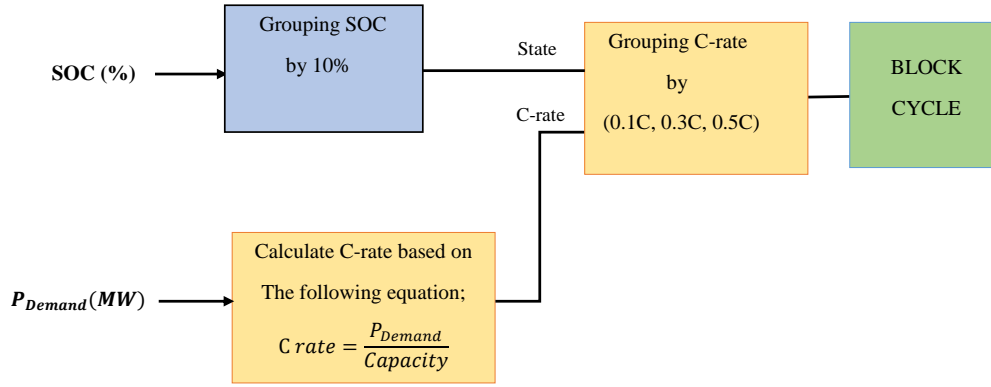
Figure. 4.11 Scheme of EFCs considering C-rate & SOC

Figure 4.11 shows the scheme of the EFCs counting method used to calculate the number of equivalent full cycles by considering both C-rate & SOC. The methodology is similar to as shown in Figure 4.10 and the only difference is that, adding SOC data that has been obtained from the simulation of DFR & DC service for Jan-2019 frequency data. The C-rate was grouped by (0.1C, 0.3C, 0.5C) while SOC was grouped by (10%, 20%, 30%, 40%, 50%, 60%, 70%, 80%, 90%) in order to calculate the number of equivalent full cycles at each range of C-rate and SOC. Once the number of cycles is obtained then the battery degradation rate for considering both C-rate and SOC can be calculated using eq.4.4;

$$Battery\ Degradation\ at\ each\ C_{rate},\ for\ each\ SOC\ (\%)$$
$$= \frac{No\ of\ cycles\ at\ each\ C\ for\ each\ SOC}{Maximum\ No\ of\ cycles} \times 100 \quad (4.4)$$

Simulation results of the EFCs considering both C-rate & SOC Effects on Battery Lifetime for both DFR & DC services for Jan-2019 frequency data

In this section, the proposed EFCs counting method used to calculate the number of full cycles by considering the effects of both C-rate & SOC for BESS used to deliver DFR and DC services separately for Jan-2019. To calculate LTO battery degradation rate, the assumed number of cycles with SOC ranges as shown in Table 4.5, and use eq.4.4 with the results shown in the below tables;

Table. 4.12 Number of cycles obtained from the (EFCs) based on different C-rates and grouped of SOC battery used to deliver DFR service for Jan-2019 frequency data

		C-rate (C)								
		C ≤ 0.1			0.1<C ≤ 0.3			0.3<C ≤ 0.5		
		Total Imp. Energy (MWh)	Total Exp. Energy (MWh)	No.of Cycles (Cycle)	Total Imp. Energy (MWh)	Total Exp. Energy (MWh)	No.of Cycles (Cycle)	Total Imp. Energy (MWh)	Total Exp. Energy (MWh)	No.of Cycles (Cycle)
SOC(%)	≤ 10	-30.86	15.46	0.5789	-85.99	84.21	2.13	-5.07	9.61	0.183
	10-20	-22.03	27.83	0.6233	-147.05	124.53	3.39	-17.15	15.75	0.411
	20-30	-22.72	20.47	0.5399	-122.53	108.37	3.21	-10.01	12.19	0.277
	30-40	-25.62	19.78	0.5675	-121.54	110.41	2.99	-8.55	11.35	0.248
	40-50	-17.81	14.72	0.4066	-76.91	70.64	1.84	-6.78	6.89	0.171
	50-60	-16.50	7.76	0.3032	-63.79	65.16	1.61	-8.69	4.52	0.165
	60-70	-9.16	10.32	0.2434	-53.29	43.95	1.22	-5.47	3.43	0.111
	70-80	-8.23	6.55	0.1848	-39.30	32.29	0.89	-3.21	6.15	0.117
	80-90	-4.59	1.47	0.0757	-16.71	16.82	0.42	-1.24	1.96	0.040
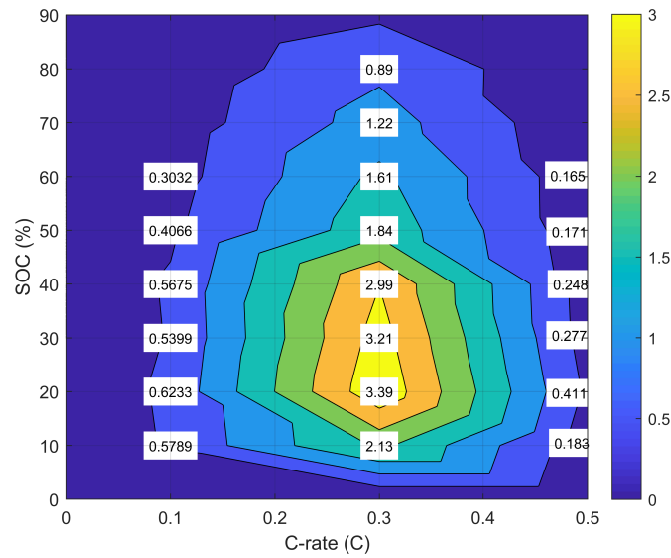
Figure. 4.12 Simulation results of the EFCs based on different C-rate for each grouped SOC for DFR model for Jan-2019. (Maximum scale is 3.39 cycles)

85

Table. 4.13 Degradation results obtained from the EFCs based on different C-rate values and grouped SOC battery delivering DFR service for Jan-2019 frequency data

		C-rate (C)		
		C$\leq$ 0.1	0.1<C$\leq$ 0.3	0.3<C$\leq$ 0.5
SOC(%)	$\leq$ 10	0.00219	0.009064	0.000851
	10 - 20	0.002397	0.01474	0.00196
	20 - 30	0.00212	0.01427	0.00135
	30 - 40	0.00227	0.01359	0.00124
	40 - 50	0.00166	0.00856	0.00088
	50 - 60	0.00126	0.00767	0.00087
	60 - 70	0.00104	0.00595	0.0006
	70 - 80	0.00080	0.00445	0.00065
	80 - 90	0.00034	0.00215	0.00023

Total of LTO battery degradation rate = 0.103152%

Table 4.12, Figure 4.12, and Table 4.13 show the simulation results of the EFCs and degradation rates by considering the effects of both C-rate and SOC on the battery lifetime delivering DFR service for the whole of Jan-2019. It is clear that BESS mostly operated at (0.1<C$\leq$0.3) for SOC range ($\leq$10% - 40%), and it's subjected to the greatest number of full cycles at the same C-rate for SOC range (10% - 20%) with the value equating to almost 3.39 cycles and caused a degradation rate equating to ~0.01474%, and this means that the battery spends most of its operation time in this region. Therefore, the degradation rates should be considered in such regions. At both C-rate ranges (C$\leq$0.1, and 0.3<C$\leq$0.5) for all SOC ranges, the number of cycles is less than one Cycle which means that the battery is rarely operating in such regions, however, the battery at 0.3<C$\leq$0.5 with will be degraded faster than at $\leq$ 0.1C.

86

Table. 4.14 Simulation results of total energy export/import and number of cycles obtained from the (EFCs) counting the method based on different C-rate values and groups of SOC batteries used to deliver DC service without submitting a P_{Base} for Jan-2019 frequency data

		C-rate (C)								
		C≤ 0.1			0.1<C ≤ 0.3			0.3<C ≤ 0.5		
		Total Imp. Energy (MWh)	Total Exp. Energy (MWh)	No.of Cycles (Cycle)	Total Imp. Energy (MWh)	Total Exp. Energy (MWh)	No.of Cycles (Cycle)	Total Imp. Energy (MWh)	Total Exp. Energy (MWh)	No.of Cycles (Cycle)
SOC(%)	≤ 10	-13.36	12.08	0.318	-0.22	0.07	0.0037	0	0	0
	10-20	-40.06	37.73	0.972	-0.19	0.56	0.0095	0	0.27	0.0034
	20-30	-11.01	14.08	0.314	-0.16	0.29	0.0056	-0.76	0.17	0.0116
	30-40	-24.15	25.62	0.622	-0.46	0.37	0.0104	-0.08	0.06	0.0017
	40-50	-5.62	8.96	0.183	0	0	0	0	0	0
	50-60	-0.69	0.64	0.017	0	0	0	0	0	0
	60-70	0	0	0	0	0	0	0	0	0
	70-80	0	0	0	0	0	0	0	0	0
	80-90	0	0	0	0	0	0	0	0	0

Figure. 4.13 Simulation results of the EFCs based on different C-rate for each grouped SOC for DC model without submitting a P_{Base} for Jan-2019. (Maximum scale is 0.972 cycles)

Table. 4.15 Degradation results obtained from the EFCs under different C-rates and grouped SOC battery delivering DC service model without submitting a P_{Base} for Jan-2019 frequency data

		C-rate (C)		
		C≤ 0.1	0.1<C≤ 0.3	0.3<C≤ 0.5
SOC(%)	≤ 10	0.0012	0.0000157	0
	10 - 20	0.003739	0.0000413	0.0000162
	20 - 30	0.0012314	0.0000249	0.0000566
	30 - 40	0.002488	0.0000473	0.0000085
	40 - 50	0.000747	0	0
	50 - 60	0.000071	0	0
	60 - 70	0	0	0
	70 - 80	0	0	0
	80 - 90	0	0	0

Total of LTO battery degradation rate = 0.009687%

Table. 4.16 Simulation results of total energy export/import and number of cycles obtained from the (EFCs) counting the method based on different C-rates and groups of SOC batteries used to deliver DC service with submitting a baseline power(±3MW) for Jan-2019 frequency data

		C-rate (C)								
		C≤ 0.1			0.1<C≤ 0.3			0.3<C≤ 0.5		
		Total Imp. Energy (MWh)	Total Exp. Energy (MWh)	No.of Cycles (Cycle)	Total Imp. Energy (MWh)	Total Exp. Energy (MWh)	No.of Cycles (Cycle)	Total Imp. Energy (MWh)	Total Exp. Energy (MWh)	No.of Cycles (Cycle)
SOC(%)	≤ 10	0	0	0	0	0	0	0	0	0
	10-20	0	0	0	0	0	0	0	0	0
	20-30	-24.50	22.93	0.59289	-0.45	0.21	0.00833	-0.65	0.18	0.01038
	30-40	-67.50	61.03	1.60663	-0.81	1.03	0.02299	-0.05	0.17	0.00282
	40-50	-9.21	12.21	0.26770	0	0	0	0	0	0
	50-60	-0.64	0.59	0.01533	0	0	0	0	0	0
	60-70	0	0	0	0	0	0	0	0	0
	70-80	0	0	0	0	0	0	0	0	0
	80-90	0	0	0	0	0	0	0	0	0

Figure. 4.14 Simulation results of the EFCs based on different C-rate for each grouped SOC for DC model with submitting a baseline power($\pm$3MW) for Jan-2019. (Maximum scale is ~ 1.6 cycles)

Table. 4.17 Degradation results obtained from the EFCs under different C-rate values and grouped SOC battery delivering DC service model with submitting a P_{Base} ($\pm$3MW) for Jan-2019 frequency data

		C-rate (C)		
		C$\leq$ 0.1	0.1<C$\leq$ 0.3	0.3<C$\leq$ 0.5
SOC(%)	$\leq$ 10	0	0	0
	10 - 20	0	0	0
	20 - 30	0.002325	0.000037	0.0000506
	30 - 40	0.006427	0.000105	0.000014
	40 - 50	0.001093	0	0
	50 - 60	0.0000639	0	0
	60 - 70	0	0	0
	70 - 80	0	0	0
	80 - 90	0	0	0

Total of LTO battery degradation rate = 0.010116%

Table 4.14, Figure 4.13, and 4.15 show the simulation results for the EFCs counting method applied to BESS used to deliver DC service without submitting a baseline power for the whole of Jan-2019 with considering the effects of both C-rate & SOC on the battery lifetime. It can be noticed that the battery was subjected to the highest number of cycles at $C \leq 0.1$ for the SOC range ($\leq$10% - 20%) with ~ 0.972 Cycle, and the

degradation rate equates to almost 0.003739%. The second greatest number of cycles was at the same C-rate for (30% - 40%) SOC range with $\sim$ 0.622 cycles and with 0.002488% degradation rate. The third and fourth highest number of cycles have occurred at the same C-rate for $\leq$10% SOC, and for (30% - 40%) SOC range with the values equating to approximately 0.318, and 0.3184 cycles, and with 0.00219%, and 0.00227 % degradation rate, respectively. This means that the battery operates most of its lifetime at $C \leq 0.1$ for SOC range from $\leq$10% - 40%, however, the degradation rates should be considered in this range. Moreover, at a C-rate range (0.3C - 0.5C), and for SOC ranges from $\leq$10% - 40 %, the number of cycles is very small compared to $C \leq 0.1$, and the degradation rate is almost equal to zero. From Table 4.16, Figure 4.14, and Table 4.17, it is clear that the highest number of cycles that were obtained from EFCs for BESS used to deliver DC service for the whole Jan-2019 with submitting $\pm$3MW of P_{Base} has occurred at the same region as for no submitting a baseline, but for (30% - 40%) SOC range with $\sim$1.607 Cycle, and with degradation rate equating to almost 0.006427%. The second highest EFCs were at the same C-rate but for (20% - 30%) SOC range with $\sim$ 0.593 Cycle, and with a degradation rate equate to approximately 0.002325%. Additionally, at the same C-rate, the third highest EFCs were obtained for the (40% - 50%) SOC range with the value equating to around 0.268 cycles and 0.001093% degradation rate. This means that BESS used to deliver DC service with submitting a baseline power operates most of its lifetime at $\leq 0.1C$ for 20% SOC - 50% SOC, however, it should be considered the degradation rates in such regions. Additionally, at all C-rates regions (from 0.1C to 0.5C), for $\leq 10\%$ SOC - 20% SOC, the battery did not operate in such regions therefore, the number of cycles equates to zero and this is because the submitted baselines power was based on SOC limitations as discussed in Chapter 3, Subsection 3.4.4 which means that the baseline power will keep SOC at the agreed limits. For example, if SOC is below SOC$_{lower}$= 25%, the power will be set to zero. Moreover, for DC service with and without submitting a baseline power at $\leq 0.1C$ for 60% SOC - 90% SOC, and 0.3< C $\leq$0.5 for 40% SOC - 90% SOC the EFCs equates to zero, which means that the battery rarely operates in these regions for delivering DC service.

4.5.5 Fast CCM

In this thesis, another method used to calculate micro charge-discharge cycles is called CCM which is implemented in the MATLAB/Simulink base on the flow chart shown in Figure 2.7, Section 2.4.2, Chapter 2. In this section, the proposed CCM is used to calculate partial charge-discharge full cycles based on the SOC profile that is obtained from BESS used to deliver DFR & DC services using real grid frequency data for the full month of Jan-2019, and the whole year-2019. The simulation results of CCM are shown below;

A. Simulation results of CCM for BESS used to deliver DFR service for Jan-2019 frequency data
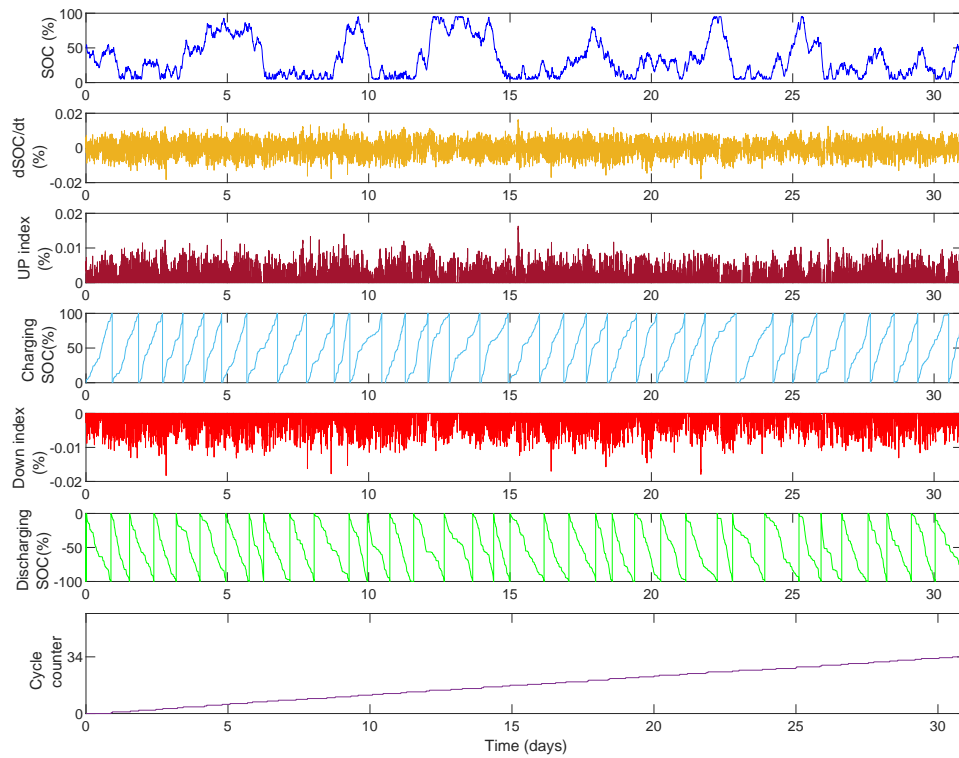
Figure. 4.15 The operation principles of the proposed CCM based on SOC profile obtained from the simulation results of BESS used to deliver DFR service for Jan-2019 frequency data.

B. Simulation results of CCM for BESS used to deliver DC service with and without submitting a baseline power for Jan-2019 frequency data
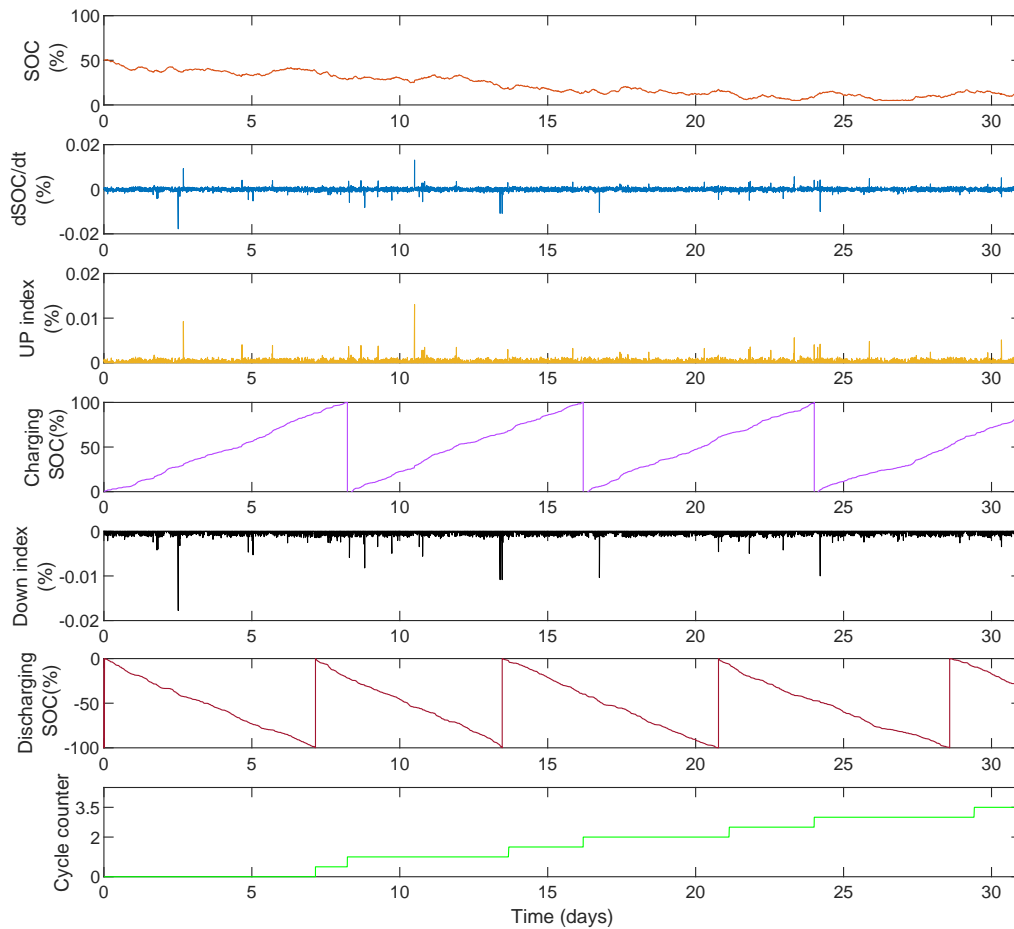
Figure. 4.16 The operation principles of the proposed CCM based on SOC profile that has been obtained from the simulation results of BESS used to deliver DC service without submitting a baseline power for Jan-2019 frequency data.
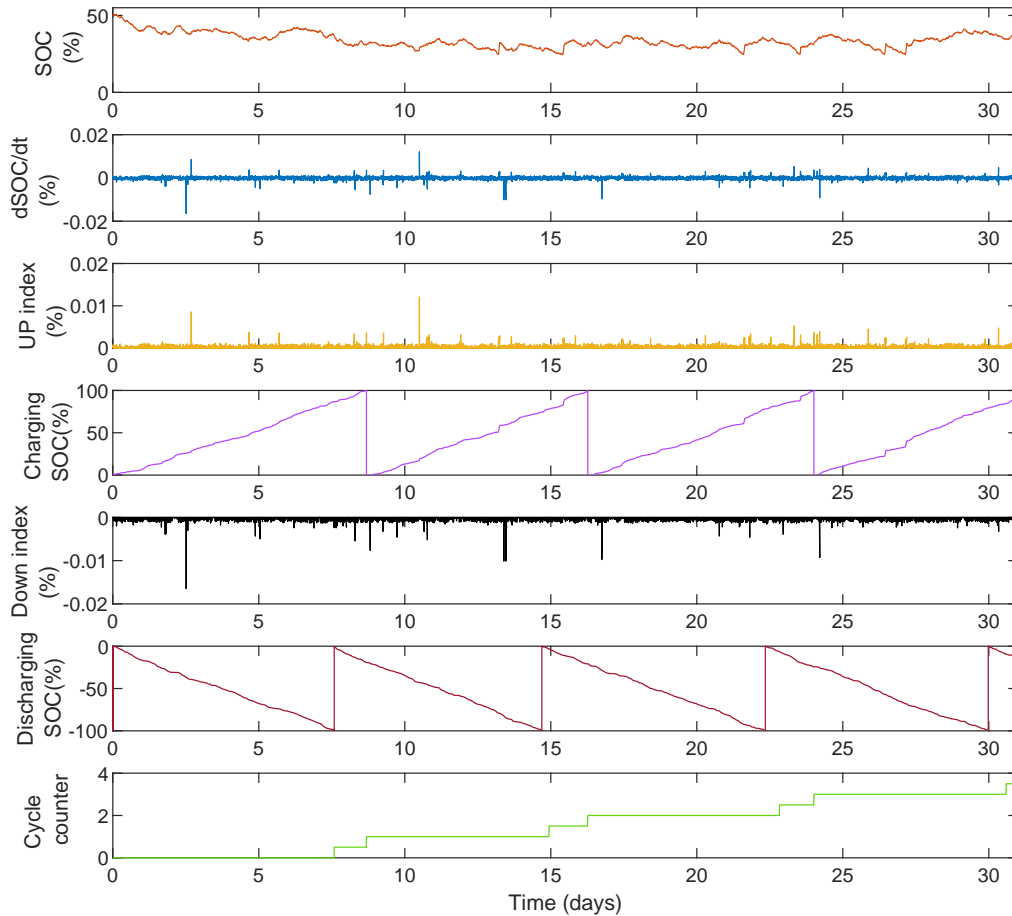
Figure. 4.17 The operation principles of the proposed CCM based on SOC profile obtained from the simulation results of BESS were obtained to deliver DC service by submitting a baseline power (±3MW) for Jan-2019 frequency data.

Table. 4.18 The findings regarding the number of full cycles achieved by CCM and the degradation rate were obtained using the Miner Rule's Method for an LTO battery that had undergone 12,000 cycles(manufacturer cycling) used to deliver DFR & DC service for the whole year of 2019 frequency data, 40MWh profile

Services	Baseline Power (MW)	Total no of Cycles (cycle)	LTO battery degradation (%)
DFR	0	401.5	3.3458
DC	0	37.5	0.3125
	±1	38.0	0.3167
	±2	37.5	0.3125
	±3	36.5	0.3042

Figure 4.15, Figure 4.16, and Figure 4.17 Illustrate the operation principles of the proposed CCM that is used to calculate the partial charge-discharge cycles based on SOC that are obtained from simulation results of BESS used to deliver both DFR & DC service for the whole of Jan-2019. It can be seen that from the obtained SOC profile, ΔSOC (dSOC/dt) has been extracted second by second then the algorithm will detect the change

in the sign of the ΔSOC, so if ΔSOC>0 then the battery is charging while if ΔSOC<0 then the battery is discharging. In the next step, all positive (UP) indexes and negative (Down)indexes will be summed up separately until the total of each index reaches 100 then one charge and one discharge will be counted. As we can see from Figure 4.15 where BESS used to deliver DFR service for the whole of Jan-2019, the average of ΔSOC is $\leq$2% which caused many micro cycles produced by the change in the real frequency data second by second. Therefore, the total number of full charge-discharge cycles produced by applying CCM to deliver DFR service for the whole of Jan-2019 is almost 34 cycles. The main reason behind that is according to NG specification that relates to DFR service, there is no SOC management as in DB there is no opportunity to charge or discharge the battery which means the power equates to zero and this will result in the increase in the number of charge and discharge cycles.

Figure 4.16, and Figure 4.17 show the operation principles of CCM that have been applied to the BESS used to deliver DC service with and without submitting a P$_{Base}$ with the same methodology that has been explained above for DFR service. From the above figures, it is clear to see that, the average of ΔSOC that has been obtained from the simulation results of DC service with and without submitting a baseline power is very small compared to DFR service which is $\leq$0.005% which caused many microcycles produced by the change in the real frequency data second by second. Therefore, the total charge-discharge full cycles will be very small compared to the DFR service. The highest number of full cycles was obtained from BESS used to deliver DC service with submitting baselines power ($\pm$1MW, $\pm$2MW) which is ~4cycles, while the lowest number of full cycles was obtained from BESS used to deliver DC service without submitting a baseline and with submitting a baseline power ($\pm$3MW) with a value=~3.5cycles.

a. The effects of C-rate on battery degradation

In this section, the proposed method called fast CCM with the algorithm shown in Section 2.4.2 Chapter 2 has been improved by considering the effects of C-rate on the battery lifetime. It is used herein to calculate the number of micro charge-discharge cycles based on the SOC data that has been obtained from BESS used to deliver both DFR & DC services for the whole of Jan 2019. The scheme of the proposed CCM considering C-rate is shown in Figure 4.18.
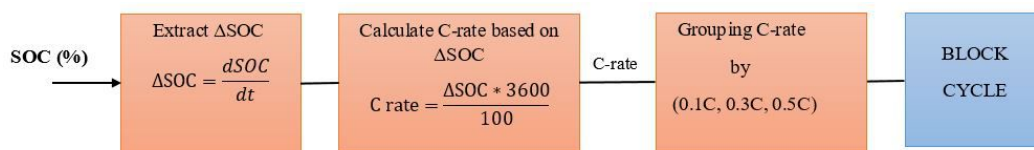
Figure. 4.18 Scheme of CCM considering only C-rate

Figure 4.18 represents the scheme of the proposed CCM that is used to calculate the

partial charge-discharge cycles using the SOC data profile that has been obtained from the simulation results of Jan-2019 with considering grouping different C-rates as (0.1C, 0.3C, 0.5C). The C-rate is calculated based on ΔSOC using the following equation;

$$C_{rate} = \frac{\Delta SOC \times 3600}{100} \tag{4.5}$$

The obtained C-rate is measured second by second grouped by (0.1C, 0.3C, 0.5C) in order to calculate the micro charge-discharge cycles at each C-rate. In the last step, the approximated number of cycles which are represented by the last block shown in Figure 4.18 called (BLOCK CYCLE) is calculated using eq.2.3 which is shown in Section 2.4.2, Chapter 2. To calculate the LTO battery degradation rate by considering the effect of C-rate on the battery lifetime, use (Date1) which assumes that the number of cycles for each C-rate is constant (12,000 cycles), and use the assumed number of cycles with C-rate ranges called (Data2) which are shown in Figure 4.6, and calculated using e.q.4.4.

Simulation results of the CCM considering C-rate effects on LTO battery Lifetime for delivering both DFR & DC services for Jan-2019 frequency data

In this section, the proposed CCM is used to calculate the number of micro charge-discharge cycles for BESS with a different C-rates value used to deliver DFR and DC services separately for Jan-2019 with the results shown in Table 4.19, and Table 4.20.

Table. 4.19 The number of cycles and degradation results obtained from the CCM based on different C-rates for BESS delivering DFR for Jan 2019 frequency data

C-rate	No of Cycles (Cycle)	LTO Battery degradation at each C-rate (%)
C$\leq$ 0.1	7.5	0.03409
0.1C$<$ C $\leq$ 0.3C	27	0.14211
0.3C$<$C $\leq$ 0.5C	1.5	0.00882

Table. 4.20 The number of cycles and degradation results obtained from the CCM for BESS used to deliver DC service with and without submitting a P_{Base} for Jan 2019 frequency data, **at C$\leq$ 0.1**

P_{Base} (MW)	No of Cycles (Cycle)	LTO Battery degradation at each C-rate (%)
0	3.5	0.01591
$\pm$1	4	0.01818
$\pm$2	4	0.01818
$\pm$3	3.5	0.01591

Table 4.19 shows that, the simulation results that were obtained from CCM considering the effects of C-rate on BESS lifetime used to deliver DFR service for the whole of Jan-2019, and it can be noticed that, the battery subjected to the greatest number of cycles that were occurred at the same C-rate range as in EFCs which is $(0.1< C \leq 0.3)$ but it has been increased by $\sim 45.46\%$, and caused an increment in the degradation rate with almost 43.64% compared to EFCs, also, the lowest number of cycles occurred at C-rate ranging from 0.3C to 0.5C which was the same as EFCs, but it has been decreased by approximately 13.43% and caused decrement in degradation rate by $\sim 13.53\%$ compared to EFCs. Therefore, the obtained results from both EFCs & CCM illustrate that, by considering the effects of C-rate on the battery lifetime, BESS spends most of its time operation at $(0.1< C \leq 0.3)$ and rarely operates at $(0.3< C \leq 0.5)$, therefore, the obtained results from CCM show that BESS is subjected to the highest number of cycles and degraded faster compared to EFCs.

Table 4.20 presents the total number of micro charge-discharge cycles and degradation rates that are obtained from applying CCM for BESS used to deliver DC service with and without submitting a different baseline power for the the whole of Jan-2019 while considering the effects of C-rate on the battery lifetime. It can be seen that in all cases of DC service, the battery only operates at $\leq 0.1C$, but for EFCs, it was operated at all C-rate ranges, at $\leq 0.1C$, Compared to EFCs, the obtained number of cycles from CCM for BESS used to deliver DC service without submitting P_{Base} was increased by almost 36.29%, with increment in a degradation rate equates to $\sim 36.32\%$, while the number of cycles that were obtained by CCM for DC service with submitting a different P_{Base} for charge/discharge purpose which includes; ($\pm 1MW$, $\pm 2MW$, and $\pm 3MW$) was increased by almost 43.56%, 44.33%, and 40.97%, and caused increment in the degradation rates by 43.55%, 44.32%, and 40.99% respectively. This means that BESS spends its operating time only in the region where C-rate is at $\leq 0.1C$, and did not operate at C-rate ranges $(0.1< C \leq 0.5)$. Therefore, by submitting a baselines power ($\pm 1MW$, $\pm 2MW$), the number of cycles will increase compared to DC without submitting a baseline power, while at ($\pm 3MW$), the number of cycles remained the same with a value (3.5 cycles), and this is because the contracted power was significantly decreased. For both methodologies (EFCs & CCM) considering the effects of C-rate on the battery lifetime, BESS used to deliver DFR service will be more degraded than DC service.

b. The Effects of both C-rate & SOC on Battery Degradation

In this section, the proposed method (CCM) with the algorithm shown in Section 2.4.2 Chapter 2 is improved considering the effects of both C-rate and SOC on battery lifetime. It is used herein to calculate the partial number of charge and discharge cycles based on the SOC data that has been obtained from BESS used to deliver both DFR & DC services

for the whole of Jan-2019. The scheme of such a method considering both C-rate & SOC is shown in Figure 4.19.
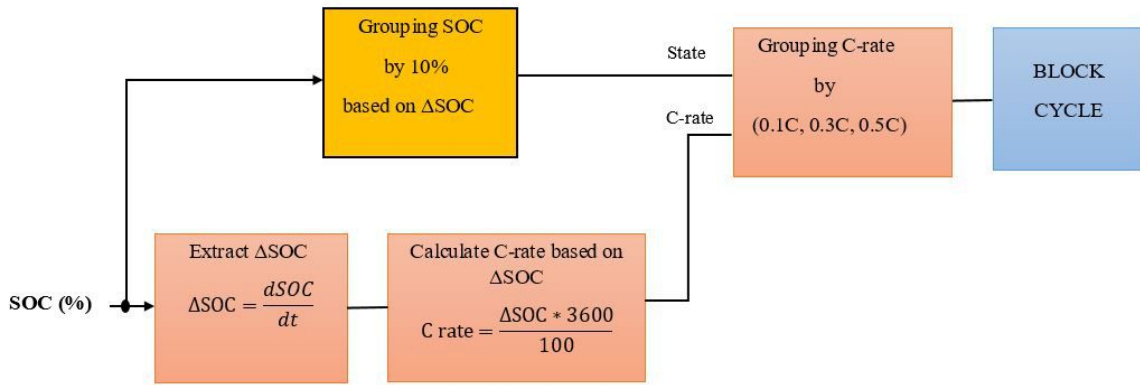
Figure. 4.19 Scheme of the Fast CCM considering C-rate & SOC.

Figure 4.19 illustrates the scheme of the proposed CCM that is used to calculate the partial charge-discharge cycles using the SOC data profile that has been obtained from the simulation results of Jan-2019 while considering grouping different C-rates as (0.1C, 0.3C, 0.5C) as well as grouping of SOC levels. The C-rate is calculated second-by-second based on ΔSOC using eq.(4.5. In the following step, the obtained C-rate is measured second-by-second with grouped of C-rate (0.1C, 0.3C, 0.5C) and grouped SOC (10%, 20%, 30%, 40%, 50%, 60%, 70%, 80%, 90%) in order to improve the accuracy of CCM. In addition to that, the obtained approximated number of cycles which is represented by the last block in Figure4.19 named (BLOCK CYCLE) and calculated as shown in Figure (2.7 in Subsection 2.4.2, Chapter 2. Lastly, the LTO battery degradation rate for considering the effects of both C-rate and SOC on battery lifetime can be calculated using the assumed number of cycles with SOC ranges as shown in Table 4.5, and using e.q.4.4.

Simulation results of the CCM considering the effects of both C-rate & SOC Effects on Battery Lifetime that has been used to deliver both DFR & DC services for Jan-2019 frequency data

In this section, the proposed CCM is used to calculate the number of charge-discharge micro cycles for BESS with a different C-rate and based on a grouped SOC used to deliver DFR and DC services separately for Jan 2019. The obtained number of cycles and degradation rates are shown in the below tables;

Table. 4.21 The number of cycles obtained from the CCM based on different C-rates and grouped of SOC Battery delivering DFR Service for Jan-2019 Frequency Data

		C-rate (C)			
		C≤ 0.1	0.1<C≤ 0.3	0.3<C≤ 0.5	Total Number of Cycles (Cycle)
SOC(%)	≤ 10	1.5	4.5	0	6
	10 - 20	1.5	6.5	0.5	8.5
	20 - 30	2.5	5	0.5	8
	30 - 40	0.5	1.5	0	2
	40 - 50	1.5	3	0.5	5
	50 - 60	0	1.5	0	1.5
	60 - 70	0	0.5	0	0.5
	70 - 80	0	1.5	0	1.5
	80 - 90	0	2.5	0	2.5
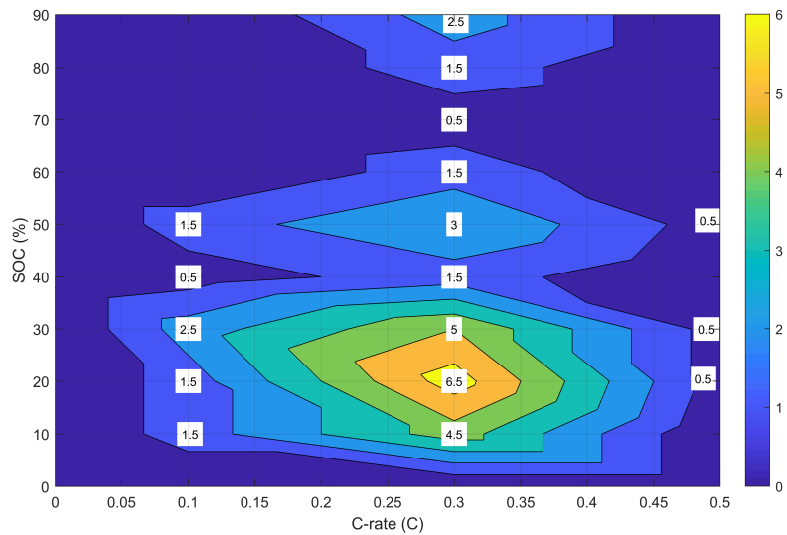
Figure. 4.20 Simulation results of the CCM based on different C-rates for each grouped SOC for DFR model for Jan-2019 frequency data. (Maximum scale is ~ 6.5 cycles)

Table. 4.22 Degradation results obtained from the CCM based on different C-rates and grouped SOC battery delivering DFR service model for Jan-2019 frequency data

		C-rate (C)		
		C≤ 0.1	0.1<C≤ 0.3	0.3<C≤ 0.5
SOC(%)	≤ 10	0.00566	0.01915	0
	10 - 20	0.005769	0.028261	0.002381
	20 - 30	0.009804	0.022222	0.002439
	30 - 40	0.002000	0.006818	0
	40 - 50	0.006122	0.013954	0.002564
	50 - 60	0	0.007143	0
	60 - 70	0	0.002439	0
	70 - 80	0	0.007500	0
	80 - 90	0	0.012820	0

Total LTO battery degradation rate = 0.157046%

Table 4.21, Figure 4.20, and Table 4.22 show the simulation results of the CCM, considering the effects of both C-rate and SOC on the battery lifetime delivering DFR service for the whole of Jan-2019. It can be noticed that BESS was mostly operated at the same C-rate for EFCs, which is (0.1< C ≤0.3), and for SOC range (≤10%−30%), while for EFCs with SOC range (≤10%−40%), it was subjected to the highest number of micro charge-discharge cycles for (≤10−20%) SOC range, which is the same as EFCs. However, the number of cycles is increased by almost 62.89% compared to EFCs, and with an increment in the degradation rate, equating to approximately 82.59%. This means that the battery spends most of its operation time at 0.1C−0.3C for all SOC ranges, so the degradation rates in such regions should be considered. At ≤ 0.1C, where the SOC ranges from 50%−90%, at 0.3C−0.5C for ≤10%, (30%−40%), and from (50%−90%), the total number of full cycles equates to zero. That's to say, the battery was rarely operating in such regions; however, in such regions, for EFCs, the number of cycles was >0 and <1.

Table. 4.23 Number of cycles obtained from the CCM based on different C-rate values and grouped of SOC battery delivering DC service without submitting a P_{Base} for Jan-2019 frequency data

		C-rate (C)			
		C≤ 0.1	0.1<C≤ 0.3	0.3<C≤ 0.5	Total Number of Cycles (Cycle)
SOC(%)	≤ 10	0.5	0	0	0.5
	10 - 20	2	0	0	2
	20 - 30	0.5	0	0	0.5
	30 - 40	0.5	0	0	0.5
	40 - 50	0	0	0	0
	50 - 60	0	0	0	0
	60- 70	0	0	0	0
	70 - 80	0	0	0	0
	80 - 90	0	0	0	0
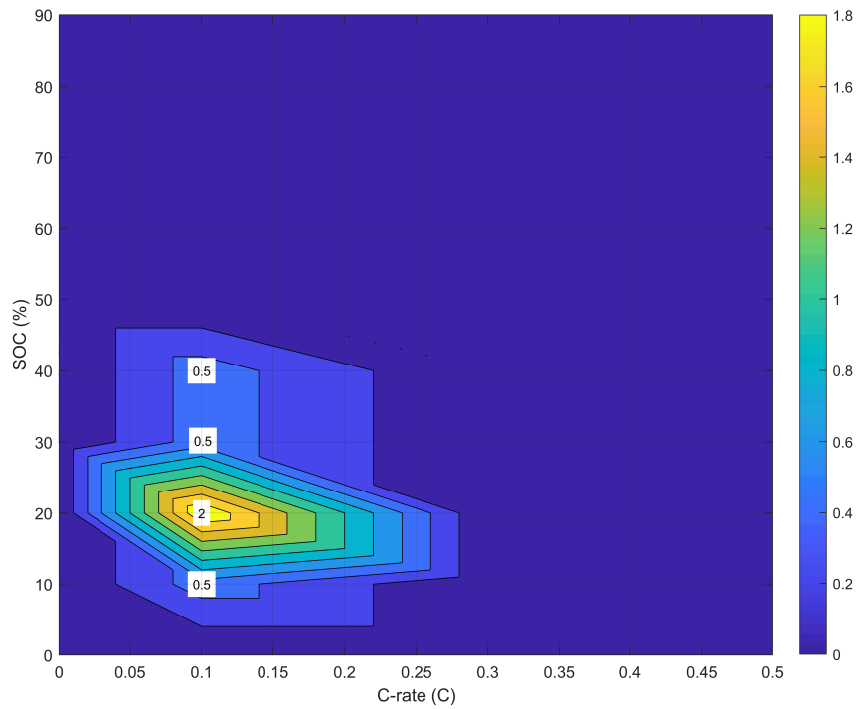
Figure. 4.21 Simulation results of CCM based on different C-rate for each grouped SOC for battery delivering DC without submitting a P_{Base} for Jan-2019. (Maximum scale is 2 cycles)

Table. 4.24 Degradation results obtained from the EFCs based on different C-rates and grouped SOC battery delivering DC service model without submitting a P_{Base} for Jan-2019 frequency data

		C-rate (C)		
		C≤ 0.1	0.1<C≤ 0.3	0.3<C≤ 0.5
SOC(%)	≤ 10	0.001887	0	0
	10 - 20	0.007692	0	0
	20 - 30	0.001961	0	0
	30 - 40	0.002000	0	0
	40 - 50	0	0	0
	50 - 60	0	0	0
	60 - 70	0	0	0
	70 - 80	0	0	0
	80 - 90	0	0	0

Total LTO battery degradation rate = 0.013540%

Table. 4.25 Number of cycles obtained from the CCM based on **C-rate (C≤ 0.1)** and grouped of SOC battery delivering DC service with submitting a different P_{Base} for Jan-2019 frequency data

		P_{Base} **(MW)**		
		±1	±2	±3
SOC(%)	≤ 10	0	0	0
	10 - 20	0	0	0
	20 - 30	2.5	1	0.5
	30 - 40	1.5	3	3
	40 - 50	0	0	0
	50 - 60	0	0	0
	60 - 70	0	0	0
	70 - 80	0	0	0
	80 - 90	0	0	0
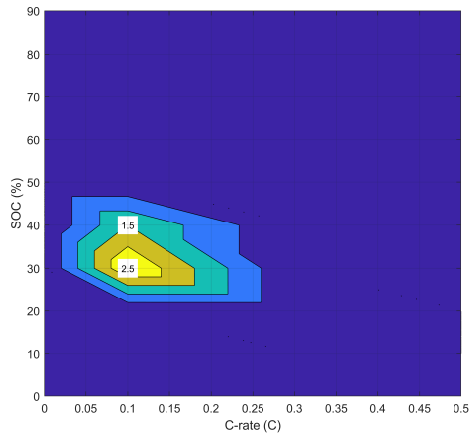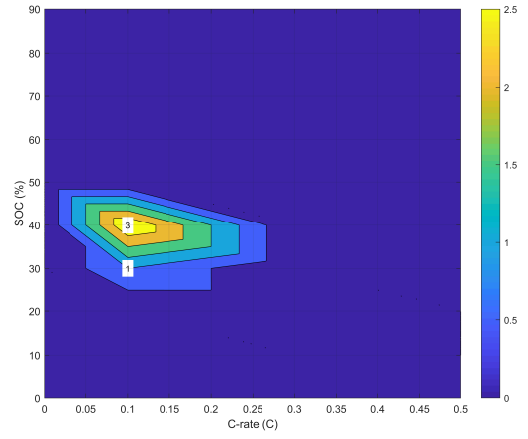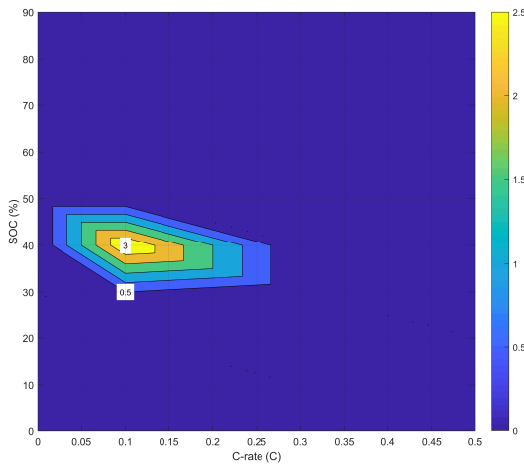
Figure. 4.22 Simulation results of CCM based on different C-rate for each grouped SOC for BESS used to deliver DC service with submitting a different P_{Base} for Jan-2019 frequency - (a) $P_{Base}(\pm 1MW)$, Maximum scale is 2.5 cycles (b) P_{Base} $(\pm 2MW)$, Maximum scale is 3 cycles (c) P_{Base} $(\pm 3MW)$, Maximum scale is 3 cycles.

Table. 4.26 Degradation results obtained from the CCM based on **C-rate (C≤ 0.1)** and grouped of SOC battery delivering DC service with submitting a different P_{Base} for Jan-2019 frequency data

		P_{Base} **(MW)**		
		±1	±2	±3
SOC(%)	≤ 10	0	0	0
	10 - 20	0	0	0
	20 - 30	0.009804	0.00392	0.00196
	30 - 40	0.006000	0.01200	0.01200
	40 - 50	0	0	0
	50 - 60	0	0	0
	60 - 70	0	0	0
	70 - 80	0	0	0
	80 - 90	0	0	0

Total LTO battery degradation rate = 0.045684%

Table 4.23, Figure 4.21, Table 4.24, Table 4.29, Figure 4.22a, Figure 4.22b, and Figure 4.22c, Illustrate the simulation results that obtained from CCM for BESS used to deliver DC service with and without submitting a P_{Base} for the whole of Jan-2019 with considering the effects of both C-rate & SOC on the battery lifetime. It can be seen that, in all cases of DC service, BESS was only operated at 0.1<C, and in the case where the DC service has been delivered without submitting a P_{Base}, the battery only operates at the same C-rate for SOC range (≤10% - 40%), and subject to the higher number of cycles for (≤10% - 20%) SOC range which is the same as EFCs with the value increased by almost 69.17% and caused increment by approximately 0.007692% degradation rate, however, for EFCs, at same C-rate, the battery was mostly operated SOC range (≤10% - 60%). This means that, for CCM, the battery delivering such service operates at such C-rate and SOC regions, but mostly spent its lifetime at (≤10% - 20%) SOC range, and the degradation rate should be considered in such region. Moreover, when the C-rate is higher than 0.1C for all SOC groups, the number of full cycles equates to zero which means the battery might not operate in such regions for delivering DC service.

In the case where DC service with submitting a P_{Base} takes place, the obtained results illustrate that the battery only operates at ≤0.1C for 20% SOC - 40% SOC, while for EFCs, at the same C-rate, the battery was mostly operated for SOC range (20% - 60%). This means by applying CCM, BESS spent most of its operation time in a such region, however, degradation should be considered in such a region. The main reason behind that is to comply with NG specification, a baseline power needs to be submitted one hour ahead in order to manage SOC if it falls below 25% or goes above 75%. In the case of submitting a ±1MW of a baseline power, BESS was subject to the greatest number of cycles for (20% - 30%) SOC range with increments equating to almost 74.02% which

caused the increase in the degradation rate by approximately 74.03% compared to EFCs, and for ±2MW, and ±3MW, the greatest number of cycles occurred at (30% - 40%) SOC range with increment equates ∼ 71.81%, and 60.49%, respectively, and caused increasing of almost 71.80%, and 60.49% in the degradation rate, respectively, compared to EFCs. Therefore, at ≤0.1C, the number of cycles is increased by increasing the value of baseline power, particularly at such C-rate for (30% - 40%) SOC range. The total number of cycles obtained from CCM considering both C-rate & SOC for BESS used to deliver DC service without and with submitting a different baseline power (±0MW, ±1MW, ±2MW, and ±3MW) equates to almost (3.5, 4, 4, and 3.5) cycles, respectively, and this means that the number of cycles obtained from CCM was higher than EFCs. /

4.5.6   Experimental Degradation of DFR & DC Services

To carry out the experimental degradation, two SOC experimental samples have been used, the first sample is a SOC obtained from the simulation results of DC service for 24 hours for Jan-2019 frequency data, while the second SOC experimental sample is obtained from the simulation results of BESS used to deliver DFR service for almost four days as shown in Figure 4.23, and Figure 4.24
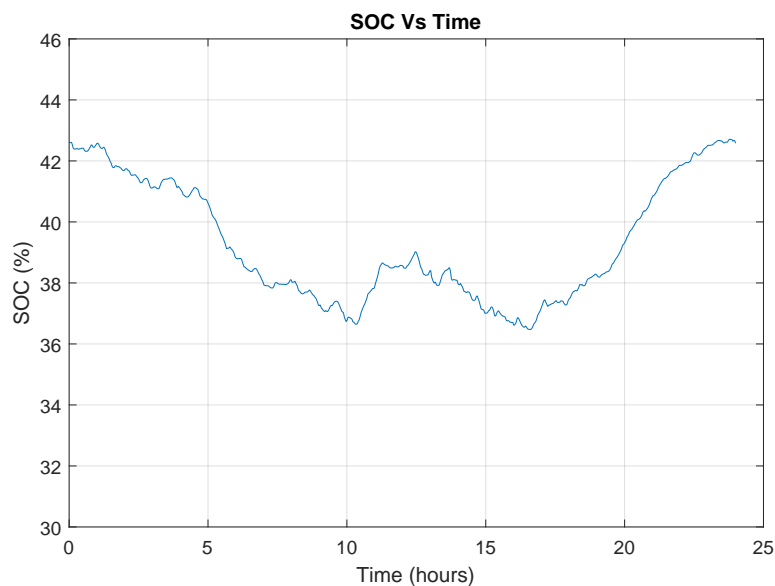
Figure. 4.23 Simulation results of DC service for Jan-2019, SOC experimental sample for ∼24 hours
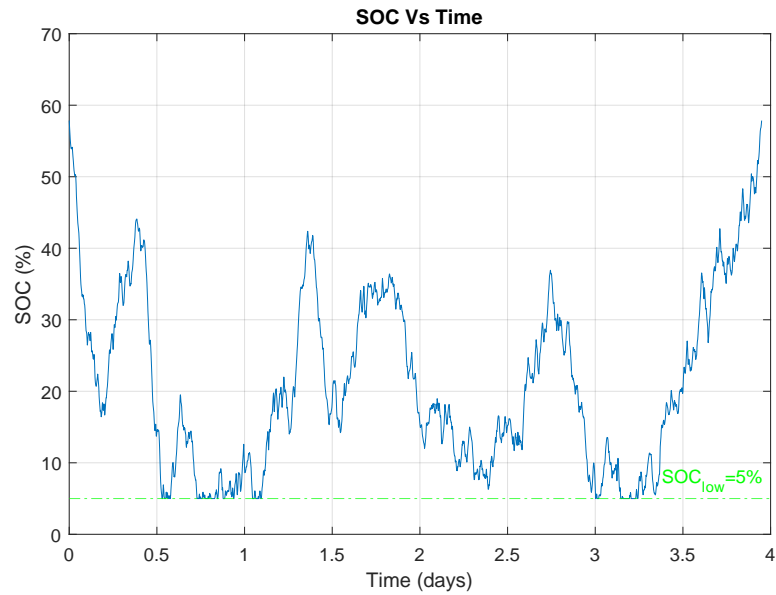
Figure. 4.24 Simulation results of DFR service for Jan-2019, SOC experimental sample for ∼94.78 hours

As we can see from Figure 4.23, and Figure 4.24, the SOC samples have been chosen based on a condition which is SOC_{start}=SOC_{end} which is considered a cell battery is doing one cycle then the charge/discharge power profile that has been obtained from the same simulation findings for each service has been taken and scaled to 12.18W which came from (2.9A x 4.2V) to charge and discharge the battery cell. The charging currents have positive values whereas discharging currents are represented by negative values. In reality, the only important readings are the lowest and highest cell voltage as a full charge/discharge cycle must end or change when one cell reaches its upper or lower voltage limit. In this section, the Lithium-ion Rechargeable battery with the cell type N18650CL-29 and the chemistry type Nickel Manganese Cobalt (NMC) has been chosen to carry out the experiment. This was the most common type of battery in 2020 when the cells were tested. The battery cell is shown in Figure 4.25 with parameters presented in Table A2, see Appendix B.

Figure. 4.25 BAK N18650CL-29 2900mAh Li-ion Battery Cell [133]

4.5.7 Test procedure

To track the degradation of the 8 cells, a standardized monitoring procedure was periodically conducted at varying temperatures (4 cells at 25C° and the other 4 at 35C°). This procedure involved a constant current (CC) charging phase utilizing a low charging current of 2.9A, followed by a constant current constant voltage (CCCV) charging phase to determine C_{actual}. Positive values were assigned to charging currents, while negative values were used to indicate discharging currents in this context. The experiment was conducted utilizing Maccor, as depicted in Figure 4.26. An outline of the hardware setup for employing Maccor battery testing equipment and the steps involved in the experiment operation are detailed in Appendix B.

Figure. 4.26 Maccor

4.5.8 Capacity Test

In this section, the capacity test has been carried out for the 8 cells in order to investigate the effects of varying temperatures on the battery cells capacity used to deliver DC & DFR services for a certain time, and the obtained results are shown in Table 4.27, and Table 4.28.

Table. 4.27 Experiments results of the Capacity test for 4 cells used to deliver **DFR service** under different temperatures (25C°, and 35C°)

Cell Number	Number of Days	Capacity (Ah)	Normalised Capacity	SOH Loss (%)	Loss per day (%)
Cell-1 (25)-25C°	0	2.7373	1	0	0
	140	2.7278	0.9965	0.35	0.0025
	170	2.7264	0.9959	0.40	0.0029
Cell-1 (17)-35C°	0	2.8362	1	0	0
	140	2.8244	0.9958	0.42	0.0030
	170	2.8238	0.9957	0.44	0.0031
Cell-2 (26)-25C°	0	2.7572	1	0	0
	140	2.7489	0.9970	0.30	0.0021
	170	2.7478	0.9966	0.34	0.0024
Cell-2 (18)-35C°	0	2.8432	1	0	0
	140	2.8319	0.9960	0.40	0.0029
	170	2.8287	0.9949	0.51	0.0036
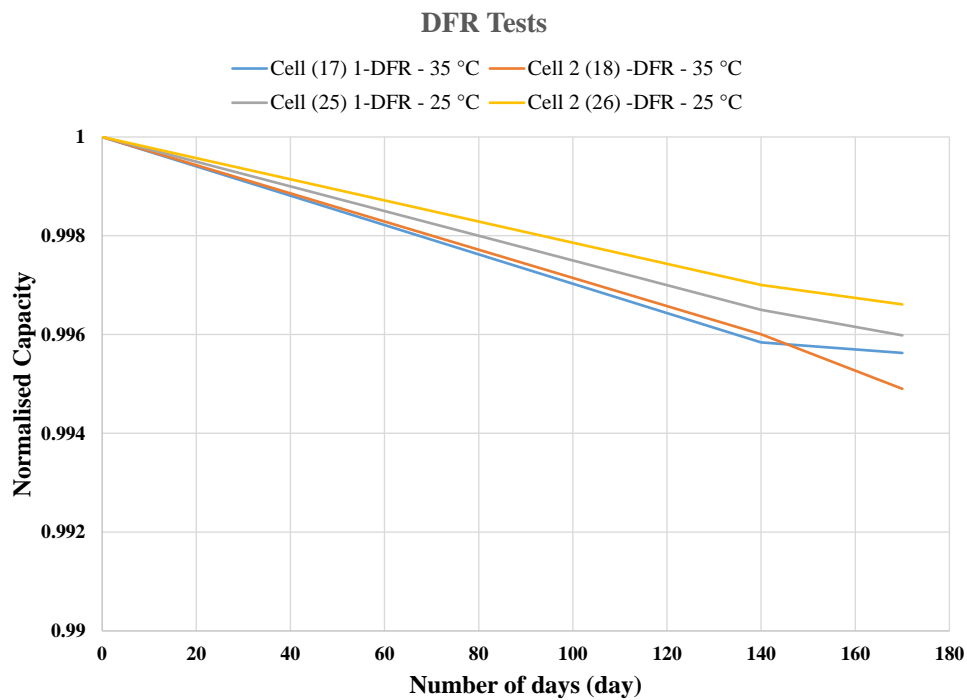
Figure. 4.27 Experiments results of the Capacity test for 4 cells used to deliver DFR service under different temperatures (25C°, and 35C°).

Table 4.27, and Figure 4.27 illustrate the experimental results for the capacity test for four LTO Rechargeable Cells used to deliver DFR service under different temperatures, 25C° and 35C°, are illustrated in the graph. It can be seen that the Li-ion cells lose their capacity under various temperatures. For Cell-1 (25) with an initial capacity of around 2.737340 Ah, after approximately 140 days at 25C°, the cell lost approximately 0.35% of its original capacity, which means that the cell loses almost 0.0025% per day. Moreover,

the largest capacity loss was almost 0.40% and it occurred after 170 days, with the loss per day increasing to approximately 0.0029%, as the time increased to one month.

For Cell-1 (17), despite the initial capacity being higher than Cell-1 (25) by almost 0.098884 Ah, after 140 days at 35°C, the cell lost around 0.42% of its original capacity, resulting in an increase in the loss to around 0.0030 per day. Additionally, the losses increased to almost 0.44% of the original capacity after approximately 170 days, causing an increment in the losses per day to almost 0.0001% compared to 140 days.

For Cell-2 (26) at 25°C, with an original capacity of 2.75718 Ah, the cell lost almost 0.30% of its capacity after 140 days, which means that it had lost approximately 0.0021% per day from its capacity. The capacity loss increased to almost 0.34% after 170 days, which caused an increase in the losses per day to almost 0.0024%. In addition, for Cell-2 (18) under 35C°, despite the initial capacity being higher than Cell-2 (26), after 140 days, the losses increased by almost 0.10% from the original capacity compared to Cell-2 (26), resulting in a rise in the losses per day by almost 0.008%. Moreover, for Cell-2 (18) under the same temperature, when the number of days increased from 140 to 170 days, the loss of capacity increased by approximately 0.11%, resulting in an increase in the losses per day with approximately 0.0007%.

That is to say, when the number of days increased at the same temperature, the capacity losses increased. Moreover, the highest capacity losses were obtained at a high temperature, which increased the cell degradation and decreased its lifetime.

Table. 4.28 Experiments results of the Capacity test for 4 cells used to deliver **DC service** under different temperatures (25C°, and 35C°)

Cell Number	Number of Days	Capacity (Ah)	Normalised Capacity	SOH Loss (%)	Loss per day (%)
Cell-1 (27)-25C°	0	2.7458	1	0	0
	140	2.7440	0.9995	0.06	0.0005
	170	2.7404	0.9980	0.20	0.0012
Cell-1 (19)-35C°	0	2.8275	1	0	0
	140	2.8185	0.9968	0.32	0.0023
	170	2.8143	0.9953	0.47	0.0027
Cell-2 (28)-25C°	0	2.7342	1	0	0
	140	2.7322	0.9993	0.07	0.0005
	170	2.7279	0.9977	0.23	0.0014
Cell-2 (20)-35C°	0	2.8264	1	0	0
	140	2.8185	0.9972	0.28	0.0020
	170	2.8165	0.9965	0.35	0.0021

DC Tests
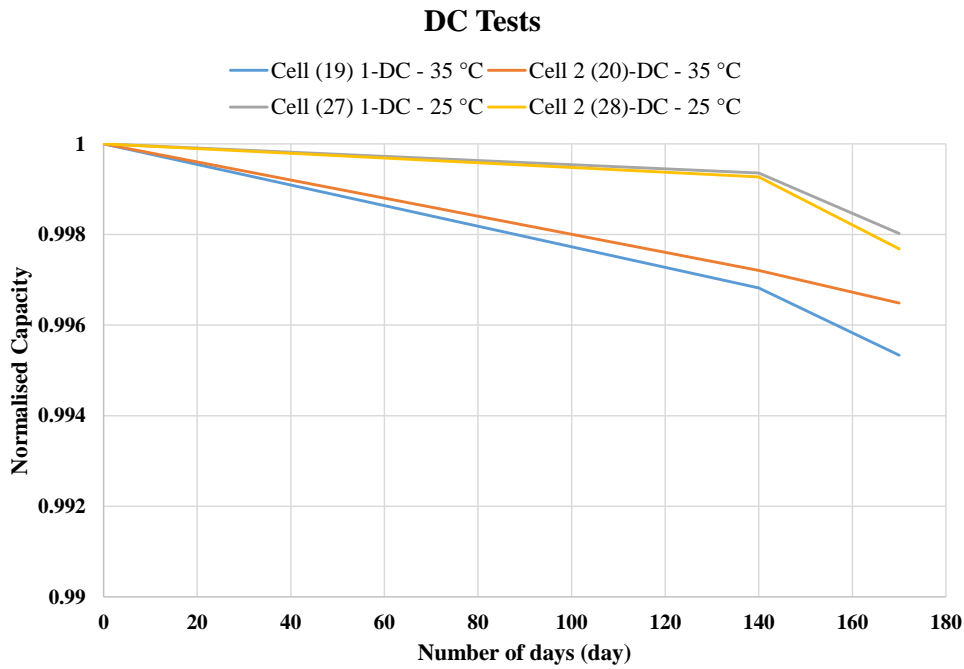
Figure. 4.28 Experiments results of the Capacity test for 4 cells used to deliver DC service under different temperatures (25C°, and 35C°).

Table 4.28, and Figure 4.28 illustrate the experimental results for the capacity test of four rechargeable LTO cells used to provide DC service at varying temperatures of 25C° and 35C°. It can be observed that Cell-1 (27), operating at 25C° with an initial capacity of 2.745805 Ah, experienced a capacity loss of around 0.06% from its original capacity after 140 days, while after 170 days, the capacity losses increased by approximately 0.14% compared to 140 days. Cell-1 (19) at 35C° exhibited a higher capacity loss despite having a higher initial capacity than Cell-1 (27). Specifically, the capacity losses increased to approximately 0.32% and 0.47% when cycled at 140 and 170 days, respectively, leading to an increment in the loss per day to almost 0.004% compared to 140 days.

On the contrary, the lowest capacity losses were obtained from cell-2 (28) at 25C°, and cell-2 (20) at 25C°, where the value equalled almost 0. 07% of its original capacity when cycled at 140 cycles. However, the highest capacity losses of almost 0.23% were observed from Cell-2 (20) at 35C° when the number of days increased to approximately 170 days.

Consequently, the results indicate that battery cells utilised to deliver DC service experience lower capacity losses and degradation rates than those used for DFR service at the same temperature. The battery cell used for DFR service under 35C° for 170 days exhibited the highest loss per day, while the lowest losses per day were observed from the battery cell used for DC service under 25C° for 140 days. The calculation of aging due to cycling for each Cell is shown in Table 4.29, and Table 4.30.

4.5.9 Calculations for life-time based on cycle ageing

Table. 4.29 Experiments results of aging due to cycling for battery cells used to deliver **DC service** under different temperatures (25C°, and 35C°)

Cell Number	Number of days (day)	Loss per day (%)	Time for the battery to reach 20% (losses of the initial capacity) (day)	Number of years*
Cell-1 (27)-25C°	140	0.0005	40,000	109.59
	170	0.0012	16,666.67	45.66
Cell-2 (28)-25C°	140	0.0005	40,000	109.59
	170	0.0014	14,285.71	39.14
Cell-1 (19)-35C°	140	0.0023	8,695.65	23.82
	170	0.0027	7,407.41	20.29
Cell-2 (20)-35C°	140	0.0020	10,000	27.39
	170	0.0021	9,523.81	26.09

*There is uncertainty regarding whether the battery cells will last for the estimated 109.59 years, with inconclusive results. Therefore, it is recommended that the cells undergo sufficient cycling to linearize the degradation.

Table. 4.30 Experiments results of aging due to cycling for battery cells used to deliver **DFR service** under different temperatures (25C°, and 35C°)

Cell Number	Number of days (day)	Loss per day (%)	Time for the battery to reach 20% (losses of the initial capacity) (day)	Number of years
Cell-1 (25)-25C°	140	0.0025	8,000	22.22
	170	0.0029	6,896.55	19.16
Cell-2 (26)-25$C°$	140	0.0021	9,523.81	26.46
	170	0.0024	8,333.33	23.15
Cell-1 (17)-35C°	140	0.0030	6,666.67	18.52
	170	0.0031	6,451.61	17.92
Cell-2 (18)-35$C°$	140	0.0029	6,896.55	19.16
	170	0.0036	5,555.56	15.43

Table 4.30 and Table 4.29 present experimental results detailing the aging of battery cells under different temperatures (25C° and 35C°) due to cycling. These cells are used to deliver both DC and DFR services for a period ranging from 140 to 170 days. The results exhibit variability for different cells and temperatures, illustrating the impact of cycling and temperature on battery aging. It is evident that under 25C°, the battery cells have a longer lifetime compared to 25C° for both services. However, battery cells delivering DC service are expected to last longer than those delivering DFR service. The anticipated aging due to cycling is very low, given that the average power of the services is less than 5% for DFR and less than 0.5% for DC. Nevertheless, it is clear that the battery cells

won't last as long as estimated, and calendar aging would likely lead to the end of life well before those extensive estimates. The timeframe is indeed too short to draw conclusive results. In a related study, the author in [134] explored capacity degradation and identified three regions, as shown in Figure 4.29.
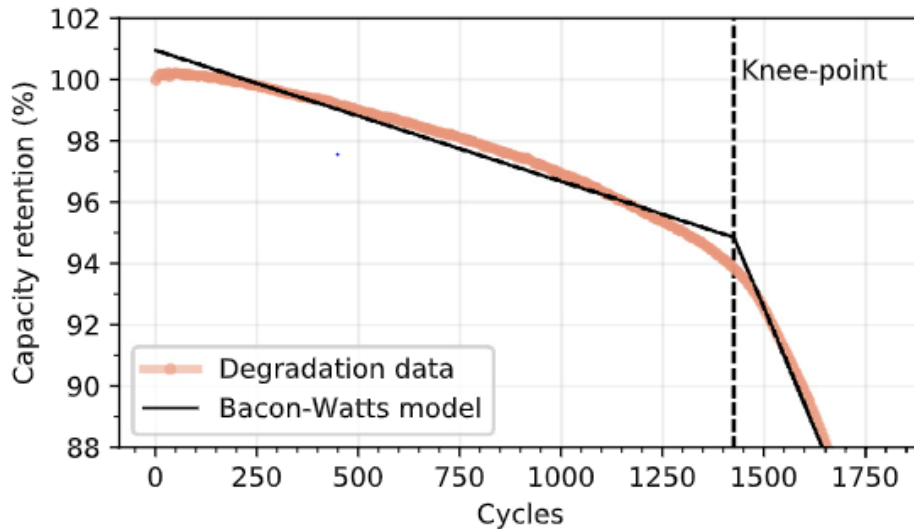
Figure. 4.29 Data on capacity degradation for a specific cell, b3c45, within the A123 dataset, along with the knee-point determined by applying the Bacon-Watts model. The width of the 95% confidence interval for the estimated knee-points, computed through a non-parametric bootstrap procedure, averaged at 6.1 cycles.

1. Early Life Region: This region refers to the initial stage of battery degradation when the capacity loss is minimal and the battery is considered to be in good condition.

2. Knee Region: This region is characterised by a sudden increase in the rate of capacity degradation, which is marked by the knee-point and knee-onset. These points represent the onset of accelerated degradation and are critical in estimating the remaining useful life of the battery.

3. Wear-Out Region: This region is marked by a significant decrease in the battery's capacity, indicating the end of its useful life. This region is reached after the knee-point and knee-onset, where the degradation rate continues to increase until the battery is no longer usable.

As we can see from Figure 4.29 there are three regions, and the experimental work is still in region 1 and therefore cannot be conclusive on the results. So, cells still need to cycle enough to be well in region 2 (the linear part) to be able to 'linearize' the degradation.

Summary

This study conducts a sensitivity analysis of the power-to-energy ratio for ESS providing both DFR and DC services as well as the battery lifetime analysis. The key findings

include:

- DFR services require low C-rates ($< 2C$) to maintain good availability, while DC services can utilize higher C-rates ($< 10C$), leading to increased availability and reduced cycles.

- Compliance with contracted service terms, specifically sustaining power delivery at Maximum Export/Import Limits for 15 minutes, is better achieved by ESS delivering DC services at lower C-rates (0.05C to 0.5C). DFR services achieve 100% compliance only at 0.05C due to the absence of SOC management.

- Implementing SOC management for DC service allows the use of higher C-rates, although this comes at the cost of reduced contracted service power and revenue. High-rate technologies like supercapacitors and flywheels are suggested as alternatives for frequency response services.

- The study introduces two cycle counting methodologies (EFCs and CCM) to quantify battery degradation rates. EFCs generally result in higher degradation rates, with DFR services causing more significant battery degradation compared to DC services.

- The analysis considers the impact of C-rate and SOC on battery lifetime, emphasizing the need to account for both factors for accurate calculations. DFR services subject batteries to more cycles and faster degradation as a result of the absence of SOC management, while DC services with a baseline power degrade faster except in cases of significant contract power reduction.

- Experimental degradation tests with lithium-ion rechargeable cells reveal that higher temperatures cause a more significant capacity loss during cycling. Cells used for DC services experience fewer cycles, reduced capacity loss, slower degradation, and long lifetime compared to those used for DFR services, highlighting the need for further testing to better understand battery behavior.

In the upcoming chapter, we embark on a detailed exploration of the recently introduced DR, a novel frequency response service within the GB electrical grid. Our study not only establishes essential control parameters but also pioneers an innovative approach to energy management, pushing the boundaries of the permissible service envelope. The chapter unveils two distinctive control methods: the first, a benchmark for standard response, and the second, a dynamic control approach strategically exploiting the extremities of the allowable service envelope. Additionally, a lifetime analysis will be carried out based on two proposed cycle counting methods, including EFCs and CCM, which will be examined and discussed in detail using BESS to deliver DR services with and without applying dynamic control.

Chapter 5

Control for New Frequency Response Services (case study)

5.1 Introduction

In this chapter, the primary focus is on the dynamic regulation (DR) service, delving into the presentation of the service envelope for both dynamic regulation high (DR-HF) and dynamic regulation low (DR-LF). The conducted simulations across six electricity forward agreement (EFA) blocks, operating under different scenarios (S1 & S2), bring to light the substantial impact of dynamic control implementation.

Scenario S1, where dynamic control is absent, is compared with Scenario S2, introducing dynamic control with both fast and slow responses. The results highlight how dynamic control can significantly enhance the availability of a battery energy storage system, potentially resulting in increased revenues and a reduction in equivalent full cycles.

The chapter further explores the strategic use of dynamic control to enhance availability, avoiding penalty payments and placing a strong emphasis on minimizing cycle numbers. This strategic approach is put into action by delivering both DR-HF & DR-LF services in a stacked bid.

In addition, the chapter incorporates the two-cycle counting methods (EFCs & CCM) discussed in Chapter 4 to deliver DR services throughout January 2019 and the entire year of 2019.

DR-LF Service Envelope
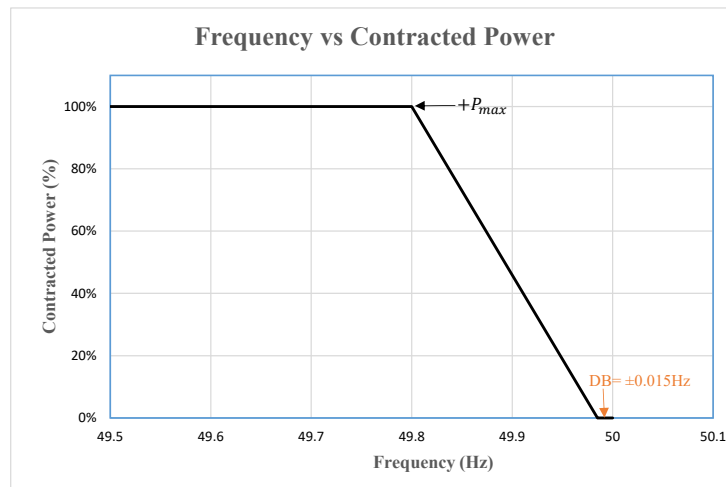
Figure. 5.1 Power vs frequency for DR-LF service.

DR-HF Service Envelope
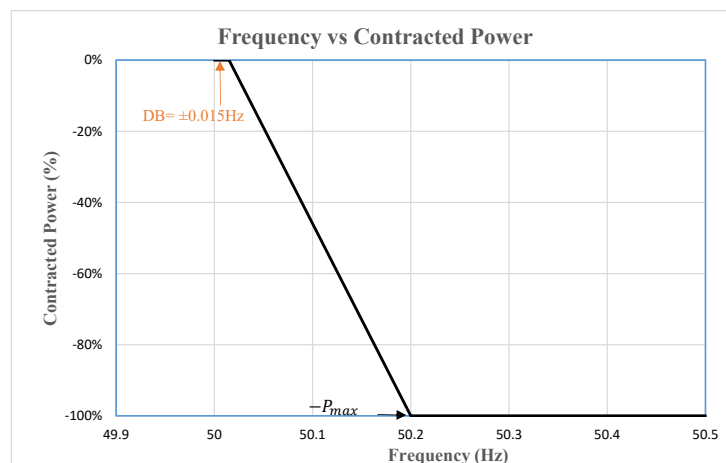
Figure. 5.2 Power vs frequency for DR-HF service.

Figure 5.1 and Figure 5.2 show the relationship between P_{DR} and the frequency data for DR-LF and DR-HF service, respectively. In these services, the assets must respond to low or high-frequency events by exporting and importing power.

115

5.1.1   Simulation Results of DR-HF Service Model
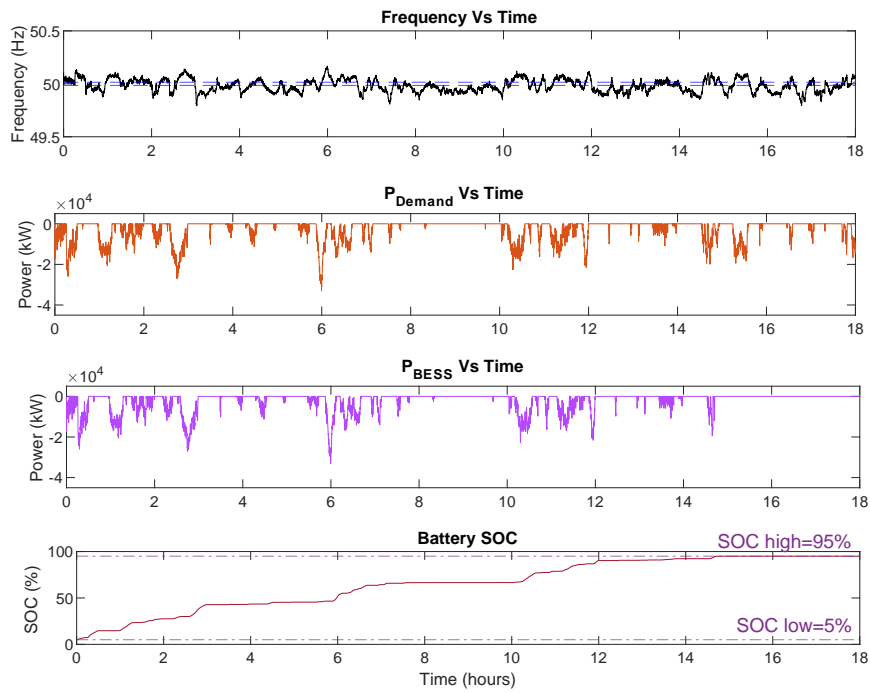
Figure. 5.3 Simulation Results of DR-HF Service for first (18 hours) of Jan-2019 (40MW/40MWh ESS).

Figure 5.3 shows the simulation results of a BESS delivering DR-HF, contracted for 40MW, for the first (18 hours) of Jan-2019 for frequency, P_{Demand}, P_{BESS}, and SOC. In this section, SOC_{start} has been set to 5%, and the SOC limits for the BESS are SOC_{high}=95%, and SOC_{low}=5% and it is shown that SOC_{high} is not breached in the simulation. If the BESS reaches the higher limit, as it does at 14.7 hours, then the system can only export power and P_{BESS} will be set to zero.

5.1.2 Simulation Results of DR-LF Service Model
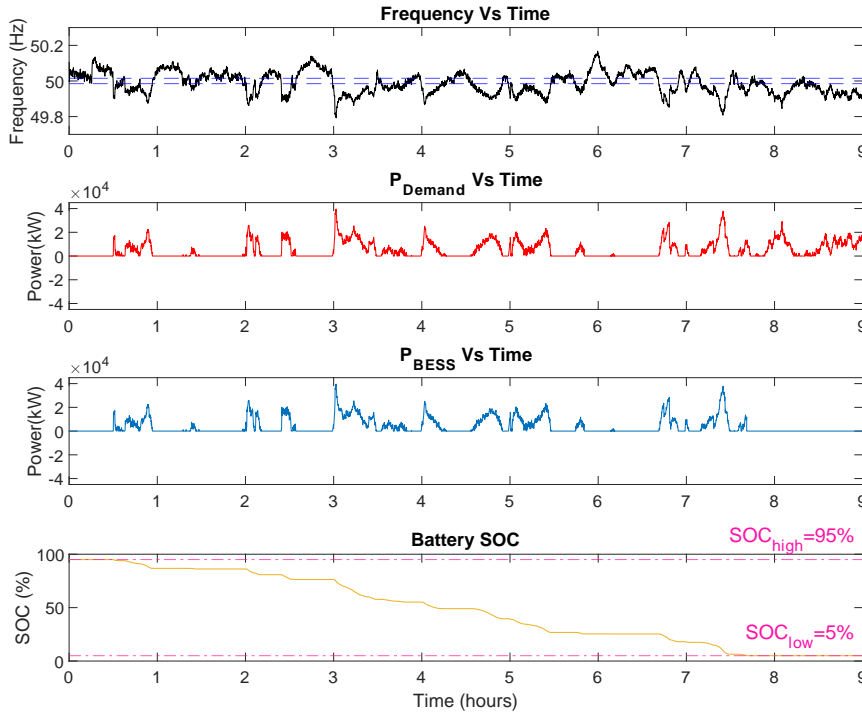
Figure. 5.4 Simulation Results of DR-LF Service for first (9 hours) of Jan-2019 (40MW/40MWh BESS).

Figure 5.4 presents the simulation results of a BESS delivering DR-LF, contracted for 40MW, for the first (9 hours) of Jan-2019 for frequency, P_{Demand}, P_{BESS}, and SOC. In this section, the SOC_{start} has been set to 95%, and SOC limits for the BESS are set as the same values as in DR-HF, and it is clear that SOC_{low} is not breached in the simulation. If the BESS reaches this limit, as it does at 7.4 hours, then the system can only import power, and P_{BESS} will be set to zero.

5.1.3 Dynamic Control of DR-LF or DR-HF

The objective of implementing the dynamic control is that there is an opportunity to exploit the speed of the control response to assist with SOC management as there is no opportunity in the DB. In this section, we consider the ESS delivering either DR-LF or DR-HF and do not consider the case of delivering both in a stacked bid [117]. The strategy in this work is to minimize the energy throughput for either service by responding fast to decreases in P_{DR} and slow to increases in P_{DR}, the sign of which depends on the service being delivered. The fast response will use a 100% p.u./sec ramp rate for P_{Demand}, resulting in the power being delivered within 1 second. The slow response follows the slower limits of the service specification in that P_{DR} must be delivered no later than 10 seconds with a minimum delay period of 2 seconds. This is implemented using a fixed control delay of 2 seconds and a ramp rate of 12.5% p.u./sec.

Dynamic Control of DR-HF

For DR-HF delivery, the SOC_{start} will be set at the lower limit (SOC_{low}=5%). The fast response will be delivered if the changing of DR-HF power ($\Delta P_{(DR-HF)} > 0$), whereas the slow response is implemented if ($\Delta P_{(DR-HF)} < 0$).
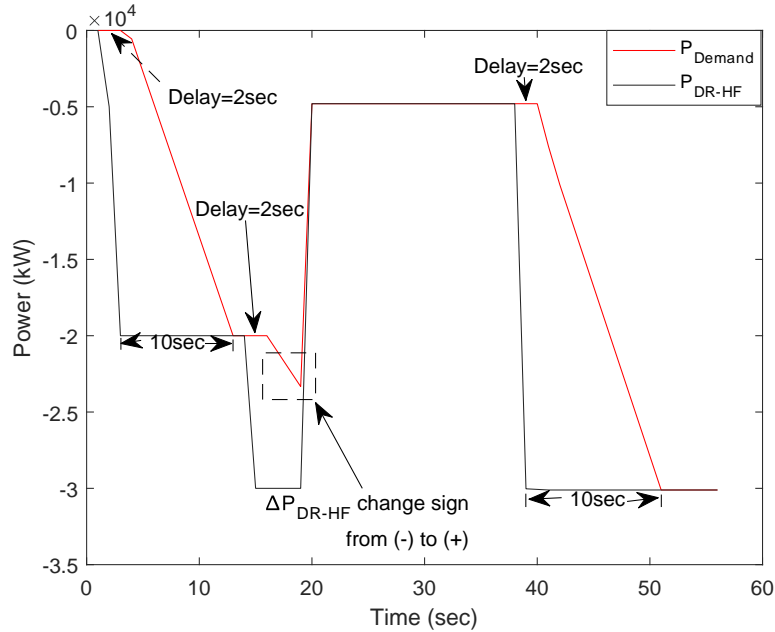
Figure. 5.5 Simulation Results of DR-HF with Dynamic Control using test inputs.

Figure 5.5 shows the simulation results of DR-HF for fast and slow responses using an illustrative example input which represents $P_{(DR-HF)}$. It can be seen that when $P_{(DR-HF)}$ increases ($\Delta P_{(DR-HF)} < 0$) then the slow control response is applied, while when ($\Delta P_{(DR-HF)} > 0$) then a fast response is used. In this methodology for DR-HF, the control is switching between ramp rates and uses the maximum allowable delay to minimize the charging power.

Dynamic Control of DR-LF

For DR-LF, the SOC_{start} will be set at higher limit (SOC_{high}=95%). The fast response will be delivered if the changing of DR-LF power ($\Delta P_{(DR-LF)} < 0$), whereas, a slow response could be implemented if ($\Delta P_{(DR-HF)} > 0$).
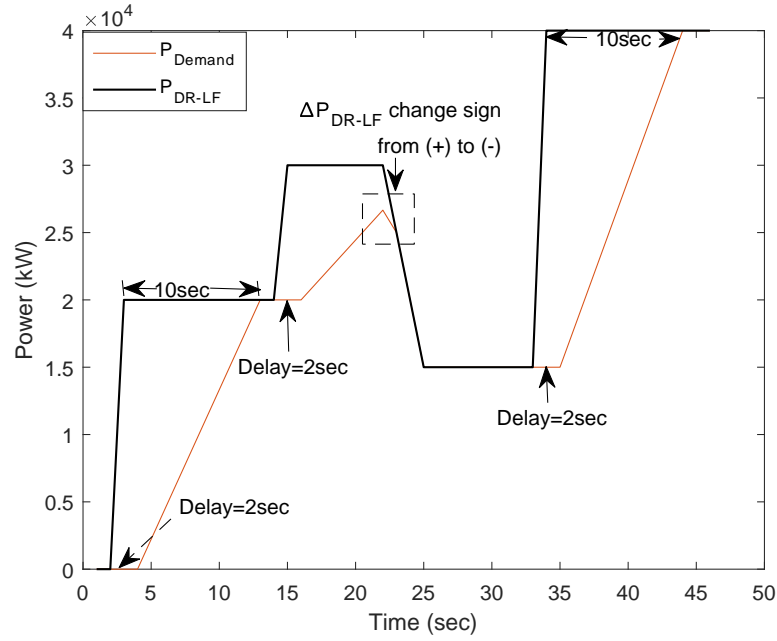
Figure. 5.6 Simulation Results of DR-LF with Dynamic Control, using test inputs.

Figure 5.6 illustrates the simulation results of DR-LF for both fast and slow responses again by using an illustrative example that represents $P_{(DR-LF)}$. It can be seen that, when $P_{(DR-LF)}$ increases ($\Delta P_{(DR-LF)} > 0$) a slow control response is applied, when ($\Delta P_{(DR-LF)} < 0$) then fast response is used. For DR-LF this means that the discharging power is minimized. The result is, that for both DR-HF and DR-LF the energy throughput is minimized over the service delivery with the aim of extending the time before the SOC limits are reached.

5.1.4 Penalty Payment

To define load profiles throughout the day, there are six Electricity Forward Agreement (EFA) blocks in 24 hours, and each EFA block represents four hours of the day [135]. These are the minimum units of time an ESS can bid to deliver a service. Each half-hour period of the day is referred to as the Settlement Period (SP) and is used as a time unit for the purposes of energy trading and balancing. To calculate the penalty payment for the service, we need to define the upper and lower bounds of the service. Based on the scenarios presented in this thesis, these correlate with the fast ($P_{DR(upper)}$) and slow ($P_{DR(lower)}$) control response. If the P_{BESS} is on or between these bounds then the error is calculated as zero. However, if P_{BESS} is outside of these bounds, then the error can be calculated by taking the difference between P_{BESS} and the upper or lower bounds [136]. The error e_m for one-time measurement and metered response (P_{BESS}) can be calculated

using eq.5.1 and implemented as shown in Figure.5.7;

$$e_m = \begin{cases} P_{DR_{(lower)}} - P_{BESS} & P_{BESS} < P_{DR_{(lower)}} \\ 0 & P_{DR_{(lower)}} \leq P_{BESS} \leq P_{DR_{(upper)}} \\ P_{BESS} - P_{DR_{(upper)}} & P_{BESS} > P_{DR_{(upper)}} \end{cases} \qquad (5.1)$$
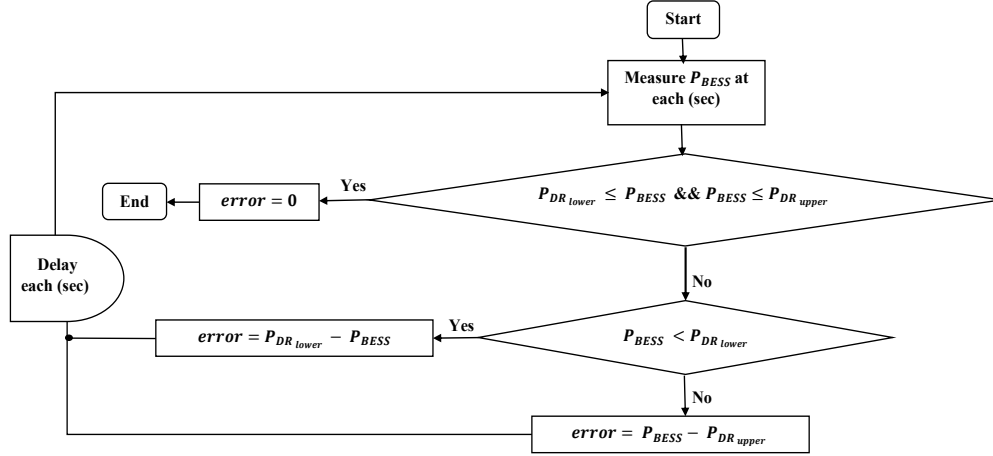
Figure. 5.7 Implemented error calculation (e_m) for DR service model.

The scaled error (es_m) for one measurement is given by

$$es_m = \frac{e_m}{P_{contract}} \qquad (5.2)$$

Where (e_m) is the calculated error, and $P_{contract}$ is the contracted quantity that the provider is contracted to deliver, in this work the example is 40MW. For each settlement period (SP), the performance score can be calculated using;

$$E = \max_m \left(\underset{over\ 2\ seconds}{rolling\_mean\ es_m} \right) \qquad (5.3)$$

and the factor for each SP, can be calculated as shown in eq.5.4

$$K_j = \begin{cases} 1 & E < A \\ 1 - \frac{E-A}{B-A} & A \leq E \leq B \\ 0 & E > B \end{cases} \qquad (5.4)$$

Where A=0.03 and B=0.07 For each contracted EFA block, the K_e factor can be calculated as shown in eq.5.5;

$$K_e = \min_j K_j \qquad (5.5)$$

The payment adjustment (K_e factor) curve is shown in Figure.5.8
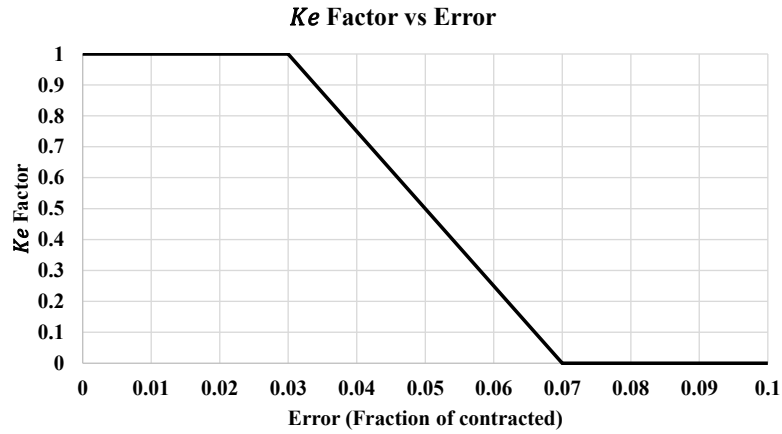
Figure. 5.8 The payment adjustment (K_e Factor) curve [136].

5.1.5 Analysis of BESS used to deliver DR-LF or DR-HF service

In this section, each service has been procured for six EFA blocks, and each two EFA blocks have been simulated back-to-back together. Two scenarios have been applied in order to examine both services (DR-LF & DR-HF) and they include;

- **(S1)** - The base case that uses a fixed delay (2 sec) and maximum ramp rate.

- **(S2)** - Using the dynamic control as previously described.

Each pair of EFA blocks has been simulated in MATLAB and to illustrate the differences in penalty payment between the two scenarios the SOC_{start} for both DR-LF and DR-HF are set to 55%, EFCs is calculated using eq.2.3, Section 2.4.3, Chapter 2, and availability is calculated using eq.4.1, Section 4.3.1, Chapter 4. The results are shown in Table 5.1 and Table 5.2.

Table. 5.1 Simulation results of DR-LF service with the two different scenarios for the first 6 EFA blocks of Dec-2019 frequency data

Number of Blocks	SOC_{start} & SOC_{end} (%)	Total Export Energy (MWh)	Avg. Availability (%)	EFCs (Cycle)	Performance score (E) for each SP	K_e Factor	scenarios
Block1	55−5.39	18.67	100	0.233	0	1	S1
	55− 7.47	17.89	100	0.224	0	1	S2
Block2	5.39−4.99	0.15	1.55	0.002	0.041	0.74	S1
	7.47−4.99	0.93	9.27	0.012	0.014	1	S2
Block3	55−26.94	10.56	100	0.132	0	1	S1
	55−29.52	9.59	100	0.119	0	1	S2
Block4	26.94−4.99	8.26	88.71	0.103	0	1	S1
	29.52−4.99	9.23	99.92	0.115	0	1	S2
Block5	55−18.69	13.66	100	0.171	0	1	S1
	55−21.75	12.50	100	0.156	0	1	S2
Block6	18.68−4.99	5.15	45.04	0.064	0	1	S1
	21.74−4.99	6.30	53.28	0.079	0	1	S2

Table 5.1 presents the simulation results that are obtained by implementing DR-LF service for the first six EFA blocks of Dec-2019 based on the two different scenarios. It can be seen that the worst scenario was S1, where a penalty payment has occurred in EFA block2 with K_e factor (0.74), this means that the providers will receive a 100% penalty payment and therefore not get paid for providing the service. In contrast, in S2 in all EFA blocks providers can get a full payment because K_e factor is equal to 1, and therefore the providers will have no penalty payment. In addition, the results show that in the EFA odd blocks (1,3, and 5) where the SOC_{start} =55% in both scenarios (S1&S2) the availability of BESS is 100%, however, in S1 the total export energy and a number of equivalent full cycles are higher compared to S2. This is because in S2 the control is minimising the export power by following the dynamic control response and it is apparent that SOC_{end} is higher compared to S1. In the EFA even blocks (2,4 and 6) where SOC_{end} = 4. 99%, the availability of BESS, average SOC, number of equivalent full cycles and export power for S1 is lower compared to S2, and this is because the SOC in S1 will reach the SOC_{lower} limit faster than S2.

Table. 5.2 Simulation results of DR-HF service with the two different scenarios for the first 6 EFA blocks of Jan-2019 frequency data

Number of Blocks	SOC_{start} & SOC_{end} (%)	Total Import Energy (MWh)	Avg. Availability (%)	EFCs (Cycle)	Performance score (E) for each SP	K_e Factor	scenarios
Block1	55−93.45	-16.34	100	0.204	0	1	S1
	55−90.52	-15.09	100	0.189	0	1	S2
Block2	93.45−95	-0.66	12.46	0.008	0.0811	0.28	S1
	90.52−95	-1.91	48.66	0.024	0	1	S2
Block3	55−79.64	-10.47	100	0.131	0	1	S1
	55−77.65	-9.63	100	0.120	0	1	S2
Block4	79.64−95	-6.53	51.27	0.082	0	1	S1
	77.65−93.77	-6.85	100	0.086	0	1	S2
Block5	55−68.24	-5.63	100	0.070	0	1	S1
	55−66.88	-5.05	100	0.063	0	1	S2
Block6	68.24−95	-11.37	53.78	0.142	0	1	S1
	66.88−95	-11.94	61.28	0.149	0	1	S2

Table 5.2 presents the simulation results of DR-HF service for the first six EFA blocks of Jan-2019 with two different scenarios. As we can see, in all EFA blocks for S2, the K_e factor is always equal to 1 which means that there is no performance payment penalty and the service is delivered according to NGET specification. However, S1 is considered the worst case, because a penalty payment occurs in EFA block2 with a K_e factor of 0.28, therefore, the providers of the service will receive a 100% penalty payment. Additionally, the results show that in the EFA odd blocks where the SOC_{start} =55%, in both scenarios the availability of BESS is 100%, however, in S1 the total import energy, and a number of equivalent full cycles are higher compared to S2. This result is due to the fact that the BESS in S2 takes longer to charge, as shown by SOC_{end} being lower compared to S1. In the EFA even blocks where SOC_{end} = 95% or 93. 77%, the availability of BESS for S1 is lower compared to S2, and this is because the SOC in S1 will hit the upper limit (95%) before it does in S2. This results in the total import energy, and the number of EFC in the EFA even blocks is higher compared to S1.

5.1.6 Simulation Results of both DR-HF & DR-LF services
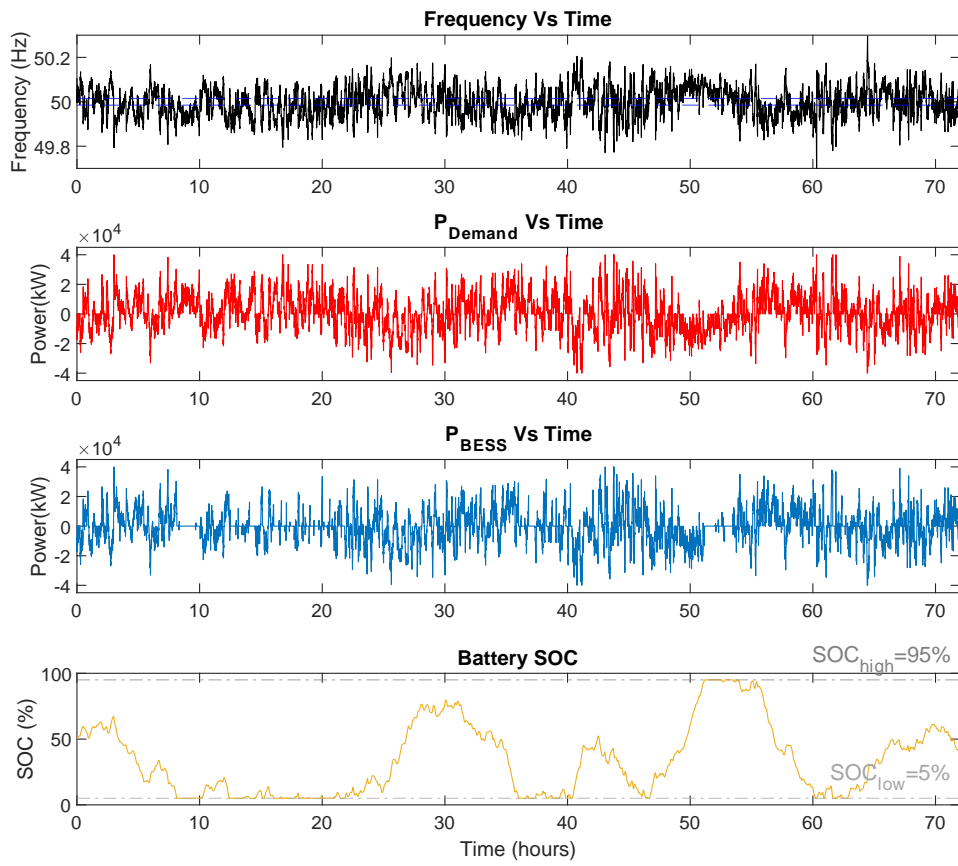
Figure. 5.9 Simulation Results of DR-HF & DR-LF Services for the first 3 days of Jan-2019 (40MW/40MWh BESS).

Figure 5.9 shows the simulation results of a BESS delivering DR-HF & DR-LF, contracted for 40MW, for the first 3 days of Jan-2019 for frequency, P_{Demand}, P_{BESS}, and SOC. In this section, SOC_{start} has been set to 50%, and the SOC limits for the BESS are SOC_{high}=95%, and SOC_{low}=5%. It can be seen that P_{Demand} and P_{BESS} are changing proportionally with change in the frequency data that is obtained from NG [114] second by second and the DB is shown as the area between the two blue dashed lines with the limits ($\pm$0.015Hz) and in this area, there is no opportunity for BESS to manage SOC, which means power equates zero. Also, it shows that both SOC_{high} and SOC_{low} are not breached in the simulation. If the BESS reaches a higher limit as it is shown in this figure, then the system can only export power and BESS will be set to zero, whereas if the BESS reaches the lower limit as it does in this figure, then the system can only import power and PBESS will be set to zero.

5.1.7 Dynamic Control of DR-LF & DR-HF

In this section, BESS has been procured for the stacking DR-LF & DR-HF services. The SOC_{start} will be set at 50%, and fast & slow response will be delivered based on the

dynamic control SOC_{higher} & SOC_{lower} setpoints. Therefore, four steps will be taken into account and they include;

1. For DR-LF delivery, the slow response will be delivered if ($\Delta P_{DR(t-1)} > 0$) && ($\Delta P_{DR(t)} > 0$) && (SOC$<SOC_{lower}$), whereas the fast response, is implemented if ($\Delta P_{DR(t-1)} < 0$) && ($\Delta P_{DR(t)} < 0$) && (SOC$<SOC_{lower}$), and the results are shown in Figure.5.10.
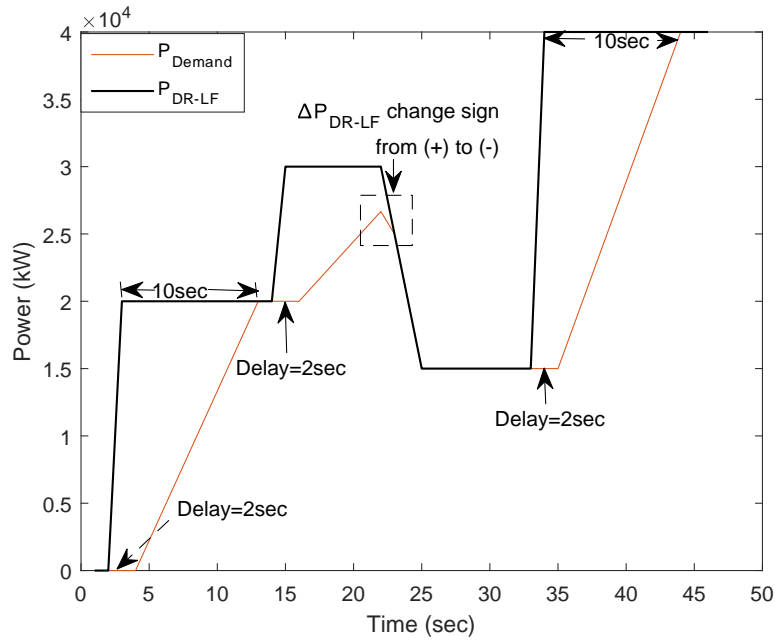
Figure. 5.10 Simulation Results of DR-LF with Dynamic Control, (SOC$<SOC_{lower}$), using test inputs.

Figure 5.10 illustrates the simulation results of DR-LF for both fast and slow responses again by using an illustrative example which represents $P_{(DR-LF)}$ when (SOC$<SOC_{lower}$). It can be seen that when $P_{(DR-LF)}$ increases ($P_{DR-LF(t-1)} > 0$) && ($\Delta P_{DR-LF(t)} > 0$) a slow control response is applied, when ($P_{DR-LF(t-1)} < 0$) && ($\Delta P_{DR-LF(t)} < 0$) then the fast response is used. For DR-LF this means that the discharging power is minimized.

2. For DR-HF delivery, the slow response will be delivered if ($\Delta P_{DR(t-1)} > 0$) && ($\Delta P_{DR(t)} > 0$) && (SOC$<SOC_{lower}$), whereas the fast response is implemented if ($\Delta P_{DR(t-1)} < 0$) && ($\Delta P_{DR(t)} < 0$) && (SOC$<SOC_{lower}$), and the results are shown in Figure 5.11.
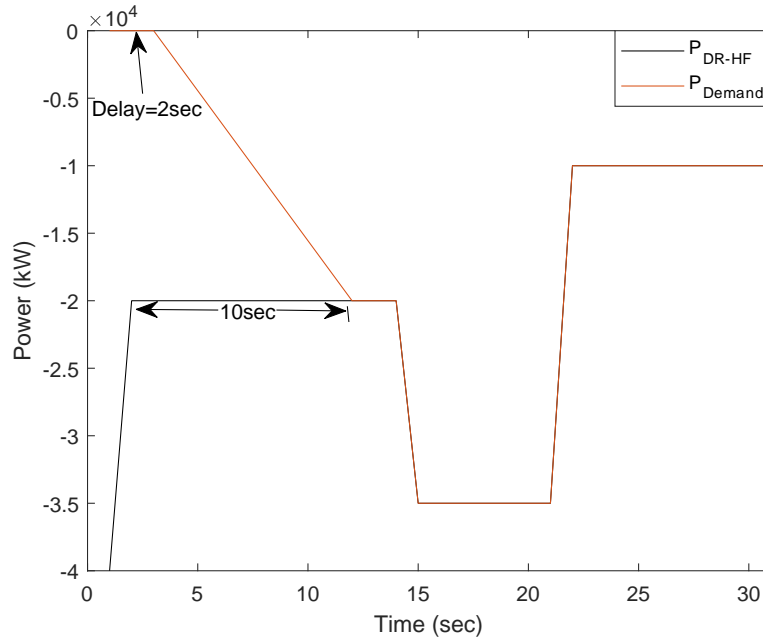
Figure. 5.11 Simulation Results of DR-HF with Dynamic Control, (SOC$<SOC_{lower}$), using test inputs.

Figure 5.11 presents the simulation results of DR-HF for both fast and slow responses by using an illustrative example input which represents the $P_{(DR-HF)}$ when SOC$<SOC_{lower}$. It can be noticed that when $P_{(DR-HF)}$ decrease which means ($P_{DR-HF(t-1)}>0$) && ($\Delta P_{DR-HF(t)}>0$) a slow control response is applied, while when ($P_{DR-HF(t-1)}<0$) && ($\Delta P_{DR-HF(t)}<0$) then the fast control response is applied. The aim of this methodology for DR-HF, control is switching between ramp rates and using the maximum allowable delay to minimise the discharging power when SOC$<SOC_{lower}$.

3. For DR-HF delivery, the slow response will be delivered if ($\Delta P_{DR(t-1)}<0$) && ($\Delta P_{DR(t)}<0$) && (SOC$>SOC_{higher}$), whereas the fast response is implemented if ($\Delta P_{DR(t-1)}>0$) && ($\Delta P_{DR(t)}>0$) && (SOC$>SOC_{higher}$), and the results are shown in Figure 5.12.
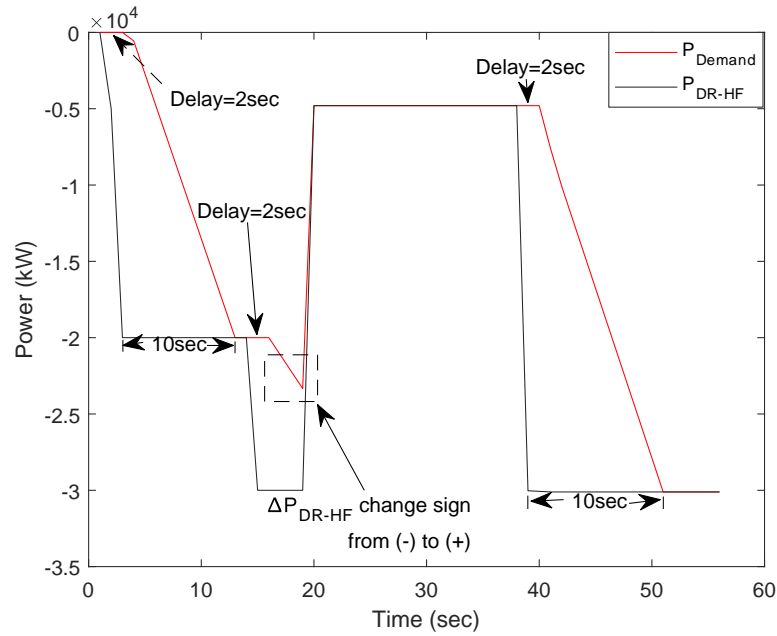
Figure. 5.12 Simulation Results of DR-HF with Dynamic Control, (SOC>SOC_{higher}), using test inputs.

Figure 5.12 shows the simulation results of DR-HF for both fast and slow responses by using an illustrative example input which represents $P_{(DR-HF)}$. It can be seen that when $P_{(DR-HF)}$ increase ($\Delta P_{(DR-HF)} < 0$) then the slow control response is applied, whereas, when ($\Delta P_{(DR-HF)} > 0$) then a fast response is used. In this methodology, the target of the dynamic control for DR-HF is to be used to minimize the charging power when SOC>SOC_{higher}.

4. For DR-LF delivery, the slow response will be delivered if ($\Delta P_{DR(t-1)} < 0$) && ($\Delta P_{DR(t)} \leq 0$) && (SOC>SOC_{higher}), whereas the fast response is implemented if ($\Delta P_{DR(t-1)} > 0$) && ($\Delta P_{DR(t)} > 0$) && (SOC>SOC_{higher}), and the results are shown in Figure 5.13.
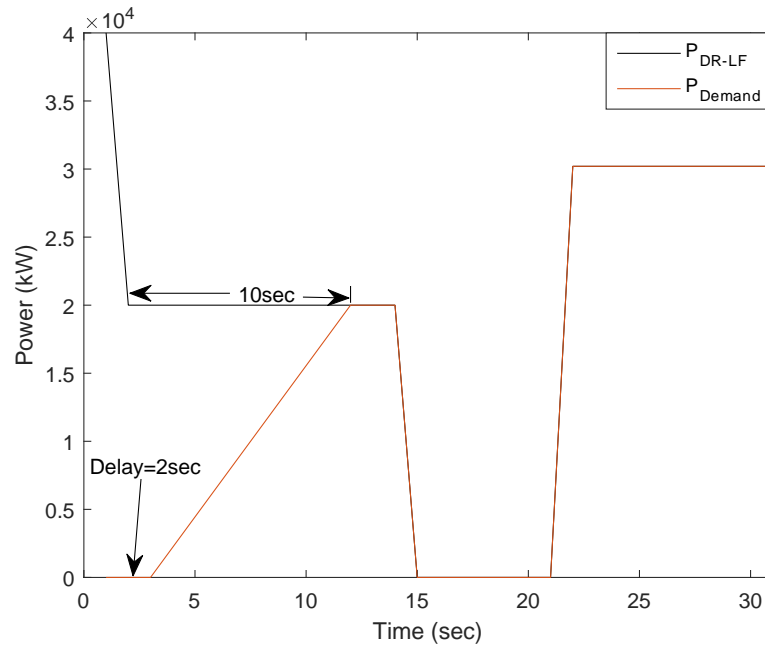
Figure. 5.13 Simulation Results of DR-LF with Dynamic Control, (SOC$>SOC_{higher}$), using test inputs.

Figure 5.13 illustrates the simulation results of DR-LF for both fast and slow responses by using an illustrative example input which represents $P_{(DR-LF)}$ when $SOC>$SOC$_{higher}$. It is clear that when $P_{(DR-LF)}$ increase (ΔP$_{(DR-HF)} >0$) then the fast control response is implemented, whereas, when (ΔP$_{(DR-LF)} <0$) then a slow response is used. This methodology aims to exploit the dynamic control for DR-HF to minimize the charging power when $SOC>$SOC$_{higher}$.

5.1.8 Analysis of the availability of BESS used to deliver DR-LF & DR-HF services based on a grouped dynamic control SOC setpoints

In this section, BESS availability has been calculated using eq.4.1 in Section 4.3.1 Chapter 4, and based on a grouped of dynamic control SOC setpoints (SOC_{higher}) & (SOC_{lower}) in order to select the optimum range of dynamic control SOC setpoints which will have high average availability. The SOC_{lower} grouped as (10%, 15%, 20%, 25%, 30%, 35%, 40%, 45%, 50%), while SOC_{higher} grouped as (45%, 50%, 55%, 60%, 65%, 70%, 75%, 80%, 85%, 90%), and the results are shown in Table 5.3 Figure 5.14.

Table. 5.3 Simulation results of average availability of BESS used to deliver DR-HF & DR-LF services based on a group of dynamic control SOC setpoints for the first 6 EFA blocks for Nov-2019 frequency data

		$SOC_{lower}(\%)$								
		10	15	20	25	30	35	40	45	50
$SOC_{higher}(\%)$	90	89.3809	89.4055	89.4310	89.4672	89.5051	89.5385	89.5595	89.5104	89.4488
	85	89.4645	89.4891	89.5139	89.5506	89.5886	89.6213	89.6340	89.5894	89.5467
	80	89.5540	89.5785	89.6033	89.6419	89.6799	89.7126	89.7218	89.6599	89.6129
	75	89.5954	89.6192	89.6439	89.6816	89.7198	89.7527	89.7660	89.7096	89.6643
	70	89.6889	89.7127	89.7381	89.7759	89.8138	89.8471	89.8561	89.7783	89.7163
	65	89.7163	89.7400	89.7647	89.8039	89.8430	89.8751	89.8886	89.8072	89.7469
	60	89.7472	89.7711	89.7965	89.8342	89.8722	89.9050	89.9159	89.8374	89.7955
	55	89.9423	89.9626	89.9882	90.0252	90.0638	90.0963	90.0764	89.9693	89.9060
	50	90.2584	90.2813	90.3090	90.3458	90.3913	90.4154	90.4177	90.0893	90.0007
	45	90.3262	90.3499	90.3775	90.4144	90.4607	90.4848	90.4879	90.1967	90.1967
	40	90.3611	90.3615	90.3620	90.3708	90.3859	90.3956	90.4160	90.2393	90.2390
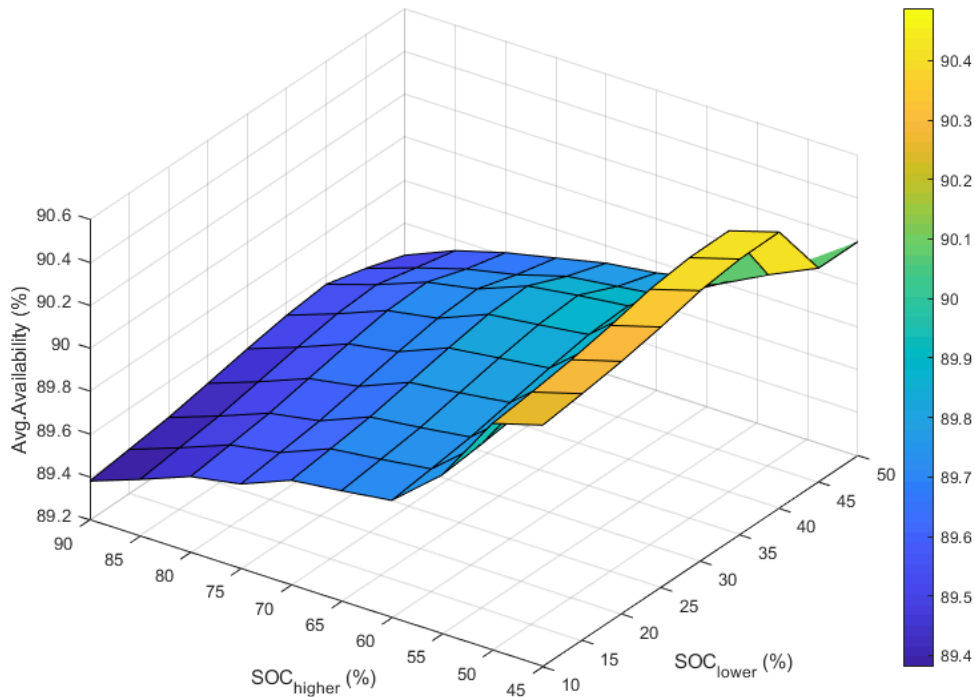
Figure. 5.14 Simulation Results of BESS used to deliver DR-HF&DR-LF with dynamic control for the first 6 EFA blocks for Nov-2019 frequency data, Avg. availability vs Dynamic Control SOC setpoint.

From Table 5.3, Figure 5.14, it is clear that, from (10% - 40%) SOC_{lower} range and at all ranges of SOC_{higher}, the average availability increases by the increase in SOC_{lower} and with the decrease in SOC_{higher} and vice versa. The highest value of average availability

was at 45% SOC_{higher} and 40% SOC_{lower} with a value equalling $\sim$ 90.49%. However, when SOC_{lower}>40% at all ranges of SOC_{higher}, the average availability was decreased gradually compared to SOC_{lower} when it was equal to 40%. Therefore, the suitable range of Dynamic control SOC setpoint is (40%SOC_{lower} - 45% SOC_{higher}).

5.1.9 Analysis of the EFCs of BESS used to deliver DR-LF & DR-HF services based on a grouped Dynamic control SOC setpoints

In this section, the number of cycles has been obtained from the EFCs counting method using eq.2.3 Subsubsection 2.4.7 Chapter 2 and based on a group of dynamic control SOC set-points which are demonstrated in Subsubsection 5.1.8, and the results are shown in Table 5.4, Figure 5.15.

Table. 5.4 The number of cycles obtained from the EFCs counting method based on grouped dynamic control SOC setpoint using BESS used to deliver DR-LF & DR-HF services with implementing dynamic control for the first 6 EFA blocks for Nov-2019 frequency data

		SOC_{lower}(%)								
		10	15	20	25	30	35	40	45	50
SOC_{higher}(%)	90	2.0559	2.0546	2.0524	2.0493	2.0489	2.0469	2.0454	2.0396	2.0356
	85	2.0559	2.0546	2.0524	2.0493	2.0489	2.0469	2.0453	2.0396	2.0357
	80	2.0559	2.0546	2.0525	2.0494	2.0489	2.0471	2.0453	2.0396	2.0357
	75	2.0557	2.0544	2.0522	2.0492	2.0487	2.0468	2.0452	2.0394	2.0355
	70	2.0557	2.0544	2.0522	2.0491	2.0487	2.0468	2.0451	2.0394	2.0355
	65	2.0557	2.0544	2.0522	2.0491	2.0487	2.0468	2.0451	2.0394	2.0355
	60	2.0551	2.0537	2.0516	2.0485	2.0481	2.0462	2.0445	2.0387	2.0348
	55	2.054	2.0533	2.0511	2.0480	2.0476	2.0457	2.0440	2.0383	2.0344
	50	2.0526	2.0515	2.0502	2.0478	2.0477	2.0459	2.0444	2.0387	2.0348
	45	2.0523	2.0512	2.0498	2.0475	2.0474	2.0456	2.0439	2.0383	2.0383
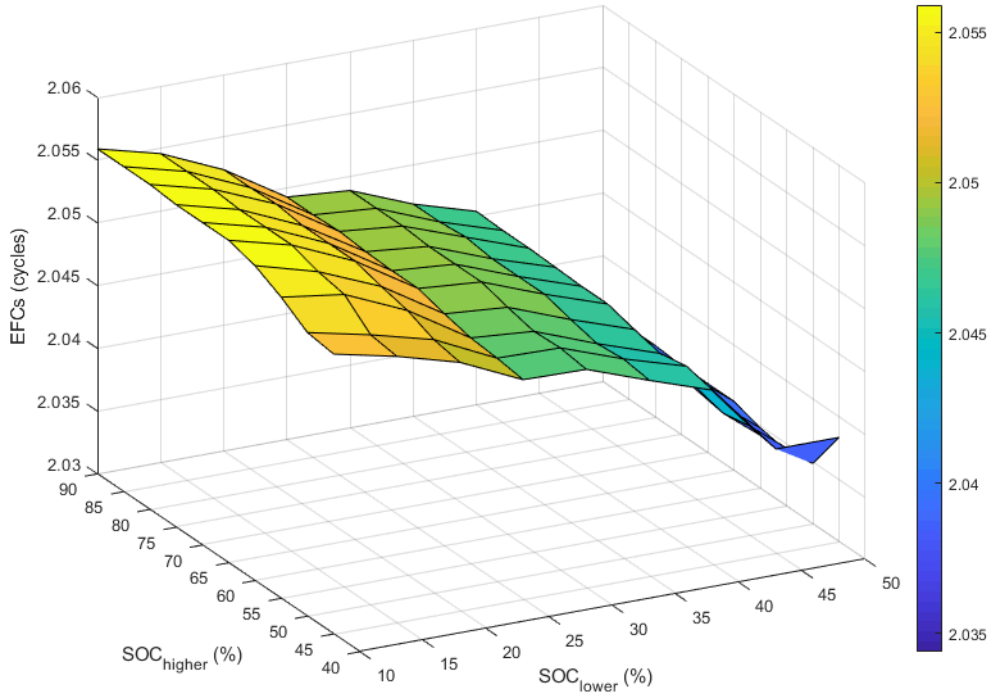
Figure. 5.15 The obtained number of cycles from EFCs for BESS used to deliver DR-HF&DR-LF with Dynamic Control, based on grouped dynamic control SOC setpoint for the first 6 EFA blocks for Nov-2019 frequency data.

From Table 5.4, Figure 5.15 it can be seen that the number of equivalent full cycles is decreased with the increase in SOC_{lower} and decrease in SOC_{higher} and vice versa. The highest number of full cycles was at SOC_{lower}= 10% and SOC_{higher}= 80%, 85%, and 90%, whereas the lowest number of full cycles was at SOC_{lower}= 50% and SOC_{higher}= 50%. However, based on the results that are obtained from Section 5.1.10, the availability of BESS in this region was lower compared to the region which is (SOC_{lower}= 40% and SOC_{higher}= 45%). When it comes to the revenue, the higher availability is more important than the higher number of full cycles for example; if we have BESS (Li-ion) with a capacity of 40MWh, a total number of cycles (10,000 cycles), and Purchase Cost (£200/kWh), this value includes the other costs such as; battery inverter (£/kW), electrical balancing of the system (BOS) (£/kW), Structural balancing of the system (BOS) (£/kW), operation and maintenance (O & M) (£/kW-yr). The BESS cost per cycle can be calculated using;

$$\text{Cost per cycle} = \frac{Cost\,of\,BESS\,(\pounds/MWh)}{Number\,of\,cycles\,(cycle)} \tag{5.6}$$

$$= \frac{\pounds 200/kWh \times 40MWh}{10,000\,cycle} \qquad = \frac{\pounds 8,000,000}{10,000\,cycle}$$

$$= \pounds 800/cycle$$

131

As we discussed above the highest number of cycles for the first 6 EFA blocks for Nov-2019 was 2.0559 cycle, therefore;

the cost per cycle/day=£800/cycle x 2.0559 cycle=£1,644.72

In case of availability, we assume that the capacity of BESS is still the same as in the above example, and it is used to deliver DR- HF & DR-LF services for the first 6 EFA blocks for Nov-2019, and DR service price for year-2022 is (£19.37/MW) [137], So the revenue can be calculated using;

$$Revenue = Contracted\,Volume(MW) \times Service\,Price(\pounds/MW/Hour) \times$$
$$24 Hour \times Days\,of\,month \quad (5.7)$$

$$Revenue = 40MW \times (\pounds19.37/MW)/Hour \times 24 Hours \times 1$$
$$= \pounds18,595.2$$

Therefore, based on the obtained results, we can decide that the highest availability is more important than the highest number of cycles, so the range which is SOC_{lower}= 40% and SOC_{higher}= 45% will be considered as in this thesis when it comes to calculating the number of cycles.

5.1.10 Analysis of BESS used to deliver DR-LF & DR-HF services

In this section, each service has been procured for six EFA blocks, and each two EFA blocks have been simulated back-to-back together. Two scenarios are applied as they have been explained in Section 5.1.5 in order to examine the stacking of both services (DR-LF & DR-HF), Each pair of EFA blocks has been simulated in MATLAB and to illustrate the differences between the two scenarios, the SOC_{start} for the stacking of DR$-$LF and DR$-$HF are set to different values (30%, 50%, 70%), and dynamic control SOC setpoints are set to (SOC_{higher}=45%), and (SOC_{lower}=40%), the results are shown in Table 5.5, Table 5.6, Table 5.7, Figure 5.16, and (Figure A1, Figure A2, see Appendix C).

Table. 5.5 Simulation results of DR-HF & DR-LF services with the two different scenarios for the first 6 EFA blocks for Dec-2019 frequency data, SOC_{start}=50%

Number of Blocks	SOC_{start} & SOC_{end} (%)	Total Import Energy (MWh)	Total Export Energy (MWh)	Avg. Availability (%)	EFCs	Performance score (E) for each SP	K_e Factor	scenarios
Block1	50 − 27.77	-11.63	18.67	100	0.379	0	1	S1
	50 − 29.06	-11.32	18.17	100	0.373	0	1	S2
Block2	27.77−5.46	-8.93	16.30	99.58	0.315	0	1	S1
	29.06−5.48	-8.87	16.47	99.72	0.334	0	1	S2
Block3	50−49.18	-11.58	10.56	100	0.277	0	1	S1
	50−49.86	-11.22	10.29	100	0.269	0	1	S2
Block4	49.18−70.85	-21.42	10.83	100	0.403	0	1	S1
	49.87−68.73	-19.78	10.78	100	0.382	0	1	S2
Block5	50−53.63	-16.97	13.66	100	0.383	0	1	S1
	50−54.67	-15.71	13.59	100	0.366	0	1	S2
Block6	53.62−57.55	-19.34	15.66	100	0.438	0	1	S1
	54.66−54.85	-18.25	15.57	100	0.423	0	1	S2

Table. 5.6 Simulation results of DR-HF & DR-LF services with the two different scenarios for the first 6 EFA blocks for Dec-2019 frequency data, SOC_{start}=30%

Number of Blocks	SOC_{start} & SOC_{end} (%)	Total Import Energy (MWh)	Total Export Energy (MWh)	Avg. Availability (%)	EFCs	Performance score (E) for each SP	K_e Factor	scenarios
Block1	30−15.60	-11.63	15.72	98.90	0.342	0	1	S1
	30−15.58	-11.59	15.69	99.14	0.341	0	1	S2
Block2	15.61−5.46	-8.93	11.73	95.89	0.258	0	1	S1
	15.58−5.48	-8.88	11.67	96.78	0.257	0	1	S2
Block3	30−29.18	-11.58	10.56	100	0.277	0	1	S1
	30−31.76	-11.51	9.59	100	0.264	0	1	S2
Block4	29.19−50.85	-21.42	10.83	100	0.403	0	1	S1
	31.77−53.27	-21.31	10.77	100	0.388	0	1	S2
Block5	30−33.63	-16.97	13.66	100	0.383	0	1	S1
	30−34.31	-16.41	13.30	100	0.371	0	1	S2
Block6	33.62−37.55	-19.34	15.66	100	0.4375	0	1	S1
	34.31−39.16	-18.99	15.12	100	0.426	0	1	S2

Table. 5.7 Simulation results of DR-HF & DR-LF services with the two different scenarios for the first 6 EFA blocks for Dec-2019 frequency data, SOC_{start}=70%

Number of Blocks	SOC_{start} & SOC_{end} (%)	Total Import Energy (MWh)	Total Export Energy (MWh)	Avg. Availability (%)	EFCs	Performance score (E) for each SP	K_e Factor	scenarios
Block1	70 −47.77	-11.63	18.67	100	0.379	0	1	S1
	70−44.52	-11.04	18.59	100	0.370	0	1	S2
Block2	47.78−18.64	-8.93	18.87	100	0.348	0	1	S1
	44.53−19.04	-8.55	18.47	100	0.338	0	1	S2
Block3	70−69.18	-11.58	10.56	100	0.277	0	1	S1
	70−67.70	-10.52	10.49	100	0.263	0	1	S2
Block4	69.19−85.13	-18.99	10.83	98.69	0.373	0	1	S1
	67.71−84.76	-19.76	10.78	99.97	0.382	0	1	S2
Block5	70−69.38	-15.17	13.66	97.29	0.360	0	1	S1
	70−69.53	-15.12	13.59	98.90	0.359	0	1	S2
Block6	69.37−73.30	-19.34	15.66	96.01	0.438	0	1	S1
	69.52−71.23	-18.25	15.57	97.95	0.423	0	1	S2

(a) BLOCK1&2

(b) BLOCK3&4

(c) BLOCK5&6
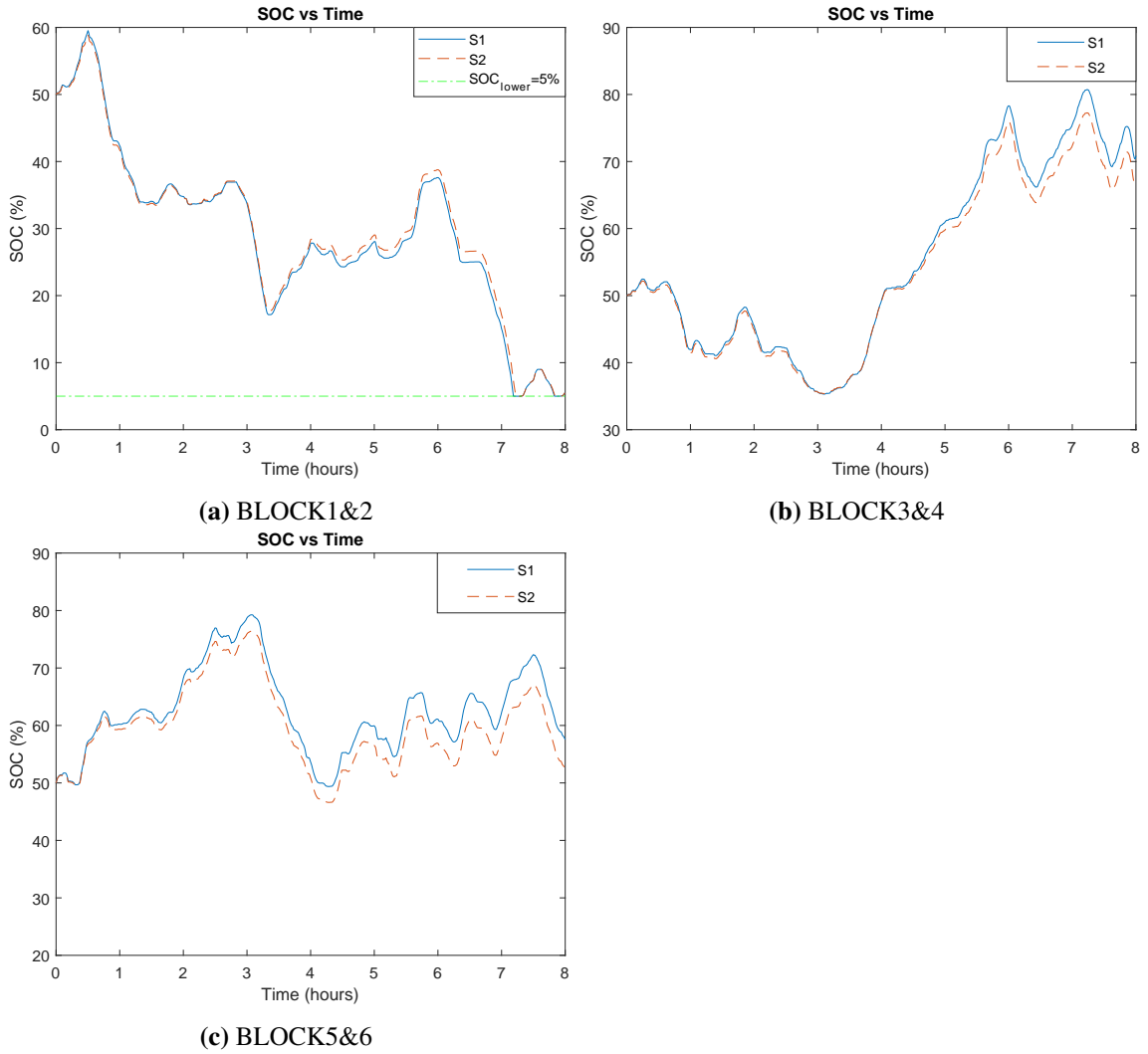
Figure. 5.16 Simulation results for battery SOC for different scenarios (S1&S2) for the first six EFA blocks of Dec-2019 frequency data, SOC_{start}=50%.

Figure 5.16, Table 5.5, Table 5.6, and Table 5.7 present the simulation results that are obtained by implementing both DR-LF & DR-HF services for the first six EFA blocks of Dec-2019 based on the two different scenarios (S1 & S2). From all these Tables, it can be noticed that, in all scenarios, the penalty payment has not occurred at any EFA blocks because the K_e factor equates to (1), which means that the providers can get a full payment. In addition to that, the obtained results that are shown in the EFA odd blocks (1, 3 and 5) for all different SOC_{start} illustrate that at S2, the total export/import energy is minimized over the time compared to S1, and this has led to decrease the total number of cycles that are obtained from EFCs, and the main reason behind this is that the implemented dynamic control has allowed more time for BESS to be charged or discharged. Moreover, from Table 5.6, the results show that in all EFA odd blocks where the SOC_{start} =50% in both scenarios (S1&S2) the average availability of BESS is 100%, whereas, at the same EFA blocks and for SOC_{start} =30%, the average availability for BESS reaches 100% for the EFA blocks 3 & 5 but for EFA block1 at S1, it equates to almost 98.90%, and for S2, it was increased to approximately 99.14%, when SOC_{start}

135

=70%, the battery reach 100% of average availability for both scenarios at EFA blocks (1 & 3) but for block5, at (S1) it was $\sim$ 97.29% and it increased to almost 98.90% for S2.

In the EFA even blocks (2, 4, and 6), for SOC_{start}=50%, the average availability of BESS reached 100% except for block2 it was with almost 99.58% for S1, and it increased to $\sim$99.72, however, for SOC_{start}=30%, the average availability was equated to 100% for both S1 & S2, for EFA blocks (4 & 6), but for block2, it equates to almost 95.89% for S1, and it increased to approximately 96.78%, and for SOC_{start}=70%, BESS has reached 100% of average availability at only EFA block2 the main reason why BESS did not reach 100% of average availability for the first and second EFA blocks although a dynamic control has been applied is that the battery reached (SOC_{lower}=5%) which made it unavailable for a certain time.

5.2 Battery aging and DR Service Model

In this section, the two different types of cycle counting methodologies which include; CCM with the algorithm shown in Figure 2.7, Subsubsection 2.4.2, Chapter 2, and EFCs which is explained and calculated using eq.2.3 in Subsubsection 2.4.3, Chapter 2 are used herein to calculate the number of cycles obtained from BESS used to deliver DR service based on two different scenarios (S1 & S2, as explained in Subsubsection 5.1.5) for Jan-2019 frequency data, and dynamic control SOC setpoints are set to (SOC_{higher}=45%), and (SOC_{lower}=40%) as discussed in Subsubsection 5.1.9. These cycle counting methods are assessed by studying the effects of only C-rate, and both C-rate & SOC on the battery lifetime. The process of implementation of such methods is the same as discussed in Chapter 4.

5.2.1 EFCs

In this section, the EFCs is calculated using eq.2.3 and explained in Subsubsection 2.4.2, Chapter 2. This method is used herein to present the subjected number of full cycles for BESS used to deliver DR service based on S1 & S2 using real grid frequency data for Jan-2019 [114].

Simulation Results of DR Service Model for Jan-2019 Frequency data

In this thesis, once the total energy throughput is obtained from the simulation results of BESS delivered DR service then using eq.2.3 in Subsubsection 2.4.3, Chapter 2 in order to calculate the generic number of cycles then utilising the manufacturer cycling (12,000 cycles for LTO battery) and using eq.2.4 to calculate battery degradation rate with the results shown in Table 5.8, and Table 5.9.

Table. 5.8 The results regarding the number of full cycles achieved by EFCs and the degradation rate were obtained using the Miner Rule's Method for an LTO battery that had undergone 12,000 cycles(manufacturer cycling) used to deliver DR service for different scenarios (S1 & S2) for **the full of Jan-2019** frequency data, 40MWh profile

Scenarios	Total Import Energy (MWh)	Total Export Energy (MWh)	Total no of Cycles (cycle)	LTO battery degradation(%)
S1	-3,034.67	2,675.27	71.37	0.59475
S2	-2,973.72	2,622.00	69.95	0.58292

Table. 5.9 The results regarding the number of full cycles achieved by EFCs and the degradation rate were obtained using the Miner Rule's Method for an LTO battery that had undergone 12,000 cycles(manufacturer cycling) used to deliver DR service for different scenarios (S1 & S2) for **the whole year of 2019** frequency data, 40MWh profile

Scenarios	Total Import Energy (MWh)	Total Export Energy (MWh)	Total no of Cycles (cycle)	LTO battery degradation(%)
S1	-33,263.91	29,439.85	783.79	6.53158
S2	-32,622.31	28,873.94	768.70	6.40583

5.2.2 The effects of C-rate on battery degradation

In this section, the EFCs counting method that is calculated using eq.2.3 which is shown in Subsubsection 2.4.3, Chapter 2 has been improved by considering the effects of grouped C-rates (0.1C, 0.3C, and 0.5C) on the battery lifetime analysis with the scheme shown in Figure 4.10, and the methodology is described in Section 4.5.3, Chapter 4. In this section, when the approximate number of full cycles is obtained then use eq.4.3, Subsubsection 4.5.3, Chapter 4 to calculate the battery degradation rate for considering the only effect of C-rate on the battery lifetime.

Simulation results of the EFCs with considering the effects of C-rate on battery lifetime delivered DR service based on the two different scenarios (S1 & S2) for Jan-2019 frequency data

In this section, the proposed EFCs counting method was used to calculate the number of full cycles for the LTO battery based on the grouped C-rates used to deliver DR service for S1 & S2 for Jan-2019. To calculate LTO battery degradation, as discussed in Subsubsection 4.4, Chapter 4, the two proposed cycling data will be considered herein, (Data1) which is about to consider the number of cycles constant and equates to 12,000 cycles for each cycle, while (Data2) is regarding the assumed number of cycles is varied for each C-rate as it's shown in Figure 4.6, then used eq.(4.3). The obtained results of

the number of cycles and LTO battery degradation rate using (Data2) are shown in Table 5.10, Table 5.11, and Table 5.12.

Table. 5.10 The number of cycles and degradation findings obtained from the EFCs counting method under different C-rates for BESS used to deliver DR service based on the two different scenarios (S1 & S2) for Jan-2019 frequency data, SOC_{start}=50%

C-rate (C)	Total Import Energy (MWh)	Total Export Energy (MWh)	No of Cycles (cycle)	LTO battery degradation (%)	Scenarios
C≤ 0.1	-53.74	45.56	1.241	0.0056	S1
	-59.92	43.59	1.294	0.0059	S2
0.1C< C ≤ 0.3C	-501.38	472.34	12.172	0.0641	S1
	-548.42	440.59	12.363	0.0651	S2
0.3C<C ≤ 0.5C	-681.23	743.10	17.804	0.1047	S1
	-735.61	662.93	17.468	0.1028	S2

Table. 5.11 The number of cycles and degradation findings obtained from the EFCs counting method under different C-rates for BESS used to deliver DR service with implementing dynamic control (S1 & S2) for Jan-2019 frequency data, SOC_{start}=30%

C-rate (C)	Total Import Energy (MWh)	Total Export Energy (MWh)	No of Cycles (cycle)	LTO battery degradation (%)	Scenarios
C≤ 0.1	-57.52	40.95	1.2309	0.0056	S1
	-59.89	43.65	1.2943	0.0058	S2
0.1C< C ≤ 0.3C	-543.01	420.73	12.0467	0.0634	S1
	-548.77	438.65	12.3428	0.0649	S2
0.3C<C≤ 0.5C	-737.69	664.45	17.5269	0.1031	S1
	-736.25	659.63	17.4484	0.1026	S2

Table. 5.12 The number of cycles and degradation findings obtained from the EFCs counting method under different C-rates for BESS used to deliver DR service based on (S1 & S2) for Jan-2019 frequency data, SOCstart= 70%

C-rate (C)	Total Import Energy (MWh)	Total Export Energy (MWh)	No of Cycles (cycle)	LTO battery degradation (%)	Scenarios
C≤ 0.1	-57.46	41.34	1.235	0.0056	S1
	-59.92	43.83	1.297	0.0059	S2
0.1C< C ≤ 0.3C	-542.92	426.06	12.112	0.0638	S1
	-548.32	443.55	12.398	0.0653	S2
0.3C<C ≤ 0.5C	-737.70	672.47	17.627	0.1037	S1
	-735.61	666.98	17.532	0.1031	S2

Table 5.10, Table 5.11, and Table 5.12 present the simulation results for the number of cycles obtained from EFCs and degradation rates, considering the effects of different C-rates on the lifetime of LTO batteries used to deliver DR services for two different scenarios (S1 & S2) throughout Jan-2019, with different SOC_{start} levels (50%, 30%, and 70%). In all cases of SOC_{start}, it is evident that for both S1 and S2, the highest number of cycles and total degradation rates occurred in the C-rate range of When comparing all SOC_{start} levels, for scenario S1, within the C-rate range of $0.3 < C \leq 0.5$.

At an SOC_{start} of 50% in scenario S1, the number of cycles and degradation rate were approximately 17.804 cycles and 0.1047%, respectively. However, in scenario S2, these values decreased by almost 1.91% and 1.83%, respectively. In the case of an SOC_{start} of 30% at the same C-rate, for S1, the number of cycles and degradation rate was ∼ 17.5269 cycles and 0.1031%, respectively, while for S2, these values decreased by 0.45% and 0.49%, respectively. Additionally, at an SOC_{start} of 70%, for S1, the number of cycles and degradation rate was approximately 17.627 cycles and 0.1037%, respectively, while in S2, these values decreased by almost 0.54% and 0.58%, respectively.

This indicates that BESS mostly operates in these regions, with a higher proportion of its operation time spent in S1. This is because, in S2, a dynamic control mechanism has been used to extend the charge/discharge time for the battery, minimising energy throughput, reducing the total number of cycles, decreasing battery degradation, and extending the battery's lifetime.

In all cases of SOC_{start}, the lowest number of cycles and battery degradation rates for both scenarios (S1 & S2) were observed at C-rates less than or equal to 0.1C.

At an SOC_{start} of 50%, for S1, the number of cycles and degradation rate were ∼ 1.241 cycles and 0.0056%, respectively. However, for S2, these values increased by almost 4.18% and 5.23%, respectively. In the case of an SOC_{start} of 30%, for S1, at the same C-rate, these values were approximately 1.2309 cycles and 0.0056%, respectively, while for S2, they increased by approximately 5.02% and 3.51%, respectively. Moreover,

at an SOC_{start} of 70%, for S1, at the same C-rate, the number of cycles and degradation rate was almost 1.235 cycles and 0.0056%, respectively, whereas, for S2, they increased by approximately 4.89% and 5.21%, respectively. This suggests that BESS rarely operates in this region, but it spends more time operating in S2 compared to S1.

When comparing all SOC_{start} levels, for S1, in the C-rate range of When comparing all SOC_{start} levels, for scenario S1, within the C-rate range of $0.3 < C \leq 0.5$, the number of cycles at an SOC_{start} of 50% was almost 1.57% higher than at 30% and 1% higher than at 70%. For S2, it increased by approximately 0.11% compared to 30% but decreased by almost 0.37% compared to 70%.

For S1, in the C-rate range of $\leq 0.1C$, the number of cycles at an SOC_{start} of 50% showed a slight increase of approximately 0.82% and 0.49% compared to 30% and 70%, respectively. In the case of S2, it remained the same as 30% but decreased by 0.23% compared to 70%.

5.2.3 The effects of both C-rate & SOC on battery Degradation

In this section, the proposed EFCs counting method has been improved by considering the effects of both C-rate & SOC on battery lifetime. The scheme of such a method is shown in Figure 4.11. As we have discussed in Subsubsection 4.5.4, Chapter 4, the C-rate was grouped by (0.1C, 0.3C, 0.5C) while SOC was grouped by 10% of SOC in order to calculate the number of equivalent full cycles at each range of C-rate and SOC. When the number of equivalent full cycles is obtained then the battery degradation rate for considering both C-rate and SOC can be calculated using eq.4.4; Subsubsection 4.5.4, Chapter 4.

Simulation Results of the EFCs with considering the effects of both C-rate & SOC on Battery Lifetime used to deliver both DR services based on (S1 & S2)

In this section, after obtaining the number of full cycles by considering the effects of both C-rate & SOC for BESS was used to deliver DR service based on S1 & S2 for Jan-2019, SOC_{start} = (50%, 30% & 70%), then the assumed number of cycles for LTO battery which is shown in Table 4.5, Subsubsection 4.4, Chapter 4 is used to calculate the battery degradation rate by using eq.4.4; Subsubsection 4.5.4, Chapter 4. The obtained results are shown in the below Figures [5.18 - 5.23], and Tables [5.14 - 5.25]. 5.20).

Table. 5.13 Number of cycles obtained from (EFCs) counting method for different C-rates and grouped of SOC battery used to deliver DR service based on (S1) for Jan-2019 frequency data, $SOC_{start} = 50\%$

		C-rate (C)								
		C ≤ 0.1			**0.1<C ≤ 0.3**			**0.3<C ≤ 0.5**		
		Total Imp. Energy (MWh)	Total Exp. Energy (MWh)	No.of Cycles (Cycle)	Total Imp. Energy (MWh)	Total Exp. Energy (MWh)	No.of Cycles (Cycle)	Total Imp. Energy (MWh)	Total Exp. Energy (MWh)	No.of Cycles (Cycle)
SOC(%)	≤ 10	-14.12	4.37	0.2311	-96.38	46.34	1.784	-72.42	73.64	1.8258
	10-20	-8.89	6.17	0.1883	-83.56	67.01	1.8821	-116.61	105.03	2.7705
	20-30	-5.65	5.62	0.1409	-67.95	60.79	1.6093	-94.95	88.24	2.2899
	30-40	-5.70	5.97	0.1459	-52.23	53.62	1.3231	-86.42	80.64	2.0883
	40-50	-5.03	5.69	0.1340	-54.24	55.41	1.3706	-93.88	79.06	2.1618
	50-60	-4.83	4.21	0.1130	-50.42	44.64	1.1883	-76.49	71.28	1.8471
	60-70	-5.55	3.28	0.1104	-52.72	34.09	1.0851	-70.91	58.31	1.6153
	70-80	-4.99	2.64	0.0954	-47.07	28.58	0.9456	-54.73	51.96	1.3336
	80-90	-4.29	4.22	0.1064	-43.49	35.37	0.9858	-59.15	51.55	1.3838
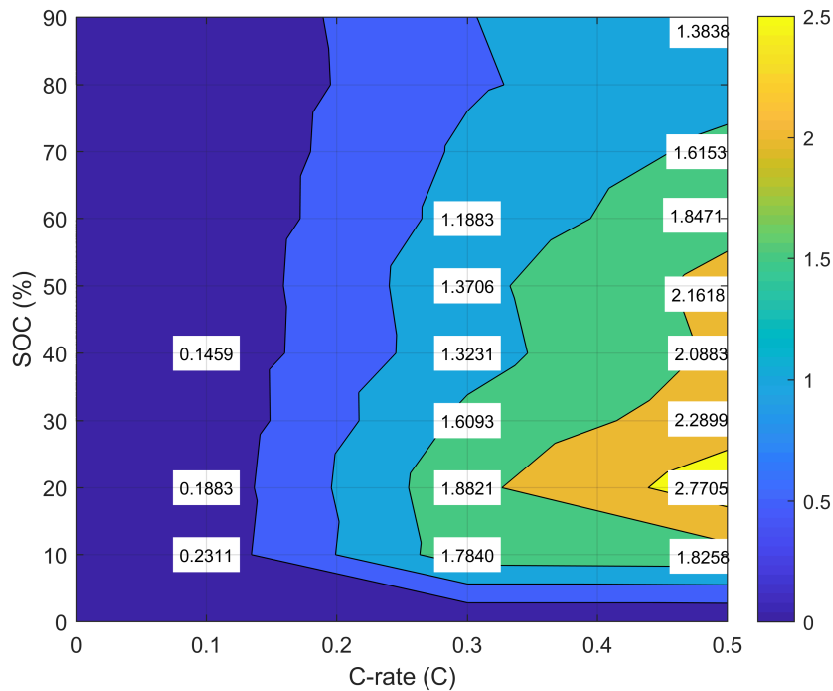
Figure. 5.17 Simulation results of the EFCs based on different C-rates for each grouped SOC for DR model without implementing dynamic control (S1) for Jan-2019, SOC_{start}=50%. (Maximum scale is 2.7705 cycles).

Table. 5.14 Degradation results obtained from the EFCs under different C-rate values and grouped SOC battery delivering DR service based on (S1) for Jan-2019 frequency, data$SOC_{start} = 50\%$

		C-rate (C)		
		C≤ 0.1	0.1<C≤ 0.3	0.3<C≤ 0.5
SOC(%)	≤ 10	0.0009	0.0076	0.0085
	10 - 20	0.0007	0.0082	0.0132
	20 - 30	0.00055	0.0072	0.0112
	30 - 40	0.00058	0.0060	0.0104
	40 - 50	0.00054	0.00638	0.01109
	50 - 60	0.00047	0.0057	0.00972
	60 - 70	0.00047	0.00529	0.00873
	70 - 80	0.00041	0.00473	0.00741
	80 - 90	0.00047	0.00506	0.00791

Total of LTO battery degradation rate = 0.14941%

Table. 5.15 Number of cycles obtained from (EFCs) counting method for different C-rates and grouped of SOC battery used to deliver DR service based on (S2) for Jan-2019 frequency data, $SOC_{start} = 50\%$

		C-rate (C)								
		C ≤ 0.1			**0.1<C ≤ 0.3**			**0.3<C ≤ 0.5**		
		Total Imp. Energy (MWh)	Total Exp. Energy (MWh)	No.of Cycles (Cycle)	Total Imp. Energy (MWh)	Total Exp. Energy (MWh)	No.of Cycles (Cycle)	Total Imp. Energy (MWh)	Total Exp. Energy (MWh)	No.of Cycles (Cycle)
SOC(%)	≤ 10	-13.27	5.22	0.23109	-91.83	49.23	1.7632	-67.08	70.94	1.7253
	10-20	-8.91	6.92	0.19783	-82.81	67.48	1.8786	-112.88	101.88	2.6844
	20-30	-5.82	6.53	0.15429	-73.13	64.66	1.7224	-89.92	87.22	2.2142
	30-40	-5.87	7.37	0.16551	-57.27	64.19	1.5182	-98.65	86.44	2.3136
	40-50	-5.93	5.76	0.14614	-58.19	56.59	1.4349	-95.00	81.29	2.2038
	50-60	-5.70	4.04	0.12179	-52.29	45.77	1.2258	-74.07	67.25	1.7665
	60-70	-5.85	2.96	0.11008	-53.00	31.51	1.0564	-67.82	56.49	1.5539
	70-80	-4.96	2.49	0.09321	-42.44	27.09	0.8692	-58.69	48.22	1.3364
	80-90	-4.89	3.58	0.10593	-40.91	35.06	0.9497	-56.16	51.99	1.3519
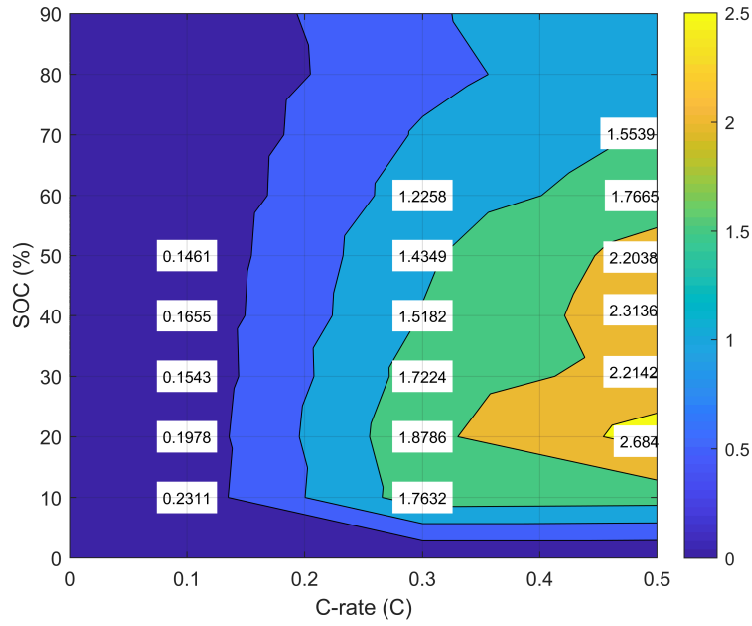
Figure. 5.18 Simulation results of the EFCs based on different C-rates for each grouped SOC for DR model with implementing a dynamic control (S2) for Jan-2019, SOC$_{start}$=50%. (Maximum scale is 2.6844 cycles).

Table. 5.16 Degradation results obtained from the EFCs base on different C-rate values and grouped SOC battery delivering DR with implementing a dynamic control (S2) for Jan-2019 frequency data, $SOC_{start} = 50\%$

		C-rate (C)		
		C$\leq$ 0.1	0.1<C$\leq$ 0.3	0.3<C$\leq$ 0.5
SOC(%)	$\leq$ 10	0.000872	0.007503	0.008025
	10 - 20	0.000761	0.008168	0.012783
	20 - 30	0.000605	0.007655	0.010801
	30 - 40	0.000662	0.006901	0.011568
	40 - 50	0.000596	0.006674	0.011302
	50 - 60	0.000507	0.005837	0.009297
	60 - 70	0.000468	0.005153	0.008399
	70 - 80	0.000405	0.004346	0.007424
	80 - 90	0.000471	0.004870	0.007725

Total of LTO battery degradation rate = 0.14978%

143

Table. 5.17 Number of cycles obtained from (EFCs) counting method based on different C-rate values and grouped of SOC battery used to deliver DR service without dynamic control (S1) for Jan-2019 frequency data, SOC_{start}=30%

		C-rate (C)								
		C ≤ 0.1			**0.1<C ≤ 0.3**			**0.3<C ≤ 0.5**		
		Total Imp. Energy (MWh)	Total Exp. Energy (MWh)	No.of Cycles (Cycle)	Total Imp. Energy (MWh)	Total Exp. Energy (MWh)	No.of Cycles (Cycle)	Total Imp. Energy (MWh)	Total Exp. Energy (MWh)	No.of Cycles (Cycle)
SOC(%)	≤ 10	-14.42	4.39	0.2354	-96.46	46.86	1.7916	-72.78	73.84	1.8328
	10-20	-8.91	6.21	0.1889	-85.28	67.42	1.9088	-117.44	106.87	2.8039
	20-30	-5.49	5.64	0.1392	-66.97	59.85	1.5853	-93.78	87.13	2.2613
	30-40	-6.08	6.12	0.1525	-55.24	54.87	1.3764	-91.02	82.83	2.1730
	40-50	-5.24	5.57	0.1352	-56.04	53.82	1.3732	-95.12	79.09	2.1776
	50-60	-4.35	4.00	0.1044	-46.11	42.38	1.1061	-71.89	65.72	1.7202
	60-70	-5.31	3.28	0.1074	-50.93	33.84	1.0595	-69.66	56.95	1.5827
	70-80	-4.99	2.64	0.0954	-47.08	28.58	0.9457	-54.73	51.96	1.3336
	80-90	-4.29	4.22	0.1063	-43.48	35.37	0.9856	-59.16	51.55	1.3839
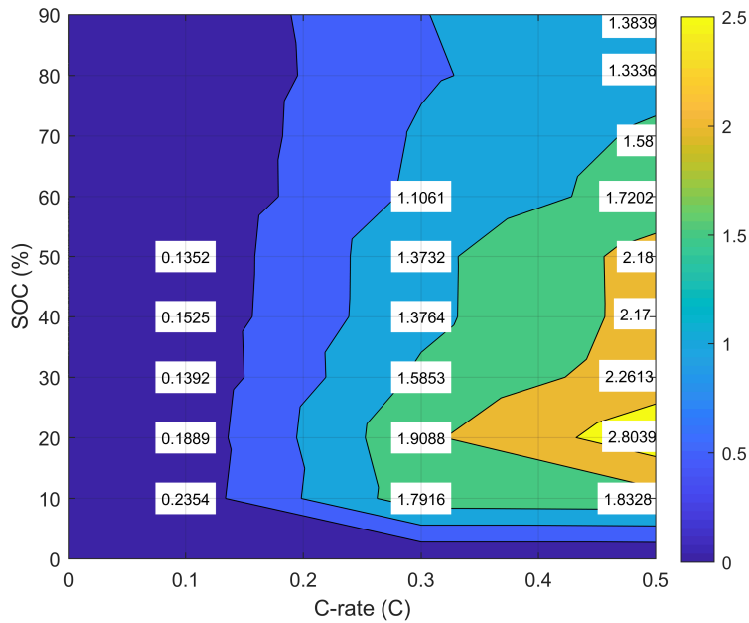
Figure. 5.19 Simulation results of the EFFs based on different C-rate for each grouped SOC for the DR model with implementing dynamic control (S1) for Jan-2019, SOC_{start}=30%. (Maximum scale is 2.8039 cycles).

Table. 5.18 Degradation results obtained from the EFCs based on different C-rate values and grouped SOC battery delivering DR service without dynamic control (S1) for Jan-2019 frequency data, $SOC_{start} = 30\%$

		C-rate (C)		
		C≤ 0.1	0.1<C≤ 0.3	0.3<C≤ 0.5
SOC(%)	≤ 10	0.000888	0.007624	0.008525
	10 - 20	0.000727	0.008299	0.013352
	20 - 30	0.000546	0.007046	0.011031
	30 - 40	0.000610	0.006256	0.010865
	40 - 50	0.000552	0.006387	0.011167
	50 - 60	0.000435	0.005267	0.009054
	60 - 70	0.000457	0.005168	0.008555
	70 - 80	0.000415	0.004729	0.007409
	80 - 90	0.000472	0.005054	0.007908

Total of LTO battery degradation rate = 0.14879%

Table. 5.19 Number of cycles obtained from (EFCs) counting method based on different C-rate values and grouped of SOC battery used to deliver DR service with implementing dynamic control (S2) for Jan-2019 frequency data, $SOC_{start}=30\%$

		C-rate (C)								
		C ≤ 0.1			0.1<C ≤ 0.3			0.3<C ≤ 0.5		
		Total Imp. Energy (MWh)	Total Exp. Energy (MWh)	No.of Cycles (Cycle)	Total Imp. Energy (MWh)	Total Exp. Energy (MWh)	No.of Cycles (Cycle)	Total Imp. Energy (MWh)	Total Exp. Energy (MWh)	No.of Cycles (Cycle)
SOC(%)	≤ 10	-13.55	5.32	0.2359	-91.94	50.40	1.7792	-67.46	70.93	1.7298
	10-20	-8.96	6.94	0.1988	-84.48	67.49	1.8996	-113.67	103.39	2.7134
	20-30	-5.53	6.55	0.1509	-72.02	63.36	1.6923	-88.75	86.52	2.1908
	30-40	-6.25	7.59	0.1731	-60.48	65.71	1.5773	-103.09	87.99	2.3885
	40-50	-6.27	5.62	0.1486	-60.25	54.80	1.4382	-96.27	82.19	2.2308
	50-60	-5.04	3.85	0.1111	-47.49	43.92	1.1427	-69.88	61.03	1.6363
	60-70	-5.74	2.96	0.1087	-51.81	31.41	1.0402	-66.93	56.16	1.5386
	70-80	-4.96	2.49	0.0932	-42.44	27.09	0.8692	-58.69	48.22	1.3364
	80-90	-4.89	3.58	0.1059	-40.91	35.07	0.9497	-56.16	51.99	1.3519
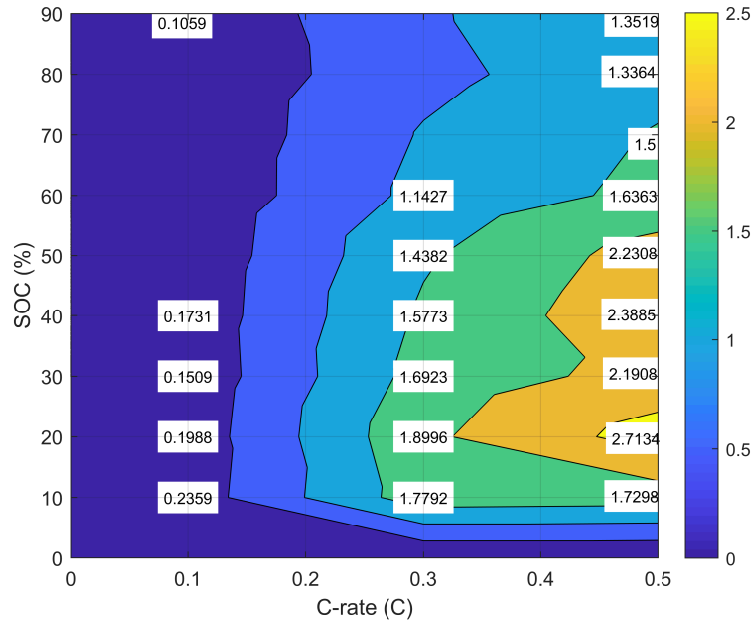
Figure. 5.20 Simulation results of the EFCs under different C-rates for each grouped SOC for DR service based on (S2) for Jan-2019, SOC_{start} = 30%. (Maximum scale is 2.7134 cycles).

Table. 5.20 Degradation findings obtained from the EFCs under different C-rate values and grouped SOC battery delivering DR service based on (S2) for Jan-2019 frequency data, SOC_{start}=30%

		C-rate (C)		
		C$\leq$ 0.1	0.1<C$\leq$ 0.3	0.3<C$\leq$ 0.5
SOC(%)	$\leq$ 10	0.0008902	0.00757	0.00805
	10 - 20	0.0007646	0.00826	0.01292
	20 - 30	0.0005918	0.00752	0.01069
	30 - 40	0.0006924	0.00717	0.01194
	40 - 50	0.0006065	0.00669	0.01144
	50 - 60	0.0004629	0.00544	0.00861
	60 - 70	0.0004626	0.00507	0.00832
	70 - 80	0.0004052	0.00435	0.00742
	80 - 90	0.000472	0.00505	0.007908

Total of LTO battery degradation rate = 0.1497662%

Table. 5.21 Number of cycles obtained from (EFCs) counting method based on different C-rate values and grouped of SOC battery used to deliver DR service without dynamic control (S1) for Jan-2019 frequency data, SOC_{start}=70%

		C-rate (C)								
		C ≤ 0.1			**0.1<C ≤ 0.3**			**0.3<C ≤ 0.5**		
		Total Imp. Energy (MWh)	Total Exp. Energy (MWh)	No.of Cycles (Cycle)	Total Imp. Energy (MWh)	Total Exp. Energy (MWh)	No.of Cycles (Cycle)	Total Imp. Energy (MWh)	Total Exp. Energy (MWh)	No.of Cycles (Cycle)
SOC(%)	≤ 10	-14.12	4.37	0.2311	-96.37	46.79	1.7895	-72.44	73.89	1.8292
	10-20	-8.63	6.15	0.1847	-83.56	66.89	1.8807	-116.27	105.39	2.7708
	20-30	-5.48	5.77	0.1407	-66.39	59.36	1.5719	-93.77	87.19	2.2619
	30-40	-5.85	5.97	0.1478	-50.93	53.93	2.6213	-86.74	79.38	2.0765
	40-50	-5.18	5.68	0.1357	-55.79	56.36	1.4019	-95.07	80.29	2.1921
	50-60	-4.46	4.05	0.1064	-47.41	43.39	1.1349	-71.89	69.09	1.7622
	60-70	-5.33	3.41	0.1092	-50.93	35.69	1.0826	-69.66	58.28	1.5993
	70-80	-5.47	2.85	0.1040	-51.38	30.83	1.0277	-59.32	57.53	1.4608
	80-90	-4.53	4.22	0.1094	-45.29	35.62	1.0113	-60.41	52.89	1.4163
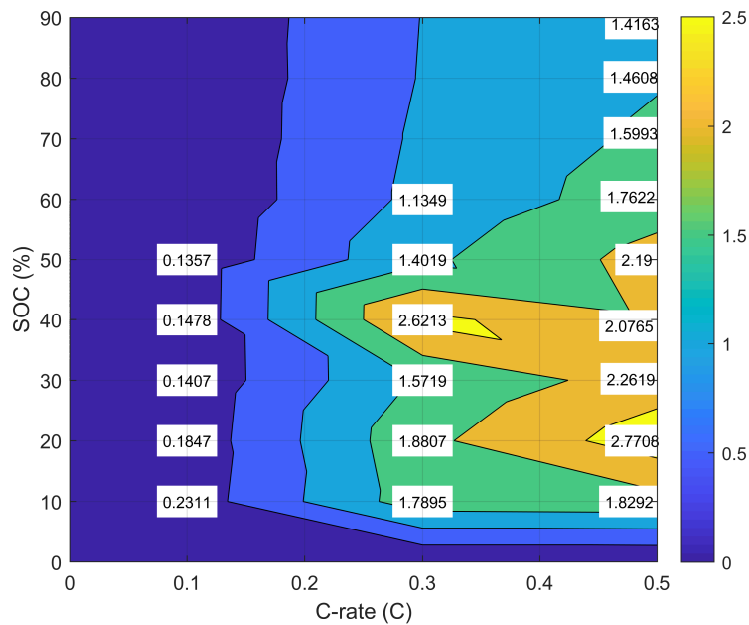
Figure. 5.21 Simulation results of the EFCs based on different C-rate for each grouped SOC for DR service without implementing dynamic control (S1) for Jan-2019, SOC_{start}=70%.(Maximum scale is 2.7708 cycles).

Table. 5.22 Degradation results obtained from the EFCs based on different C-rate values and grouped SOC battery delivering DR service without dynamic control (S1) for Jan-2019 frequency data, SOC_{start}=70%

		C-rate (C)		
		C≤ 0.1	0.1<C≤ 0.3	0.3<C≤ 0.5
SOC(%)	≤ 10	0.000872	0.007615	0.008508
	10 - 20	0.000710	0.008177	0.013194
	20 - 30	0.000552	0.006986	0.011034
	30 - 40	0.000591	0.011915	0.010383
	40- 50	0.000554	0.006520	0.011242
	50 - 60	0.000443	0.005404	0.009275
	60 - 70	0.000465	0.005281	0.008645
	70 - 80	0.000452	0.005139	0.008116
	80 - 90	0.000486	0.005186	0.008093

Total of LTO battery degradation rate = 0.15584%

Table. 5.23 Number of cycles obtained from (EFCs) counting method based on different C-rate values and grouped of SOC battery used to deliver DR service with dynamic control (S2) for Jan-2019 frequency data, SOC_{start}=70%

		C-rate (C)								
		C ≤ 0.1			0.1<C ≤ 0.3			0.3<C ≤ 0.5		
		Total Imp. Energy (MWh)	Total Exp. Energy (MWh)	No.of Cycles (Cycle)	Total Imp. Energy (MWh)	Total Exp. Energy (MWh)	No.of Cycles (Cycle)	Total Imp. Energy (MWh)	Total Exp. Energy (MWh)	No.of Cycles (Cycle)
SOC(%)	≤ 10	-13.27	5.22	0.2311	-91.83	49.51	1.7667	-67.08	71.26	1.7293
	10-20	-8.67	6.89	0.1947	-82.81	67.59	1.8801	-112.52	101.68	2.6775
	20-30	-5.53	6.59	0.1514	-71.45	62.81	1.6782	-88.76	86.75	2.1938
	30-40	-6.11	7.39	0.1687	-56.36	64.67	1.5129	-99.01	85.13	2.3017
	40-50	-6.21	5.75	0.1495	-60.09	57.09	1.4647	-96.17	82.92	2.2386
	50-60	-5.05	3.88	0.1116	-47.70	44.94	1.1579	-69.89	63.99	1.6736
	60-70	-5.74	3.11	0.1106	-51.82	33.46	1.0659	-66.93	57.28	1.5526
	70-80	-5.63	2.69	0.1039	-47.23	28.93	0.9520	-62.88	54.45	1.4665
	80-90	-4.99	3.59	0.1073	-42.11	35.16	0.9659	-57.05	52.32	1.3671
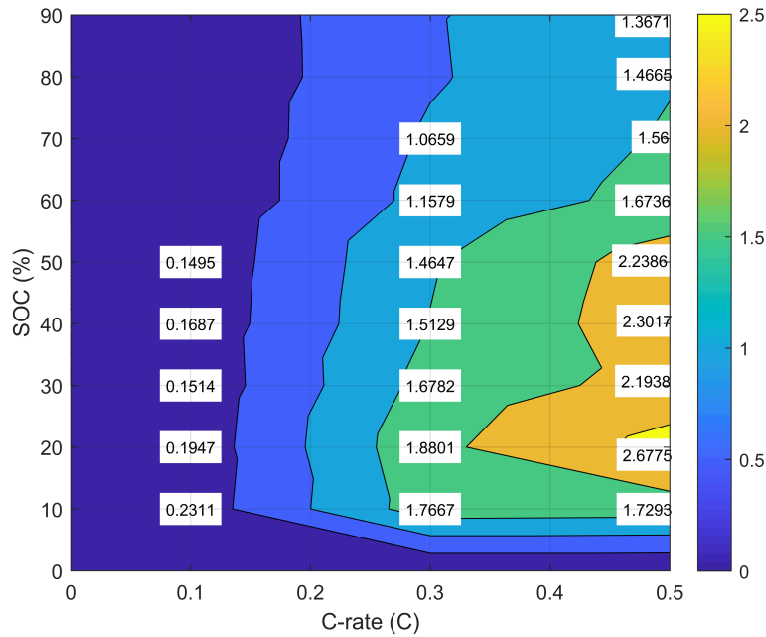
Figure. 5.22 Simulation results of the EFCs based on different C-rates for each grouped SOC for the DR model with implementing a dynamic control (S2) for Jan-2019, SOC$_{start}$=70%. (Maximum scale is 2.6775 cycles).

Table. 5.24 Degradation results obtained from the EFCs based on different C-rate values and grouped SOC battery delivering DR service with implementing a dynamic control (S2) for Jan-2019 frequency data, SOC$_{start}$=70%

		C-rate (C)		
		C$\leq$ 0.1	0.1<C$\leq$ 0.3	0.3<C$\leq$ 0.5
SOC(%)	10	0.000872	0.007518	0.008043
	20	0.000749	0.008174	0.012750
	30	0.000594	0.007459	0.010701
	40	0.000675	0.006877	0.011509
	50	0.000610	0.006813	0.011480
	60	0.000465	0.005514	0.008808
	70	0.000471	0.005200	0.008392
	80	0.000452	0.004760	0.008147
	90	0.000477	0.004953	0.007812

Total of LTO battery degradation rate = 0.15028%

Figures 5.18 to 5.23 and Tables 5.14 to 5.25 present the simulation results for the number of cycles obtained from EFCs and the corresponding degradation rates. These results consider the effects of both C-rate and SOC_{start} on the lifetime of LTO batteries used to deliver DR service, based on scenarios S1 & S2, for the entire month of January 2019, with different SOC_{start} values (50%, 30%, and 70%).

In the cases of SOC_{start} at 50% and 30%, it is evident that for both scenarios (S1 & S2), BESS primarily operated within the C-rate range of When comparing all SOC_{start}

149

levels, for scenario S1, within the C-rate range of $0.3 < C \leq 0.5$, with SOC_{start} values ranging from 10% to 50%. The highest number of cycles and degradation rates for both scenarios occurred at the same C-rate but within the SOC_{start} range of 10% to 20%. For instance, at an SOC_{start} of 50% in scenario S1, these values were approximately 2.7705 cycles and 0.0132% degradation, whereas in scenario S2, these values decreased by about 3.16% and 3.20%, respectively. Similarly, at an SOC_{start} of 30%, in scenario S1, the values were approximately 2.8039 cycles and 0.013352% degradation, while in S2, they decreased by approximately 3.28% and 3.29%, respectively.

For scenario S1 at an SOC_{start} of 70%, BESS mainly operated within the C-rate range of When comparing all SOC_{start} levels, for scenario S1, within the C-rate range of $0.3 < C \leq 0.5$, with SOC_{start} values from 10% to 50%, as well as within the C-rate range of 0.1C to 0.3C, with SOC_{start} values from 30% to 40%. In scenario S2, it mostly operated within the C-rate range of When comparing all SOC_{start} levels, for scenario S1, within the C-rate range of $0.3 < C \leq 0.5$, with SOC_{start} values from 10% to 50%. The highest number of cycles and degradation rates for both scenarios occurred at When comparing all SOC_{start} levels, for scenario S1, within the C-rate range of $0.3 < C \leq 0.5$ within the SOC_{start} range of 10% to 20%. For example, in scenario S1, these values were approximately 2.7708 cycles and 0.013194% degradation, while in scenario S2, they decreased by about 3.43% and 3.43%, respectively.

This suggests that BESS frequently operates within these specific regions, with a higher proportion of its operation time in scenario S1. This is attributed to the dynamic control mechanism employed in S2, extending the charge/discharge time for the battery, minimising energy throughput, reducing the total number of cycles, decreasing battery degradation, and extending the battery's lifetime.

In all cases of SOC_{start}, the lowest number of cycles and the lowest battery degradation rates for both scenarios (S1 & S2) were observed at C-rates of less than or equal to 0.1C. In these cases, the number of cycles was less than one cycle, indicating that the battery rarely operates within these regions. However, it's worth noting that batteries within the C-rate range of When comparing all SOC_{start} levels, for scenario S1, within the C-rate range of $0.3 < C \leq 0.5$ are subject to faster degradation compared to those with C-rates less than or equal to 0.1C.

At an SOC_{start} of 50%, for scenario S1, the number of cycles and degradation rate were approximately 1.241 cycles and 0.0056%, respectively. However, for scenario S2, these values increased by around 4.18% and 5.23%, respectively. At an SOC_{start} of 30%, in scenario S1, the values were approximately 1.2309 cycles and 0.0056%, while for S2, they increased by approximately 5.02% and 3.51%, respectively. Similarly, at an SOC_{start} of 70% in scenario S1, the number of cycles and degradation rate were around 1.235 cycles and 0.0056%, respectively, but in scenario S2, they increased by approximately 4.89% and 5.21%, respectively. This suggests that BESS rarely operates within this specific range, but it has spent more time operating in scenario S2 compared

to S1.

When comparing all SOC_{start} levels, for scenario S1, within the C-rate range of When comparing all SOC_{start} levels, within the C-rate range of $0.3 < C \leq 0.5$, the number of cycles at an SOC_{start} of 50% was almost 1.57% higher than at 30% and 1% higher than at 70%. For scenario S2, it increased by approximately 0.11% compared to 30% but decreased by almost 0.37% compared to 70%. In the case of scenario S1, within the C-rate range of C≤0.1, the number of cycles at an SOC_{start} of 50% showed a slight increase of approximately 0.82% and 0.49% compared to 30% and 70%, respectively. For scenario S2, it remained the same at 30% but decreased by 0.23% compared to 70%.

5.2.4 Fast Cycle Counting Method (CCM)

In this section, the Fast CCM is used to calculate the micro charge-discharge cycles based on the SOC profile that is obtained from BESS used to deliver DR service based on S1 & S2 for Jan-2019 frequency data. The algorithm of such a method is shown and explained in Figure 2.7, Section 2.4.2 in Chapter 2.

5.2.5 Simulation Results of BESS-Based DR Services Using CCM and SOC Profile: Jan-2019 Frequency Data
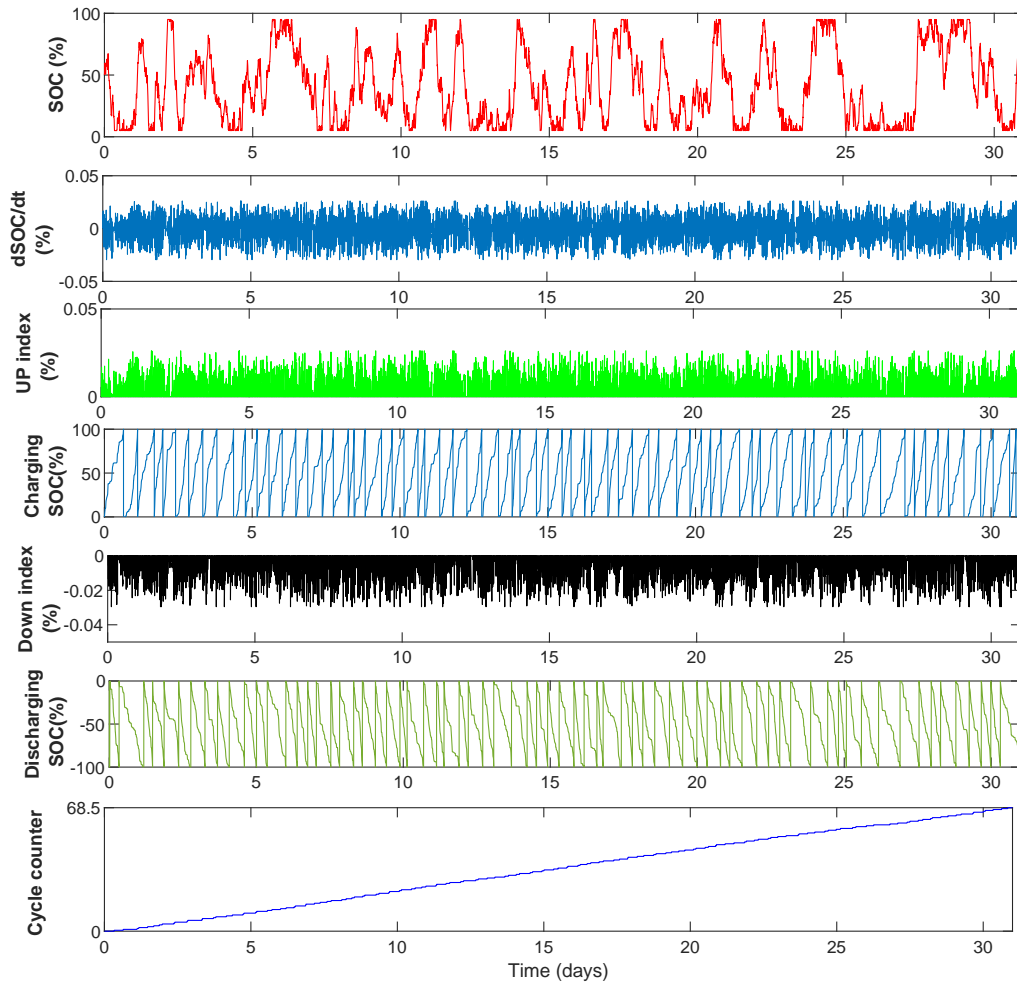
Figure. 5.23 The operation principles of proposed CCM used to count the micro charge-discharge cycles based on SOC profile that has been obtained from simulation results BESS used to deliver DR Service without dynamic control (S1) for Jan-2019 frequency data.
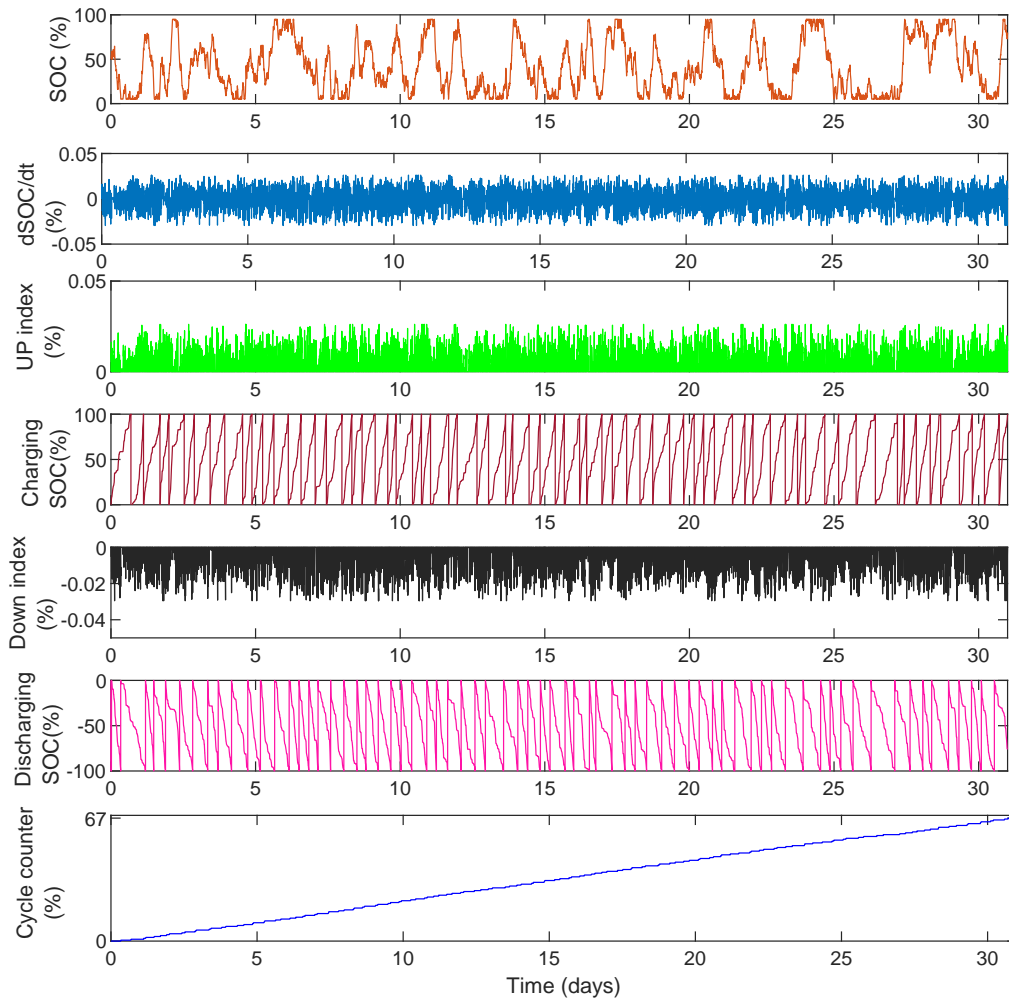
Figure. 5.24 The number of cycles using CCM based on SOC profile that has been obtained from simulation results of BESS used to deliver DR Service with dynamic control (S2) for Jan-2019 frequency data.

Table. 5.25 The findings regarding the number of full cycles achieved by CCM and the degradation rate were obtained using the Miner Rule's Method for an LTO battery that had undergone 12,000 cycles(manufacturer cycling) used to deliver DR service for different scenarios (S1 & S2) for Jan-2019 frequency data, 40MWh profile

Scenarios	Total no of Cycles (cycle)	LTO battery degradation rate (%)
S1	68.5	0.5708
S2	67	0.5583

153

Table. 5.26 The findings regarding the number of full cycles achieved by CCM and the degradation rate were obtained using the Miner Rule's Method for an LTO battery that had undergone 12,000 cycles(manufacturer cycling) used to deliver DR service for different scenarios (S1 & S2) for the full year-2019 frequency data, 40MWh profile

Scenarios	Total no of Cycles (cycle)	LTO battery degradation(%)
S1	753	6.275
S2	737.50	6.146

Figure 5.23, Figure 5.24, Illustrate the operation principles of the proposed CCM which is explained in Chapter 4, Subsubsection 4.5.5 that is used herein to calculate the partial charge-discharge cycles based on SOC that are obtained from simulation results of BESS used to deliver DR service for the whole of Jan-2019 based on (S1 & S2). As we can see from both Figures, the average of ΔSOC is $\sim$ 0.0053569 which caused many micro cycles resulting from the change in the real frequency data second by second. Comparing S1 to S2, based on the results shown in Table 5.25, and Table 5.26, it is clear that, BESS that has been used to deliver DR service based on S1 for Jun-2019 was subject to the highest total number of cycles which equates $\sim$68.5 cycle and with a higher degradation rate equates $\sim$ 0.5708%, while in S2, the battery was subject to less number of cycles as well as less degradation rate which are equating to almost $\sim$ 67 cycles, and 0.5583%, respectively. In addition to that, for the whole year of 2019, and based on S1, BESS has been subjected to the greatest number of cycles as well as the highest degradation rate with the values equating to approximately 753 cycles, and 6.275%, respectively. However, in S2, the total number of cycles has been reduced to 737.50 cycles, and the degradation rate decreased to almost 6.146%. The main reason behind that is, in S1, there was no SOC management which led to an increase in the total charge-discharge cycles and fast degradation which led to a decrease in the battery lifetime, while in S2, there was an opportunity for SOC management, and dynamic control has been used to allow more time for battery SOC to be charged or discharged, and this had resulted in the decrease in the total number of cycles and slow degradation and increase the battery lifetime.

a. The Effects of C-rate on Battery Degradation

In this section, the proposed method called fast CCM with the algorithm shown in Subsubsection 2.4.2, Chapter 2 has been improved by considering the effects of C-rate on the battery lifetime. It is used herein to calculate the number of micro charge-discharge cycles based on the SOC data that has been obtained from BESS used to deliver DR service based on (S1 & S2) for the whole of Jan-2019. The scheme of the proposed CCM considering the C-rate is shown in Figure 4.18 and discussed in Subsubsection 4.5.5, Chapter 4. The C-rate is calculated based on ΔSOC using eq.4.5.

The obtained C-rate is measured second by second grouped by (0.1C, 0.3C, 0.5C) in

order to calculate the partial charge-discharge cycles at each C-rate. To calculate the LTO battery degradation rate by considering the only effect of C-rate on the battery lifetime, Data2 has been used as shown in Figure 4.6 and calculated using e.q.4.3.

Simulation results of the CCM considering only C-rate effects on LTO battery Lifetime for delivering DR service based on (S1 & S2) for Jan-2019 frequency data

In this section, the proposed CCM is used to calculate the number of micro charge-discharge cycles for BESS with a different C-rate value used to deliver DR service based on (S1 & S2) for Jan-2019. The obtained results of the number of cycles and LTO battery degradation rate using (Data2) are shown in the below Tables [5.28 - 5.30].

Table. 5.27 Number of cycles and degradation findings obtained from the CCM based on different C-rate ranges for BESS delivering DR service using (S1 & S2) for Jan-2019 frequency data, SOCstart= 50%

C-rate (C)	No of Cycles (Cycle)	Battery degradation rate at each C-rate (%)	Scenarios
C≤ 0.1	1	0.0046	S1
	3.5	0.0159	S2
0.1C< C ≤ 0.3C	19	0.100	S1
	23.5	0.1237	S2
0.3C<C ≤ 0.5C	25	0.1471	S1
	21	0.1235	S2

Table. 5.28 Degradation results obtained from the CCM based on different C-rate values for BESS delivering DR service using (S1 & S2) for Jan-2019 frequency data, SOC_{start}=30%

C-rate (C)	No of Cycles (Cycle)	Battery degradation rate at each C-rate (%)	Scenarios
C≤ 0.1	1	0.0046	S1
	5	0.0227	S2
0.1C< C ≤ 0.3C	20	0.1053	S1
	22.5	0.1184	S2
0.3C<C ≤ 0.5C	25.5	0.1500	S1
	25.5	0.1500	S2

Table. 5.29 Number of cycles and degradation results obtained from the CCM based on different C-rate ranges for BESS delivering DR service using (S1 & S2) for Jan- 2019 frequency data, SOC_{start}=70%

C-rate (C)	No of Cycles (Cycle)	Battery degradation rate at each C-rate (%)	Scenarios
C≤ 0.1	1	0.0046	S1
	1.5	0.0068	S2
0.1C< C ≤ 0.3C	21	0.1132	S1
	17	0.0895	S2
0.3C<C ≤ 0.5C	22	0.1294	S1
	30	0.1765	S2

Table 5.27, Table 5.28, and Table 5.29 display the simulation results for the number of cycles and degradation rate obtained from the proposed CCM, considering the effects of the C-rate on LTO battery lifetime used for delivering DR service under scenarios S1 and S2 throughout Jan-2019, with different SOC_{start} (50%, 30%, and 70%).

It is evident that, for all SOC_{start} cases, the C-rate range of $0.3 < C \leq 0.5$ resulted in the highest number of cycles and the greatest total degradation rate for both S1 and S2. At SOC_{start}=50%, S1 experienced an increase of approximately 33.62% in both the number of cycles and degradation rate compared to the EFC results, while for S2, these figures increased by approximately 18.36% and 18.29%, respectively. Similarly, at SOC_{start}=30%, for S1, the number of cycles and degradation rate increased by 37.06%, while for S2, they increased by 37.49%. At SOC_{start}=70%, both S1 and S2 showed increases of approximately 22.07% in the number of cycles and 22.05% in the degradation rate.

In summary, BESS operations were predominantly concentrated in the aforementioned C-rate range. At SOC_{start}=50%, the majority of BESS operation time was spent in S1. Conversely, at SOC_{start}=30%, the operation time for BESS was consistent between S1 and S2. At SOC_{start}=70%, BESS favored S2, and this was attributed to the dynamic control implemented in S2, extending the charge/discharge time for the battery, minimising energy throughput, reducing the total number of cycles, and decreasing battery degradation while extending the battery's lifetime.

In all SOC_{start} scenarios, the lowest number of cycles and degradation rates occurred at a C-rate $\leq$ 0.1C. At SOC_{start}=50%, for S1, both the number of cycles and degradation rate decreased by approximately 21.51% and 19.61%, respectively, while for S2, they increased by almost 92.03% and 91.74%, respectively. At SOC_{start}=30%, for S1, both these parameters decreased by approximately 20.70% and 19.61%, respectively, whereas for S2, they increased by approximately 117.76% and 118.59%, respectively. Similarly, at SOC_{start}=70%, for S1, both the number of cycles and degradation rate were reduced by 21.03% and 19.61%, respectively, while for S2, they increased by approximately 14.52%

and 14.17%, respectively. Consequently, BESS rarely operated in the lower C-rate region, but it spent more time operating in S2 compared to S1.

b. The effects of both C-rate & SOC on Battery Degradation

In this section, the proposed method (CCM) with the algorithm shown in Subsubsection 2.4.2, Chapter 2 is improved by considering the effects of both C-rate and SOC on the battery lifetime. It is used herein to calculate the partial number of charge and discharge cycles based on the SOC data that has been obtained from BESS used to deliver DR service based on S1 & S2 for the whole of Jan-2019. The scheme of such a method considering both C-rate SOC is shown in Figure 4.19 and explained in Subsubsection 4.5.5, Chapter 4.

The LTO battery degradation rate for considering the effects of both C-rate and SOC on battery lifetime can be calculated using the assumed number of cycles with SOC ranges as shown in Table 4.5, and using e.q. 4.4.

Simulation results of the CCM considering the effects of both C-rate SOC on battery lifetime that have been used to deliver DR service based on S1 & S2 for Jan-2019 frequency data

In this section, the proposed CCM is used to calculate the number of charge-discharge micro cycles for BESS based on a grouped C-rate & SOC used to deliver DR service for Jan 2019. The obtained number of cycles and degradation rates are shown in the Figures [5.25−5.30], and Tables [5.30−5.41].

Table. 5.30 Number of cycles findings obtained from the Fast CCM under different C-rate values and grouped SOC battery delivering DR without Dynamic Control (S1) for Jan-2019 frequency data, SOC_{start}=50%

		C-rate (C)			
		C≤ 0.1	0.1<C≤ 0.3	0.3<C≤ 0.5	Total Number of Cycles (Cycle)
SOC(%)	C≤ 10	0	3.5	1.5	5
	10 - 20	0	4	2.5	6.5
	20 - 30	0	1.5	5.5	7
	30 - 40	0	2	4.5	6.5
	40 - 50	0	2.5	2	4.5
	50 - 60	0.5	1	2	3.5
	60 - 70	0	2.5	3	5.5
	70 - 80	0.5	1.5	0.5	2.5
	80 - 90	0	0.5	2	2.5
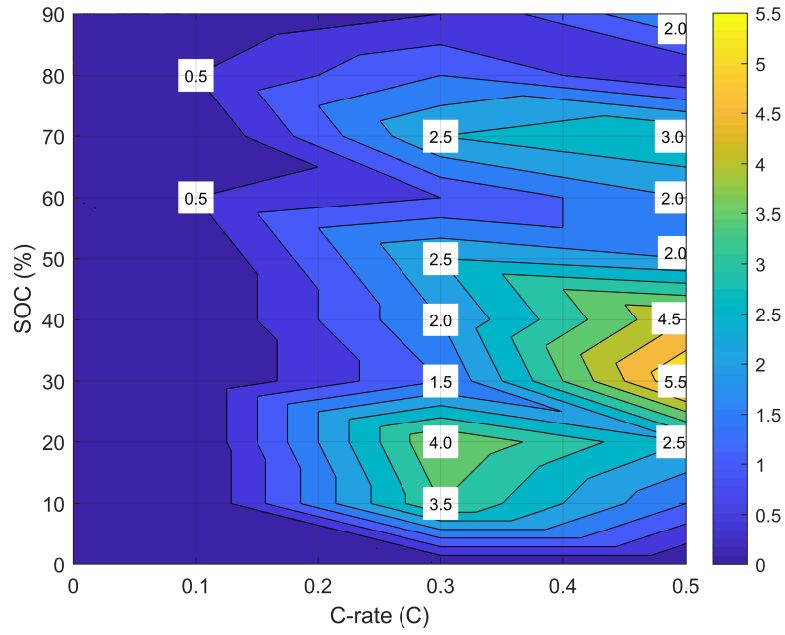
Figure. 5.25 Simulation results of the CCM under different C-rates for each grouped SOC for the DR model based on S1 for Jan-2019 frequency data, SOC_{start}=50%. (Maximum scale is 5.5 cycles)

Table. 5.31 Degradation results obtained from the Fast CCM under different C-rate values and grouped SOC battery delivering DR based on (S1) for Jan-2019 frequency data, SOC_{start}=50%

		C-rate (C)		
		C$\leq$ 0.1	0.1<C$\leq$ 0.3	0.3<C$\leq$ 0.5
	$\leq$ 10	0	0.0149	0.0069
	10 - 20	0	0.0174	0.0119
	20 - 30	0	0.0067	0.0268
	30 - 40	0	0.0091	0.0225
SOC(%)	40 - 50	0	0.0116	0.0103
	50 - 60	0.0021	0.0048	0.0105
	60 - 70	0	0.0122	0.0162
	70 - 80	0.0022	0.0075	0.0028
	80 - 90	0	0.0026	0.0114

Total of LTO battery degradation rate = 0.21040%

Table. 5.32 The number of cycles findings obtained from the Fast CCM based on different C-rate values and grouped of SOC battery delivering DR service with implementing a dynamic control (S2) for Jan-2019 frequency data, SOC_{start}=50%

		C-rate (C)			
		C≤ 0.1	0.1<C≤ 0.3	0.3<C≤ 0.5	Total Number of Cycles (Cycle)
SOC(%)	≤ 10	1	4.5	2	7.5
	10 - 20	0	4.5	3	7.5
	20 - 30	0	1.5	3	4.5
	30 - 40	1.5	0.5	3.5	5.5
	40 - 50	0	1	3	4
	50 - 60	0.5	4.5	1	6
	60 - 70	0.5	4.5	1	6
	70 - 80	0	3	1	4
	80 - 90	0	3	2	5
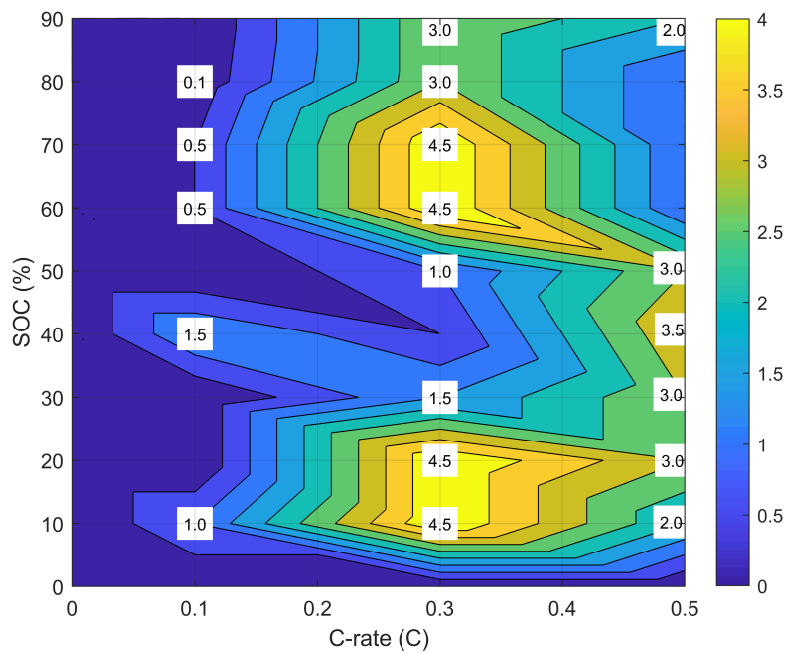
Figure. 5.26 Simulation results of the CCM under different C-rates for each grouped SOC for the DR service based on S2 for Jan-2019, SOC_{start}=50%. (Maximum scale is 4.5 cycles)

Table. 5.33 Degradation results obtained from the CCM under different C-rate values and grouped SOC battery delivering DR with implementing a dynamic control (S2) for Jan-2019 frequency data, SOC_{start}=50%

		C-rate (C)		
		C≤ 0.1	0.1<C≤ 0.3	0.3<C≤ 0.5
SOC(%)	≤ 10	0.003774	0.019149	0.009302
	10 - 20	0.000000	0.019565	0.014286
	20 - 30	0.000000	0.006667	0.014634
	30 - 40	0.006000	0.002273	0.017500
	40 - 50	0.000000	0.004651	0.015385
	50 - 60	0.002083	0.021429	0.005263
	60 - 70	0.002128	0.021951	0.005405
	70 - 80	0.000000	0.015000	0.005556
	80 - 90	0.000000	0.015385	0.011429

Total of LTO battery degradation rate = 0.23882%

Table. 5.34 Number of cycles findings obtained from the CCM based on different C-rate values and grouped of SOC battery delivering DR without Dynamic Control (S1) for Jan-2019 frequency data, SOC$_{start}$=30%

|		C-rate (C)			Total Number of Cycles (Cycle)
		C≤ 0.1	0.1<C≤ 0.3	0.3<C≤ 0.5	
SOC(%)	≤ 10	0	3	1.5	4.5
	10 - 20	0	4	2.5	6.5
	20 - 30	0	4.5	4	8.5
	30 - 40	0.5	1	3.5	5
	40 - 50	0	3	1	4
	50 - 60	0.5	1.5	3.5	5.5
	60 - 70	0	2	1.5	3.5
	70 - 80	0	2	0.5	2.5
	80 - 90	0	0.5	2.5	3
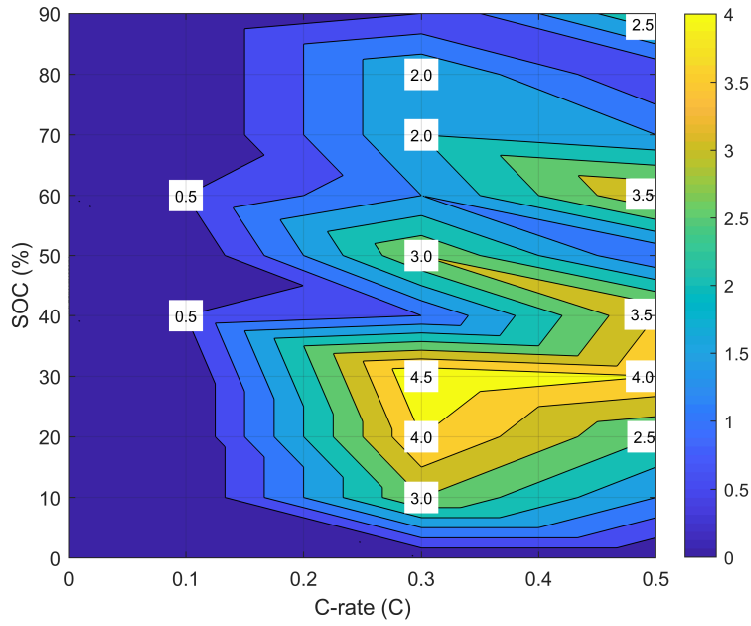
Figure. 5.27 Simulation results of the CCM based on different C-rate for each grouped SOC for the DR model without implementing dynamic control (S1) for Jan-2019, SOC_{start}=30%. (Maximum scale is 4 cycles)

Table. 5.35 Degradation results obtained from the CCM based on different C-rate values and grouped SOC battery delivering DR service without applying a dynamic control (S1) for Jan-2019 frequency data, SOC_{start}=30%

		C-rate (C)		
		$C \leq 0.1$	$0.1 < C \leq 0.3$	$0.3 < C \leq 0.5$
SOC(%)	≤ 10	0.000000	0.012766	0.006977
	10 - 20	0.000000	0.017391	0.011905
	20 - 30	0.000000	0.020000	0.019512
	30 - 40	0.002000	0.004545	0.017500
	40 - 50	0.000000	0.013953	0.005128
	50 - 60	0.002083	0.007143	0.018421
	60 - 70	0.000000	0.009756	0.008108
	70 - 80	0.000000	0.010000	0.002778
	80 - 90	0.000000	0.002564	0.014286

Total of LTO battery degradation rate = 0.20682%

161

Table. 5.36 Number of cycles obtained from the CCM based on different C-rate values and grouped of SOC battery delivering DR with applying Dynamic Control (S2) for Jan-2019 frequency data, SOC_{start}=30%

		C-rate (C)			
		C≤ 0.1	0.1<C≤ 0.3	0.3<C≤ 0.5	Total Number of Cycles (Cycle)
SOC(%)	≤ 10	1.5	4.5	2	8
	10 - 20	0	2.5	3.5	6
	20 - 30	0	3.5	4.5	8
	30 - 40	0	2	3.5	5.5
	40 - 50	0	3	2	5
	50 - 60	0.5	2.5	3	6
	60 - 70	0.5	0.5	0.5	1.5
	70 - 80	0	1	4	5
	80 - 90	1.5	1.5	1.5	4.5
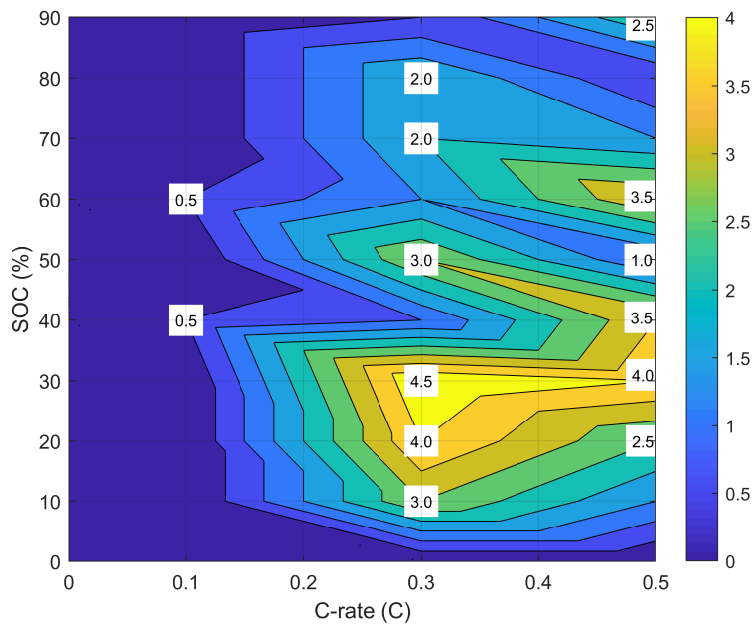
Figure. 5.28 Simulation results of the CCM based on different C-rate for each grouped SOC for the DR model with implementing dynamic control for Jan-2019, SOC_{start}=30%. (Maximum scale is 4.5 cycles).

Table. 5.37 Degradation results obtained from the CCM based on different C-rate values and grouped SOC battery delivering DR service with implementing a dynamic control (S2) for Jan-2019 frequency data, SOC_{start}=30%

		C-rate (C)		
		C≤ 0.1	0.1<C≤ 0.3	0.3<C≤ 0.5
SOC(%)	≤ 10	0.005660	0.019149	0.009302
	10 - 20	0.000000	0.010870	0.016667
	20 - 30	0.000000	0.015556	0.021951
	30 - 40	0.000000	0.009091	0.017500
	40 - 50	0.000000	0.013953	0.010256
	50 - 60	0.002083	0.011905	0.015789
	60 - 70	0.002128	0.002439	0.002703
	70 - 80	0.000000	0.005000	0.022222
	80 - 90	0.006667	0.007692	0.008571

Total of LTO battery degradation rate = 0.23715 %

Table. 5.38 Number of cycles obtained from the CCM based on different C-rate values and grouped of SOC for battery delivering DR without applying Dynamic Control (S1) for Jan-2019 frequency data, SOC_{start}=70%

		C-rate (C)			Total Number of Cycles (Cycle)
		C≤ 0.1	0.1<C≤ 0.3	0.3<C≤ 0.5	
SOC(%)	≤ 10	0	3.5	2	5.5
	10 - 20	0	5	2.5	7.5
	20 - 30	0	3	4	7
	30 - 40	0	2.5	2	4.5
	40 - 50	0	2	2.5	4.5
	50 - 60	1	1	2	4
	60 - 70	0	1	2	3
	70 - 80	0	1.5	0.5	2
	80 - 90	0	2	3	5
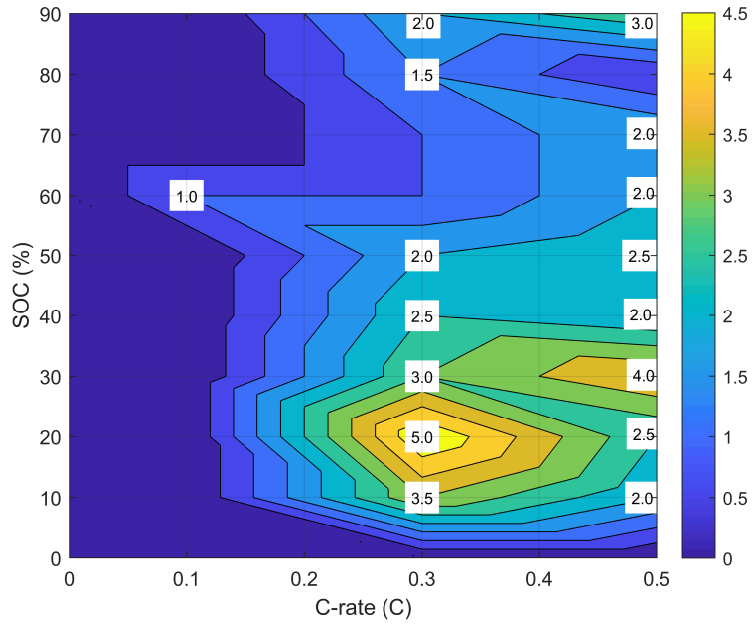
Figure. 5.29 Simulation results of the CCM based on different C-rate for each grouped SOC for the DR model without implementing dynamic control (S1) for Jan-2019, SOC_{start}=70%. (Maximum scale is 5 cycles).

Table. 5.39 Degradation results obtained from the CCM based on different C-rate values and grouped SOC for battery delivering DR service without implementing a dynamic control (S1) for Jan-2019 frequency data, SOC_{start}=70%

		C-rate (C)		
		C≤ 0.1	0.1<C≤ 0.3	0.3<C≤ 0.5
SOC(%)	≤ 10	0.000000	0.014894	0.009302
	10 - 20	0.000000	0.021739	0.011905
	20 - 30	0.000000	0.013333	0.019512
	30 - 40	0.000000	0.011364	0.010000
	40 - 50	0.000000	0.009302	0.012821
	50 - 60	0.004167	0.004762	0.010526
	60 - 70	0.000000	0.004878	0.010811
	70- 80	0.000000	0.007500	0.002778
	80 - 90	0.000000	0.010256	0.017143

Total of LTO battery degradation rate = 0.20699%

164

Table. 5.40 Number of cycles findings obtained from the CCM based on different C-rate values and grouped of SOC battery delivering DR with applying Dynamic Control (S2) for Jan-2019 frequency data, $SOC_{start}=70\%$

| | | **C-rate (C)** | | | Total Number of Cycles   (Cycle) |
		$C\leq 0.1$	$0.1<C\leq 0.3$	$0.3<C\leq 0.5$	
SOC(%)	≤ 10	0.5	3.5	6	10
	10 - 20	0.5	1.5	3	5
	20 - 30	0	0.5	5	5.5
	30 - 40	0	3	3.5	6.5
	40 - 50	0.5	2	2.5	5
	50 - 60	0	1	3	4
	60 - 70	0	1.5	3	4.5
	70 - 80	0	1.5	1.5	3
	80 - 90	0	2	1	3
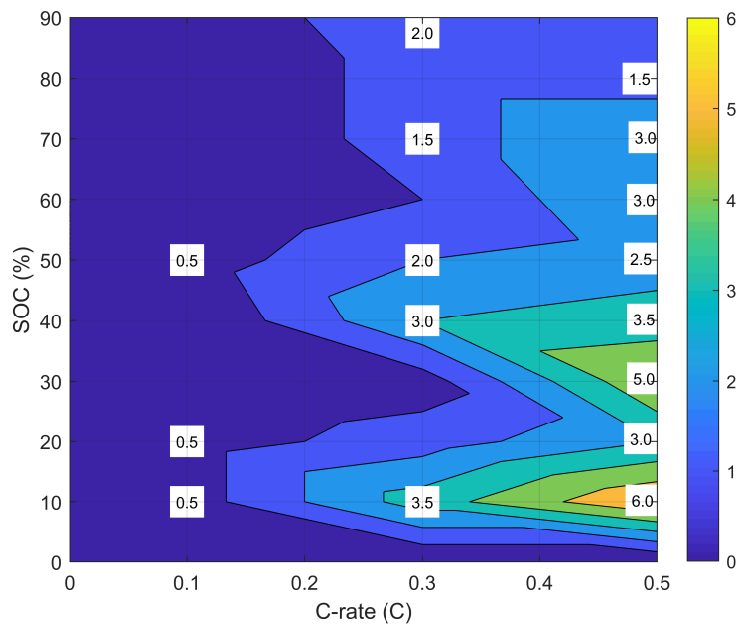
Figure. 5.30 Simulation results of the CCM based on different C-rates for each grouped SOC for the DR model with implementing dynamic control (S2) for Jan-2019, $SOC_{start}=70\%$. (Maximum scale is 6 cycles).

Table. 5.41 Degradation results obtained from the CCM based on different C-rate values and grouped SOC battery delivering DR service with implementing a dynamic control (S2) for Jan-2019 frequency data, SOC$_{start}$=70%

		C-rate (C)		
		C$\leq$ 0.1	0.1<C$\leq$ 0.3	0.3<C$\leq$ 0.5
SOC(%)	$\leq$ 10	0.001887	0.014894	0.027907
	10 - 20	0.001923	0.006522	0.014286
	20 - 30	0.000000	0.002222	0.024390
	30 - 40	0.000000	0.013636	0.017500
	40 - 50	0.002041	0.009302	0.012821
	50 - 60	0.000000	0.004762	0.015789
	60 - 70	0.000000	0.007317	0.016216
	70 - 80	0.000000	0.007500	0.008333
	80 - 90	0.000000	0.010256	0.005714

Total of LTO battery degradation rate = 0.20699%

Figures [5.25−5.30], and Tables [5.30−5.41] present the simulation results concerning the number of cycles and degradation rates. These results are based on the application of the CCM method and account for the impact of both the C-rate and SOC on the lifetime of LTO batteries used for delivering DR service under scenarios S1 and S2 throughout January 2019. These scenarios consider different initial states of charge, specifically 50%, 30%, and 70%.

When considering a SOC_{start} of 50%, it becomes evident that in S1, the Battery Energy Storage System (BESS) predominantly operated within the C-rate range of 0.3 < C $\leq$ 0.5, coupled with a SOC range of 20% to 40%. It exhibited the highest number of cycles and degradation rates within this C-rate range and SOC range (20% to 30%). The specific values were approximately 5.5 cycles and a degradation rate of 0.0268%. In contrast, for S2, BESS's operational pattern was primarily within the C-rate range of 0.3 < C $\leq$ 0.5, with a SOC range of 30% - 40%, resulting in the highest number of cycles at 4.5. Comparing this to the EFC method at the same SOC_{start}, BESS operated within the same C-rate range, but the number of cycles was approximately 3.16% lower.

When the initial state of charge was set to SOC_{start}=30%, BESS in S1 mostly operated within the C-rate range of 0.3 < C $\leq$ 0.5 and the SOC range of 20% - 30%. This operation resulted in the highest number of cycles at around 4.5, accompanied by a degradation rate of approximately 0.02%. In S2, BESS again operated mostly within the same C-rate ranges but exhibited slightly different SOC ranges (20% - 30% and 70% - 80%). The highest number of cycles was achieved within this C-rate range, although it was reduced by almost 3.28% compared to S2. Similarly, when comparing these results to those obtained through the EFC method at the same SOC_{start}, BESS operated predominantly within the C-rate range of 0.3 < C $\leq$ 0.5 and exhibited the highest number of cycles at around 2.80 cycles for S1, while for S2, the number of cycles was reduced by

almost 3.28% when compared to the results of the EFCs method.

In the scenario where the initial state of charge was SOC_{start}=70%, BESS in S1 operated mostly within the C-rate range of $0.3 < C \leq 0.5$ for a SOC range of 20% - 30%. Within this operational range, it exhibited the highest number of charge-discharge cycles, almost 5 cycles, and a degradation rate of approximately 0.02%. In comparison, for S2, BESS was operated within the C-rate range of $0.3 < C \leq 0.5$. The SOC range for these results was $< 10\%$ and 20% - 30%. The number of cycles obtained was approximately 6, with a degradation rate of 0.027907%. When comparing these results to those obtained through the EFC method at the same SOC_{start}, it is noted that for S1, BESS was primarily operating within the same C-rate range and SOC range (10% - 20%) and was subject to the highest number of cycles. However, for S2, this number of cycles was reduced by approximately 3.43%.

In summary, BESS mostly operates within the C-rate range of $0.1 < C \leq 0.5$, depending on the SOC_{start}, S1, and S2 scenarios. However, it spends more of its operational time in scenario S1. This preference for S1 is due to the dynamic control applied in S2, which extends the charge/discharge time for the battery. This extension results in the minimisation of energy usage, which, in turn, decreases the total number of cycles, reduces battery degradation, and extends the battery's lifetime.

In all cases of SOC_{start}, BESS's lowest number of cycles and lowest battery degradation rate occurred when the C-rate was $\leq 0.1C$, regardless of the SOC range. In these cases, the number of cycles was less than one cycle, signifying that the battery rarely operates in such conditions.

Comparing all the cases of SOC_{start}, the results obtained from the CCM show that the total number of cycles for SOC_{start}=50% is the highest, and for SOC_{start}=70% is the lowest when compared to SOC_{start}=30%. Additionally, the number of cycles obtained through the CCM method exceeded those obtained through the EFC method.

Summary

A brief summary of this chapter:

- Dynamic control for DR services, incorporating slow and fast ramp rates for DR-HF and DR-LF, aims to minimize energy throughput.

- The goal of dynamic control is to extend the time before SOC limits are reached, enhancing BESS availability and reducing penalty payments.

- The analysis reveals a decrease in EFCs when compared to a baseline control response, showing potential for more consecutive EFA blocks without penalties.

- Dynamic control is developed in MATLAB/Simulink to manage SOC for a stacked DR-HF and DR-LF contract, optimizing for high revenue and availability.

- Simulation results for DR-LF and DR-HF services in different scenarios indicate that penalty payments are avoided, and total export/import energy is reduced over time, enhancing average availability.

- Two cycle counting methodologies, EFCs and CCM, are introduced to approximate the number of cycles.

- EFCs result in a higher total number of cycles compared to CCM, and the analysis of battery degradation shows faster BESS degradation in S1 compared to S2 due to the absence of applied dynamic control in S1.

- The study highlights the importance of considering both C-rate and SOC for precise battery lifetime calculations.

In the forthcoming chapter, a techno-economic assessment will be conducted for grid-connected batteries providing frequency response services such as DFR, DC, and DR in the UK.

Chapter 6

Techno-economic assessment of Grid Connected Batteries providing Frequency Response Services in Great Britain

6.1 Introduction

In this chapter, the three frequency response services, namely DFR, DC, and DR, all provided by BESS, will be examined. These services will be evaluated with varying C-rates, and their financial implications shall be scrutinized by employing divergent charging methodologies within the context of the GB energy market.

Furthermore, the analysis will encompass considerations of service availability, wherein a financial metric known as Net Present Value (NPV), as well as the calculation of the Capacity Factor (CF), will be employed. These financial and operational parameters shall be investigated across a spectrum of C-rates and SOC management strategies, allowing assessment of different operational scenarios for LTO battery over a 15-year lifespan.

6.2 Real-world battery costs

Batteries are considered the most common technology that has been used for storing electrical energy and successfully demonstrated at the grid-level as well as in microgrid applications [62], [14] to manage the frequency deviation of electricity supply. [138] reports that, over the last 10-15 years, LTO batteries have been considered the most developed batteries which made them ideal candidates for grid use due to their technical performance. In recent years, the cost of batteries has been decreasing which will make them highly profitable for large-scale grid applications. In regards to the cost, besides the battery cells themselves, there are other costs that relate to BESS components that need to be taken into account when it comes to calculating BESS capital cost [139]. The components of BESS include batteries, inverters of different types such as (DC-DC or AC-DC), balancing of the system (BOS) that is needed for the installations of electrical structural works, battery management systems, and installation labour & equipment [140]. According to [141] the cost of a BESS can be calculated based on power capacity cost which is expressed in (£/kW) or energy capacity cost which is expressed in (£/kWh) depending on which attribute is prioritized. Systems designed for power output are meant

to generate high amounts of instantaneous power but for a short period. They are not suitable for sustaining this level of power output for a long duration. These systems may have higher costs per kW but their costs per kWh tend to be lower. [142] states that, if we have, for instance, a £12 million battery system with a nameplate power capacity of 10 MW and nameplate energy capacity of 4 MWh would have relatively low power costs (£1,200/kW) and relatively high energy costs (£3,000/ kWh). In regards to operation and maintenance (O & M) costs, they normally occur during the system life cycle and include labour, and electricity purchasing (energy storage charging cost). In this thesis, the Li-ion battery has been chosen to be used in the BESS model duo to its several advantages which include; high efficiency, power density, and long lifetime over other battery types [2]. Table 6.1 gives a detailed cost breakdown for a Li-ion BESS that is used in this thesis with references that are shown in the last column of this table.

Table. 6.1 Parameters and costs breakdown for Lithium-ion BESS

BESS component	Values	References
Battery Li-ion Purchase Cost (£/kWh)	130 – 300	[2], [143], [144], [145], [146], [147]
Battery central inverter price (£/kW)	60 – 70	[140]
Electrical BOS (£/kW)	70 – 140	[140]
Structural BOS (£/kW)	10 – 50	[140]
Operational and Maintenance costs (£/kW-yr)	1.7 – 7.8	[2], [148], [147], [149]
Total Capital Cost (£/kWh)	441	[146]
Battery lifetime (years)	15	[145], [150]

6.3 Revenue Anlaysis

6.3.1 Analysis of DFR vs DC vs DR Service

Table. 6.2 Analysis of DFR vs DC vs DR Service for the full month of Jun-2019 frequency data

Contracted Service Power (MW)	C-rate (C)	Total Import Energy (MWh)	Total Export Energy (MWh)	Avg.Availability (%)	Services
±40	0.5	1,521.09	1,358.31	96.05	DFR
	1	1,503.56	1,325.84	93.93	
	2	1,436.32	1,263.47	89.72	
±40	0.5	156.19	161.63	100	DC
	1	156.19	152.64	99.63	
	2	156.19	144.18	98.24	
±40	0.5	3,050.96	2,686.02	93.50	DR
	1	2,873.71	2,527.98	89.12	
	2	2,572.05	2,269.36	83.84	
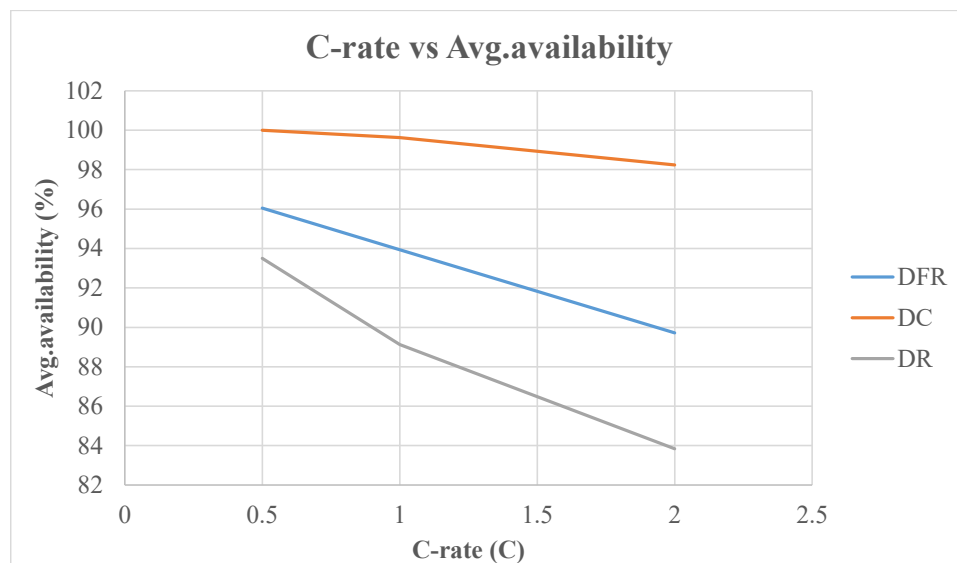
Figure. 6.1 Simulation results for DFR, DC & DR services for Jun-2019, Avg.Availability vs C-rate

Table 6.2 and Figure 6.1 illustrate the simulation results of a BESS that has delivered the three services (DFR, DC & DR) separately for the full month of Jun-2019, and it is clear that a higher total (import/export) energy is required for the delivery of DR compared with DFR & DC services. It is almost double DFR and 16 times higher than DC. In terms of average availability vs C-rate, it can be seen that when the C-rate increases the

average availability decreases and vice versa, and the highest average availability is for DC compared to DFR, and DR, while, the lowest average availability is for DR service.

6.4 Grid connected battery cost

In the UK, charges for using the electricity system network are imposed on all users of the GB electricity network to pay to use it. Several types of charges will be described in this section which include;

6.4.1 RO – Renewable Obligation

In the UK, renewable obligation is considered a mechanism that has been designed to support large-scale renewable electricity generation. In 2002, the scheme was implemented in England, Wales, and Scotland, and it came into effect in Northern Ireland in 2005. It is conditioned by three separate RO Orders to reflect the responsibilities of the devolved administrations [151]. The strategy of RO imposes an obligation on suppliers to provide a specified number of Renewable Obligation Certificates (ROCs) per MWh of electricity supplied. The required obligation will be based on the forecast of the amount of electricity that will be supplied in the GB as well as the number of ROCs that Ofgem will issue to eligible renewable generators. Essentially, it will be set annually by the Department for Business, Energy & Industrial Strategy (BEIS) and administered by Ofgem [152]. The RO charge is calculated annually and is based on the compliance period that starts from 1 April and ends on 31 March. [153] presents the progression of the obligation level in ROC/MWh for the period 2010-2023, and it is noticed that from 2010 to 2023 the buy-out price increased from £36.99 to £52.88 respectively. The buy-out price refers to the cost that electricity suppliers must pay for each (ROC) that they are unable to present to the regulator as evidence of their compliance with the government's renewable energy targets. This is the result of the increase in the penetration level of renewable generators that are integrated into the power grid, which are largely supported by the UK government through funds for renewable projects. In this thesis, the rate used is for 2022/2023. Therefore, the calculations for each service are given below.

$$
\begin{aligned}
Rate &= ROC(\pounds) \times ROCs/MWh \\
&= \pounds 52.88 \ \times \ 0.491/MWh \\
&= \pounds 25.96/MWh
\end{aligned}
\tag{6.1}
$$

The supplier, therefore, charges at this rate for imported energy. The cost can be calculated based on eq.(6.2), and the results are shown in Table 6.3.

$$
Cost = Import\,Energy(MWh) \times \pounds/MWh
\tag{6.2}
$$

Table. 6.3 Analysis of **RO** for DFR vs DC vs DR delivered
by BESS for Jun-2022, using Jun-2019 frequency data

Services	C-rate(C)	Cost (£)
DFR	0.5	39,487.49
	1	39,032.42
	2	37,286.87
DC	0.5	4,054.69
	1	4,054.69
	2	4,054.69
DR	0.5	79,202.92
	1	74,601.51
	2	66,770.42

As we can see from Table 6.3, the RO cost for both DFR & DR services increases with the decrease in the C-rate. This indicates that lower C-rates result in higher energy throughput. However, for DC service, the cost remains constant for all C-rates. The main reason for this is that the battery imports the same amount of energy from the grid for all C-rates.

6.4.2 CFD – Contract for Difference

This contract is called a private law contract that needs to be signed between a low-carbon electricity generator and the government-owned company, Low Carbon Contracts Company (LCCC). This contract will be based on an agreed fixed rate for electricity generated for a certain number of years that is settled at auctions. The main reason behind that is to incentivise companies in the UK to commit to producing low-carbon energy, and this can be achieved by providing them stability and predictability to future revenue streams. [154] reporters that, the object of CFD is to guarantee a fixed price for energy generation companies, called the 'strike rate', and will be based on wholesale rates. The strategy of this charge methodology will be implemented based on three conditions as set below;

- If the generator sells some energy with a cost the same as the strike price, then no further action will be taken place.

- If the energy cost by generators is below the strike price, then the supplier must be committed to triggering top-up payments to the generators.

- If the generators sell some energy at a price that is higher than the strike price then it will result in generators paying back the difference.

The CfD charge methodology for the generator is shown in Figure 6.2.
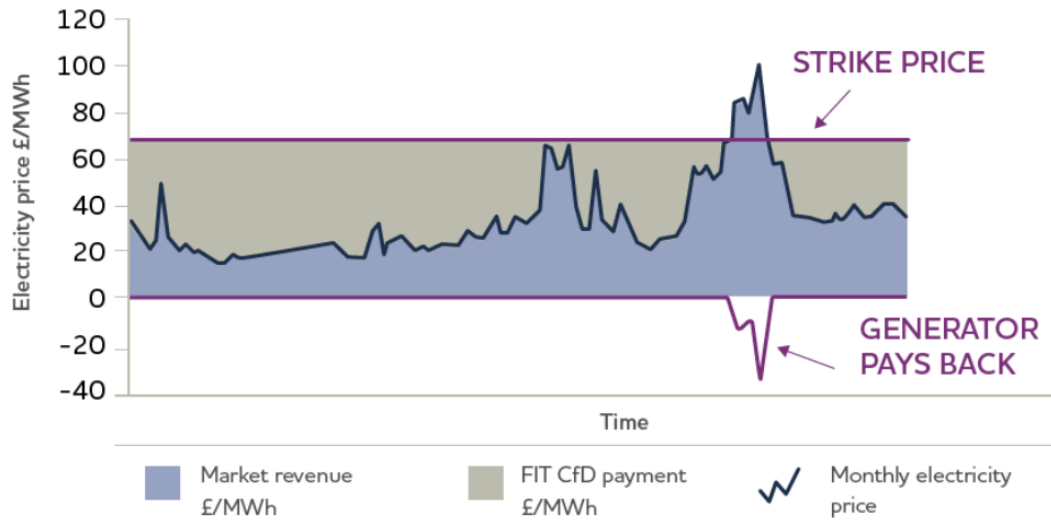
Figure. 6.2 CfD generator example [155]

The CfD model guarantees a stable premium for generators over a 15-20 year time-frame. In the UK, CfDs were issued by the Energy Act 2013 to replace RO, and the main reason behind that is many viewed as having considered CfDs to be an expensive method for incentivizing renewables. In April 2014, the first Contract for Difference (CfD) received parliamentary approval from the Secretary of State. During this period, the UK set a primary objective of achieving a 30% share of renewable electricity generation by the year 2020. Consequently, eight investment contracts were granted in anticipation that these agreements would contribute to the generation of 15 terawatt-hours (TWh) of energy by 2020. Currently, there are another three allocation rounds or competitive auctions that relate to CfDs, starting in 2015, 2017, and 2019 [156]. [157] reports that on 24 November 2020, a consultation decision was published by the Department for Business, Energy & Industry Strategy (BEIS) that relates to the proposed amendments to the CfD Scheme, and it states that the fourth allocation round (AR4) of CfD will be opened by the end of 2021, and BEIS has announced that there will an expansion of the CfD scheme which will include the increase in the capacity that has been offered at AR3 in 2019 from 5.8GW to 12GW, which means more than doubling. Renewable technologies have been grouped into pots; however, each pot will differ from the others in terms of funding, and the parameters of the bids. For instance, there was no funding for the last two allocation rounds for the pot 1 technologies which included onshore wind, and solar. The proposed pots for AR4 are as follows:

- Pot 1 (established technologies): Onshore wind (>5MW), Energy from Waste with CHP, Solar Photovoltaic (PV) (>5MW), Hydro (>5MW and <50MW), Landfill Gas and Sewage Gas.

- Pot 2 (less established technologies): ACT, Anaerobic digestion (AD) (>5MW),

remote island wind ($> 5MW$), tidal stream, wave-dedicated biomass with Micro combined heat and power (CHP), floating offshore wind and geothermal.

- New Pot 3 (offshore wind): offshore wind.

A change has been made which includes a new third pot has been introduced in AR4, ring-fencing offshore wind into its own class. However, It was in pot 2 of the previous rounds, this action has led to placing offshore wind in the same pot as well as putting it in direct competition with smaller-scale and more nascent technologies. The results obtained from the third round show that there were almost 95% of the CfD awards were allocated by (MW) to offshore wind. Previously, in the past, it was possible to add storage to CfD sites so long as they complied with the terms and conditions of their respective contract; however, they had to be metered separately on the basis of they are not considered a part of the facility itself. According to [158] Allocation Round 5 (AR5) will be opened in March 2023. The proposed updates to CfD can be found in [159] that detail the changes in technology pots, energy storage, and negative pricing. All GB-based licensed electricity suppliers (Supplier Obligation) must be committed to making payments to CfD Generators which is funded by a statutory levy. The payments are described below;

- A pre-payments must be paid by suppliers on eligible demand on a daily basis which consists of a unit cost fixed Interim Levy Rate (ILR), and the charge will be given as a £/MWh.

- At the beginning of each quarterly obligation period, lump sum Individual Supplier Reserve Amount payments should be taken into account.

For a given quarter, the Low Carbon Contracts Company (LCCC) will be responsible for giving forecasting the amount of the ILR and Total Reserve on a quarterly basis, before the start of the preceding quarter [160]. In this thesis, the rate that has been used for billing is £0.0879/MWh. This comprises the ILR plus the Operational Costs Levy (OCL). The OCL has published for the year ahead a flat rate across the financial year (Apr22-Mar23) which it is £0.0879/MWh [161], and the adjusted rate for ILR from 1 April 2022 to 30 Jun 2022 is £0/MWh [162]. The cost is calculated based on eq.6.3, and the results are given in Table 6.4.

$$Cost = (ILR + OCL) \times Import\ Energy(MWh) \qquad (6.3)$$

Table. 6.4 Analysis of **CFD** for DFR, DC & DR delivered by
BESS for Jun-2022, using Jun-2019 frequency data

Services	C-rate (C)	Cost (£)
DFR	0.5	133.70
	1	132.16
	2	126.25
DC	0.5	13.73
	1	13.73
	2	13.73
DR	0.5	268.18
	1	252.59
	2	226.08

6.4.3   FiT – Feed in Tariff

The feed-in tariffs (FIT) scheme was known as an environmental program introduced and designed by the government. The objective of such a scheme is to promote the uptake of renewable and low-carbon electricity generation technologies. In April 2019, this program has been closed to new applicants. however, the scheme was open to anyone who installed one of the following technology types with the maximum capacity of 5MW or 2kW for CHP, and they include; Solar photovoltaic (solar PV), Wind, Micro combined heat and power (CHP), Hydro, and Anaerobic digestion (AD). The payment will depend on the technology type and the date that suppliers joined the scheme and it is the supplier's responsibility to pay the generator for the electricity generated and exported back to the grid [163]. [164] statues that at the start of the scheme (April 2010) rates varied from 4.5p/kWh for 1.5MW-5MW Wind to 45.4p/kWh for 4kW solar panels installations. However, in 2018 rate for 4kW solar was 3.93p/kWh. Although the scheme is now closed to new applications it still needs to be paid for through a FiT levy to suppliers. The rate used for billing was £7.50 / MWh. Rates are not published but instead confirmed with suppliers via quarterly and annual levelisation invoicing processes, which reconcile and update forecasts on an ongoing basis. The cost is calculated based on eq.6.4, and the results are shown in Table 6.5.

$$Cost = Import\,Energy(MWh) \times £/MWh \qquad (6.4)$$

Table. 6.5 Analysis of **FiT** for DFR vs DC vs DR delivered by
BESS for Jun-2022, using Jun-2019 frequency data

Services	C-rate (C)	Cost (£)
DFR	0.5	11,408.18
	1	11,276.70
	2	10,772.40
DC	0.5	1,171.43
	1	1,171.43
	2	1,171.43
DR	0.5	22,882.2
	1	21,552.83
	2	19,290.38

6.4.4 AAHEDC-Assistance for Areas with High Electricity Distribution Costs

AAHEDC is a levy that is used to recover costs for the North of Scotland is considered the only area that needs assistance. The amount of assistance will be recovered through a charge to all suppliers and the cost will be passed on to Scottish Hydro Electric Power Distribution Ltd to decrease the distribution charges in the North of Scotland [165]. In each year, AAHEDC tariffs will be published by 15 July and applied on the first of April retrospectively. The AAHEDC tariff is applied to the net usage. For 2022/2023 the rate is 0.040670 p/kWh [166]. The cost is calculated based on eq.6.5, and the results are shown in Table 6.6.

$$Cost = (Export\ Energy(MWh) - Import\ Energy(MWh)) \times (p/kWh) \quad (6.5)$$

Table. 6.6 Analysis of **AAHEDC** for DFR vs DC vs DR delivered
by BESS for Jun-2022, using Jun-2019 frequency data

Services	C-rate (C)	Cost (£)
DFR	0.5	66.20
	1	72.28
	2	70.29
DC	0.5	2.21
	1	1.44
	2	4.89
DR	0.5	148.42
	1	140.61
	2	123.10

6.4.5 CM-Capacity Market

All Suppliers in the UK should be committed to funding the Capacity Market(CM) arrangements through the Settlement Costs Levy and the Capacity Market Supplier Charge. Suppliers will only be charged for a period from 4 pm to 7 pm on working days between Nov-Feb. CM is charged on a supplier's gross demand rather than net demand, and this method makes CM not qualify as an embedded benefit [167]. It is possible for a battery to participate in the auction for year-ahead delivery although the derating for batteries is currently high so would not add much in the way of revenue. The calculation of CM supplier charge payment and supplier's Settlement Costs Levy Payments are illustrated in eq.6.6, and eq.6.7.

$$Monthly\,CM\,supplier\,charge\,for\,supplier = Total\,annual\,capacity$$
$$provider\,payments \times (Monthly\,weighting\,factor)$$
$$\times (Suppliers\,gross\,demand\,for\,peak\,period)/(Gross\,demand\,of$$
$$all\,suppliers\,for\,peak\,demand) \quad (6.6)$$

$$Monthly\,Settlement\,Cost\,Levy\,for\,Supplier =$$
$$(Total\,Settlement\,Cost \times (Suppliers\,Gross\,Demand))$$
$$/(Gross\,demand\,of\,all\,Suppliers)/12 \quad (6.7)$$

For the period 2021-2022, the Jun weighting factor is 7.132%, total annual capacity payment = £609,476,116.40 [168], Settlement Costs Levy = £6,954,000.00, and Gross

demand of all Suppliers = 11,527,490.02 MWh [169]. In this thesis, the calculations of suppliers' gross demand for the peak period for each service (DFR, DC & DR) are shown in Table6.7.

Table. 6.7 Analysis of Suppliers' Gross Demand for Peak period for each Service (DFR, DC & DR) for the full month of Jun-2019

Services	C-rate (C)	Suppliers Gross Demand for Peak Period (MWh)
DFR	0.5	724.80
	1	720.64
	2	686.33
DC	0.5	77.41
	1	77.41
	2	77.41
DR	0.5	1,503.20
	1	1,408.76
	2	1,303.14

Herein, we have taken a 0.5C battery which has been used to deliver DFR service for Jun-2019 as an example to calculate CM. The calculation is given below;

$$Monthly\,CM\,supplier\,charge\,for\,supplier = £609,476,116.40\times$$
$$(0.07131951809 \times 724.80MWh/(11,527,490.02MWh) = £2,733.06$$

$$Monthly\,Settlement\,Cost\,Levy\,for\,Supplier = (£6,954,000.00\times$$
$$724.80MWh/(11,527,490.02MWh))/12 = £36.44$$

The calculations of CM for BESS with different C-rates and used to deliver different frequency response services (DFR, DC & DR) are shown in Table 6.8.

Table. 6.8 Analysis of **CM** for DFR vs DC vs DR delivered by BESS for Jun-2022, using Jun-2019 frequency data

Services	C-rate (C)	Monthly Settlement Cost Levy for Supplier (£)	Monthly CM supplier charge for supplier (£)
DFR	0.5	36.44	2,733.06
	1	36.23	2,717.37
	2	34.50	2,587.99
DC	0.5	3.89	291.89
	1	3.89	291.89
	2	3.89	291.89
DR	0.5	75.57	5,668.23
	1	70.82	5,312.11
	2	65.51	4,913.85

6.4.6 Balancing Services Use of System (BSUoS)

NGESO uses a detailed methodology to establish a daily BSUoS charge, taking into account the actual costs of balancing the system for each (HH) period, they then provide a monthly forecast of BSUoS charges and suppliers will reconcile this in arrears to charge the customer. According to [109] BSUoS charges are paid by both generators and suppliers. Figure 6.3 shows that the rate for Jun-2022 varied on a half-hour period between £0.54 /MWh to £34.06 with the average being £9.85/MWh [170].

Figure. 6.3 BSUoS Charges on the full month of Jun-2022

The BSUoS charge can be calculated using;

$$BSUoS\,charge \quad = \quad BSUoS\,Tariff \quad \times \quad (Metered\,Volume \quad \times \quad TLM) \quad (6.8)$$

Where; BSUoS Tariff is the price in £/MWh, Metered volume is the import/export energy over a period of time measured by MWh, and TLM is called Transmission Loss Multiplier which is produced by Elexon and can be calculated by dividing Transmission Loss (TL) between demand and generation users and using a parameter called the Generation/Demand (G/D) split which is currently considered as 45% of the losses deducted from the metered volume of generators and the remaining which is 55% will be added to the metered volume of the demand users [171].

The TLM can be calculated using;

$$TLM(for\,a\,generator\,unit) = (1 + TLF + GenLossAdjustment)$$

Where; Gen Loss Adjustment= - (Average transmission loss x G/D split)

$$TLM(for\,a\,demand\,unit) = (1 + TLF + DemandLossAdjustment)$$

Where; Demand Loss Adjustment=Average transmission loss x (1- G/D split)

In this thesis, the Transmission Loss Factor and Average transmission loss have been chosen for Zone 5 (Midlands) with values 0.007420 and 2% respectively [172]. Herein, the example of showing the calculations of BSUoS (Demand/Generation) for BESS with 0.5C used to deliver DFR service for the whole of Jun-2019 is shown below;

181

BSUoS/Generation

$$BSUoS\,charge = BSUoS\,Tariff \times Metered\,volume$$
$$\times (1 + TLF + Gen\,Loss\,Adjustment) \quad (6.9)$$

For DFR service;

$$BSUoS\,charge = £9.85/MWh \times (1,358.31MWh)\times$$
$$[1 + (0.0074207) + (-1 \times 2\% \times 45\%)] = £13,358.22$$

BSUoS/Demand

$$BSUoS\,charge = BSUoS\,Tariff \times (Metered\,Volume$$
$$\times TLM) = BSUoS\,Tariff \times Metered\,Volume\,volume$$
$$\times (1 + TLF + Demand\,Loss\,Adjustment) \quad (6.10)$$

For DFR service;

$$BSUoS\,charge = £9.85/MWh \times (1,521.09MWh)\times$$
$$[1 + (0.007420) + (1 \times 2\% \times (1 - 45\%))] = £15,258.72$$

The calculation of BSUoS is carried out using eq.6.9, and eq.6.10, and the results are illustrated in Table 6.9.

Table. 6.9 Analysis of **BSUoS** for DFR vs DC vs DR at different battery C-rate for the full month of Jun-2019

Services	C-rate (C)	Cost (£)	Revenue (£)
DFR	0.5	15,258.72	13,358.22
	1	15,082.87	13,038.89
	2	14,408.35	12,425.53
DC	0.5	1,566.81	1,589.54
	1	1,566.81	1,501.13
	2	1,566.81	1,417.93
DR	0.5	30,605.51	26,415.51
	1	28,827.44	24,861.28
	2	25,801.36	22,317.89

6.4.7 Distribution Use of System (DUoS)

DUoS is the cost of maintaining the regional network operated by the DNO (Distribution Network Operator) for the area for imported energy. This charge relates to consumers who installed the half-hourly meters and connected to the grid below 22kV, the charge is varied and depends on the time used, it's defined by three different bands which include; Red, Amber, or Green bands. The Red band is considered the highest charge where the consumer uses electricity during peak demand periods. Whereas, Amber and Green bands are currently charged at significantly lower rates [173]. The time period for each band is shown in [174]. DNOs publish their charging statements which will take effect from 1st April for each year, and in this thesis, the charge is taken for 2022 and applied to the West Midlands. The charges for ESS can be found under the LV Site Specific No Residual tariff with DUoS charges of £12.84/MWh, £2.24/MWh, and £0.09/MWh for red, amber, and green time bands, respectability [174]. In this thesis, BESS with different C-rates (0.5C, 1C, 2C) is procured to deliver frequency response services (DFR, DC & DR) 24/7 separately and the results are shown in Table 6.10, Table 6.11, and Table 6.12. The results illustrate that for all services, the cost increases when the C-rate decreases and vice versa, the highest cost was for BESS with 0.5C used to deliver DR service for the whole of Jun-2019 and the lowest cost was for BESS with 2C used to deliver DC service for the whole of Jun-2019. Moreover, in most charge-bands the costs are different however, for DC service where C-rate equates to 0.5C or 1C, the cost remains with the same value which equates (£320.14).

Table. 6.10 DUoS for BESS with a different C-rate delivering DFR services for Jun-2022 using Jun-2019, frequency data (Import)

	DFR (0.5C)			DFR (1C)			DFR (2C)		
	Import			Import			Import		
	Red	Orange	Green	Red	Orange	Green	Red	Orange	Green
Mon-Fri Energy (MWh)	143.37	533.23	422.07	141.31	531.86	415.14	137.51	395.52	385.03
Mon-Fri Cost (£)	1,840.87	1,194.44	37.99	1,814.42	1,191.37	37.36	1,765.63	885.96	34.65
Sat-Sun Energy (MWh)			507.59			500.25			477.54
Sat-Sun Cost (£)			45.68			45.02			42.98
Total unit charges (£)	3,118.98			3,088.17			2,729.22		

Table. 6.11 DUoS for BESS with a different C-rate delivering DC services for Jun-2022 using Jun-2019, frequency data, (Import)

	DC (0.5C)			DC (1C)			DC (2C)		
	Import			Import			Import		
	Red	Orange	Green	Red	Orange	Green	Red	Orange	Green
Mon-Fri Energy (MWh)	14.62	55.30	43.30	14.62	55.30	43.30	14.62	55.30	41.05
Mon-Fri Cost (£)	187.72	123.87	3.89	187.72	123.87	3.89	187.72	123.87	3.69
Sat-Sun Energy (MWh)			51.78			51.78			51.78
Sat-Sun Cost (£)			4.66			4.66			4.66
Total unit charges (£)	320.14			320.14			319.94		

Table. 6.12 DUoS for BESS with a different C-rate delivering DR services for Jun-2022, using Jun-2019 frequency data, (Import)

	DR (0.5C)			DR (1C)			DR (2C)		
	Import			Import			Import		
	Red	Orange	Green	Red	Orange	Green	Red	Orange	Green
Mon-Fri Energy (MWh)	287.61	1101.07	823.77	287.29	1034.15	764.77	242.15	890.76	720.61
Mon-Fri Cost (£)	3,692.91	2,466.39	74.14	3,688.80	2316.49	68.83	3,109.21	1,995.30	64.86
Sat-Sun Energy (MWh)			1013.96			947.11			846.26
Sat-Sun Cost (£)			91.25			85.23			76.16
Total unit charges (£)	6,324.69			6,159.35			5,245.53		

6.4.8 Generator Distribution Use of System (GDUoS)

Charges relate to the positive charges and negative credits associated with the local distribution of exported electricity onto the grid. The charge bands are the same as the DUoS and they appear on the DNOs charging statement, and for ESS appear under the HV Generation Site Specific tariff, £18/MWh, £3.13/MWh, and £0.17/MWh for red, amber, and green time bands, respectively [174]. The results are shown in Table 6.13, Table 6.14, and Table 6.15. The results show that, for all services, the revenue increases with the decrease in the C-rate and vice versa, and the highest revenue was obtained from BESS with 0.5C used to deliver DR service for the whole Jun-2019 however, the lowest revenue was obtained from the BESS with 2C used to deliver DC service for the whole Jun-2019.

Table. 6.13 DUoS for BESS with a different C-rate delivering DFR services for Jun-2022, using Jun-2019 frequency data, (Export)

	DFR (0.5C)			DFR (1C)			DFR (2C)		
	Export			Export			Export		
	Red	Orange	Green	Red	Orange	Green	Red	Orange	Green
Mon-Fri Energy (MWh)	139.23	430.07	409.78	139.23	409.11	409.78	137.51	395.52	382.45
Mon-Fri Cost (£)	2,506.14	1,346.12	69.66	2,506.14	1,280.51	69.66	2,475.18	1,237.98	65.01
Sat-Sun Energy (MWh)			458.41			446.91			423.07
Sat-Sun Cost (£)			77.93			75.98			71.92
Total unit charges (£)	3,999.85			3,932.29			3,850.09		

Table. 6.14 DUoS Charge for BESS with a different C-rate delivering DC services for Jun-2022, using Jun-2019 frequency data, (Export)

	DC(0.5C)			DC (1C)			DC (2C)		
	Export			Export			Export		
	Red	Orange	Green	Red	Orange	Green	Red	Orange	Green
Mon - Fri Energy (MWh)	15.98	52.11	53.37	15.96	48.90	50.72	15.65	46.49	42.24
Mon - Fri Cost (£)	287.64	163.10	30.96	287.28	153.06	29.42	281.7	145.51	24.49
Sat-Sun Energy (MWh)			50.19			46.56			46.56
Sat-Sun Cost (£)			8.53			7.92			7.92
Total unit charges (£)		490.23			477.68			459.62	

Table. 6.15 GDUoS Charge for BESS with a different C-rate delivering DR services for Jun-2022, using Jun-2019, frequency data (Export)

	DR (0.5C)			DR (1C)			DR (2C)		
	Export			Export			Export		
	Red	Orange	Green	Red	Orange	Green	Red	Orange	Green
Mon-Fri Energy (MWh)	282.32	829.52	843	272.76	799.17	767.84	236.42	718.44	697.21
Mon-Fri Cost (£)	5,081.76	2,596.39	143.31	4,909.68	2,501.40	130.53	4,255.56	2,248.72	118.53
Sat-Sun Energy (MWh)			893.65			839.94			745.29
Sat-Sun Cost (£)			151.92			142.79			126.69
Total unit charges (£)		7,973.38			7,684.4			6,749.5	

6.4.9 TNUoS – Transmission Network Use of System

This type of charge is used to recover the cost of installing and maintaining the transmission system in the zones that include; England, Wales, Scotland, and Offshore. Each year, NGESO publishes TNUoS tariffs which should take effect from 1 April up to the end of March next year. The charging method involves 'Triads' which are defined by NGESO as the three highest half-hour periods of demand which are separated by a clear window of at least ten days during the winter season which starts from 1 November and ends on the 28th/29th of February [175]. To determine how much the payment is each year for TNUoS, take the average demand over the three Triad periods and multiply it by the regional tariff. Typically, NGESO announces the Triads at the end of the winter months which can be by late March or early April. During the winter season, the estimation of transmission charges will be considered while after the Triads have been announced reconciliation will be taken place [176].
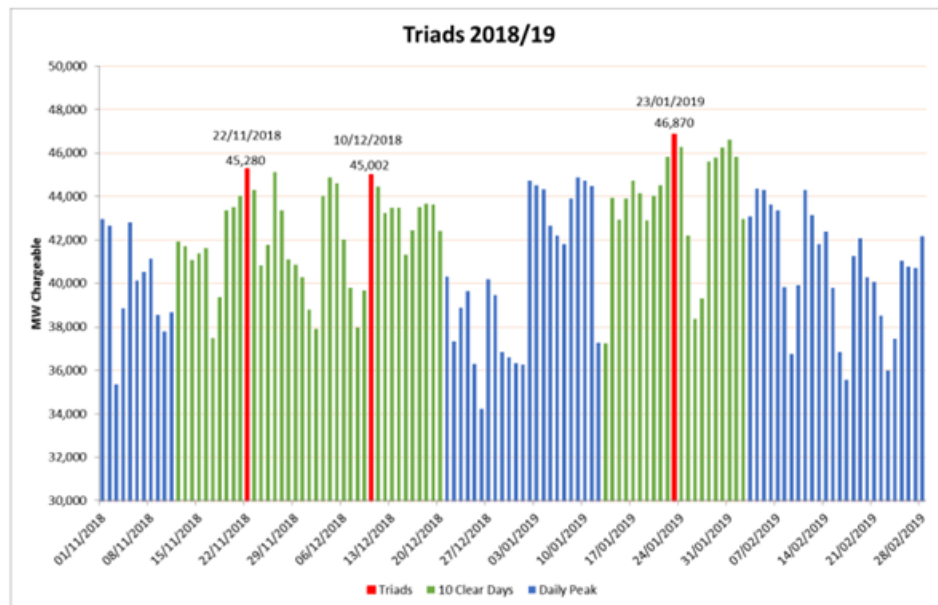
Figure. 6.4 Triads 2018/19 [177]

Figure 6.4 Illustrates the Triads for the year 2018/2019 which will be taken place herein in this thesis to calculate TNUoS charge. The charge is broken down into two categories which include (demand & generation).

TNUoS/Demand

The average Tariff for the year 2022/2023 is £55.063/kW [178]. The cost over the year can be calculated using eq.6.11 and the results are shown in Table 6.16.

$$Cost \quad = \quad Average\,Import\,Power\,at\,Triad(kW) \quad \times \quad Avg.Tariff(£/kW) \quad (6.11)$$

Table. 6.16 Analysis of TNUoS/Demand Charge for DFR vs DC vs DR at different battery C-rate for the full year-2022, using year-2019 frequency data

Services	C-rate (C)	Avg.Import Power over Triads (kW)	Cost (£)
DFR	0.5	1,422.03	78,300.98
	1	1,422.03	78,300.98
	2	1,422.03	78,300.98
DC	0.5	125.24	6,896.07
	1	125.24	6,896.07
	2	125.24	6,896.07
DR	0.5	2,503.13	137,829.39
	1	2,503.13	137,829.39
	2	2,503.13	137,829.39

TNUoS/Generation

The average Tariff for the year 2022/2023 is £11.622/kW [178]. The revenue over the year can be calculated using eq.6.12 and the results are shown in Table 6.17.

$$Revenue = Average\,Export\,Power\,at\,Triad(KW)$$
$$\times Avg.Tariff(£/kW) \quad (6.12)$$

Table. 6.17 Analysis of TNUoS/Generation Charge for DFR vs DC vs DR at different battery C-rate for the full year-2022, using year-2019 frequency data

Services	C-rate (C)	Avg.Export Power over Triads (kW)	Revenue (£)
DFR	0.5	732.34	8,511.50
	1	732.34	8,511.50
	2	732.34	8,511.50
DC	0.5	54.35	631.67
	1	54.35	631.67
	2	54.35	631.67
DR	0.5	1,083.97	12,598.26
	1	1,083.97	12,598.26
	2	1,070.39	12,440.43

As we can see from Table 6.17, the revenue obtained from BESS with different C-rates used to deliver DFR, DC, and DR for the entire year 2022 using TNUoS/Generation Charge is equal for each C-rate for the same service. The main reason is that the BESS exports the same power over the Triads for each C-rate. However, compared to these services, the revenue obtained from DR is the greatest, while that from DC is the lowest.

6.4.10 Elexon

This is a cost that Elexon charges all suppliers for being part of the Balancing and Settlement Code (BSC) and an active participant in the GB electricity markets. Whilst there is a published list of Elexon charges it's difficult to reconcile a specific supplier's cost because of the different methods of charging (per MWh, per meter, fixed) which leads to a different charge per supplier based on their portfolio makeup (number of Supplier Volume Allocation (SVA) meters, number of Central Volume Allocation (CVA) meters, number of additional or secondary BMUs, etc.) [179]. For the Jun-2022 invoice a rate of £0.20/MWh was applied, see the WESS invoice which is shown in Appendix D. The calculation is carried out using eq.6.13 and the results are shown in Table 6.18.

$$Cost = (Export\,Energy\,(MWh) + Import\,Energy$$
$$(MWh)) \times £0.20/MWh \quad (6.13)$$

Table. 6.18 Analysis of **Elexon** charge for DFR vs DC vs DR at different battery C-rate for the whole of Jun-2022, using Jun-2019, frequency data

Services	C-rate (C)	Cost (£)
DFR	0.5	575.88
	1	565.88
	2	539.96
DC	0.5	63.56
	1	61.77
	2	60.07
DR	0.5	1,147.39
	1	1,080.34
	2	968.28

6.4.11   TNUoS EET – Embedded Export Tarrif

One other part of TNUoS is called EET. It was established as a new tariff under code modifications CMP264/265. Based on the HH metered generation export volumes during the Triads, the tariff is paid to embedded generators. The tariff will take effect from 1 April each year. It is payable to both exporting HH demand customers as well as embedded generators (less than 100MW) [180]. The embedded generator (BESs) might licence exempt because it has a capacity of less than 100MW. TNUoS is also charged to suppliers of both half-hourly and non-half-hourly demand [178]. The calculation herein is based on the HH period and it is carried out using eq.6.14 The results are shown in Table 6.19.

TNUoS EET/Generation

The average EET tariff for the year 2022/2023 is £2.075/kW [178].

$$Revenue = Avg. Export\,power\,over\,Triad \times\ Avg. EET\,tariff \qquad (6.14)$$

Table. 6.19 Analysis of TNUoS EET- Embedded Export Charge for BESS delivering DFR vs DC vs DR at different C-rate for the whole of Jun-2022, using Jun-2019 frequency data

Services	C-rate (C)	Avg.Export Power over Triads (kW)	Revenue (£)
DFR	0.5	732.34	1,519.84
	1	732.34	1,519.84
	2	732.34	1,519.84
DC	0.5	54.35	112.79
	1	54.35	112.79
	2	54.35	112.79
DR	0.5	1,083.97	2,249.58
	1	1,083.97	2,249.58
	2	1,070.39	2,221.40

TNUoS EET/Demand

In this thesis, BESS is considered an embedded generator with a capacity of (40MW), so it can be license-exempt because it has a capacity of less than 100MW. Therefore, the charge is zero.

6.4.12   FFR–Fast Frequency Response

In this thesis, FFR is considered as the income paid for BESS providing whether (DFR, DC & DR) service during the month of Jun-2019. Figure 6.5 shows the reference price for the existing frequency response service for the year 2022.
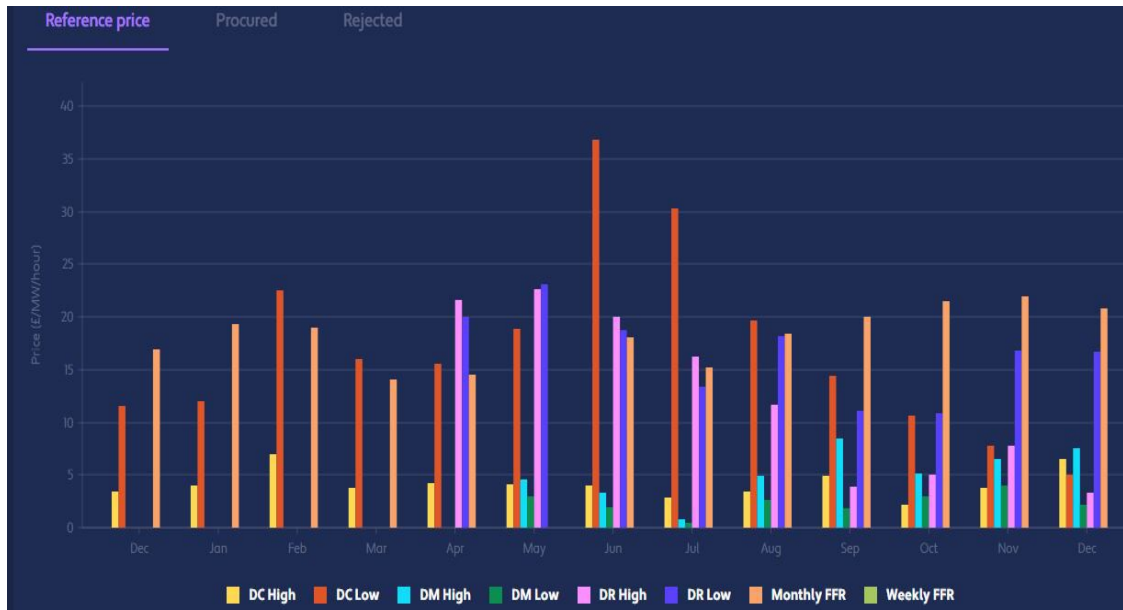
Figure. 6.5 The reference price for the existing frequency response service for the year-2022 [137]

In this thesis, the contracted amount is 40MW. As we can see from Figure 6.5, the prices for Jun-2022 of the frequency services that are used herein in this thesis are different from one service to another and they include; the monthly price for DFR is £18.10/MW/Hour, the price of DC-HF & DC-LF is £3.96/MW/hour, £36.78/MW/hour respectively, so the total price of DC service is £40.74/MW/hour, and the price of DR-HF & DR-LF is £20.02/MW/hour, £18.71/MW/hour respectively, so the average price of DR service is £19.37/MW/hour. The revenue calculation of each service is carried out by using eq.6.15;

$$Revenue = Contracted\ Volume(MW) \times Service\ Price(\pounds/MW/Hour) \times$$
$$24 Hour \times Days\ of\ month \quad (6.15)$$

- For DFR service

$$Revenue = 40MW \times (\pounds18.10/MW)/Hour \times 24Hours \times 30$$
$$= -\pounds521,280$$

- For DC Service

$$Revenue = 40MW \times (\pounds40.74/MW)/Hour \times 24Hours \times 30$$
$$= -\pounds1,173,312$$

- For DR Service

$$Revenue = 40MW \times (19.37/MW)/Hour \times 24Hours \times 30$$
$$= -£557,856$$

6.4.13 Imbalance

Each settlement period comprises two types of imbalance prices. These are; system buys price (SSP) and system sell price (SBP). However, both prices will be considered equal, which means that there will be only a single price that will be applied. ELEXON has applied such prices to Parties' imbalances to determine their imbalance charges. So, if a Party's generation or consumption does not comply with a contracted energy volume then a party is in imbalance. That is to say, if a party has generated less energy or over-consumed energy compared to the contracted volume then the shortfall of energy will be bought at SBP. Whereas, if a Party has under-consumed and over-generated compared to the agreed contracted energy then the extra energy can be sold at SSP [181]. In this thesis, BESS has delivered (DFR, DC & DR) services according to the contracted volume. Therefore, the imbalance charge will be considered here as zero.

6.4.14 DUoS Fixed

In the GB, DNO has set daily fixed DUoS charges which are known as 'Fixed charge p/MPAN/day' and it is based on consumers' contracted connection capacity. The rate for 2021/2022 is 90.06 p/MPAN/day [174]. For all services (DFR, DC & DR), the cost is calculated as given;

$$Cost = p/MPAN/day \times 30days \qquad (6.16)$$
$$= 90.06p/MPAN/day \times 30days$$
$$= £27.02$$

6.4.15 DUoS Capacity

This charge is related to the maximum import capacity in MVA that is mentioned in the connection agreement with the DNO. It is important for customers and suppliers to know that they only sign up for the capacity that they realistically need because the higher maximum import capacity that they might sign up for will result in the higher capacity charge [182]. The charge rate for 2021/2022 is 5.18p/kVA/day [174]. In this thesis, the connection capacity of a 1C battery is 40MVA. For all services (DFR, DC & DR) delivered by BESS with different C-rates, the cost is the same and it can be calculated

using the following formulae:

$$Cost = kVA \times Charge\ Rate(p/kVA/day) \quad (6.17)$$
$$= 40,000kVA \times 5.18p/kVA/day \times 30days$$
$$= 40,000kVA \times 0.0518\pounds/kVA/day \times 30days$$
$$= \pounds62,160$$

6.4.16   MOP DA/DC – Meter Operator / Data Aggregation / Data Collection

In the GB, Half-hourly (HH) metering must be installed for all businesses that have a peak load electricity usage over 100kW as well as any meters that are covered by P272 (05 – 08 NHH profiles) [183]). It is compulsory for all HH meters to have a Meter Operator (MOP), and a Data Collection/Data Aggregation (DC/DA) provider. The payment that relates to these services is considered a part of the non-commodity costs in the customer's invoice and is a pass-through from the providers of these services, [183]. The price related to such services for Jun-2022 is £1.5/day [174]. The cost for all services (DFR, DC, & DR) is calculated as given below;

$$Cost = \pounds1.5/day \times 30days = \pounds45 \quad (6.18)$$

6.4.17   Reactive Power

In general, to avoid Reactive power charges payment, at Metering Point, the power factor should be maintained between 0.95 to unity, and this can be achieved by best practice design of the properties' electrical installation. In this method, the charge will take place for all time periods [174]. It is possible to calculate reactive power charge by taking the reactive power outside of 0.95 in kvar, then multiplying it by the rate, and dividing the result by 100 [182]. In this section, charges relating to reactive power in p/kVarh have not taken place, and it is considered zero.

6.4.18   Excess Capacity

This charge methodology relates to the usage of excess power over the agreed amount specified in the connection contract agreement with the DNO. So, if the desired capacity has been exceeded, then the penalty will be raised to three times higher than the standard rate [174]. According to the discrepancy between the Maximum Import Capacity (MIC)/ Maximum Export Capacity (MEC) and the actual capacity used, the exceeding portion of the capacity will be charged at the excess capacity fee p/kVA/day rate. This will be billed for the whole billing cycle during which the breach of the contract takes place. This is determined in pounds by dividing the number of days by 100 and multiplying the rate by the difference between the maximum kVA consumed in the month and the chargeable

agreed capacity [182]. In this thesis, the agreed capacity has not been exceeded as BESS has delivered all services (DFR, DC & DR) according to NG specifications. Therefore, the excess capacity charge is equal to zero.

6.5 Revenue vs C-rate

In this section, the results obtained from the different charging methodologies discussed in this chapter will be analyzed based on cost and revenue. The system provided DFR, DC, or DR each day separately. The breakdown illustrated in the electricity supply invoice for Jun-2022, which relates to the proposed invoices, shows the individual cost/revenue elements classified as either a cost (positive) or revenue (negative).

The supplier provides a breakdown of the export and import energy per (HH) for a certain time period. In this section, we will consider two different time periods (month/year) of the proposed electricity supply invoice, and we will assess the obtained revenue against BESS with different C-rates.

6.5.1 Analysis of revenue vs C-rate for BESS used to deliver DFR, DC & DR for the whole of Jun-2022

In this section, BESS has delivered three frequency response services, namely DFR, DC, and DR, using different C-rates throughout Jun-2022. These services will be assessed by analyzing the cost and revenue. An example of the electricity supply invoice for Jun-2022 for BESS with 1C is shown in Table 6.20, and additional examples of supply invoices for BESS with different C-rates are presented in Table A3, Table A4, Table A5 (see Appendix D).
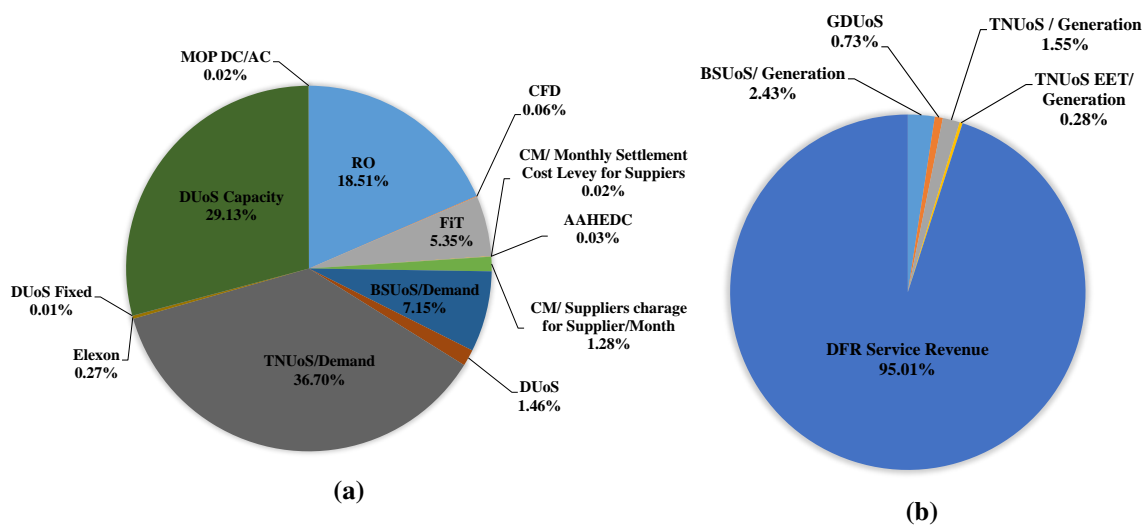
Figure. 6.6 Analysis findings of Cost (a), and Revenue (b) for BESS with 0.5C used to deliver DFR service for Jun-2022, using frequency data of Jun-2019.

As we can see from Figure 6.6, (Table A3, Figure A4, and Figure A6, see Appendix

D), where BESS with different C-rates has been used to deliver DFR service using Jun-2019 frequency data, the highest cost for at all C-rates (0.5C, 1C & 2C) was TNUoS/Demand which representing almost 36.70%, 33.84%, and 37.45% of the total cost, respectively. The second highest cost for all C-rates was DUoS Capacity which represented approximately 29.13%, 29.25%, and 29.73% of the total cost of each C-rate, respectively. The third greatest cost for all C-rates was RO which represented around 18.51%, 18.36%, and 17.83% of the total cost of each C-rate, respectively. The fourth highest Cost for all C-rates was BSUoS/Demand which represents ∼7.15%, 7.10%, and 6.89% of the total cost of each C-rate. The fifth highest cost for all C-rate was FiT which represents almost 5.35%, 5.31%, and 5.15% of the total cost of each C-rate, respectively. In addition to that, for all C-rates, the other costs represent a very small percentage (less than 1.5%) of the total cost, and some of them with same value for each C-rate.

Regarding the revenue, Figure 6.6 (b), (Table A3, Figure A4(b), and Figure A6(b). See Appendix D), it is clear that the highest revenue for all C-rates (0.5C, 1C & 2C) is DFR services revenue which represents almost 95.01%, 95.08%, and 95.20% of the total revenue of each C-rate, respectively, and the second and third greatest revenue for all C-rates were BSUoS/Generation and GDUoS, and they are with the highest values for 0.5C and with the lowest value for 2C, and this has led the DFR services revenue for 0.5C represented with the lower percentage from the total revenue compared to other C-rates, however these cost categories were represented with the small percentage of the total revenue(less that 2.5%). That is to say, in overall, compared to the different C-rates, the cost of 0.5C was the highest, and the cost of 2C was the lowest, and this made 2C with the highest total cost (cost & revenue) while 0.5 with the lost total cost.

(a)   **(b)**
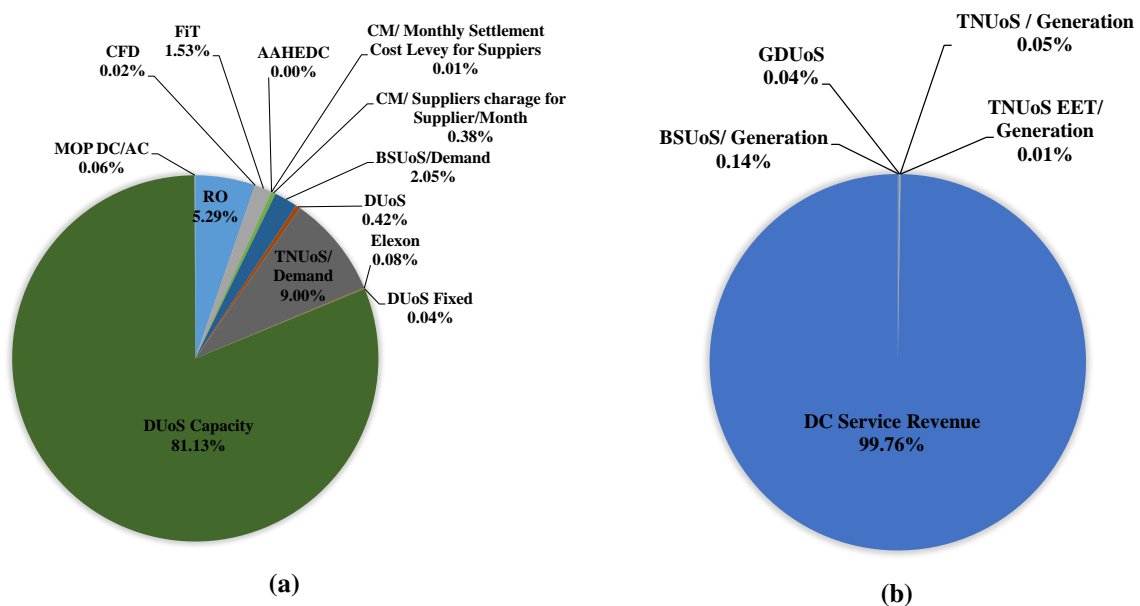
Figure. 6.7 Analysis findings of Cost (a), and Revenue (b) for BESS with 0.5C used to deliver DC service for Jun-2022, using frequency data of Jun-2019.

It can be noticed that from Figure 6.7 (a), (Table A4, Figure A7, and Figure A8) see

Appendix D, where BESS with different C-rates (0.5C, 1C & 2C) has been used to deliver DC service using Jun-2019 frequency data, for the cost (a), all costs were almost with the same values for all C-rates, and the highest cost was DUoS Capacity, and the second and third greatest costs were RO, and TNUoS. The main reason for the cost was getting the same value at each C-rate because BESS imported the same amount of energy for Jun-2019.

From Figure 6.7 (b), (Table A4, Figure A7, and Figure A8) see Appendix D, it is clear that the highest revenue for all C-rates (0.5C, 1C, and 2C) was DC service revenue which representing around 99.76%, 99.77%, and 99.78% of the total revenue for each C-rate.£1,173,312, and represent almost 99.76%, 99.75%, 99.78% of the total revenue for each C-rate, respectively, and the main reason behind getting these values is because of compared to other C-rates, BESS with 0.5C made a higher income from other charge methodologies such as BSUoS/ Generation, and TNUoS/Generation. The lowest revenue for all C-rates was TNUoS EET/Generation which represents almost 0.01% of the total revenue for each C-rates. Therefore, the highest total cost was obtained from 0.5C, while the lowest total cost was obtained from 2C.
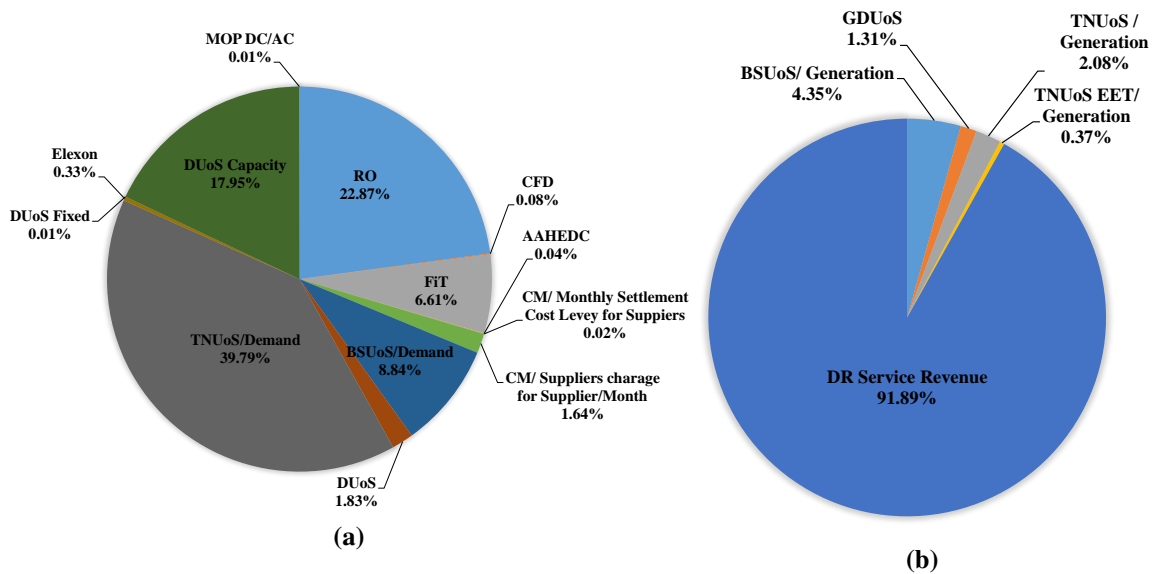
Figure. 6.8 Analysis findings of Cost (a), and Revenue (b) for BESS with 0.5C used to deliver DR service for Jun-2022, using frequency data of Jun-2019.

From Figure 6.8 (a), (Table A5, Figure A9, and Figure A10) see Appendix D, where BESS with different C-rates has been used to deliver DR service without implementing a dynamic control for using Jun-2019 frequency data, for the cost (a), it is clear to see that, for all C-rates (0.5C, 1C & 2C), the highest cost was TNUoS/Demand which representing $\sim$ 39.79% for 0.5C, and 42.61% for both 1C &2C from the total cost of each C-rate, respectively. The second greatest cost for all C-rates was RO which represented almost 22.87%, 23.06%, and 20.46% of the total cost for each C-rates, respectively. The third highest cost for all C-rates was DUoS Capacity which represented approximately 17.95% of the total cost of 0.5C and represented the same value for both C1 &C2 which was

almost 19.22% of the total cost of each of these C-rates. The fourth and fifth highest costs for all C-rates were BSUoS/Demand and FiT which represented almost 8.84%, 6.61% of the total cost of 0.5C, representing 8.91%, and 6.66% of the total cost of 1C, and representing ∼7.98%, and 5.96% of the total cost of 2C. The other costs represent very small values (less than 2%) of the total cost which means that they have had a significantly lower effect on the total cost for each C-rate.

In the regard to the revenue, From Figure 6.8 (b), (Table A5, Figure A9, and Figure A10) see Appendix D, it can be noticed that the highest revenue for all C-rates (0.5C, 1C & 2C) was DR service revenue which representing almost 91.89%, 92.17%, and 92.73% of the total revenue of each C-rate, respectively. Therefore, BESS with 0.5C was generating the highest revenue while at 0.2C was generating lower revenue, however, at 0.5C BESS was with the highest cost so, the greatest total cost (cost % revenue) was gained from BESS with 2C. Compared to all three services, DC at 0.5C was with the highest total cost while the lowest total cost was obtained from DR at 0.5C.

Table. 6.20 Energy supply invoice for Jun-2022, BESS with 1C-rate used to deliver DFR, DC & DR Service for Jun-2019 frequency data

Cost Breakdown					
Cost		Charger Point	Cost/Revenue DFR	Cost/Revenue DC	Cost/Revenue DR
RO		MSP	£39,032.42	£4,054.69	£74,601.51
CFD		NBP	£132.16	£13.73	£252.59
FiT		MSP	£11,276.70	£1,171.43	£21,552.83
AAHEDC		GSP	£72.28	£1.44	£140.61
CM	Monthly Settlement Cost Levy for Supplier	NBP	£36.23	£3.89	£70.82
	Monthly CM supplier charge for supplier	NBP	£2,717.37	£291.89	£5,312.11
BSUoS	Generation	NBP	-£13,038.89	-£1,501.13	-£24,861.28
	Demand	NBP	£15, 082.87	£1,566.81	£28,827.44
DUoS		MSP	£3,088.17	£320.14	£6,159.35
GDUoS		MSP	-£3,932.29	-£477.68	-£7,684.4
TNUoS	Demand	MSP	£78,300.98	£6,896.07	£137,829.39
	Generation	MSP	-£8,511.50	-£631.67	-£12,598.26
Elexon		GSP	£565.88	£61.77	£1,080.34
TNUoS EET	Generation	NBP	-£1,519.848	-£112.79	-£2,249.58
	Demand	NBP	0	0	0
Frequency Response Revenue		GSP	-£521,280	-£1,173,312	-£557,856
DUoS Fixed		Supply	£27.02	£27.02	£27.02
DUoS Capacity		Site	£62,160	£62,160	£62,160
MOP DC/AC		Supply	£45	£45	£45
Total Cost		-	-£350,828.32	-£1,099,421.39	-£267,190.51

6.5.2 Analysis of revenue vs C-rate for BESS used to deliver DFR, DC & DR for the whole of the year- 2022

In this section, the three frequency response services which include; (DFR, DC & DR) have been delivered by BESS with different C-rates for the whole of the year-2022, and these services will be assessed by the analysis of the cost and revenue. The supplier provides a breakdown of the total export and import energy per half hour for the whole of the year-2022 which are shown in Table 6.22. Herein, we have applied all charges methodologies that have been used for Jun-2022 on the year-2022 in order to calculate

the total cost by taking the difference between cost and revenue over the year, and two things needed to be considered;

- Take the average frequency service price over the year.

- TNUoS for demand & generation will be paid in one time (lump sum) which is paid in Jun-2022.

The calculation of total unit charge for both DUoS & GDUoS over the year-2022 can be found in, Table A7, Table A8, Table A9, Table A10, Table A11, see Appendix D. An example of the electricity supply invoice for the year-2022 for BESS with 1C is shown in Table 6.21, and the other examples of supply invoices for BESS with different C-rates are shown in Table A12, Table A13 (see Appendix D).

Table. 6.21 Analysis of DFR vs DC vs DR for the full Year-2019 frequency data

Contracted Service Power (MW)	C-rate (C)	Total Import Energy (MWh)	Total Export Energy (MWh)	Avg. Availability (%)	Services
±40	0.5	18,074.63	16,257.09	96.51	DFR
	1	17,789.19	15,807.78	94.45	
	2	16,704.54	14,785.29	90.02	
±40	0.5	1,847.47	1,884.56	100	DC
	1	1,847.47	1,820.87	99.78	
	2	1,847.47	1,720.33	98.43	
±40	0.5	35,823.25	31,804.42	94.14	DR
	1	33,263.91	29,439.85	89.40	
	2	29,784.61	26,390.07	83.18	

Table. 6.22 Energy supply invoice of year 2022 for BESS with 1C used to deliver DFR, DC & DR Service for the full year-2019 frequency data

| Cost Breakdown					
Cost		Charger Point	Cost/Revenue DFR	Cost/Revenue DC	Cost/Revenue DR
RO		MSP	£461,807.37	£47,960.32	£863,531.10
CFD		NBP	£1,563.67	£162.39	£2,923.89
FiT		MSP	£133,418.93	£13,856.03	£249,479.33
AAHEDC		GSP	£801.02	£10.76	£1,545.95
CM	Settlement Cost Levy for Supplier/ Year	NBP	£445.52	£47.86	£870.93
	CM supplier charge for supplier/Year	NBP	£41,543.55	£4,462.54	£81,212.38
BSUoS	Generation	NBP	–£155,460.70	-£17,907.24	-£289,524.60
	Demand	NBP	£178,451.10	£18,532.78	£333,684.80
DUoS		MSP	£40,165.12	£4,161.21	£78,189.71
GDUoS		MSP	-£45,775.86	-£5,898.87	-£95,649.54
TNUoS	Demand	MSP	£78,300.98	£6,896.07	£137,829.39
	Generation	MSP	-£8,511.50	-£631.67	-£12,598.26
Elexon		GSP	£6,719.39	£733.67	£12,540.75
TNUoS EET	Generation	NBP	-£1,519.84	-£112.79	-£2,249.58
	Demand	NBP	0	0	0
Frequency Response Revenue		GSP	-£5,509,164	-£7,622,660	-£3,781,838
DUoS Fixed		Supply	£328.72	£328.72	£328.72
DUoS Capacity		Site	£756,280	£756,280	£756,280
MOP DC/AC		Supply	£547.50	£547.50	£547.50
Total Cost		-	-£4,020,059.03	-£6,793,230.72	-£1,662,895.53
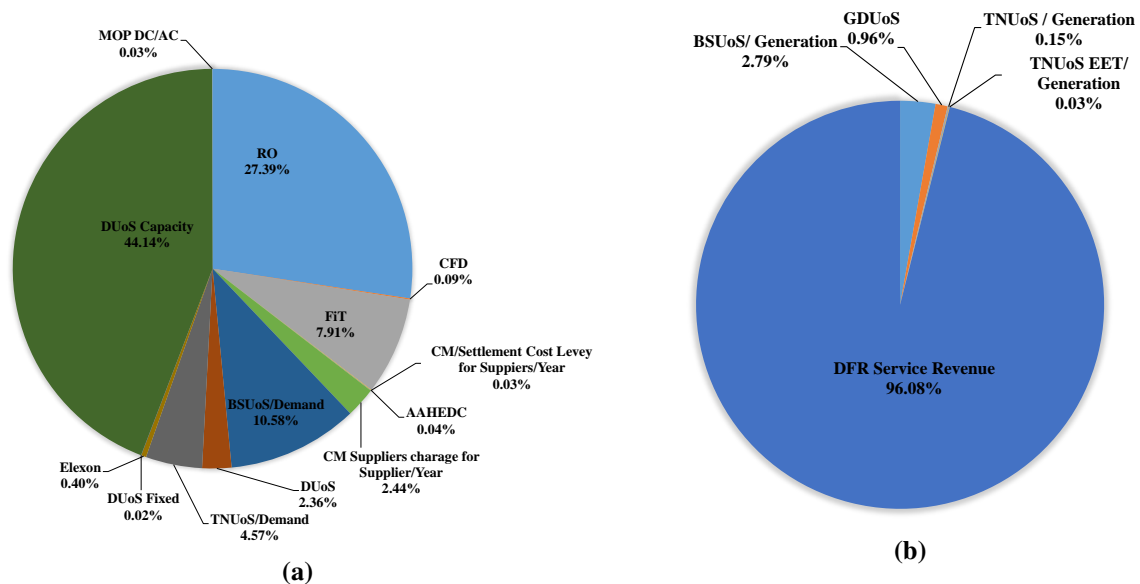
Figure. 6.9 Analysis findings of Cost (a), and Revenue (b) for BESS with 0.5C used to deliver **DFR** service for the whole year-2022, using frequency data of year-2019.

As we can see from Table 6.21, Figure 6.9 (a), Table A12, Table A13, Figure A11, Figure A16, see Appendix C, where BESS with different C-rates (0.5C, 1C & 2C) has been used to deliver DFR service for the whole year-2022, using year-2019 frequency data, for all C-rates, DUoS Capacity was the highest cost and compared to the obtained results from Jun-2022, it was representing increment equates to almost 15.1%, 15.23%, and 16.13% of the total cost, respectively. However, TNUoS/Demand was representing a decrement equating to $\sim$ 31.5%, 32.24%, and 32.7% of the total cost, respectively, and the main reason behind decreased this cost in the year, this is because it has been considered as a lump sum (one payment) paid on Jun-2022 as discussed earlier in Section 6.4.9. Additionally, for all C-rates and compared to the Jun-2022 cost, RO was representing almost the same increment which equates to $\sim$8.8% of the total cost of each C-rate. The lowest cost for all C-rates was DUoS Fixed which represents almost 0.02% of the total cost for each C-rate and compared to Jun-2022, it has been increased by a very small amount represented by almost 0.01%.

In regard to the revenue, from Table 6.21, Figure 6.9 (b), and Table A12, Table A13, Figure A11, Figure A16, see Appendix C, it is clear that for all C-rates (0.5C, 1C & 2C), DFR service revenue was the highest revenue representing increment compared to Jun-2022 equates to almost 1.07%, 4.54%, 1.32% of the total revenue for each C-rate, respectively. TNUoS/Generation represented a significantly lower revenue compared to Jun-2022 which is less than 0.035% of the total revenue.

202
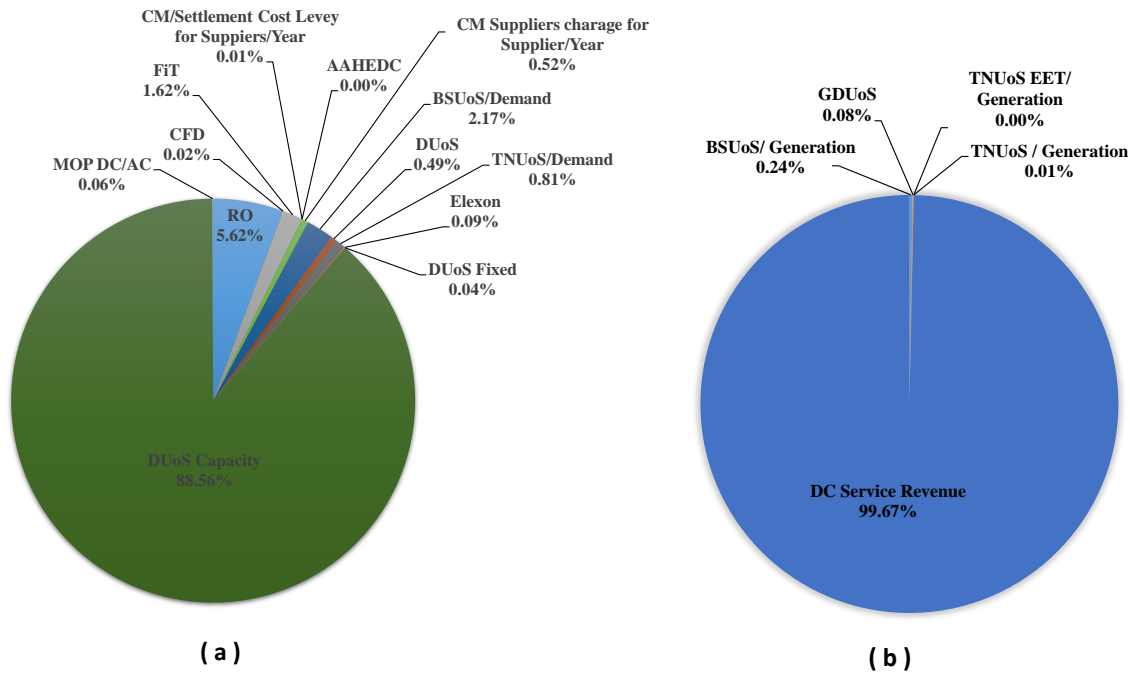
Figure. 6.10 Analysis findings of Cost (a), and Revenue (b) for BESS with 0.5C used to deliver **DC** service without submitting a P_{Base} for the whole year-2022, using frequency data of year-2019.

From Table 6.21, Figure 6.10 (a), and Table A12, Table A13, Figure A12, Figure A15, see Appendix B, where BESS with different C-rates (0.5C, 1C & 2C) has been used to deliver DC service without submitting a P_{Base} for the whole year-2022, using frequency data for the year-2019, it is clear that, DUoS Capacity was the highest cost for all C-rates (0.5C, 1C & 2C) and compared to Jun-2022, it represents the same increment equates to almost 7.43% of the total cost of each C-rate, and the main reason behind for this cost has got a significantly highest value compared to other costs as well as compared to other services (DFR, & DR) is because of BESS delivered DC service imported a very small amount of energy from the grid. At all C-rates and compared to Jun-2022, RO was almost with the same increment equates to 0.33%, of the total cost of each C-rate. Some of the rest of the costs represented the same value while the others were slightly increased compared to Jun-2022. However, TNUoS/Generation represented a significant decrement for all C-rates (0.5C, 1C, and 2C), amounting to almost 8.96% of the total cost

In the case of the revenue, from Table 6.21, Figure 6.10 (b), and Table A12, Table A13, Figure A12, Figure A15, (see Appendix D), it can be noticed that the highest revenue for all C-rates (0.5C, 1C & 2C) was the DC service revenue, and compared to Jun-2022, it was representing a decrement equates to almost 0.09%, 0.09%, and 0.08% of the total revenue for each C-rate, respectively. The lowest revenue for all C-rates was TNUoS/Generation which represents a very small value equating to 0.5C almost 0.05%, considered 0% for both 1C & 2C of the total revenue. Therefore, when it comes to calculating the total cost for each C-rate, 0.5C will have the highest total cost compared to 1C & 2C.
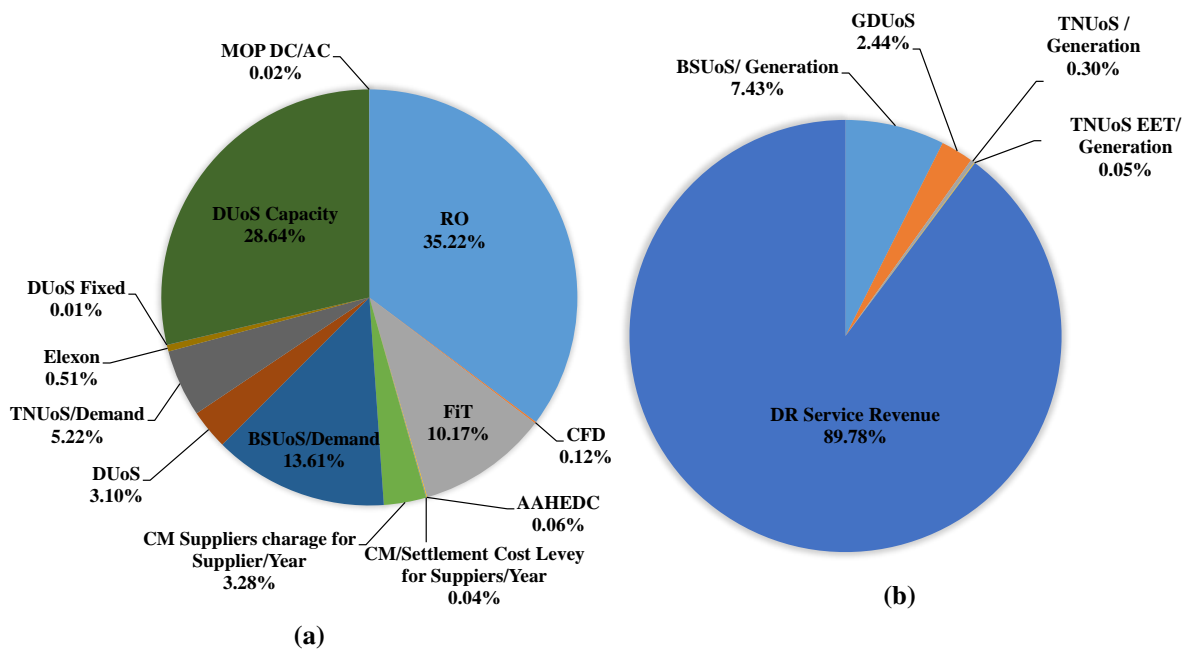
Figure. 6.11 Analysis findings of Cost (a), and Revenue (b) for BESS with 0.5C used to deliver **DR** service without implementing a dynamic control for the whole year-2022, using frequency data of year-2019.

From Table 6.21, Figure 6.11 (a), and Table A12, Table A13, Figure A13, Figure A14b, see Appendix D, where the BESS with a different C-rates (0.5C, 1C, 2C) used to deliver DR service without implementing a dynamic control for the whole year-2022, using frequency data of Jun-2019, it can be seen that RO was the highest cost for all C-rates (0.5C, 1C & 2C) and compared to Jun-2022, it has been represented an increment equates to approximately 12.35%, 11.22%, and 12.13% of the total cost of each C-rate. The second highest cost for all C-rates was DUoS Capacity which represented almost 10.69%, 10.08%, and 12.84% of the total cost of each C-rate, respectively. In contrast, for 0.5C, 1C & 2C and compared to Jun-2022, TNUoS/Demand represented a decrement equates to almost 34.57%, 37.14%, and 36.77% of the total cost for each C-rate. For all C-rates, BSUoS/demand with the increment equates to approximately 4.77%, 4.34%, and 4.68% of the total cost of each C-rate, respectively. The other costs were slightly increased. The lowest cost for all C-rates was MOP DC/AC which represented a very small increment equates to almost 0.01% of the total cost for each C-rate.

In the case of the revenue, from Table 6.21, Figure 6.11 (b), and Table A12, Table A13, Figure A13, Figure A14b, it is clear that the highest revenue for 0.5C, 1C & 2C and compared to Jun-2022 was the DR service revenue which represented a decrement equated to almost 2.11%, 1.74%, and 1.40% of the total revenue for each C-rate. The lowest revenue was TNUoS EET/Generation which represents a very small value equates to almost 0.05% of the total revenue. Therefore, when it comes to calculating the total cost (cost & revenue) for BESS with 2C used to deliver DR service was with the highest total cost while 0.5C was with the lowest total cost.

6.6 Net Present Value (NPV)

Net present value (NPV) is a financial method that can be calculated by taking the difference between the present value (PV) of cash inflows and the present value (PV) of cash outflows for a specific time period [184]. The NPV can be calculated using,

$$NPV = \sum_{t=1}^{n} \frac{R_t}{(1+i)^t} \tag{6.19}$$

where Rt is a difference between Net cash inflow and out flows during a single period (t), i= discount rate or investment rate, and t=Number of timer periods [2].

6.6.1 Capacity Factor (CF)

CF is mathematically represented by eq.6.20 and is defined as the ratio of the actual energy supplied by BESS over a year in MWh to the amount of energy that BESS could deliver if it is operated at full rated power (installed capacity in MW), for 24h per day for a year [185].

$$CF = \frac{E_{BESS}(MWh/yr)}{P_R(MW) * 8760(h/yr)} \tag{6.20}$$

Where E_{BESS} is the actual energy that BESS could be generated over a year in MWh, P_R is the maximum rated power in (MW).

6.6.2 NPV for BESS with a different C-rates (0.5C, 1C, 2C) used to deliver (DFR, DC & DR) services for the whole year-2022

In this thesis, the installed capacity of BESS is equal to (40MW) and such a battery should be able to absorb or deliver energy from or to the grid 24/7 for each month of 2022. As we can see from Table 6.1, battery prices range from £130/kWh to £300/kWh, so, in this thesis, we assumed a constant per-energy-unit battery price of £209/kWh with a capital cost of 441k(/MWh), and O&M cost will be 2.5% of battery purchase cost which equal to (£5.225/kW-yr), and the investment rate is expected to pay 8% per year. In this thesis, it is assumed that there are nine scenarios as listed in Table 6.30, and in each project, BESS was modeled as 24/7 and it will be used to deliver DFR, DC & DR service for 15 years based on the lifetime of cells. In this thesis, a 1C battery (40MW/40MWh) is used to deliver each service separately. Therefore, the capital cost and the annual maintenance cost for each project are calculated below;

$$Capital\,Cost = £441k(/MWh) \times 40(MWh) = £17,640,000$$

$$Annual\,Maintenance\,Cost = £5.225k/MW \times 40MW$$
$$= £209,000$$

The calculations of NPV are carried out using eq.(6.19) and the results are shown in Table 6.23.

The calculation of NPV for BESS with different C-rates used to deliver DFR, DC & DR service for 15 years

In this section, nine scenarios listed from A−I will be examined in terms of average availability, C-rate, NPV, and CF. These scenarios include those from A−C, which focus on BESS with different C-rates used to deliver DFR service; scenarios from D−F, which pertain to BESS with different C-rates used to deliver DC service; and the last scenarios from G−I, which concern BESS with different C-rates used to deliver DR service. The delivery time is assumed to be 15 years based on the LTO battery lifetime. The results are shown in Table 6.23 and Table 6.24.

Table. 6.23 Analysis NPV for BESS with different C-rates used to deliver DFR, DC & DR for 15 years

Services	C-rate (C)	Battery Capital Cost (£)	The PV of net cash flows (£)	The PV of Operation & Maintenance cost (£)	NPV (£)
DFR	0.5	-17,640,000	34,415,655.32	-1,788,931.05	14,986,724.28
	1	-17,640,000	34,409,609.59	-1,788,931.05	14,980,678.55
	2	-17,640,000	34,737,765.28	-1,788,931.05	15,308,834.24
DC	0.5	-17,640,000	58,153,400.36	-1,788,931.05	38,724,469.31
	1	-17,640,000	58,146,513.57	-1,788,931.05	38,717,582.52
	2	-17,640,000	58,135,777.84	-1,788,931.05	38,706,846.80
DR	0.5	-17,640,000	13,452,633.84	-1,788,931.05	-5,976,297.20
	1	-17,640,000	14,233,518.85	-1,788,931.05	-5,195,412.20
	2	-17,640,000	15,252,048.88	-1,788,931.05	-4,176,882.17

Table. 6.24 Analysis C-rate vs Avg.availability vs CF vs NPV

Services	C-rate (C)	Avg.availability (%)	CF(%)	NPV(£)	Scenarios
DFR	0.5	96.51	4.64	14,986,724.28	A
	1	94.45	4.51	14,980,678.55	B
	2	90.02	4.22	15,308,834.24	C
DC	0.5	100	0.54	38,724,469.31	D
	1	99.78	0.52	38,717,582.52	E
	2	98.43	0.49	38,706,846.80	F
DR	0.5	94.14	9.08	-5,976,297.20	G
	1	89.4	8.40	-5,195,412.20	H
	2	83.18	7.53	-4,176,882.17	I
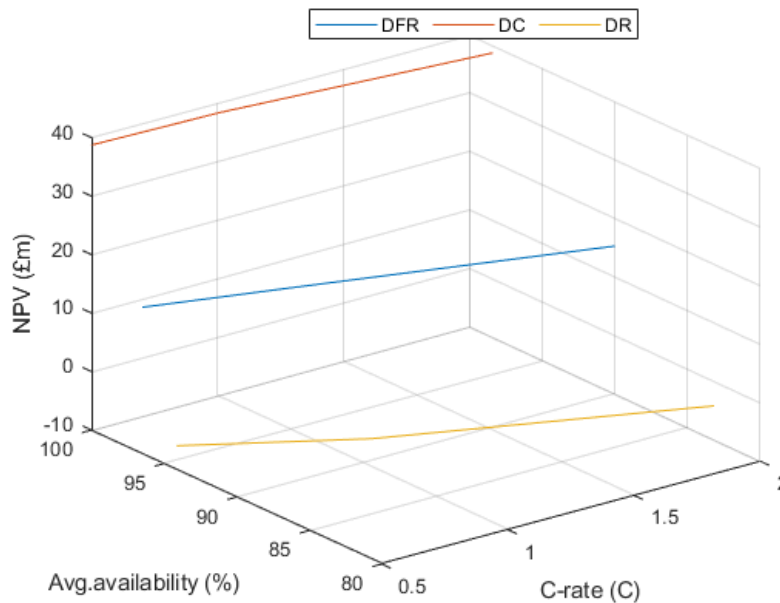
Figure. 6.12 NPV vs C-rate vs Avg. availability

Table 6.24, and Figure 6.12 show the relationship between C-rate, NPV, and average availability for BESS to deliver DFR, DC & DR services for 15 years period. It is clear that compared to all different scenarios, scenario (D) was the best option where BESS with the highest average availability reached 100% and achieved the greatest NPV, while in scenario (F) when C-rate increased to 2C, both average availability and NPV have been decreased by almost 1.57%, and 0.05%, respectively, however, these values still the highest compared to other services. For DFR service, the highest average availability was obtained at 0.5C, however, the greatest NPV was in scenario (C) where the C-rate is equal to 2C. Regarding DR service, the average availability increases with the decrease in the C-rate and vice versa, the highest average availability was obtained at 0.5C but it is still the smallest value compared to the other services, and in terms of NPV, it is increased by

the increase in C-rate, however, for this service with all scenarios (F - I), the NPV was equated to zero which means these scenarios will not be accepted. That's to say, compared to all scenarios, the only scenarios that could be accepted are listed from (A -F) because they have a positive NPV, however, the more profitable scenarios are delivered by DC (D, E, F) because they have a higher NPV.
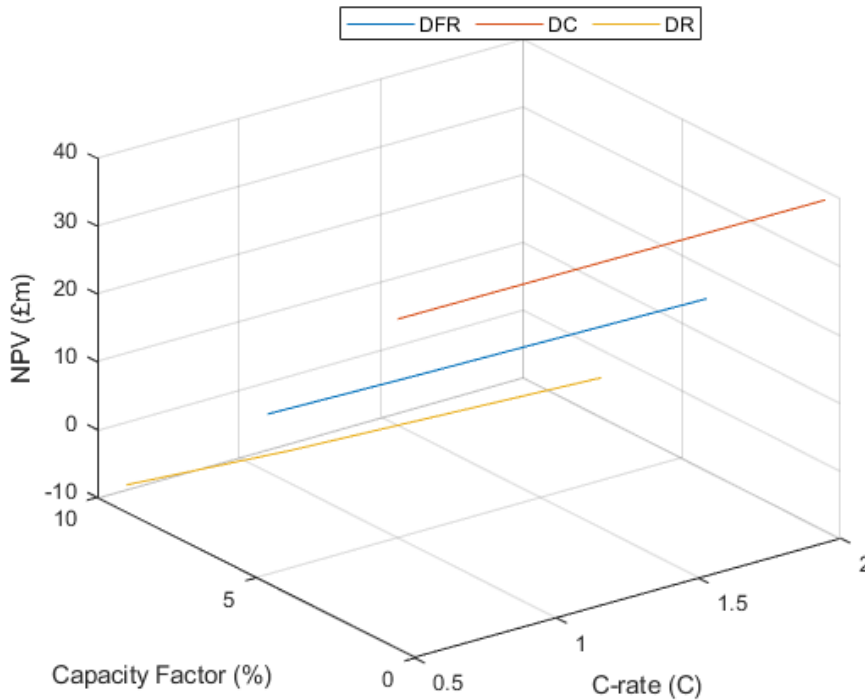
Figure. 6.13 NPV vs C-rate vs Capacity Factor

Table 6.24, and Figure 6.13 illustrate the relationship between C-rate, NPV, and CF for BESS used to deliver DFR, DC, & DR for 15 year period. It can be seen that the C-rate increases while the capacity factor decreases and vice versa. Compared to all services, the lowest values for the CF were at the DC service, specifically in scenario (F), and the highest NPV was obtained for this service in scenario (D), for this service when the C-rate decreases the NPV and CF increases and vice versa. For the DFR service, the CF was with a maximum value obtained at 0.5C (scenario A) while it was with a minimum value of 2C but with the highest NPV. Additionally, for DR service, when the C-rate decreases the NPV decreases while the CF increases and vice versa, the highest NPV was obtained in scenario (I) but the greatest CF was obtained in scenario (G), however, all scenarios (G, H & I) for this service will not be accepted because they are with a negative NPV and higher CF. In contrast, other scenarios such as (A, B, C, D, E, and F) are accepted because the NPV is positive. However, the scenarios that relate to DC service which include (D, E & F) are more profitable because they have higher NPV and lower CF compared to the other scenarios.

6.6.3 Revenue vs SOC Management

In this section, both services DC & DR will be delivered using BESS and assessed in terms of cost and revenue based on SOC management for each service. However, DFR service will not take place in such assessment because according to NG specification, in such service there is no opportunity to charge-discharge the battery in DB which means the SOC management will not be considered for DFR service.

A. Analysis DC services without baseline power vs DC with submitting a baseline power

In this section, an assessment based on the revenue vs SOC management will take place for DC service with and without P_{Base} delivered by BESS for Jun-2022, and for the whole year 2022 using frequency data of 2019, and the methodology of submitting a P_{Base} power is discussed in Chapter 3, Subsubsection 3.4.4. The simulation results of BESS used to deliver DC service for Jun-2022, and the proposed energy supply invoice for this month are shown in Table A14, and Table A15 (see Appendix E). The simulation results of BESS used to deliver DC service for the whole year-2022 can be seen in Table 6.25, the calculation of total unit charge for both DUoS GDUoS over the Jun-2022 can be found in Table A16, Table A17 (see Appendix E), and the proposed energy supply invoice for this year are shown in Table 6.26.

Table. 6.25 Simulation Results of BESS with 1C that is used to deliver DC service with and without submitting a baseline power for the full year-2019 frequency data

Contracted Service Power (MW)	Baseline power (MW)	Total Import Energy (MWh)	Total Export Energy (MWh)	Avg.Availability (%)
±40	0	1,847.47	1,820.87	99.78
±39	±1	1,929.22	1,799.97	100

Table 6.25 presents the simulation results of BESS used to deliver DC service with and without a baseline power for the whole year-2019. It can be seen that when the baseline power(±1MW) was submitted then the total export energy decreased over the year by almost 1.15% while the total import energy increased by approximately 4.33% compared to the case of without submitting the P_{Base}, also the average availability of BESS reached 100% in the case of P_{Base} while for no P_{Base} the average availability was decreased to $\sim 0.22\%$. The methodology for implementing a baseline power (P_{Base}) was explained in Chapter 3, Subsubsection 3.4.4. The analysis findings of the proposed energy supply invoice for BESS with 1C-rate used to deliver DC service without and with submitting a baseline power for the full year-2022 are shown in Table 6.26 and illustrated in Figure 6.14, and Figure A12 .

Table. 6.26 Energy supply invoice for BESS with 1C-rate used to deliver DC services with and without(P_{Base}) for the full year-2019 frequency data

Cost Breakdown				
Cost		Charger Point	Cost/Revenue without (P_{Base})	Cost/Revenue with(P_{Base})
RO		MSP	£47,960.32	£50,082.55
CFD		NBP	£162.39	£169.58
FiT		MSP	£13,856.03	£14,469.15
AAHEDC		GSP	£10.76	£52.25
CM	Settlement Cost Levy for Supplier/ Year	NBP	£47.86	£46.60
	CM supplier charge for supplier/Year	NBP	£4,462.54	£4,453.32
BSUoS	Generation	NBP	-£17,907.24	-£17,701.70
	Demand	NBP	£18,532.78	£19,352.85
DUoS		MSP	£4,161.21	£4,347.90
GDUoS		MSP	-£5,898.87	-£5,826.04
TNUoS	Demand	MSP	£6,896.07	£6,723.75
	Generation	MSP	-£631.67	-£615.85
Elexon		GSP	£733.67	£745.84
TNUoS EET	Generation	NBP	-£112.79	-£109.97
	Demand	NBP	0	0
DC Frequency Response Revenue		GSP	-£7,622,660	-£7,430,670
DUoS Fixed		Supply	£328.72	£328.72
DUoS Capacity		Site	£756,280	£756,280
MOP DC/AC		Supply	£547.50	£547.50
Total Cost		-	-£6,793,230.72	-£6,597,323.55

From Table 6.26, it can be seen that the total cost that is obtained from BESS used to deliver DC service without P_{Base} for the full year-2019 equates to £6,793,230.72 while by submitting the P_{Base} it has been decreased by almost 2.93% and those values represent the income that is obtained from the sum of cost (+ sign) and revenue (- sign). For the demonstration, the values of both cost and revenue are represented in percentages as shown in Figure 6.14, and Figure A17, see Appendix E.

Figure. 6.14 Analysis findings of (a) Cost, and (b) Revenue for 1C BESS used to deliver DC service with P_{Base} for the whole year-2022, using frequency data of Jun-2019

As we can see from Figure A17 where BESS has been used to deliver DC without P_{Base}, and Figure 6.14 where BESS has been used to deliver DC by submitting a P_{Base}, for the cost, DUoS Capacity represents the highest value equates $\sim 88.56\%$ of the total cost for DC without P_{Base} while it has been decreased by $\sim 0.42\%$ when a P_{Base} has been submitted. However, most of the other costs for DC with the submission of a P_{Base} are slightly increased compared to DC without P_{Base} such as AAHEDC, RO, FiT, BSUoS, and DUoS with values ranged as $(0\%-0.01\%, 5.62\%-5.84\%, 1.62\%-1.69\%, 2.17\%-2.26\%, 0.49\%-0.51\%)$ respectively. While TNUoS / Demand decreased by 0. 08% from the total cost, and the other costs remained the same.

In regard to the revenue, from Figure 6.14 (b), and Figure A17, it is clear that the DC service revenue was the highest value representing $\sim 99.$ 68% of the total revenue of DC without P_{Base}, while it has been decreased by $\sim 0.01\%$ when a P_{Base} has been submitted, and this is caused by the decreases of the contracted power from 40MW to 39MW and add ± 1MW for charge and discharge purposes. Furthermore, for DC without P_{Base}, BSUoS / Generation represents 0. 23% of the total revenue and has increased by almost 0. 01% of the total revenue when a P_{Base} has been submitted. Therefore, the total cost of DC service without submitting a P_{Base} is higher than DC service with submitting a P_{Base} by approximately 2.93%.

Analysis of NPV for BESS with 1C used to deliver DC Service without and with submitting a baseline power($\pm$1MW)for 15 Years

Table. 6.27 Analysis of NPV for BESS with 1C used to deliver DC Service without and with submitting a baseline power($\pm$1MW)for 15 Years

Contracted Service Power (MW)	Capital Cost (£)	The PV of net cash flows (£)	The PV of Operation & Maintenance cost (£)	NPV (£)
$\pm$40	-17,640,000	58,146,513.57	-1,788,931.05	38,717,582.52
$\pm$39	-17,640,000	56,468,057.75	-1,788,931.05	37,039,126.70

Table 6.27 gives the results of NPV for BESS with 1C used to deliver the DC service without and with submitting a baseline power($\pm$1MW) for 15 Years, and it is clear that in the cast where the P_{Base} was submitted the PV of net cash flow decreased by 2.93% compared to the case of no P_{Base}. In terms of NPV, both cases could be accepted because NPV is positive, however, in the case where the P_{Base} was submitted the NPV decreased by 4.43% compared to the case without P_{Base}. Therefore, the case that relates to DC without submitting a P_{Base} will be more profitable than DC with submitting P_{Base}.

B. Analysis of DR services with and without implementing dynamic control

In this section, an assessment based on the revenue vs SOC management will be carried out for BESS used to provide DR service throughout the year 2022 using two different scenarios (S1 & S2) as explained in Chapter 5, Subsubsection 5.1.5. For Jun-2022, the simulation results of BESS used to deliver DR service for different scenarios (S1 & S2), the calculation of total unit charge for both DUoS & GDUoS, and the proposed energy supply invoice can be seen in Table A18, Table A20, Table A21, and Table A19 (see Appendix E), and for the whole year-2022, the simulation results of BESS used to deliver DR with and without implementing a dynamic control and the proposed energy supply invoice are shown in Table 6.28, and Table 6.29, and the calculation of total unit charge for both DUoS & GDUoS is shown in Table A20, and Table A21, see Appendix E.

Simulation Results of BESS with 1C that used to deliver DR service with a different scenarios (S1 & S2) for the whole year-2019 frequency data

Table. 6.28 Simulation Results of BESS with 1C that used to deliver DR service with a different scenarios for the whole year-2019 frequency data

Contracted Service Power (MW)	Total Import Energy (MWh)	Total Export Energy (MWh)	Avg.Availability (%)	Scenarios
±40	33,263.91	29,439.85	89.40	S1
±40	32,696.21	28,938.61	90.74	S2

Table 6.28 gives simulation results of BESS with 1C that was used to deliver DR service with different scenarios for the whole year-2019. It can be noticed that at (S2) where a dynamic control was implemented, the energy throughout was minimised over the year compared to (S1). The export energy was reduced by almost 1.71%, and the imported energy was decreased by approximately 1. 72%, which has led to an increase in the average for (S2) by almost 1.5% compared to S1.

Table. 6.29 Energy supply invoice of year-2022 for BESS with 1C-rate used to deliver DR service with different scenarios for the whole year-2019 frequency data

Cost Breakdown				
Cost		Charger Point	Cost/Revenue (S1)	Cost/Revenue (S2)
RO		MSP	£863,531.10	£848,793.61
CFD		NBP	£2,923.89	£2,873.99
FiT		MSP	£249,479.33	£245,221.58
AAHEDC		GSP	£1,545.95	£1,519.09
CM	Settlement Cost Levy for Supplier/ Year	NBP	£870.93	£832.97
	CM supplier charge for supplier/Year	NBP	£81,212.38	£79,599.96
BSUoS	Generation	NBP	-£289,524.60	-£284,595.10
	Demand	NBP	£333,684.80	£327,990.00
DUoS		MSP	£78,189.71	£76,655.50
GDUoS		MSP	-£95,649.54	-£93,538.75
TNUoS	Demand	MSP	£137,829.39	£137,105.77
	Generation	MSP	-£12,598.26£	-£11,256.18
Elexon		GSP	£12,540.75	£12,326.96
TNUoS EET	Generation	NBP	-£2,249.58	-£2,009.94
	Demand	NBP	0	0
DR Frequency Response Revenue		GSP	-£3,781,838	-£3,781,838
DUoS Fixed		Supply	£328.72	£328.72
DUoS Capacity		Site	£756,280	£756,280
MOP DC/AC		Supply	£547.50	£547.50
Total cost		-	-£1,662,895.53	-£1,683,162.32

From Table 6.29, it can be seen that the total cost (cost & revenue) that has been obtained from BESS used to deliver DR service (S2) for the full year-2019 increased by almost 1.21% compared to (S1), and those values represent the income that is obtained from the sum of the cost (+ sign) and revenue (- sign). For the demonstration, the value of both cost and revenue are represented in percentages as shown in Figure 6.15, and Figure A18, see Appendix E.
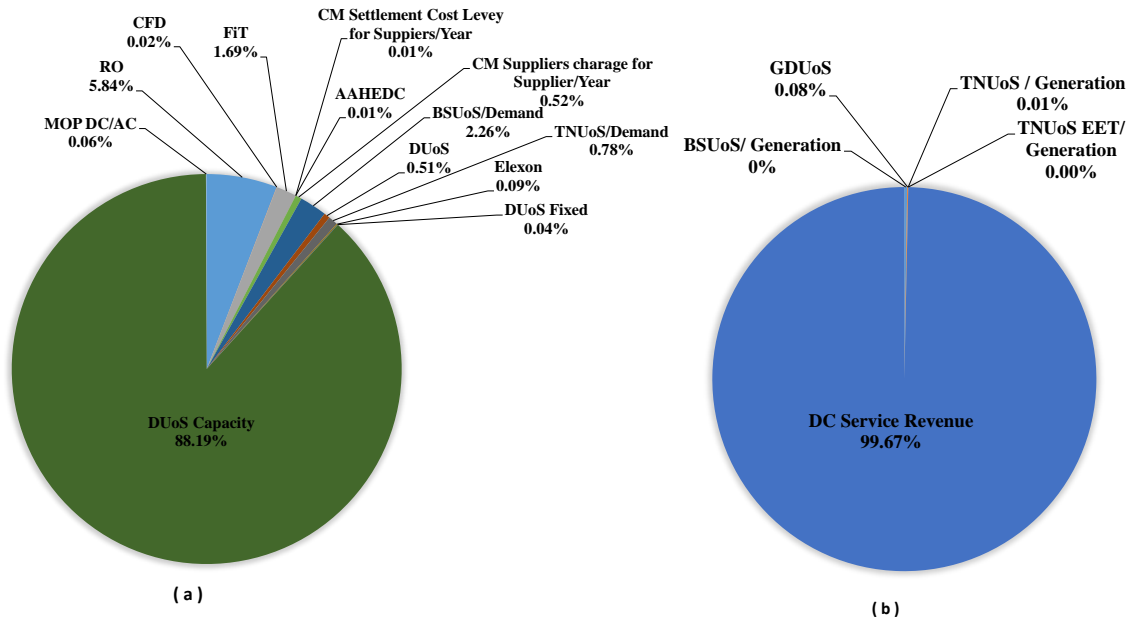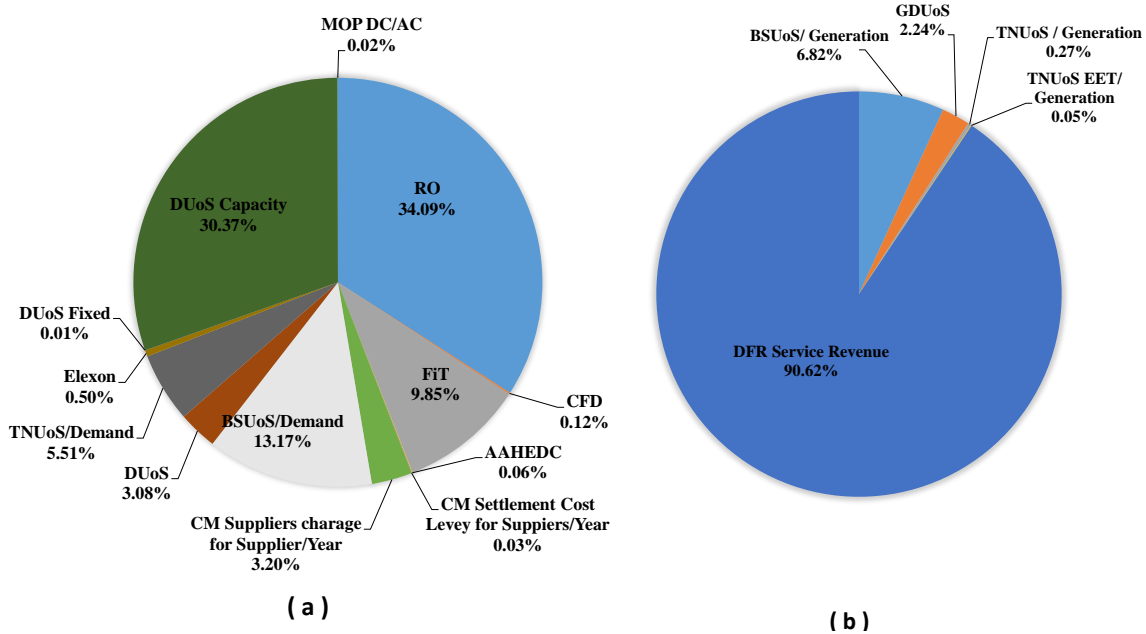
Figure. 6.15 Analysis findings of (a) Cost, and (b) Revenue for 1C BESS used to deliver DR service with implementing a dynamic control (S2) for the whole year-2022, using frequency data of Jun-2019.

As we can see from Figure A18 where BESS has been used to deliver DR service without implementing a dynamic control (S1), and Figure 6.15 where BESS has been used to deliver DR service with implementing a dynamic control (S2), for the cost (a), RO represents the highest value equates $\sim 34.28\%$ from the total cost for (S1) while in (S2) it has been decreased to $\sim 34.09\%$ from the total cost, the second highest cost for (S1) is DUoS Capacity which equates ~ 30.02 from the total cost whereas in (S2), while it has been increased by almost 1.16% compared to (S1), the third higher cost was BSUoS/Demand with $\sim 13.25\%$ of the total cost in (S1) and it has been reduced to almost 13.17% from the total cost in (S2), the forth higher cost was FiT which was with the value equates $\sim 9.90\%$ from the total cost of (S1) while it has been reduced to almost 9.85% from the total cost of (S2). The cost of TNUoS/Demand in (S1) equates to almost 5.47% from the total cost, and it has been increased to $\sim 5.51\%$ from the total cost of (S2). In addition to that, the cost of DUoS equates to almost 3.10% from the total cost of (S1) however, in (S2) it has been decreased to $\sim 3.08\%$ from the total cost of (S2). Moreover, the other costs almost remain the same value for both (S1 & S2) except the cost of CM Supplier charge for the supplier which represents 3.22% of the total cost in (S1) while it has been slightly decreased to 3.20% from the total cost in (S2). Therefore, most of the costs in (S1) have been decreased compared to (S2), and the main reason behind this is that by implementing a dynamic control, the energy throughout is minimised over the year which has led to a decrease in the cost for (S2).

In regard to the revenue, from Figure 6.15 (b), and Figure A18, it can be seen that DR service revenue was the highest, and it is the same value for both (S1 & S2) represents

$\sim 90.62\%$ of the total revenue. The second, third, and fourth highest revenues that were obtained from (S1) are BSUoS/Generation, GDUoS, and TNUoS/Generation with values equating to almost 6.94%, 2.29%, and 0.30% of the total revenues, respectively. However, in (S2), these revenues have been decreased to the values equated to 6.82%, 2.24%, and 0.27% from the total revenue, respectively, and this was caused by applied a dynamic control which has led to minimized export power to the grid and this has resulted in a decrease in the revenue for such charge methods. However, the revenue that has been obtained from TNUoS EET/Generation for both (S1 & S2) remains with the same value (0.05%) from the total revenue. Therefore, the cost in (S2) has decreased compared to (S1) and this has led to the increase in the total revenue of S2 with the increment equating to approximately 1.97% compared to (S1).

Analysis of NPV for BESS with 1C used to deliver DR Service based on two different scenarios (S1 & S2) for 15 Years, 40MW profile

Table. 6.30 Analysis of NPV for BESS with 1C used to deliver DR Service without and with implementing a dynamic control for 15 Years, 40MW profile

scenarios	Capital Cost (£)	The PV of net cash flows (£)	The PV of Operation & Maintenance cost (£)	NPV (£)
S1	-17,640,000	14,125,684.31	-1,788,931.05	-5,303,246.73
S2	-17,640,000	14,406,992.01	-1,788,931.05	-5,021,939.04

Table 6.30 presents the results of the analysis of NPV for 1C BESS used to deliver DR service for 15 years based on two different scenarios (S1 & S2). As we can see from (S2), the PV of net cash flow is slightly higher than (S1) with the increment equating to around 1.97%, and this means that BESS in S2 has generated a higher income than S1. However, the NPV for both S1 & S2 is negative, which means that both scenarios will not be accepted.

6.7   Discussion/Conclusion

The simulation results for BESS with different C-rates (0.5C, 1C, 2C) were used to provide the three services (DFR, DC, and DR) separately for the full month of Jun-2019 and the entire year 2019. The results showed that all services were delivered according to NG specifications. However, the results indicated that DC is a less demanding service compared to both DFR and DR, with the highest demand being for the DR service. The energy throughput for the DR service was almost double that of DFR and 16 times higher than DC. However, the BESS used to provide the DC service had the highest availability compared to DFR and DR, reaching 100% at 0.5C, while for DFR and DR at the same C-rate, it was 96.05% and 93.50%, respectively. The availability increased with the decrease

in the C-rate and vice versa.

Moreover, the obtained results from comparing revenue vs C-rate illustrated that DC service, specifically at 0.5C, generated the highest revenue together with the greatest total cost (cost & revenue), while the lowest revenue and total cost were for DR service.

Additionally, regarding SOC management vs revenue, at 1C, BESS used to deliver DC service with a P_{Base}. The total cost (cost & revenue) for DC service without submitting P_{Base} was the highest compared to the DC service with submitting a P_{Base}. Additionally, for SOC management vs revenue, the results showed that S2 had the highest total cost (cost & revenue) compared to S1.

In this thesis, for revenue vs C-rate, nine scenarios listed from (A - I) have been assessed in terms of which scenario is more profitable than the others. The obtained results illustrated that the only scenarios listed from A to F could be accepted because they have a positive NPV. However, the scenarios for the DC service will be more profitable than the scenarios for DFR service, and this is because they have the largest NPV compared to the DFR. The highest values were for DC service, which includes scenarios (D, E & F) with the maximum NPV equating to £38,724,469.31 at 0.5C (scenario D), and the lowest NPV was at 2C (scenario F) with £38,706,846.80. For DFR service, the maximum NPV was at 2C (scenario C) with £15,308,834.24, and the lowest NPV was at 1C (scenario B) with £14,980,678.55. In addition, the projects that relate to DC service have a higher availability and lower CF compared to both DFR and DR services. For example, at 1C, for DC service, the CF was almost 0.52%, while at the same C-rate, for DFR and DR, it increased by approximately 3.98% and 7.88%, respectively.

Regarding the analysis of NPV for revenue vs SOC management, at 1C for DC service, the NPV of DC with and without submitting a baseline power is positive, which means that both cases could be accepted. However, in the case of DC without submitting a baseline power, the NPV was the greatest, increasing by almost 4.33513% compared to DC with submitting a baseline power. Regarding the DR service for both S1 and S2, even though S2 has a higher NPV than S1, both have a negative NPV, which means that these cases will not be accepted.

However, choosing a BESS with a 2C rating might not be a good option as batteries designed for sustained higher C-rates have tended to cost more, they also require more cooling and the cost of HVAC therefore increases. This will lead to an increase in battery capital costs. However, with the correct cooling strategy, cheaper chemistries could be used.

Furthermore, at 2C, current Li-ion battery cells will have a shorter life-time because they will degrade faster than 0.5C & 1C. The author in [186] discusses the accelerated testing and degradation modelling of Li-ion batteries using an empirical mixed-model approach inspired by physics. One method of conducting accelerated testing on Li-ion batteries is by testing them at accelerated levels of discharge C-rates. This process is known as an Accelerated Degradation Test (ADT) or Accelerated Repeated Measures

Degradation Test, where the degradation indicator of the product under test is recorded continuously or at specific intervals to capture the degradation process. This author presents experimental data from two case studies on two types of Li-ion batteries, denoted as type A and type B, respectively, and the batteries have slight differences in material composition. In this work, type A Li-ion batteries are used as an example of an accelerating Li-ion battery cycle by varying the discharge C-rate. The batteries are tested for capacity fades at different discharge C-rates, including 0.2C, 0.5C, 1C, and 2C, with several samples of 2, 14, 5, and 3, respectively, while assuming that other stress factors are constant. The purpose of testing at different C-rates is to collect data on their effects on capacity fade trends. The charge-discharge cycles in this test were requested to be between 3.0V and 4.1V, and the tests were conducted under a fixed and controlled environmental temperature of 37C°. Part of this data has also been used in [187]. The testing data for type A batteries was limited to 250 cycles, and the normalized discharge capacity profiles for type A are shown in Figure 6.16.
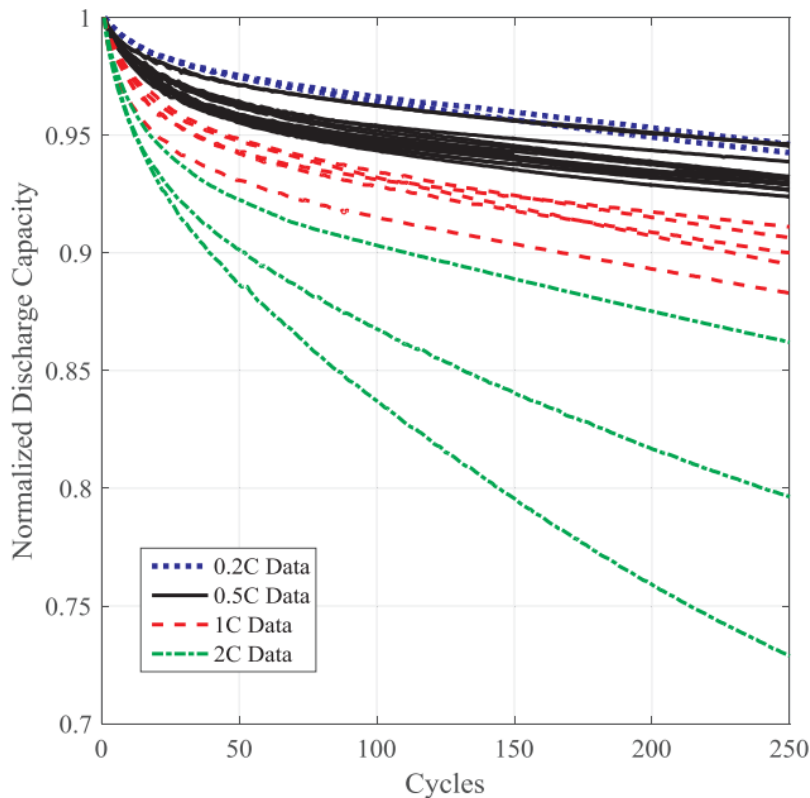
Figure. 6.16 Data on normalized discharge capacity testing for battery population type A at various C-rates [186]

As depicted in Figure 6.16, the Li-ion battery subjected to a discharge C-rate of 2C has experienced faster capacity loss than the battery subjected to a discharge C-rate of 0.2C, despite both batteries undergoing 250 cycles at the same temperature. This indicates that the battery subjected to 2C discharge C-rate is prone to faster degradation and has a shorter lifespan compared to the one subjected to 0.2C. Consequently, increasing the

discharge C-rate will accelerate the battery degradation rate (capacity fade) and reduce the time required for a full charge-discharge cycle, resulting in a two-fold acceleration. Therefore, the discharge C-rate stress factor can be utilised for the accelerated testing of Li-ion batteries.

Although the service is designed to be available 24/7, the reality is that it may not always be feasible due to various factors such as maintenance, SOC management, and success in bidding. Moreover, the market has moved away from long-term contracts to weekly bidding, providing more flexibility for the BESS to provide other services and access different revenue streams. Future pricing of the frequency response services is likely to be more volatile with downward trends predicted as required volumes saturate. For the purposes of the economic assessment, it could be increased the capital costs to install a larger battery; this would vary depending on the C-rate as we can assume that a higher C-rate would require a larger capacity battery at the start. How do we incorporate the decreased capacity? Degradation will reduce the capacity size therefore, this will lead to considering the following assumptions;

- NGESO should recognise that pricing needs to be attractive, hence introducing stacking to increase possible revenues.

- It might be necessary to reduce the capacity in the model as time goes on. i.e. each year the capacity is slightly less, which means by year 6, for example, the maximum contractible power would be 39MW to meet the energy requirements within the terms and conditions of the contract.

- Do we increase the capacity costs and install a higher capacity battery to offset the loss in energy over time?

Chapter 7

Conclusions and Future work

This section presents an overview of the research carried out in this thesis, emphasizing the importance of each chapter in accomplishing the primary objective and the degree of contribution to the existing knowledge. The chapter concludes with a comprehensive summary and suggestions for future research to extend this thesis. Although the present work in this thesis is conclusive, there are numerous areas for further exploration and development. The following list outlines potential paths for research that could be pursued based on the conclusions of this study.

7.1 Conclusion

7.1.1 Models and Experimental Validation Results for Battery and Frequency Response Services

This chapter presented the development of the generic model of BESS in MATLAB/Simulation based on the 'Bucket Model' principle, which can be easily modified and adapted for other ESS applications. The model was used to provide frequency response services, including DFR, DC, and DR, and the results showed that each service proportionally responds in power to changes in grid frequency with each service differing in the response envelope in compliance with NG specifications. However, DC service is less demanding, with significantly lower average power and energy throughput compared to DFR and DR services. The BESS model's accuracy was assessed through two verification exercises against a WESS, and the results indicated that the model achieved RMSE and MAPE values within acceptable limits, confirming its accuracy.

7.1.2 Sensitivity Analysis of Power-to-Energy Ratios and Battery Lifetime for Dynamic Frequency Response Services in UK Energy Storage Systems

Firstly, in this chapter, simulation results comparing the new DC service against the DFR service are presented and show that DC is a less demanding service with approximately 10 times lower average power and energy throughput. A sensitivity analysis for different C-rates vs availability has been presented and this shows that low (<2C) C-rates are

required to maintain good availability for DFR whilst higher (<10C) C-rates can be used for DC. Furthermore, by implementing baseline charging for DC, higher C-rates can be utilized whilst remaining compliant with sustained delivery requirements, although, this will result in a lower contracted service power and lower hence revenue. Typically, these frequency response services are provided by 1C BESS, however, this work shows that high C-rate technologies such as supercapacitor and flywheel could be utilized.

Additionally, in this chapter, two different cycle counting methodologies, EFCs and CCM, have been developed in MATLAB/Simulink to accurately quantify the number of cycles and battery degradation in BESS used for delivering DFR and DC services. The obtained results showed that EFCs and CCM can provide significantly different values for the number of cycles and degradation rate results. The results also revealed that the DFR service degrades the battery more than the DC service due to its higher power delivered to the grid in response to frequency changes. Moreover, the battery degradation was higher in DC service with P_{Base} submission than without, except when $P_{Base}=\pm3MW$.

Furthermore, grouping C-rate as (0.1C, 0.3C, 0.5C) and grouping SOC by 10% for BESS was found to provide more accurate results for degradation analysis compared to only considering the effects of C-rate on battery lifetime. The obtained results from EFCs and CCM showed that the BESS used for delivering DFR mostly operates at $0.1< C \leq0.3$ and caused almost 0.09%, and 0.14% of the degradation rate, respectively. On the other hand, for all cases of DC service ($\pm0MW$, $\pm1MW$, $\pm2MW$, $\pm3MW$) of P_{Base}, the BESS spends most of its time operating at $C\leq0.1$, and the obtained number of cycles from CCM was slightly higher than EFCs, but the degradation rate varied significantly between using Data1 and Data2. Therefore, it is recommended to consider the effects of both C-rate, & SOC and use both cycle counting methodologies with Data2 for a more accurate analysis of battery degradation in BESS used for delivering DFR and DC services.

Finally, in this chapter, an experiment was conducted to evaluate the degradation of eight lithium-ion rechargeable cells under different temperatures while delivering DFR and DC services. The cells were tested, and the results showed that delivering DFR & DC by lithium-ion rechargeable cells at different temperatures caused capacity loss, with higher temperatures leading to greater capacity loss. Cells used for DC services under the same temperature showed lower capacity loss and a lower degradation rate compared to those used for DFR services. Although aging due to cycling is expected to be low, the results are inconclusive, and more cycling is required to "linearize" the degradation.

Future Work

- Apply the sensitivity analysis in the same way for other ESS types such as supercapacitor and flywheel or hybrid with BESS.

- The degradation experiment for DFR & DC needs more cycling until to get conclusive results ("linearize" the degradation).

7.1.3   DR service and BESS degradation analysis

In Chapter 5, the study presents a dynamic control approach for DR service with the aim of minimizing energy throughput during service delivery in order to extend the time before the SOC limits are reached, thereby increasing the availability of BESS and reducing the likelihood of penalty payments for not meeting service delivery requirements. The dynamic control approach was developed using MATLAB/Simulink to manage the SOC of a stacked DR-HF and DR-LF contract where the BESS responds to both high and low-frequency events in total export/import energy was minimized over time in S2 compared to S1.

Furthermore, the study developed two different cycle counting methodologies, EFCs and CCM which are discussed in Chapter 4, to quantify the approximate number of cycles. Results showed that EFCs generated higher numbers of cycles than CCM, likely due to the latter requiring a longer time period to sum up the micro charge-discharge full cycle until reaching 100%. The obtained number of cycles was then used to calculate battery degradation based on LTO battery manufacturer cycles, and it was found that DR service with S1 degraded BESS more than DR service with S2, which used dynamic control to decrease the energy throughput over time and extend the time for SOC to hit the limits. The results of the comparison of all cases of SOC_{star} show that for both S1 and S2, the highest total number of cycles was obtained from CCM for SOC_{star}=50%, while the lowest was obtained for SOC_{star}=70% compared to SOC_{star}=30%. Additionally, the number of cycles obtained from CCM was higher than EFCs.

Additionally, the obtained results by grouping C-rate as (0.1C, 0.3C, 0.5C) and analyzing the degradation rates based on Data1 & Data2 show that the degradation rates for using Data2 are significantly lower than those for Data1. However, the results obtained illustrate that grouping both C-rate and SOC gives more accurate results for calculating battery degradation compared to considering only the effects of C-rate on battery degradation.

Future Work

The findings of this study provide a valuable contribution to the field of ESS, and future research could expand the proposed dynamic control approach together with submitting a baseline power to other ESS and exploring the potential of incorporating machine learning algorithms for improved performance.

Additionally, future work could investigate the development of novel cycle counting methodologies that can accurately capture the micro-level details of battery usage and degradation, which could lead to further insights into the behavior of battery systems and their degradation mechanisms.

7.1.4 Financial Aspects of BESS and Frequency Response Services

In this chapter, the simulation outcomes of the BESS when providing individual services (DFR, DC, and DR) with different C-rates (0.5C, 1C, and 2C) were analyzed for the entire month of Jun-2019 and the full year of 2019. The results indicate that all services were delivered according to NG specifications. However, the findings suggest that providing DR is more demanding than DFR and DC, with the DR service demonstrating the highest demand. Notably, the BESS employed for the DC service exhibited the highest availability, reaching 100% at 0.5C. In comparison, for DFR and DR at the same C-rate, the availability was decreased by 3.95% and 6.5%, respectively.

In this chapter, the study compares the costs and revenues of BESS with different C-rates used to deliver DFR, DC & DR services in the UK electricity system charge for Jun-2022 and the whole year-2022. The results show the most effective costs for all services delivered by BESS at different C-rates were DUoS Capacity and RO, while the highest revenue was frequency response revenue. The study also investigated the impact of dynamic control on DR service at (S2) with the same C-rate (1C). The analysis showed that the total cost (cost/revenue) increased by approximately 1.99146% due to the implementation of dynamic control. This was attributed to the reduction in energy throughput over the year, which resulted in a decrease in costs for (S2) and an increase in revenue. Additionally, the study presented that DC service without submitting a base power level will generate a higher revenue compared to DC with submitting a baseline power.

This chapter conducted an assessment of nine scenarios listed from A to I based on their profitability. The results indicate that only scenarios from A to F have a positive NPV and can be accepted. The scenarios related to DC service (D, E, and F) are more profitable than those related to DFR service. The DC service scenarios exhibit the highest NPV, with scenario D at 0.5C exhibiting the maximum NPV, while scenario F at 2C exhibits the lowest NPV. For DFR service, scenario C at 2C exhibits the highest NPV, and scenario B at 1C exhibits the lowest NPV. Additionally, the scenarios related to DC service exhibit higher availability and lower CF compared to DFR and DR services. At 1C, the CF for DC service was approximately 0.52%, while for DFR and DR, it was approximately 4.50% and 8.40%, respectively. Regarding the analysis of NPV for revenue vs SOC management, for DC service, the NPV of both scenarios (with and without submitting a baseline power) was positive, with the project without submitting a baseline power exhibiting a greater NPV. However, for DR service (S1 and S2), both scenarios exhibited negative NPV, indicating that they will not be accepted.

If the frequency service price is the same for all services, then the other option might be 2C BESS; however, the use of batteries designed for a higher C-rate for BESS with 2C

can result in higher capital costs due to increased cooling requirements. Additionally, BESS with 2C is expected to have a shorter lifetime and require more maintenance and SOC management due to its faster degradation rate. Furthermore, the market for frequency response services is expected to be more volatile in the future, and a larger battery could be installed by increasing capital costs to achieve higher capacity depending on the C-rate.

References

[1] X. Liang, "Emerging power quality challenges due to integration of renewable energy sources," *IEEE Transactions on Industry Applications*, vol. 53, no. 2, pp. 855–866, 2016.

[2] N. S. Rayit, J. I. Chowdhury, and N. Balta-Ozkan, "Techno-economic optimisation of battery storage for grid-level energy services using curtailed energy from wind," *Journal of Energy Storage*, vol. 39, p. 102641, 2021.

[3] T. H. Mehr, M. A. Masoum, and N. Jabalameli, "Grid-connected lithium-ion battery energy storage system for load leveling and peak shaving," in *2013 Australasian Universities Power Engineering Conference (AUPEC)*, pp. 1–6, IEEE, 2013.

[4] M. Moradiya , "Challenges Renewable Energy Sources Face ," 2019. *[Online], Available:* `https://https://www.azocleantech.com/article.aspx?ArticleID=836`,[Accessed: 17-Aug-2022].

[5] B. Kroposki, "Integrating high levels of variable renewable energy into electric power systems," *Journal of Modern Power Systems and Clean Energy*, vol. 5, no. 6, pp. 831–837, 2017.

[6] T. O. Olowu, A. Sundararajan, M. Moghaddami, and A. I. Sarwat, "Future challenges and mitigation methods for high photovoltaic penetration: A survey," *Energies*, vol. 11, no. 7, p. 1782, 2018.

[7] P. Chaudhary and M. Rizwan, "Voltage regulation mitigation techniques in distribution system with high pv penetration: A review," *Renewable and Sustainable Energy Reviews*, vol. 82, pp. 3279–3287, 2018.

[8] D. Bozalakov, T. Vandoorn, B. Meersman, and L. Vandevelde, "Overview of increasing the penetration of renewable energy sources in the distribution grid by developing control strategies and using ancillary services," in *IEEE Young Researchers Symposium*, EESA, 2014.

[9] G. O. Gil, J. I. Chowdhury, N. Balta-Ozkan, Y. Hu, L. Varga, and P. Hart, "Optimising renewable energy integration in new housing developments with low carbon technologies," *Renewable Energy*, vol. 169, pp. 527–540, 2021.

[10] S. Vazquez, S. M. Lukic, E. Galvan, L. G. Franquelo, and J. M. Carrasco, "Energy storage systems for transport and grid applications," *IEEE Transactions on industrial electronics*, vol. 57, no. 12, pp. 3881–3895, 2010.

[11] A. Diehl, "Why is Energy Storage Such an Important Part of the Renewables Mix," 2015. *[Online], Available:* https://www.greentechrenewables.com/article/why-energy-storage-such-important-part-renewables-mix, [Accessed: 06-Sep-2020].

[12] M. Niroomand, T. Feldmann, and E. Bollin, "High-performance control system for grid-tied esss," *IET Generation, Transmission & Distribution*, vol. 11, no. 8, pp. 2138–2145, 2017.

[13] K. Divya and J. Østergaard, "Battery energy storage technology for power systems—an overview," *Electric power systems research*, vol. 79, no. 4, pp. 511–520, 2009.

[14] R. E. Ciez and J. Whitacre, "Comparative techno-economic analysis of hybrid micro-grid systems utilizing different battery types," *Energy conversion and management*, vol. 112, pp. 435–444, 2016.

[15] B. Gundogdu, S. Nejad, D. T. Gladwin, and D. A. Stone, "A battery energy management strategy for uk enhanced frequency response," in *2017 IEEE 26th International Symposium on Industrial Electronics (ISIE)*, pp. 26–31, IEEE, 2017.

[16] X. Xu, M. Bishop, D. G. Oikarinen, and C. Hao, "Application and modeling of battery energy storage in power systems," *CSEE Journal of Power and Energy Systems*, vol. 2, no. 3, pp. 82–90, 2016.

[17] D. Manz, R. Piwko, and N. Miller, "Look before you leap: The role of energy storage in the grid," *IEEE Power and Energy Magazine*, vol. 10, no. 4, pp. 75–84, 2012.

[18] M. Uddin, M. F. Romlie, M. F. Abdullah, S. Abd Halim, T. C. Kwang, *et al.*, "A review on peak load shaving strategies," *Renewable and Sustainable Energy Reviews*, vol. 82, pp. 3323–3332, 2018.

[19] Y. Zhang, V. Gevorgian, C. Wang, X. Lei, E. Chou, R. Yang, Q. Li, and L. Jiang, "Grid-level application of electrical energy storage: Example use cases in the united states and china," *IEEE Power and Energy Magazine*, vol. 15, no. 5, pp. 51–58, 2017.

[20] A. Immendoerfer, I. Tietze, H. Hottenroth, and T. Viere, "Life-cycle impacts of pumped hydropower storage and battery storage," *International Journal of Energy and Environmental Engineering*, vol. 8, pp. 231–245, 2017.

[21] Electrek, "The world's largest battery storage system just got even larger," 2023. *[Online], Available:* `https://electrek.co/2023/08/03/worlds-largest-battery-storage-system-just-got-even-larger/#:~:text=Vistra%20today%20announced%20that%20it%20completed%20Moss%20Landing%E2%80%99s,that%2C%20together%2C%20house%20more%20than%20110%2C000%20battery%20modules`, [Accessed: 23-Nov-2023].

[22] B. Gundogdu, D. Gladwin, and D. Stone, "Battery energy management strategies for uk firm frequency response services and energy arbitrage," *The Journal of Engineering*, vol. 2019, no. 17, pp. 4152–4157, 2019.

[23] L. Joerissen, J. Garche, C. Fabjan, and G. Tomazic, "Possible use of vanadium redox-flow batteries for energy storage in small grids and stand-alone photovoltaic systems," *Journal of power sources*, vol. 127, no. 1-2, pp. 98–104, 2004.

[24] Z. Liu, Z. Zhang, R. Zhuo, and X. Wang, "Optimal operation of independent regional power grid with multiple wind-solar-hydro-battery power," *Applied energy*, vol. 235, pp. 1541–1550, 2019.

[25] M. Abuagreb, A. Abuhussein, *et al.*, "Sizing of energy storage system for virtual inertia emulation," in *2022 IEEE 31st International Symposium on Industrial Electronics (ISIE)*, pp. 374–379, IEEE, 2022.

[26] K. Lappalainen and S. Valkealahti, "Sizing of energy storage systems for ramp rate control of photovoltaic strings," *Renewable Energy*, vol. 196, pp. 1366–1375, 2022.

[27] Difference Between.com, "Difference between Capacitor and Battery," 2019. *[Online], Available:* `http://www.differencebetween.net/technology/difference-between-capacitor-and-battery/`,[Accessed: 04-Sep-2019].

[28] I. Hadjipaschalis, A. Poullikkas, and V. Efthimiou, "Overview of current and future energy storage technologies for electric power applications," *Renewable and sustainable energy reviews*, vol. 13, no. 6-7, pp. 1513–1522, 2009.

[29] P. Diwan, "Battery Energy Storage System," 2019. *[Online], Available:* `https://pdiwan.medium.com/battery-energy-storage-system-eb0e9a57d546`,[Accessed: 08-Sep-2022].

[30] G reen Tech Renewables, "Energy Storage: Key Metrics for Success," 2022. *[Online], Available:* `https://www.greentechrenewables.com/article/energy-storage-key-metrics-success`,[Accessed: 20-Sep-2022].

[31] S. N. Motapon, E. Lachance, L.-A. Dessaint, and K. Al-Haddad, "A generic cycle life model for lithium-ion batteries based on fatigue theory and equivalent cycle counting," *IEEE Open Journal of the Industrial Electronics Society*, vol. 1, pp. 207–217, 2020.

[32] F. Leng, C. M. Tan, and M. Pecht, "Effect of temperature on the aging rate of li ion battery operating above room temperature," *Scientific reports*, vol. 5, no. 1, p. 12967, 2015.

[33] I. Piccirilli Dorsey, "Fact Sheet: Energy Storage." *[Online], Available:* `https://www.eesi.org/papers/view/energy-storage-2019#2`,[Accessed: 07-Oct-2019].

[34] E. Hossain, H. M. R. Faruque, M. S. H. Sunny, N. Mohammad, and N. Nawar, "A comprehensive review on energy storage systems: Types, comparison, current scenario, applications, barriers, and potential solutions, policies, and future prospects," *Energies*, vol. 13, no. 14, p. 3651, 2020.

[35] Batteryuniversity.com, "Basic to Advanced Battery Information from Battery University." *[Online], Available:* `https://batteryuniversity.com/`,[Accessed: 07-Oct-2019].

[36] N. Vangapally, T. R. Penki, Y. Elias, S. Muduli, S. Maddukuri, S. Luski, D. Aurbach, and S. K. Martha, "Lead-acid batteries and lead–carbon hybrid systems: A review," *Journal of Power Sources*, vol. 579, p. 233312, 2023.

[37] M. Aneke and M. Wang, "Energy storage technologies and real life applications–a state of the art review," *Applied Energy*, vol. 179, pp. 350–377, 2016.

[38] M. Fetcenko, J. Koch, and M. Zelinsky, "Nickel–metal hydride and nickel–zinc batteries for hybrid electric vehicles and battery electric vehicles," in *Advances in battery technologies for electric vehicles*, pp. 103–126, Elsevier, 2015.

[39] T. S. Energy, "Lithium ion batteries: energy density," 2023. *[Online], Available:* `https://thundersaidenergy.com/downloads/lithium-ion-batteries-energy-density/#:˜:text=Today%E2%80%99s%20lithium%20ion%20batteries%20have%20an%20energy%20density,the%20electrolyte%20and%200.1%20kg%20in%20the%20balance`, [Accessed: 23-Nov-2023].

[40] M. Beaudin, H. Zareipour, A. Schellenberglabe, and W. Rosehart, "Energy storage for mitigating the variability of renewable electricity sources: An updated review," *Energy for sustainable development*, vol. 14, no. 4, pp. 302–314, 2010.

[41] Statista, "Lithium-ion battery price worldwide from 2013 to 2022, with a forecast for 2023," 2023. *[Online], Available:* `https://www.statista.com/statistics/883118/global-lithium-ion-battery-pack-costs/`, [Accessed: 23-Nov-2023].

[42] popular-science, "Rusty metal could be the battery the energy grid needs," 2022. *[Online], Available:* `https://www.nationalgrideso.com/document/130271/download`,[Accessed: 16-Aug-2022].

[43] L. Yaqoob, T. Noor, and N. Iqbal, "An overview of metal-air batteries, current progress, and future perspectives," *Journal of Energy Storage*, vol. 56, p. 106075, 2022.

[44] M. A. Rahman, X. Wang, and C. Wen, "High energy density metal-air batteries: a review," *Journal of the Electrochemical Society*, vol. 160, no. 10, p. A1759, 2013.

[45] M. Guarnieri *et al.*, "Introduction to electrochemical energy storage," in *Encyclopedia of Energy Storage*, vol. 2, pp. 236–249, Elsevier, 2022.

[46] E. Rodrigues, R. Godina, S. F. Santos, A. W. Bizuayehu, J. Contreras, and J. P. Catalao, "Energy storage systems supporting increased penetration of renewables in islanded systems," *Energy*, vol. 75, pp. 265–280, 2014.

[47] Alex Scott, "Flow batteries, the forgotten energy storage device," 2023. *[Online], Available:* `https://cen.acs.org/materials/energy-storage/Flow-batteries-forgotten-energy-storage/101/i25`,[Accessed: 6-Dec-2023].

[48] Activepower.com, "Active Power: Critical Power Solutions." *[Online], Available:* `https://www.activepower.com/en-GB`,[Accessed: 07-Oct-2019].

[49] K. Ding and J. Zhi, "Wind power peak-valley regulation and frequency control technology," in *Large-Scale Wind Power Grid Integration*, pp. 211–232, Elsevier, 2016.

[50] T. Bowen et al, "Rusty metal could be the battery the energy grid needs," 2021. *[Online], Available:* `https://www.nrel.gov/docs/fy21osti/76097.pdf`,[Accessed: 23-Aug-2021].

[51] Z.A.Amin, "Electricity storage and renewables: cost and markets 2030." *[Online], Available:* `https://www.irena.org/-/media/Files/IRENA/Agency/Publication/2017/Oct/IRENA_Electricity_Storage_Costs_2017.pdf`,[Accessed: 07-Oct-2019].

[52] A. Z. A. Shaqsi, K. Sopian, and A. Al-Hinai, "Review of energy storage services, applications, limitations, and benefits," *Energy Reports*, vol. 6, pp. 288–306, 2020.

[53] A. Olabi, C. Onumaegbu, T. Wilberforce, M. Ramadan, M. A. Abdelkareem, and A. H. Al-Alami, "Critical review of energy storage systems," *Energy*, vol. 214, p. 118987, 2021.

[54] M. M. Rana, M. Uddin, M. R. Sarkar, S. T. Meraj, G. Shafiullah, S. Muyeen, M. A. Islam, and T. Jamal, "Applications of energy storage systems in power grids with and without renewable energy integration—a comprehensive review," *Journal of Energy Storage*, vol. 68, p. 107811, 2023.

[55] J. D. Hunt, B. Zakeri, A. Nascimento, J. R. Gazoli, F. T. Bindemann, Y. Wada, B. van Ruijven, and K. Riahi, "Compressed air seesaw energy storage: A solution for long-term electricity storage," *Journal of Energy Storage*, vol. 60, p. 106638, 2023.

[56] X. Luo, J. Wang, M. Dooner, and J. Clarke, "Overview of current development in electrical energy storage technologies and the application potential in power system operation," *Applied energy*, vol. 137, pp. 511–536, 2015.

[57] R. J. Kerestes, G. F. Reed, and A. R. Sparacino, "Economic analysis of grid level energy storage for the application of load leveling," in *2012 IEEE Power and Energy Society General Meeting*, pp. 1–9, IEEE, 2012.

[58] T. Simpkins and C. Donnell, "Optimizing battery sizing and dispatching to maximize economic return," in *Proceedings of the Battcon 2017 International Stationary Battery Conference, At Orlando, FL, USA*, pp. 8–10, 2017.

[59] F. A. Bhuiyan and A. Yazdani, "Energy storage technologies for grid-connected and off-grid power system applications," in *2012 IEEE Electrical Power and Energy Conference*, pp. 303–310, IEEE, 2012.

[60] Nationalgrid, "Black Start." *[Online], Available:* `https://www.nationalgrid.com/sites/default/files/documents/Black%20Start%20v1.0_0.pdf`,[Accessed: 22-Nov-2023].

[61] SIEMENS energy, "Black Start & Black Grid Restoration ," 2021. *[Online], Available:* `https://assets.siemens-energy.com/siemens/assets/api/uuid:f79fcd4a-c502-4ab8-b31e-a1d38df46c0c/flyer-blackstart-final.pdf`,[Accessed: 22-Nov-2023].

[62] H. C. Hesse, M. Schimpe, D. Kucevic, and A. Jossen, "Lithium-ion battery storage for the grid—a review of stationary battery storage system design tailored for applications in modern power grids," *Energies*, vol. 10, no. 12, p. 2107, 2017.

[63] Infineon , "Battery management systems (BMS)," 2023. *[Online], Available:* `https://www.nationalgrideso.com/industry-information/balancing-services/reserve-services/fast-reserve,`[Accessed: 24-Nov-2023].

[64] A.Petrova , "Efficient Energy Management and Energy Saving with a BESS (Battery Energy Storage System)," 2021. *[Online], Available:* `https://www.integrasources.com/blog/energy-management-and-energy-saving-bess/,`[Accessed: 09-Jun-2023].

[65] K. S. Ng, C.-S. Moo, Y.-P. Chen, and Y.-C. Hsieh, "Enhanced coulomb counting method for estimating state-of-charge and state-of-health of lithium-ion batteries," *Applied energy*, vol. 86, no. 9, pp. 1506–1511, 2009.

[66] W.-Y. Chang, "The state of charge estimating methods for battery: A review," *International Scholarly Research Notices*, vol. 2013, 2013.

[67] L. Lu, X. Han, J. Li, J. Hua, and M. Ouyang, "A review on the key issues for lithium-ion battery management in electric vehicles," *Journal of power sources*, vol. 226, pp. 272–288, 2013.

[68] H. Qian, J. Zhang, J.-S. Lai, and W. Yu, "A high-efficiency grid-tie battery energy storage system," *IEEE transactions on power electronics*, vol. 26, no. 3, pp. 886–896, 2010.

[69] M. Jinhao, M. Ricco, L. Guangzhao, M. J. Swierczynski, D.-I. Stroe, A.-I. Stroe, and R. Teodorescu, "An overview of online implementable soc estimation methods for lithium-ion batteries," in *2017 International Conference on Optimization of Electrical and Electronic Equipment (OPTIM) & 2017 Intl Aegean Conference on Electrical Machines and Power Electronics (ACEMP)*, pp. 573–580, IEEE Press, 2017.

[70] Y. Zou, X. Hu, H. Ma, and S. E. Li, "Combined state of charge and state of health estimation over lithium-ion battery cell cycle lifespan for electric vehicles," *Journal of Power Sources*, vol. 273, pp. 793–803, 2015.

[71] W. Zhou, Y. Zheng, Z. Pan, and Q. Lu, "Review on the battery model and soc estimation method," *Processes*, vol. 9, no. 9, p. 1685, 2021.

[72] S. Tamilselvi, S. Gunasundari, N. Karuppiah, A. Razak RK, S. Madhusudan, V. M. Nagarajan, T. Sathish, M. Z. M. Shamim, C. A. Saleel, and A. Afzal, "A review on battery modelling techniques," *Sustainability*, vol. 13, no. 18, p. 10042, 2021.

[73] A. Suti, G. Di Rito, and G. Mattei, "Development and experimental validation of novel thevenin-based hysteretic models for li-po battery packs employed in fixed-wing uavs," *Energies*, vol. 15, no. 23, p. 9249, 2022.

[74] H. He, R. Xiong, and J. Fan, "Evaluation of lithium-ion battery equivalent circuit models for state of charge estimation by an experimental approach," *energies*, vol. 4, no. 4, pp. 582–598, 2011.

[75] M. Tomasov, M. Kajanova, P. Bracinik, and D. Motyka, "Overview of battery models for sustainable power and transport applications," *Transportation Research Procedia*, vol. 40, pp. 548–555, 2019.

[76] S. Singirikonda and Y. Obulesu, "Battery modelling and state of charge estimation methods for energy management in electric vehicle-a review," in *IOP Conference Series: Materials Science and Engineering*, vol. 937, p. 012046, IOP Publishing, 2020.

[77] R. R. Thakkar, "Electrical equivalent circuit models of lithium-ion battery," *Management and Applications of Energy Storage Devices*, 2021.

[78] M. Doyle, T. F. Fuller, and J. Newman, "Erratum: Modeling of galvanostatic charge and discharge of the lithium/polymer/insertion cell [j. electrochem. soc., 140, 1526 (1993)]," *Journal of the Electrochemical Society*, vol. 165, no. 11, p. X13, 2018.

[79] M. Petit, E. Calas, and J. Bernard, "A simplified electrochemical model for modelling li-ion batteries comprising blend and bidispersed electrodes for high power applications," *Journal of Power Sources*, vol. 479, p. 228766, 2020.

[80] T. F. Fuller, M. Doyle, and J. Newman, "Simulation and optimization of the dual lithium ion insertion cell," *Journal of the electrochemical society*, vol. 141, no. 1, p. 1, 1994.

[81] J. Meng, G. Luo, M. Ricco, M. Swierczynski, D.-I. Stroe, and R. Teodorescu, "Overview of lithium-ion battery modeling methods for state-of-charge estimation in electrical vehicles," *Applied sciences*, vol. 8, no. 5, p. 659, 2018.

[82] R. Xu, "Lithium-ion battery modeling and soc estimation," 2023.

[83] B. Gundogdu and D. T. Gladwin, "Bi-directional power control of grid-tied battery energy storage system operating in frequency regulation," in *2018 International Electrical Engineering Congress (iEECON)*, pp. 1–4, IEEE, 2018.

[84] H. Alnuman, D. Gladwin, and M. Foster, "Electrical modelling of a dc railway system with multiple trains," *Energies*, vol. 11, no. 11, p. 3211, 2018.

[85] Y. Gao, J. Jiang, C. Zhang, W. Zhang, and Y. Jiang, "Aging mechanisms under different state-of-charge ranges and the multi-indicators system of state-of-health for lithium-ion battery with li (nimnco) o2 cathode," *Journal of Power Sources*, vol. 400, pp. 641–651, 2018.

[86] G. Ning, B. Haran, and B. N. Popov, "Capacity fade study of lithium-ion batteries cycled at high discharge rates," *Journal of power sources*, vol. 117, no. 1-2, pp. 160–169, 2003.

[87] E. Wikner, *Lithium ion battery aging: Battery lifetime testing and physics-based modeling for electric vehicle applications*. Chalmers Tekniska Hogskola (Sweden), 2017.

[88] J. Wang, P. Liu, J. Hicks-Garner, E. Sherman, S. Soukiazian, M. Verbrugge, H. Tataria, J. Musser, and P. Finamore, "Cycle-life model for graphite-lifepo4 cells," *Journal of power sources*, vol. 196, no. 8, pp. 3942–3948, 2011.

[89] J. Groot, *State-of-health estimation of li-ion batteries: Cycle life test methods*. Chalmers Tekniska Hogskola (Sweden), 2012.

[90] J. Groot, *State-of-health estimation of Li-ion batteries: Ageing models*. Chalmers Tekniska Hogskola (Sweden), 2014.

[91] J. Schmalstieg, S. Käbitz, M. Ecker, and D. U. Sauer, "From accelerated aging tests to a lifetime prediction model: Analyzing lithium-ion batteries," in *2013 World electric vehicle symposium and exhibition (EVS27)*, pp. 1–12, IEEE, 2013.

[92] P. Ramadass, B. Haran, R. White, and B. N. Popov, "Capacity fade of sony 18650 cells cycled at elevated temperatures: Part i. cycling performance," *Journal of power sources*, vol. 112, no. 2, pp. 606–613, 2002.

[93] R. B. Wright, C. G. Motloch, J. R. Belt, J. P. Christophersen, C. D. Ho, R. A. Richardson, I. Bloom, S. Jones, V. S. Battaglia, G. Henriksen, *et al.*, "Calendar- and cycle-life studies of advanced technology development program generation 1 lithium-ion batteries," *Journal of power sources*, vol. 110, no. 2, pp. 445–470, 2002.

[94] E. Wikner and T. Thiringer, "Extending battery lifetime by avoiding high soc," *Applied Sciences*, vol. 8, no. 10, p. 1825, 2018.

[95] Y. Preger, H. M. Barkholtz, A. Fresquez, D. L. Campbell, B. W. Juba, J. Romàn-Kustas, S. R. Ferreira, and B. Chalamala, "Degradation of commercial lithium-ion cells as a function of chemistry and cycling conditions," *Journal of The Electrochemical Society*, vol. 167, no. 12, p. 120532, 2020.

[96] Y. Gao, J. Jiang, C. Zhang, W. Zhang, Z. Ma, and Y. Jiang, "Lithium-ion battery aging mechanisms and life model under different charging stresses," *Journal of Power Sources*, vol. 356, pp. 103–114, 2017.

[97] B. Zakeri and S. Syri, "Electrical energy storage systems: A comparative life cycle cost analysis," *Renewable and sustainable energy reviews*, vol. 42, pp. 569–596, 2015.

[98] J. Vetter, P. Novák, M. R. Wagner, C. Veit, K.-C. Möller, J. Besenhard, M. Winter, M. Wohlfahrt-Mehrens, C. Vogler, and A. Hammouche, "Ageing mechanisms in lithium-ion batteries," *Journal of power sources*, vol. 147, no. 1-2, pp. 269–281, 2005.

[99] B. Nykvist and M. Nilsson, "Rapidly falling costs of battery packs for electric vehicles," *Nature climate change*, vol. 5, no. 4, pp. 329–332, 2015.

[100] S. Yuanyuan, X. Bolun, T. Yushi, and Z. Baose, "A convex cycle-based degradation model for battery energy storage planning and operation," in *2018 Annual American Control Conference (ACC)*, pp. 4590–4596, IEEE, 2018.

[101] S. D. Downing and D. Socie, "Simple rainflow counting algorithms," *International journal of fatigue*, vol. 4, no. 1, pp. 31–40, 1982.

[102] C. Amzallag, J. Gerey, J. L. Robert, and J. Bahuaud, "Standardization of the rainflow counting method for fatigue analysis," *International journal of fatigue*, vol. 16, no. 4, pp. 287–293, 1994.

[103] I. Rychlik, "A new definition of the rainflow cycle counting method," *International journal of fatigue*, vol. 9, no. 2, pp. 119–121, 1987.

[104] B. Gundogdu and D. T. Gladwin, "A fast battery cycle counting method for grid-tied battery energy storage system subjected to microcycles," in *2018 International Electrical Engineering Congress (iEECON)*, pp. 1–4, IEEE, 2018.

[105] ENERGY STORAGE, "Every Charge Cycle Counts when It comes to Battery Degradation," 2021. *[Online], Available:* https://www.energy-storage.news/every-charge-cycle-counts-when-it-comes-to-battery-degradation/,[Accessed: 08-Sep-2021].

[106] NGESO, "Reserve services," 2023. *[Online], Available:* `https://www.nationalgrideso.com/industry-information/balancing-services/reserve-services`, [Accessed: 24-Nov-2023].

[107] NGESO , "Short term operating reserve (STOR)," 2023. *[Online], Available:* `https://www.nationalgrideso.com/industry-information/balancing-services/reserve-services/short-term-operating-reserve-stor`,[Accessed: 24-Nov-2023].

[108] NG , "Short Term Operating Reserve (STOR) ," 2018. *[Online], Available:* `https://www.nationalgrideso.com/document/115786/download`,[Accessed: 10-Jun-2023].

[109] Nationalgrid ESO, "Fast reserve," 2023. *[Online], Available:* `https://www.infineon.com/cms/en/applications/solutions/battery-management-system/`,[Accessed: 23-Nov-2023].

[110] M. Nedd, J. Browell, A. Egea-Alvarez, K. Bell, R. Hamilton, S. Wang, and S. Brush, "Operating a zero carbon gb power system in 2025: Frequency and fault current [annexes-review of system and network issues, frequency stability, power electronic devices and fault current, & market needs]," 2020.

[111] NationalGridESO , "Frequency response services," 2023. *[Online], Available:* `https://www.nationalgrideso.com/industry-information/balancing-services/frequency-response-services`,[Accessed: 16-Jan-2023].

[112] NGESO, "Historic frequency data," 2022. *[Online], Available:* `https://www.nationalgrideso.com/industry-information/balancing-services/frequency-response-services/historic-frequency-data`,[Accessed: 08-Sep-2022].

[113] W. Guo, H. Bai, G. Szatmari-Voicu, A. Taylor, J. Patterson, and J. Kane, "A 10kw 97%-efficiency llc resonant dc/dc converter with wide range of output voltage for the battery chargers in plug-in hybrid electric vehicles," in *2012 IEEE Transportation Electrification Conference and Expo (ITEC)*, pp. 1–4, IEEE, 2012.

[114] NGESO, "Dynamic Containment," 2021. *[Online], Available:* `https://www.nationalgrideso.com/industry-information/balancing-services/frequency-response-services/dynamic-containment`,[Accessed: 08-Sep-2021].

[115] A. Abdulkarim and D. T. Gladwin, "A sensitivity analysis on power to energy ratios for energy storage systems providing both dynamic firm and dynamic containment

frequency response services in the uk," in *IECON 2021–47th Annual Conference of the IEEE Industrial Electronics Society*, pp. 1–6, IEEE, 2021.

[116] NGESO , "Dynamic Containment Service Terms," 2021. *[Online], Available:* `https://www.nationalgrideso.com/document/177106/download`,[Accessed: 28-Dec-2021].

[117] NGESO , "Dynamic Regulation - Technical Requirements," 2022. *[Online], Available:* `https://www.nationalgrideso.com/industry-information/balancing-services/Frequency-Response-Services/Dynamic-Regulation/Technical-Requirements`,[Accessed: 28-December-2021].

[118] T&D World , "Lithium-Titanate Battery to Be Installed for 2MW Energy Storage System Project in UK," 2014. *[Online], Available:* `https://eepower.com/news/toshiba-to-supply-lithium-titanate-battery-for-2mw-energy-storage/`, [Accessed: 26-Jul-2021].

[119] Battery Power , "Toshiba to Supply Lithium-Titanate Battery for 2MW Energy Storage System Project in UK Led by the University of Sheffield ." *[Online], Available:* `https://www.batterypoweronline.com/news/toshiba-to-supply-lithium-titanate-battery-for-2mw-energy-storage-system-project-in-uk-led-by-the-university-of-sheffield/`,[Accessed: 28-Jul-2022].

[120] T. Feehally, A. Forsyth, R. Todd, M. Foster, D. Gladwin, D. Stone, and D. Strickland, "Battery energy storage systems for the electricity grid: Uk research facilities," 2016.

[121] NG Electrical System Operator, "Frequency response services," 2022. *[Online], Available:* `https://www.nationalgrideso.com/industry-information/balancing-services/frequency-response-servicesa`,[accessed: 09-Mar-2019].

[122] S. Mori, M. Smith, D. Gladwin, and D. Stone, "Experimental analysis of efficiencies of a large scale energy storage system," in *2020 2nd IEEE International Conference on Industrial Electronics for Sustainable Energy Systems (IESES)*, vol. 1, pp. 50–55, IEEE, 2020.

[123] B. M. Gundogdu, S. Nejad, D. T. Gladwin, M. P. Foster, and D. A. Stone, "A battery energy management strategy for uk enhanced frequency response and triad avoidance," *IEEE Transactions on Industrial Electronics*, vol. 65, no. 12, pp. 9509–9517, 2018.

[124] A. J. Hutchinson and D. T. Gladwin, "Verification and analysis of a battery energy storage system model," *Energy Reports*, vol. 8, pp. 41–47, 2022.

[125] B. Mantar Gundogdu, *Control analysis for grid tied battery energy storage system for SOC and SOH management.* PhD thesis, University of Sheffield, 2019.

[126] B. Mantar Gundogdu, D. T. Gladwin, S. Nejad, and D. A. Stone, "Scheduling of grid-tied battery energy storage system participating in frequency response services and energy arbitrage," *IET Generation, Transmission & Distribution*, vol. 13, no. 14, pp. 2930–2941, 2019.

[127] B. Yang, Y. Wang, and Y. Zhan, "Lithium battery state-of-charge estimation based on a bayesian optimization bidirectional long short-term memory neural network," *Energies*, vol. 15, no. 13, p. 4670, 2022.

[128] K. Smith, A. Saxon, M. Keyser, B. Lundstrom, Z. Cao, and A. Roc, "Life prediction model for grid-connected li-ion battery energy storage system," in *2017 American Control Conference (ACC)*, pp. 4062–4068, IEEE, 2017.

[129] Z. Wang, D. T. Gladwin, M. J. Smith, and S. Haass, "Practical state estimation using kalman filter methods for large-scale battery systems," *Applied Energy*, vol. 294, p. 117022, 2021.

[130] A. Kadri, H. Marzougui, A. Aouiti, and F. Bacha, "Energy management and control strategy for a dfig wind turbine/fuel cell hybrid system with super capacitor storage system," *Energy*, vol. 192, p. 116518, 2020.

[131] Battery University, "BU-501a Discharge Characteristics of Li-ion ," 2021. *[Online], Available:* `https://batteryuniversity.com/article/bu-501a-discharge-characteristics-of-li-ion`,[Accessed: 08-Sep-2021].

[132] HYBRIS, "Toshiba Batteries Main Features and Optimization (Part II of III)," 2021. *[Online], Available:* `https://hybris-project.eu/toshiba-batteries-main-features-and-optimization-part-ii-of-iii/`,[Accessed: 08-Dec-2022].

[133] LiTech Power, "Specification For Lithium-ion Rechargeable Cell," 2020. *[Online], Available:* `https://www.litechpower.com/product-detail/batterycellBAK%20N18650CL-29%202900mAh.html`,[Accessed: 08-Mar-2022].

[134] P. Fermín-Cueto, E. McTurk, M. Allerhand, E. Medina-Lopez, M. F. Anjos, J. Sylvester, and G. dos Reis, "Identification and machine learning prediction of

knee-point and knee-onset in capacity degradation curves of lithium-ion cells," *Energy and AI*, vol. 1, p. 100006, 2020.

[135] National Grid ESO, "Simplification and Standardisation of FFR service ," 2018. *[Online], Available:* `https://www.nationalgrideso.com/document/102071/download`, [Accessed: 06-Jan-2022].

[136] NGESO , "EBR Article 18 Dynamic Moderation (DM) and Dynamic Regulation (DR) Terms and Conditions - Closed ," 2022. *[Online], Available:* `https://www.nationalgrideso.com/calendar/ebr-article-18-dynamic-moderation-dm-and-dynamic-regulation-dr-terms-and-conditions-closed`,[Accessed: 28-Mar-2022].

[137] MODO , "Reference Price," 2022," 2022. *[Online], Available:* `https://platform.modo.energy/home`,[Accessed: 16-Jan-2023].

[138] World Energy Council, "E-storage: Shifting from cost to value Wind and solar applications," 2016. *[Online], Available:* `https://www.worldenergy.org/assets/downloads/Resources-E-storage-report-2016.02.04.pdf`,[accessed: 7-Seb-2022].

[139] J. Fleer, S. Zurmühlen, J. Meyer, J. Badeda, P. Stenzel, J.-F. Hake, and D. U. Sauer, "Techno-economic evaluation of battery energy storage systems on the primary control reserve market under consideration of price trends and bidding strategies," *Journal of Energy Storage*, vol. 17, pp. 345–356, 2018.

[140] C. Augustine and N. Blair, "Storage futures study: Storage technology modeling input data report," tech. rep., National Renewable Energy Lab.(NREL), Golden, CO (United States), 2021.

[141] I. Strategy, "Electrcity Generation Costs 2020," 2020. *[Online], Available:* `https://assets.publishing.service.gov.uk/government/uploads/system/uploads/attachment_data/file/911817/electricity-generation-cost-report-2020.pdf`, [Accessed: 06-Sep-2022].

[142] F. Mohamad, J. Teh, C.-M. Lai, and L.-R. Chen, "Development of energy storage systems for power network reliability: A review," *Energies*, vol. 11, no. 9, p. 2278, 2018.

[143] C. S. Lai, G. Locatelli, A. Pimm, Y. Tao, X. Li, and L. L. Lai, "A financial model for lithium-ion storage in a photovoltaic and biogas energy system," *Applied Energy*, vol. 251, p. 113179, 2019.

[144] C. S. Lai, Y. Jia, L. L. Lai, Z. Xu, M. D. McCulloch, and K. P. Wong, "A comprehensive review on large-scale photovoltaic system with applications of electrical energy storage," *Renewable and Sustainable Energy Reviews*, vol. 78, pp. 439–451, 2017.

[145] J. Ren and X. Ren, "Sustainability ranking of energy storage technologies under uncertainties," *Journal of cleaner production*, vol. 170, pp. 1387–1398, 2018.

[146] M. Obi, S. M. Jensen, J. B. Ferris, and R. B. Bass, "Calculation of levelized costs of electricity for various electrical energy storage systems," *Renewable and Sustainable Energy Reviews*, vol. 67, pp. 908–920, 2017.

[147] N. Lutsey and M. Nicholas, "Update on electric vehicle costs in the united states through 2030," *Int. Counc. Clean Transp*, vol. 12, 2019.

[148] W. Cole, A. W. Frazier, and C. Augustine, "Cost projections for utility-scale battery storage: 2021 update," tech. rep., National Renewable Energy Lab.(NREL), Golden, CO (United States), 2021.

[149] F. Fan, G. Zorzi, D. Campos-Gaona, G. Burt, O. Anaya-Lara, J. Nwobu, and A. Madariaga, "Sizing and coordination strategies of battery energy storage system co-located with wind farm: the uk perspective," *Energies*, vol. 14, no. 5, p. 1439, 2021.

[150] R. Fu, T. W. Remo, and R. M. Margolis, "2018 us utility-scale photovoltaics-plus-energy storage system costs benchmark," tech. rep., National Renewable Energy Lab.(NREL), Golden, CO (United States), 2018.

[151] E.ON Energy, "The Renewables Obligation explained," 2013. *[Online], Available:* `https://www.eonenergy.com/~/media/2390C47918784D15BED091AEEF4E481B.pdf`,[Accessed: 21-Jul-2021].

[152] Ofgem, "Guidance for generators that receive or would like to receive support under the Renewables Obligation (RO) scheme ," 2019. *[Online], Available:* `https://www.ofgem.gov.uk/sites/default/files/docs/2019/04/ro_generator_guidance_apr19.pdf`,[Accessed: 28-Jul-2021].

[153] Ofgem, "Renewables Obligation (RO) Buy-out Price, Mutualisation Threshold and Mutualisation Ceilings," 2022-2023. *[Online], Available:* `https://www.ofgem.gov.uk/publications/renewables-obligation-ro-buy-out-price-mutualisation-threshold-and-mutualisation-ceilings-2022-23`,[Accessed: 28-Jul-2022].

[154] The Green Age, "FiT Contract For Difference (CFD)," 2021. *[Online], Available:* `https://www.thegreenage.co.uk/tech/fit-contract-for-difference/`,[Accessed: 29-Jul-2021].

[155] EMR Settlement Limited, "Contracts for Difference," 2022-2023. *[Online], Available:* `https://www.emrsettlement.co.uk/about-emr/contracts-for-difference/`,[Accessed: 28-Jul-2022].

[156] Victoria Judd, "Financing the green transition: the evolution of contracts for difference," 2021. *[Online], Available:* `https://www.financierworldwide.com/financing-the-green-transition-the-evolution-of-contracts-for-difference#.Y6oHFEjP3IW`,[Accessed: 29-Jul-2021].

[157] Womble Bond Dickinson, "Upcoming changes to CfD Scheme for AR4 onwards," 2020. *[Online], Available:* `https://www.womblebonddickinson.com/uk/insights/articles-and-briefings/upcoming-changes-cfd-scheme-ar4-onwards`,[Accessed: 29-Jul-2022].

[158] Department for business, Energy & Industrial Strategies , "AR5 Core Parameters," 2022. *[Online], Available:* `https://assets.publishing.service.gov.uk/government/uploads/system/uploads/attachment_data/file/1124052/cfd_ar5_core_parameters.pdf`,[Accessed: 27-Dec-2022].

[159] BEIS, "Proposed Amendments to Supply Chain Plans and CfD Delivery:Government Response to Consultation ," 2022. *[Online], Available:* `https://www.gov.uk/government/consultations/contracts-for-difference-cfd-proposals-for-changes-to-\supply-chain-plans-and-cfd-delivery`,[Accessed: 6-Aug- 2022].

[160] LCCC, "CFD Levy," 2022. *[Online], Available:* `https://www.lowcarboncontracts.uk/cfd-levy`,[Accessed: 7-Aug-2022].

[161] Low Carbon Contracts Company, "Operational Costs Levy Dashboard," 2022.

[162] Low Carbon Contracts Company, "LCCC determines ILR and TRA for Q3 2022 and adjusts TRA for Q2 2022," 2022. [Online]. Available: :https://www.lowcarboncontracts.uk/news/announcement/lccc-determines-ilr-and-tra-for-q3-2022-and-adjusts-tra-for-q2-2022.

[163] TotalEnergies, "Feed-In Tariff Scheme ," 2022. *[Online], Available:* `https://business.totalenergies.uk/information-centre/more/feed-tariffs-scheme`,[Accessed: 6-Dec-2022].

[164] Ofgem, "Feed-in Tariffs (FIT)," 2021. *[Online], Available:* `https://www.ofgem.gov.uk/environmental-and-social-schemes/feed-tariffs-fit`,[accessed: 7-Aug-2021].

[165] Qrsted, "Budget with confidence," 2018. *[Online], Available:* `https://orstedcdn.azureedge.net/-/media/www/docs/corp/uk-dcs/collateral/regulatory-updates/orsted_energy-costs-update-october-2018.ashx?la=en&rev=31d7e497cdd14e34962d0887f0a257d4&hash=4e29d01759780760d7c5c369a239f58b`,[Accessed: 6-Jun-2022].

[166] NGESO, "Assistance for Areas with High Electricity Distribution Costs (AAHEDC)," 2022. *[Online], Available:* `https://www.nationalgrideso.com/electricity-transmission/document/263936/download`,[Accessed: 30-Jul-2022].

[167] EMR Settlement Limitted, "G15 - CM Supplier Payments," 2020. *[Online], Available:* `https://www.emrsettlement.co.uk/document/guidance/g15-cm-supplier-payments/`,[Accessed: 6-Aug-2021].

[168] EMR Settlement Limitted, "Key Figures for Payments in 2020/21," 2021. *[Online], Available:* `https://www.emrsettlement.co.uk/document/guidance/g15-cm-supplier-payments/`,[Accessed: 7-Aug-2021].

[169] EMR Settlement Limitted, "Key Figures for Payments in 2022/23," 2022. *[Online], Available:* `https://www.emrsettlement.co.uk/document/settlement-data/key-figures-for-payments-in-2022-23/`,[Accessed: 7-Aug- 2022].

[170] NGESO , "Current Balancing Services Use of System (BSUoS) Charges," 2021. *[Online], Available:* `https://data.nationalgrideso.com/balancing/current-balancing-services-use-of-system-bsuos-data`,[Accessed: 13-Aug-2021].

[171] National Grid , "The impact of Locational Transmission Losses on transmission charges," 2017. *[Online], Available:* `https://www.nationalgrideso.com/electricity-transmission/document/48626/download`,[Accessed: 7-Aug-2021].

[172] Elexon, "Elexon BM Unit Details," 2021. *[Online], Available:* `https://www.netareports.com/data/elexon/bmu.jsp`,[Accessed: 15-Aug-2021].

[173] Q Stark , "DUoS Red Band Charges – Your essential guide," 2021. *[Online], Available:* `https://www.stark.co.uk/resources/news/duos-red-band-charges-guide/`,[Accessed: 7-Seb-2021].

[174] Western Power Distribution , "Use of System Charging Statement," 2022. *[Online], Available:* `https://www.nationalgrid.co.uk/downloads-view-reciteme/493354`,[Accessed: 7-Seb-2022].

[175] National Grid , "Electricity Transmission network charging ," 2018. *[Online], Available:* `https://www.nationalgrid.com/sites/default/files/documents/Introduction%20to%20TNUoS%2C%20BSUoS%20and%20Connection%20Charging.pdf`,[Accessed: 27-Oct-2021].

[176] Stark , "TNUoS TransmissionElectricity Charges Guide," 2020. *[Online], Available:* `https://www.stark.co.uk/resources/news/tnuos-transmission-electricity-charges/`,[Accessed: 7-Seb-2022].

[177] NGESO, "Triads," 2018-2019. *[Online], Available:* `https://www.nationalgrideso.com/document/140446/download`,[Accessed: 21-Aug-2021].

[178] NGESO, "Final TNUoS Tariffs for 2022/23 ," 2022. *[Online], Available:* `https://www.nationalgrideso.com/document/235056/download`,[Accessed: 17-Aug-2022].

[179] Elexon BSC Portal, "Trading Charges," 2021. *[Online], Available:* `https://www.elexon.co.uk/operations-settlement/balancing-and-settlement/trading-charges/`,[Accessed: 16-Aug-2021].

[180] National Grid ESO, "TNUoS in 10 Minutes," 2018. *[Online], Available:* `https://www.nationalgrideso.com/document/130271/download`,[Accessed: 16-Aug-2021].

[181] Elexon , "Imbalance Pricing Guidance guide," 2021. *[Online], Available:* `https://www.elexon.co.uk/documents/training-guidance/bsc-guidance-notes/imbalance-pricing/`,[Accessed: 27-Oct-2021].

[182] Western Power Distribution , "DUoS Charging for LV and HV Metered Connections," 2018. *[Online], Available:* `https://www.nationalgrid.co.uk/downloads/7028`,[Accessed: 7-Seb-2022].

[183] SME Energy , "MOP DC/DA Contract Management," 2022. *[Online], Available:* `https://www.inenco.com/services/metering/mop-dcda-contract-management/#:~:text=Half%2Dhourly%20(HH)%20metering,(DC%2FDA)%20provider`,[Accessed: 8-Jun-2022].

[184] M. Beuse, M. Dirksmeier, B. Steffen, and T. S. Schmidt, "Profitability of commercial and industrial photovoltaics and battery projects in south-east-asia," *Applied Energy*, vol. 271, p. 115218, 2020.

[185] ScienceDirect, "Capacity Factor," 2012. *[Online], Available:* `https://www.sciencedirect.com/topics/engineering/capacity-factor/pdf`,[Accessed: 6-Aug-2022].

[186] S. Saxena, Y. Xing, D. Kwon, and M. Pecht, "Accelerated degradation model for c-rate loading of lithium-ion batteries," *International journal of electrical power & energy systems*, vol. 107, pp. 438–445, 2019.

[187] E. Cripps and M. Pecht, "A bayesian nonlinear random effects model for identification of defective batteries from lot samples," *Journal of Power Sources*, vol. 342, pp. 342–350, 2017.

[188] Energy Storage , "Basic to Advanced Battery Information from Battery University," 2021. *[Online],Available:* `https://batteryuniversity.com/`,[Accessed: 07-Oct-2019].

[189] M. Aneke and M. Wang, "Energy storage technologies and real life applications–a state of the art review," *Applied Energy*, vol. 179, pp. 350–377, 2016.

[190] Á. Rodríguez del Nozal, E. Romero-Ramos, and Á. L. Trigo-García, "Accurate assessment of decoupled oltc transformers to optimize the operation of low-voltage networks," *Energies*, vol. 12, no. 11, p. 2173, 2019.

[191] F. Akel, T. Ghennam, E. Berkouk, and M. Laour, "An improved sensorless decoupled power control scheme of grid connected variable speed wind turbine generator," *Energy Conversion and Management*, vol. 78, pp. 584–594, 2014.

[192] IRENA, "Electricity Storage and Renewables:Costa and Markets to 2023," 2017. *[Online], Available:* `https://www.irena.org/-/media/Files/IRENA/Agency/Publication/2017/Oct/IRENA_Electricity_Storage_Costs_2017.pdf`,[Accessed: 08- Sep-2021].

[193] T. Tuan, G. Mouloud, M. Tam, and P. Cong, "Control algorithms for micro-grid local controllers," p. 497, 2014.

[194] G. C. Konstantopoulos and A. T. Alexandridis, "Full-scale modeling, control, and analysis of grid-connected wind turbine induction generators with back-to-back ac/dc/ac converters," *IEEE journal of emerging and selected topics in power electronics*, vol. 2, no. 4, pp. 739–748, 2014.

[195] J. Hernández, J. De la Cruz, and B. Ogayar, "Electrical protection for the grid-interconnection of photovoltaic-distributed generation," *Electric Power Systems Research*, vol. 89, pp. 85–99, 2012.

[196] J. Hu, M. Marinelli, M. Coppo, A. Zecchino, and H. W. Bindner, "Coordinated voltage control of a decoupled three-phase on-load tap changer transformer and photovoltaic inverters for managing unbalanced networks," *Electric Power Systems Research*, vol. 131, pp. 264–274, 2016.

[197] C. R. Sarimuthu, V. K. Ramachandaramurthy, K. Agileswari, and H. Mokhlis, "A review on voltage control methods using on-load tap changer transformers for networks with renewable energy sources," *Renewable and Sustainable Energy Reviews*, vol. 62, pp. 1154–1161, 2016.

Appendix:A

Table. A1 List of some issues with the suggested solutions for integrating RES to the grid

Issues	Suggested solutions	Outcomes
Voltage unbalance	Three-phase grid-connected inverters.	This potential approach is used to reduce voltage imbalance in low voltage networks, which can result in enhanced voltage profiles, increased capacity for individual renewable energy sources (RES) to integrate into the network, and a reduction in overall network losses [27].
Power quality issues (Overvoltages and voltage unbalance)	Virtual synchronous machine (VSM) method.	The VSM (Virtual Synchronous Machine) technique is an excellent solution and a highly promising area for future research concerning voltage and frequency control [1]
	Synchronverter technology (Back-to-back voltage source inverter has been adopted to interface with the grid) [28].	The reason for the widespread use of this topology is its straightforward control design. Nonetheless, it exerts a considerable effect on power quality since the current it delivers to the grid is not sinusoidal. Consequently, it may cause an extra non-sinusoidal voltage drop over the line impedance, resulting in a rise in grid voltage distortion. This, in turn, can have an adverse effect on other loads and/or generators [188].

	Back-to-back converters applied in variable speed wind turbines that are provided with PMSG.	As stated by [40], the results obtained from the extended real-time simulation demonstrate that the suggested approach has the potential to enhance the wind turbine's fault ride-through capability. This improvement is achieved by ensuring that the wind turbine operates normally under regular grid conditions as well as during grid faults.
Overvoltages occurred in the low voltage (LV) grid.	Disconnected DERs from the grid and reconnected again.	The act of undertaking this action would result in a depletion of both renewable energy (RE) and financial resources for the prosumers. To address these challenges, it is necessary to strengthen the LV grid. Nonetheless, this presents a significant challenge for the DSO due to the substantial expenses involved [189].
Overvoltages and voltage unbalance	On-load tap changer (OLTC).	These gadgets are better suited for deployment in the medium voltage (MV) category and are not frequently used for low voltage (LV) tasks. Additionally, their functionality is limited to resolving overvoltage challenges and does not extend to rectifying voltage imbalances [190].
	Decoupled OLTC	The employment of decoupled OLTC is relatively infrequent in practical scenarios, and it is predominantly utilized in conjunction with medium voltage (MV) applications. [49].

	Distribution System Operators (DSOs) can leverage the deployment of certain equipment such as Dynamic Voltage Restorers (DVR) or Distribution Static Compensators (DSTATCOM) to regulate voltage control.	According to the findings of [49], these methods have demonstrated their efficacy in maintaining power quality in distribution networks. Nonetheless, it is important to note that these devices are primarily linked to the medium voltage side. While they can exert some influence on the voltage levels on the low voltage (LV) side, it is considerably more challenging for them to address voltage imbalances.
	One approach for managing reactive power is Coordinated Reactive Power Support, which involves leveraging the power and current ratings of the power electronic inverter for Renewable Energy Sources (RES) [191].	Despite the fact that the suggested algorithm shows positive outcomes, the ability of the RES's inverter to provide reactive power support was restricted by its current capacity. Furthermore, there was a substantial loss in the grid as a result of the high R/X ratios of the LV grid, which limited the impact of reactive power on the voltage profile. [192].
	Reactive power voltage control P/PF and Q/V in combination with an OLTC.	Positive outcomes have been attained, although the impact of reactive power has been limited, and it should be noted that not all MV/LV distribution transformers are outfitted with an OLTC [190].
Overvoltages and voltage unbalance.	Using battery storage together with the PV system.	The simulation results indicate that the complete mitigation of overvoltage can be accomplished. However, the problem of voltage unbalance persists, and the authors' attempts to reduce this issue have somewhat limited effectiveness due to the use of a single-phase inverter in the simulations. [193].

Power quality.	Active power curtailment.	Active power curtailment is viewed as an effective approach that seeks to enhance the hosting capacity of a feeder while preserving the power quality, sustainability, and reliability of the grid [191].
	Smart grid concepts for electric vehicle (EV) charging, which incorporate a combination of renewable energy resources and demand response, have been introduced. This includes coordinated control between photovoltaic (PV) and EV charging.	The results obtained indicate that this approach can lead to a reduction in both grid losses and the amount of energy curtailed by the PV. Nevertheless, the authors cautioned that the suggested coordinated control may not be a suitable solution, particularly in residential areas, because of the increase in the number of electric vehicles that are likely to be present during the evening period [194].
	Coordinated and uncoordinated charging of EV.	The charging of electric vehicles (EVs), whether coordinated or uncoordinated, was analyzed, and the findings indicated that the voltage unbalance factor (VUF) was reduced from 7.7% to 1.96%. While the outcomes were satisfactory, the control algorithms were observed to be more complicated and less reliable due to communication difficulties. [195].
Voltage unbalance	Three-phase damping control strategy.	This approach has the capability to withstand both zero- and negative-sequence voltage components, making it more suitable due to its ability to mitigate zero-sequence voltage unbalance [196].

	Integrating a three-phase damping control strategy with the voltage-based droop control strategy.	The results obtained demonstrate that the Distributed Energy Resource (DER) is effectively controlled at the inverter terminals by employing these two strategies. However, this approach has resulted in a reduction in some active power to ensure that phase voltages remain within their limits [197].

Appendix:B

<p align="center">**Table. A2** Cell characteristics</p>

ITEM	SPECIFICATION
Capacity	2900mAh by standard charge and discharge
Nominal voltage	3.6V
Charge cut-off voltage	4.2 V
Discharge cut-off voltage	2.5 V
Max charge current	1C (25C°), not for cycle life)
Max discharge current	3C (25C°), not for cycle life)
Storage temperature	1 year: -20-25C°, 3 months: -20-45C°, 1 month: -20-60C°
Humidity range	0-60% RH (Non-condensing)
Internal resistance	$\leq$35mΩ(AC Impedance, 1000 Hz)
Weight	$\leq$ 48g

An overview of the hardware setup for using Maccor battery testing equipment

1. Battery Test Chamber or Rack: The battery test chamber or rack is used to hold the batteries being tested and provides electrical connections to the battery testing equipment. Maccor offers a variety of test chambers and racks, ranging from small single-cell chambers to large multi-cell racks.

2. Battery Cycler: The battery cycler is the main component of the testing equipment and is used to control the charge and discharge of the batteries being tested. The cycler includes a programmable power supply, a load bank, and measurement tools for monitoring the battery's voltage, current, and temperature. Maccor's cyclers can be programmed to perform a wide range of tests, including cycling, capacity testing, and impedance testing.

3. Data Acquisition System: The data acquisition system is used to record and analyze the battery's performance data during testing. Maccor's data acquisition systems can capture a range of data, including voltage, current, temperature, and capacity,

and provide advanced analysis tools for identifying trends and anomalies in the data.

4. Safety Equipment: Maccor's battery testing equipment includes a range of safety features, such as over-current and over-voltage protection, fume hoods, and emergency shut-off switches. These safety features help ensure that the testing is conducted safely and in compliance with relevant safety regulations.

5. Computer and Software: Maccor's battery testing equipment is controlled by a computer running Maccor's proprietary software. The software provides a user-friendly interface for programming the tests, monitoring the battery's performance, and analyzing the test data.

Experiment Operation Steps

1. Start by preparing the eight cells for testing, ensuring that they are fully charged and at the same temperature.

2. Place the cells into the Maccor battery test chamber or rack, ensuring that they are properly connected to the testing equipment and any required safety features are in place.

3. Set up the testing parameters in the Maccor software, including the discharge current rate, end-of-discharge voltage, and any other relevant parameters for the specific type of cell being tested.

4. Start the test, allowing the cells to discharge at the specified current rate until they reach the end-of-discharge voltage.

5. Measure and record the capacity of each cell at the end of the test using the Maccor software or a separate capacity measurement tool.

6. Repeat the test at least two more times for each cell to ensure the accuracy and repeatability of the results.

7. Analyze the data to determine the average capacity and any variations between the cells.

8. If necessary, perform further tests or investigations to identify any factors that may be contributing to variations in capacity between the cells, such as differences in manufacturing or aging effects.

Appendix:C

(a) BLOCK1&2

(b) BLOCK3&4

(c) BLOCK5&6

Figure. A1 Simulation results for battery SOC for different scenarios (S1&S2) for the first six EFA blocks of Dec-2019 frequency data, $SOC_{start} = 30\%$.
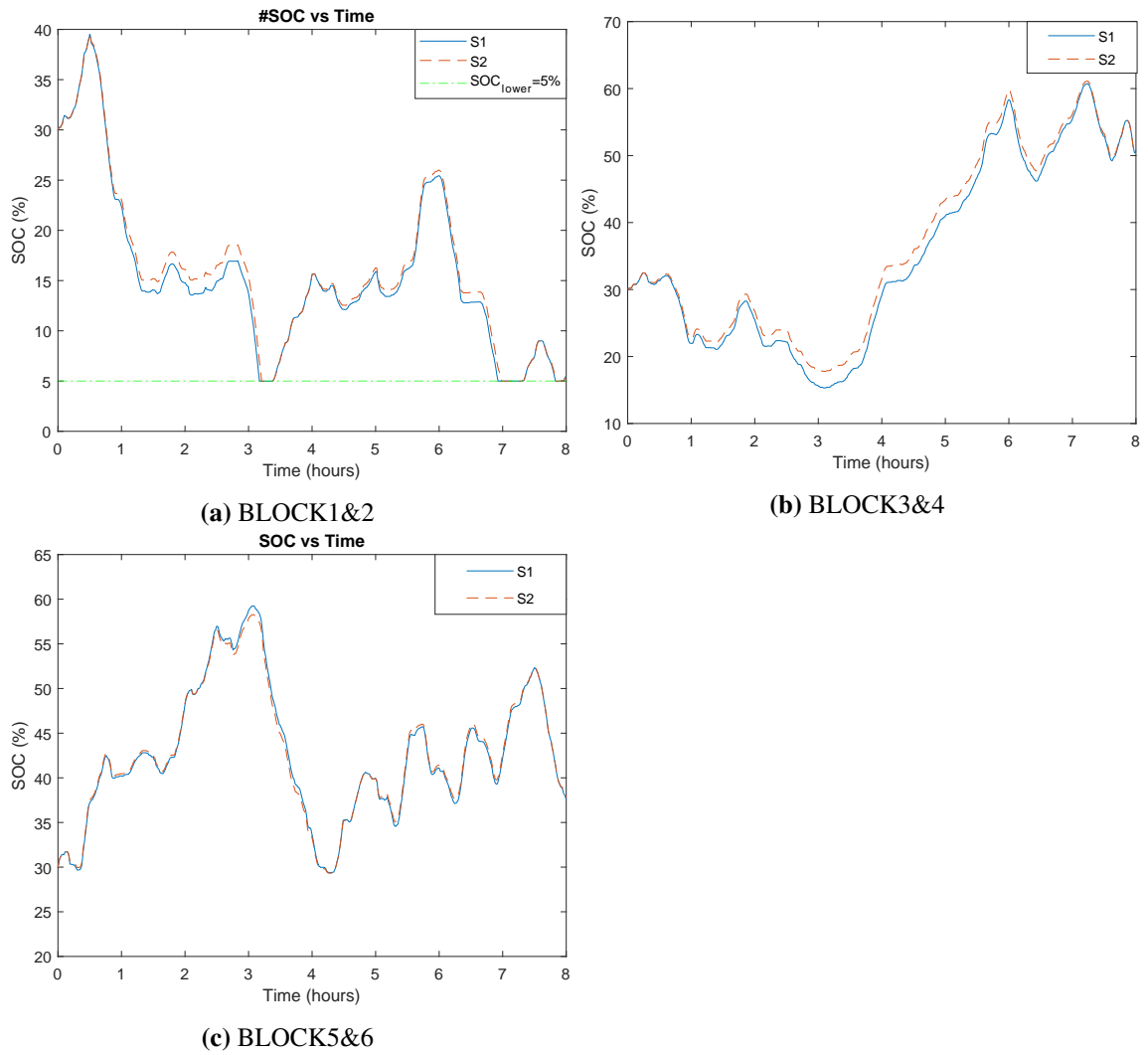
(a) BLOCK1&2

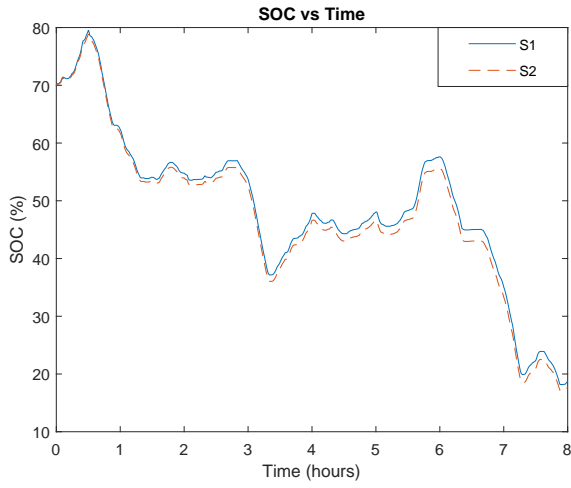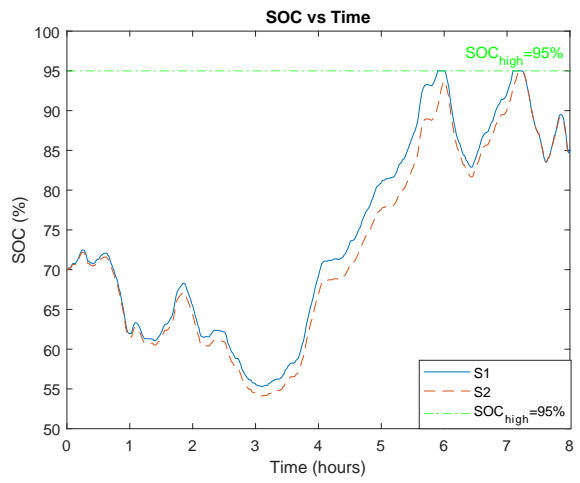**(b)** BLOCK3&4
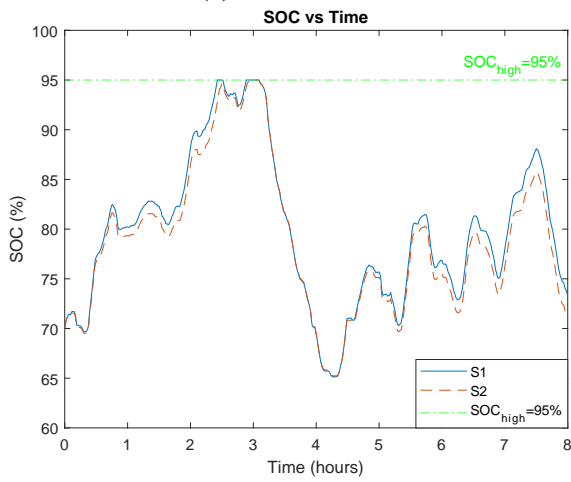
(c) BLOCK5&6

Figure. A2 Simulation results for battery SOC for different scenarios (S1&S2) for the first six EFA blocks of Dec-2019 frequency data, SOC$_{start}$ = 70%.

253

Appendix:D

Figure. A3 Jun-2022 invoice.

Energy supply invoice for Jun-2022, BESS with a different C-rates used to deliver DFR Service for Jun-2019 frequency data

Table. A3 Energy supply invoice for Jun-2022, BESS with a different C-rates used to deliver DFR Service for Jun-2019 frequency data

Cost Breakdown					
Cost		Charger Point	Cost/Revenue 0.5C	Cost/Revenue 1C	Cost/Revenue 2C
RO		MSP	£39,487.49	£39,032.42	£37,286.87
CFD		NBP	£133.70	£132.16	£126.25
FiT		MSP	£11,408.18	£11,276.70	£10,772.40
AAHEDC		GSP	£66.20	£72.28	£70.29
CM	Monthly ,Settlement Cost Levy for Supplier	NBP	£36.44	£36.23	£34.50
	Monthly CM supplier charge for supplier	NBP	£2,733.06	£2,717.37	£2,587.99
BSUoS	Generation	NBP	-£13,358.22	-£13,038.90	-£12,425.52
	Demand	NBP	£15,258.72	£15,082.87	£14,408.35
DUoS		MSP	£3,118.98	£3,088.17	£2,729.22
GDUoS		MSP	-£3,999.85	-£3,932.29	-£3,850.09
TNUoS	Demand	MSP	£78,300.98	£78,300.98	£78,300.98
	Generation	MSP	-£8,511.50	-£8,511.50	-£8,511.50
Elexon		GSP	£575.88	£565.88	£539.96
TNUoS EET	Generation	NBP	-£1,519.84	-£1,519.84	-£1,519.84
	Demand	NBP	0	0	0
DFR Service Revenue		GSP	-£521,280	-£521,280	-£521,280
DUoS Fixed		Supply	£27.02	£27.02	£27.02
DUoS Capacity		Site	£62,160	£62,160	£62,160
MOP DC/AC		Supply	£45	£45	£45
Total Cost		-	-£335,317.76	-£335,745.45	-£338,498.12
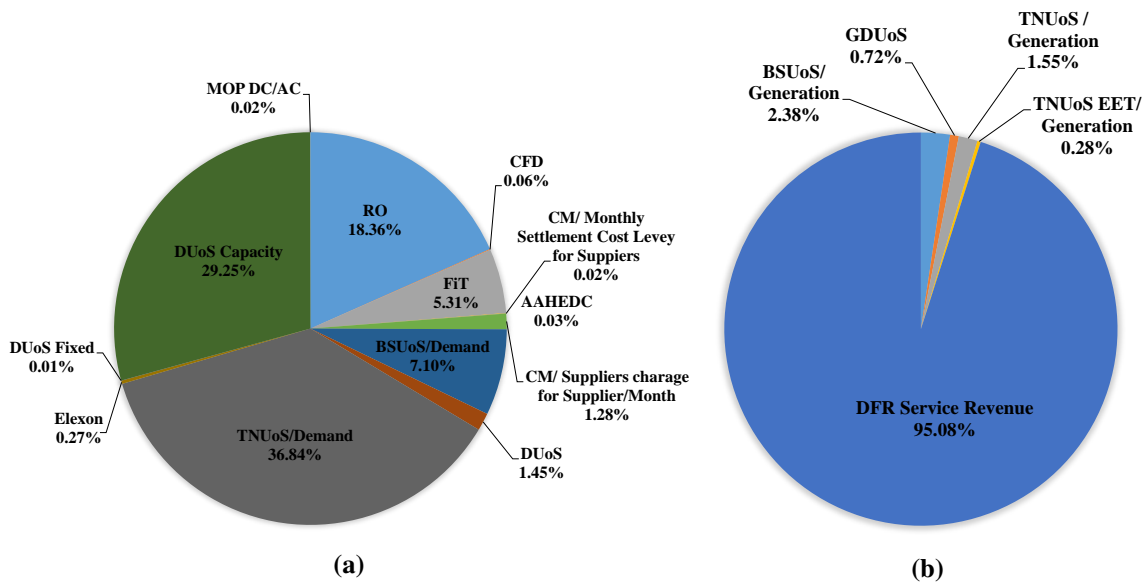
Figure. A4 Analysis findings of Cost (a), and Revenue (b) for BESS with 1C used to deliver DFR service for Jun-2022, using frequency data of Jun-2019.

(a)
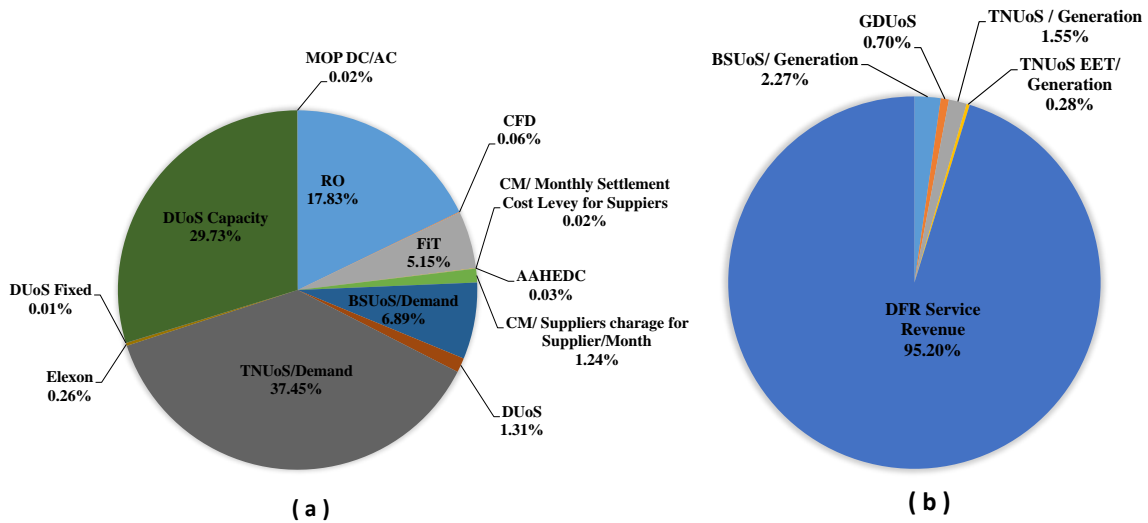
Figure. A6 Analysis findings of Cost (a), and Revenue (b) for BESS with 2C used to deliver DFR service for Jun-2022, using frequency data of Jun-2019.

Table. A4 Energy supply invoice for Jun-2022, BESS with a different C-rates used to deliver DC Service for Jun-2019 frequency data

Cost Breakdown					
Cost		Charger Point	Cost/Revenue 0.5C	Cost/Revenue 1C	Cost/Revenue 2C
RO		MSP	£4,054.69	£4,054.69	£4,054.69
CFD		NBP	£13.73	£13.73	£13.73
FiT		MSP	£1,171.43	£1,171.43	£1,171.43
AAHEDC		GSP	£2.22	£1.44	£4.89
CM	Monthly Settlement Cost Levy for Supplier	NBP	£3.89	£3.89	£3.89
	Monthly CM supplier charge for supplier	NBP	£291.89	£291.89	£291.89
BSUoS	Generation	NBP	-£1,589.54	-£1,501.13	-£1,417.93
	Demand	NBP	£1,566.81	£1,566.81	£1,566.81
DUoS		MSP	£320.14	£320.14	£319.94
GDUoS		MSP	-£490.23	-£477.68	-£459.62
TNUoS	Demand	MSP	£6,896.07	£6,896.07	£6,896.07
	Generation	MSP	-£631.67	-£631.67	-£631.67
Elexon		GSP	£63.56	£61.77	£60.07
TNUoS EET	Generation	NBP	-£112.79	-£112.79	-£112.79
	Demand	NBP	0	0	0
DC Service Revenue		GSP	-£1,173,312	-£1,173,312	-£1,173,312
DUoS Fixed		Supply	£27.02	£27.02	£27.02
DUoS Capacity		Site	£62,160	£62,160	£62,160
MOP DC/AC		Supply	£45	£45	£45
Total Cost		-	-£1,099,519.78	-£1,099,421.39	-£1,099,318.58

Figure. A7 Analysis findings of Cost (a), and Revenue (b) for BESS with 1C used to deliver DC service for Jun-2022, using frequency data of Jun-2019.

Figure. A8 Analysis findings of Cost (a), and Revenue (b) for BESS with 2C used to deliver DC service for Jun-2022, using frequency data of Jun-2019.

Table. A5 Energy supply invoice for Jun-2022, BESS with a different C-rates used to deliver DR Service for Jun-2019 frequency data

| Cost Breakdown					
Cost		Charger Point	Cost/Revenue 0.5C	Cost/Revenue 1C	Cost/Revenue 2C
RO		MSP	£79,202.92	£74,601.51	£66,770.42
CFD		NBP	£268.18	£252.59	£226.08
FiT		MSP	£22,882.20	£21,552.83	£19,290.38
AAHEDC		GSP	£148.42	£140.61	£123.10
CM	Monthly Settlement Cost Levy for Supplier	NBP	£75.57	£70.82	£65.51
	Monthly CM supplier charge for supplier	NBP	£5,668.23	£5,312.11	£4,913.85
BSUoS	Generation	NBP	-£26,415.51	-£24,861.28	-£22,317.89
	Demand	NBP	£30,605.51	£28,827.44	£25,801.36
DUoS		MSP	£6,324.69	£6,159.35	£5,245.53
GDUoS		MSP	-£7,973.38	-£7,684.4	-£6,749.50
TNUoS	Demand	MSP	£137,829.39	£137,829.39	£137,829.39
	Generation	MSP	-£12,598.26	-£12,598.26	-£12,440.43
Elexon		GSP	£1,147.39	£1,080.34	£968.28
TNUoS EET	Generation	NBP	-£2,249.58	-£2,249.58	-£2,221.40
	Demand	NBP	0	0	0
DR Service Revenue		GSP	-£557,856	-£557,856	-£557,856
DUoS Fixed		Supply	£27.02	£27.02	£27.02
DUoS Capacity		Site	£62,160	£62,160	£62,160
MOP DC/AC		Supply	£45	£45	£45
Total Cost		-	-£260,708.21	-£267,190.51	-£278,119.30
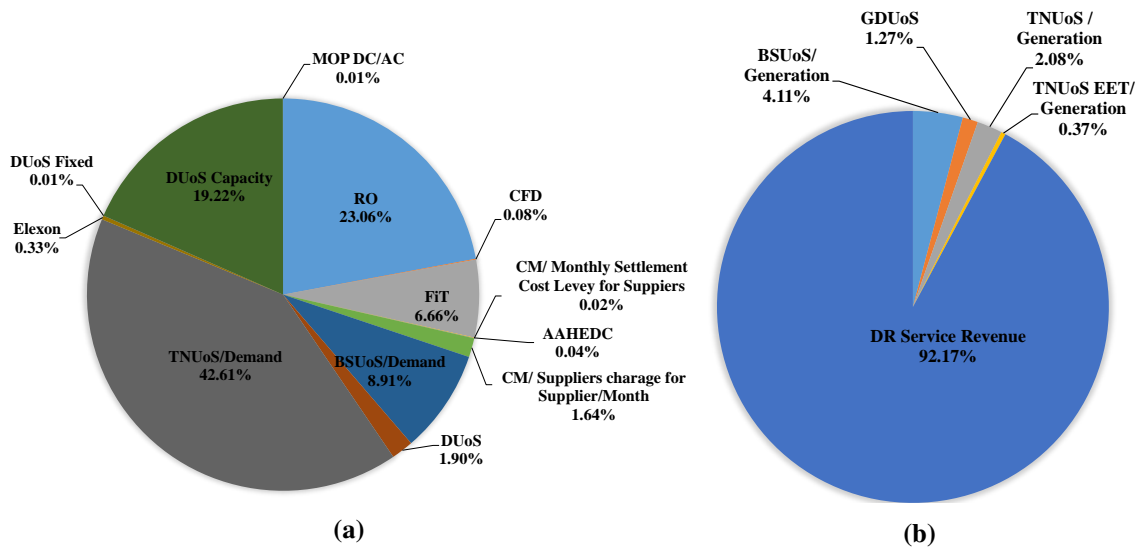
Figure. A9 Analysis findings of Cost (a), and Revenue (b) for BESS with 1C used to deliver DR service for Jun-2022, using frequency data of Jun-2019.
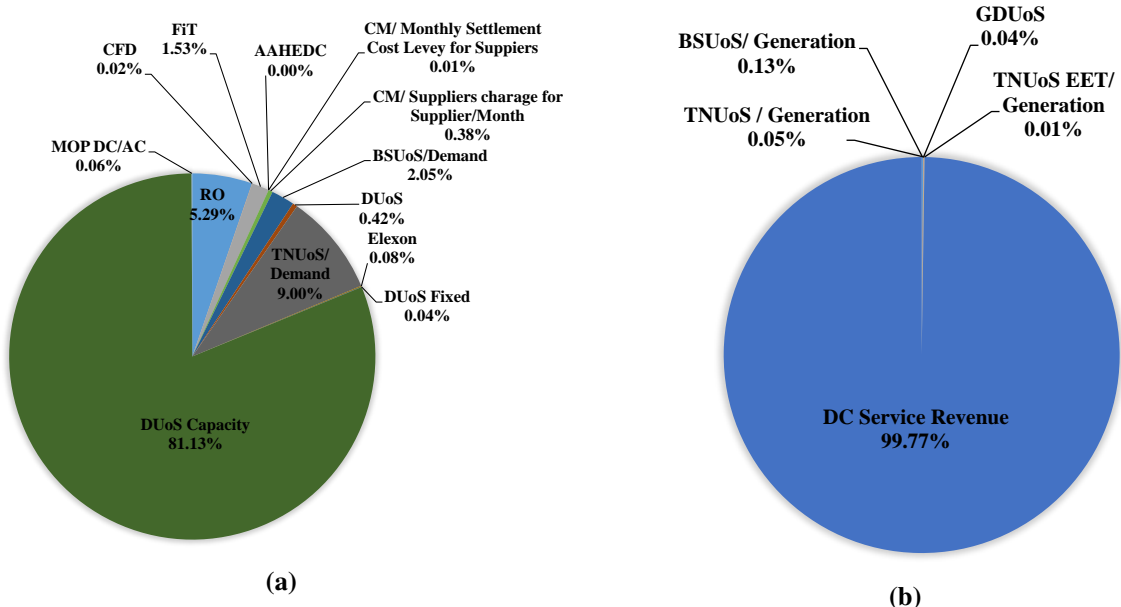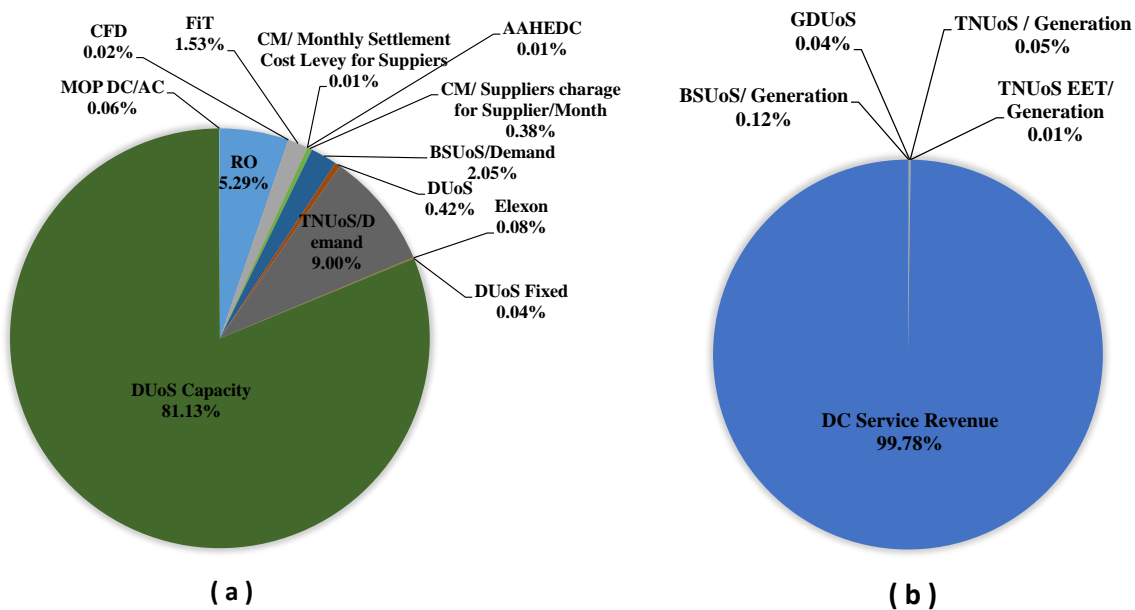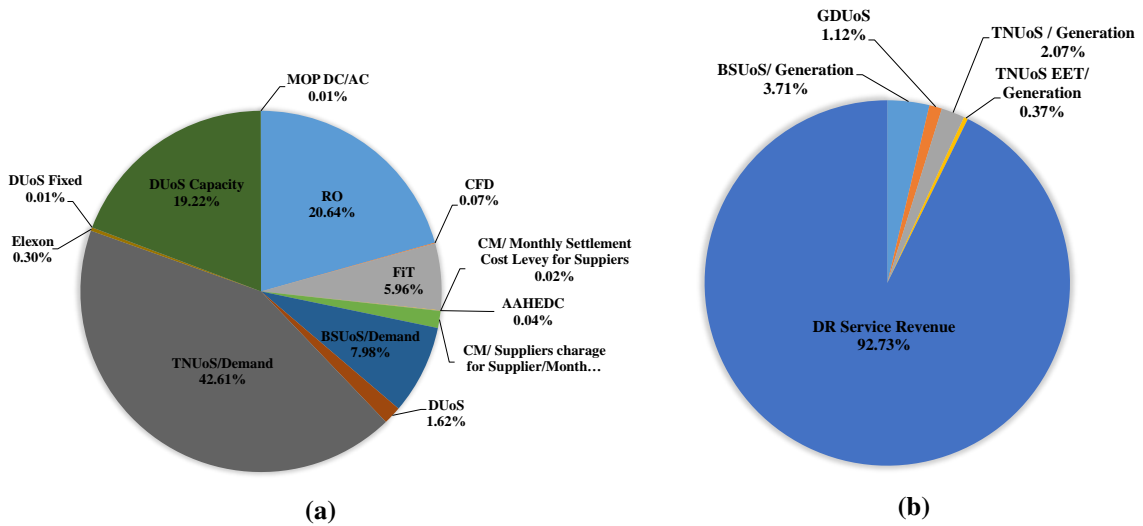

Figure. A10 Analysis findings of Cost (a), and Revenue (b) for BESS with 2C used to deliver DR service for Jun-2022, using frequency data of Jun-2019.

DUoS &GDUoS for BESS with different C-rates delivering DFR services for the full year-2022

Table. A6 DUoS for BESS with different C-rates delivering DFR services for the full year-2022 (Import)

| | DFR (0.5C) | | | DFR (1C) | | | DFR (2C) | | |
| | Import | | | Import | | | Import | | |
	Red	Orange	Green	Red	Orange	Green	Red	Orange	Green
Mon-Fri Energy (MWh)	1,957.24	6,394.63	5,794.51	1,950.74	6,323.82	5,686.06	1,892.18	6,034.34	5,175.95
Mon-Fri Cost (£)	25,130.96	14,323.97	521.51	25,047.50	14,165.36	511.75	24,295.59	13,516.92	465.84
Sat-Sun Energy (MWh)			5,006.82			4,894.50			4,616.90
Sat–Sun Cost (£)			450.61			440.51			415.52
Total unit charges (£)	40,427.05			40,165.12			38,693.87		

Table. A7 GDUoS for BESS with different C-rates delivering DFR services for the full year-2022 (Export)

| | DFR (0.5C) | | | DFR (1C) | | | DFR (2C) | | |
| | Export | | | Export | | | Export | | |
	Red	Orange	Green	Red	Orange	Green	Red	Orange	Green
Mon-Fri Energy (MWh)	1,957.24	5,814.20	5,301.91	1,752.11	5,633.99	5,176.94	1,648.71	5,265.81	4,850.32
Mon-Fri Cost (£)	35,230.32	18,198.45	901.33	31,537.98	12,620.14	880.08	29,676.78	11,795.41	824.55
Sat-Sun Energy (MWh)			4,457.16			4,339.16			4,045.58
Sat-Sun Cost (£)			757.72			737.66			687.75
Total unit charges (£)	55,087.82			45,775.86			42,984.49		

DUoS& GDUoS for BESS with different C-rates delivering DC services for the full year- 2019

Table. A8 DUoS for BESS with different C-rates delivering DC services for the full Year-2019 (Import)

| | DC (0.5C) | | | DC (1C) | | | DC (2C) | | |
| | Import | | | Import | | | Import | | |
	Red	Orange	Green	Red	Orange	Green	Red	Orange	Green
Mon-Fri Energy (MWh)	201.79	656.79	593.25	201.79	656.79	593.25	201.79	656.79	593.25
Mon - Fri Cost (£)	2,590.98	1,471.21	53.39	2,590.98	1,471.21	53.39	2,590.98	1,471.21	53.39
Sat-Sun Energy (MWh)			507.05			507.05			507.05
Sat-Sun Cost (£)			45.63			45.63			45.63
Total unit charges (£)	4,161.21			4,161.21			4,161.21		

Table. A9 GDUoS for BESS with different C-rates delivering DC services for the full year-2022 (Export)

| | DC(0.5C) | | | DC (1C) | | | DC (2C) | | |
| | Export | | | Export | | | Export | | |
	Red	Orange	Green	Red	Orange	Green	Red	Orange	Green
Mon-Fri Energy (MWh)	211.24	670.55	610.76	204.15	651.20	595.98	196.72	619.28	561.27
Mon-Fri Cost (£)	3,802.32	2,098.82	103.83	3,674.70	2,038.26	101.32	3,540.96	1,938.35	95.42
Sat-Sun Energy (MWh)			524.07			497.56			465.65
Sat-Sun Cost (£)			89.09			84.59			79.16
Total unit charges (£)	6,094.06			5,898.87			5,653.89		

DUoS&DGUoS for BESS with a different C-rates delivering DR services for the full year- 2022

Table. A10 DUoS for BESS with different C-rates delivering DR services for the full year-2019 (Import)

	DR (0.5C)			DR (1C)			DR (2C)		
	Import			Import			Import		
	Red	Orange	Green	Red	Orange	Green	Red	Orange	Green
Mon-Fri Energy (MWh)	3,974.63	12,857.24	11,372.61	3,832.39	12,162.32	10,187.19	3,509.47	10,887.37	9,037.57
Mon-Fri Cost (£)	51,034.25	28,800.22	1,023.54	49,207.89	27,243.59	916.85	45,061.59	24,387.71	813.38
Sat-Sun Energy (MWh)			9,781.76			9,126.44			8,122.93
Sat-Sun Cost (£)			880.36			821.38			731.06
Total unit charges (£)	81,738.37			78,189.71			70,993.74		

Table. A11 GDUoS for BESS with different C-rates delivering DR services for the full year-2022 (Export)

	DR (0.5C)			DR (1C)			DR (2C)		
	Export			Export			Export		
	Red	Orange	Green	Red	Orange	Green	Red	Orange	Green
Mon-Fri Energy (MWh)	3,549.12	11,400.75	10,416.92	3,310.91	10,559.60	9,661.42	2,955.46	9,415.09	8,716.31
Mon-Fri Cost (£)	63,884.16	35,684.35	1,770.88	59,596.38	33,051.55	1,642.44	53,198.28	29,469.23	1,481.77
Sat-Sun Energy (MWh)			8,675.04			7,995.14			7,167.46
Sat-Sun Cost (£)			1,474.76			1,359.17			1,218.47
Total unit charges (£)	102,814.15			95,649.54			85,367.75		

Energy supply invoice for year-2022, BESS with different C-rates used to deliver DFR, DC & DR Service for the full year-2019 frequency data

Table. A12 Energy supply invoice of year-2022 for BESS with 0.5C used to deliver DFR, DC & DR Service for the full year-2019 frequency data

Cost Breakdown					
Cost		Charger Point	Cost/Revenue DFR	Cost/Revenue DC	Cost/Revenue DR
RO		MSP	£469,217.39	£47,960.32	£929,971.57
CFD		NBP	£1,588.76	£162.39	£3,148.86
FiT		MSP	£135,559.73	£13,856.03	£268,674.38
AAHEDC		GSP	£734.77	£14.99	£1,624.69
CM	Settlement Cost Levy for Supplier/Year	NBP	£448.09	£47.86	£929.32
	CM supplier charge for supplier/Year	NBP	£41,783.37	£4,462.54	£86,656.67
BSUoS	Generation	NBP	-£159,879.40	-£18,533.60	-£312,778.80
	Demand	NBP	£181,314.50	£18,532.78	£359,358.70
DUoS		MSP	£40,427.05	£4,161.21	£81,738.37
GDUoS		MSP	-£55,087.82	-£6,094.06	-£102,814.15
TNUoS	Demand	MSP	£78,300.98	£6,896.07	£137,829.39
	Generation	MSP	-£8,511.50	-£631.67	-£12,598.26
Elexon		GSP	£6,866.35	£746.41	£13,525.53
TNUoS EET	Generation	NBP	-£1,519.84	-£112.79	-£2,249.58
	Demand	NBP	0	0	0
Frequency Response Revenue		GSP	-£5,509,164	-£7,622,660	-£3,781,838
DUoS Fixed		Supply	£328.72	£328.72	£328.72
DUoS Capacity		Site	£756,280	£756,280	£756,280
MOP DC/AC		Supply	£547.5	£547.5	£547.5
Total Cost		-	-£4,020,765.35	-£6,794,035.30	-£1,571,665.09

Table. A13 Energy supply invoice of year 2022 for BESS with 2C used to deliver DFR, DC & DR Service for the full year-2019 frequency data

Cost Breakdown					
Cost		Charger Point	Cost/Revenue DFR	Cost/Revenue DC	Cost/Revenue DR
RO		MSP	£433,649.86	£47,960.32	£773,208.48
CFD		NBP	£1,468.33	£162.39	£2,618.07
FiT		MSP	£125,284.05	£13,856.03	£223,384.58
AAHEDC		GSP	£775.89	£51.39	£1372.31
CM	Settlement Cost Levy for Supplier/Year	NBP	£424.31	£47.86	£7805.64
	CM supplier charge for supplier/Year	NBP	£39,565.64	£4,462.54	£75,123.58
BSUoS	Generation	NBP	-£145,405.10	-£16,918.49	-£259,531.70
	Demand	NBP	£167,570.50	£18,532.78	£298,782.40
DUoS		MSP	£38,693.87	£4,161.21	£70,993.74
GDUoS		MSP	-£42,984.49	-£5,653.89	-£85,367.75
TNUoS	Demand	MSP	£78,300.98	£6,896.07	£137,829.39
	Generation	MSP	-£8,511.50	-£631.67	-£12,440.43
Elexon		GSP	£6,297.97	£ 713.56	£11,234.94
TNUoS EET	Generation	NBP	-£1,519.84	-£112.79	-£2,221.40
	Demand	NBP	0	0	0
Frequency Response Revenue		GSP	-£5,509,164	-£7,622,660	-£3,781,838
DUoS Fixed		Supply	£328.72	£328.72	£328.72
DUoS Capacity		Site	£756,280	£756,280	£756,280
MOP DC/AC		Supply	£547.5	£547.5	£547.5
Total Cost		-	-£4,058,397.31	-£6,791,976.47	-£1,781,889.93

Figure. A11 Analysis findings of Cost (a), and Revenue (b) for BESS with 1C used to deliver DFR service for the whole year-2022, using frequency data of year-2019.

Figure. A12 Analysis findings of Cost (a), and Revenue (b) for BESS with 1C used to deliver DC service without submitting a P_{Base} for the whole year-2022, using frequency data of year-2019.

Figure. A13 Analysis findings of Cost (a), and Revenue (b) for BESS with 1C used to deliver DR service without implementing a dynamic control for the whole year-2022, using frequency data of year-2019.
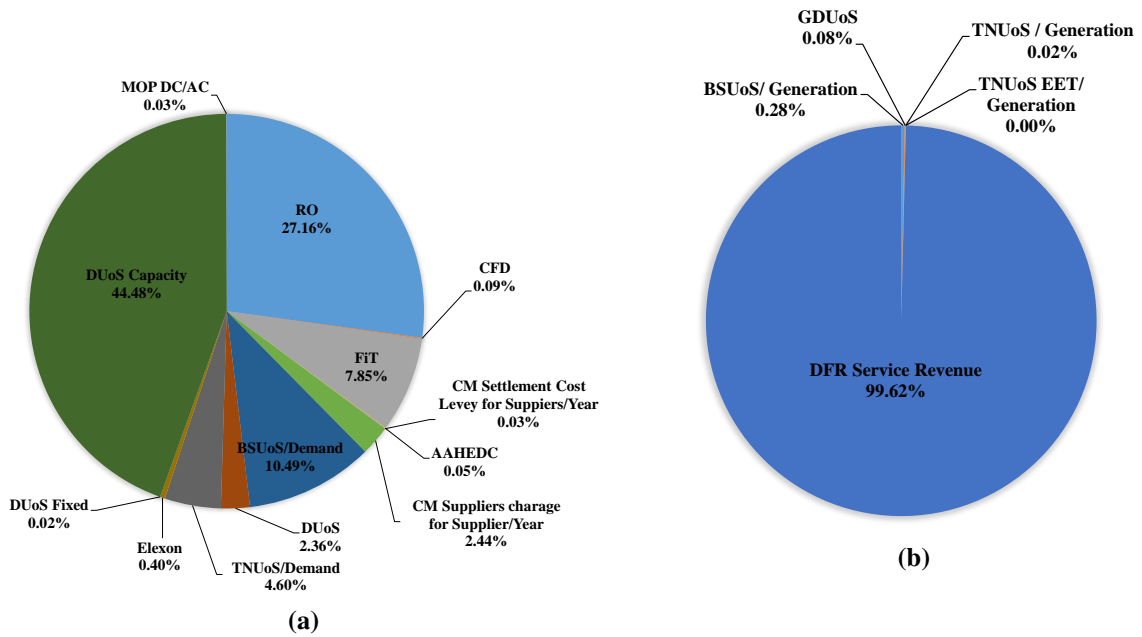

Figure. A14 Analysis findings of Cost (a), and Revenue (b) for BESS with 2C used to deliver DFR service for the whole year-2022, using frequency data of year-2019.
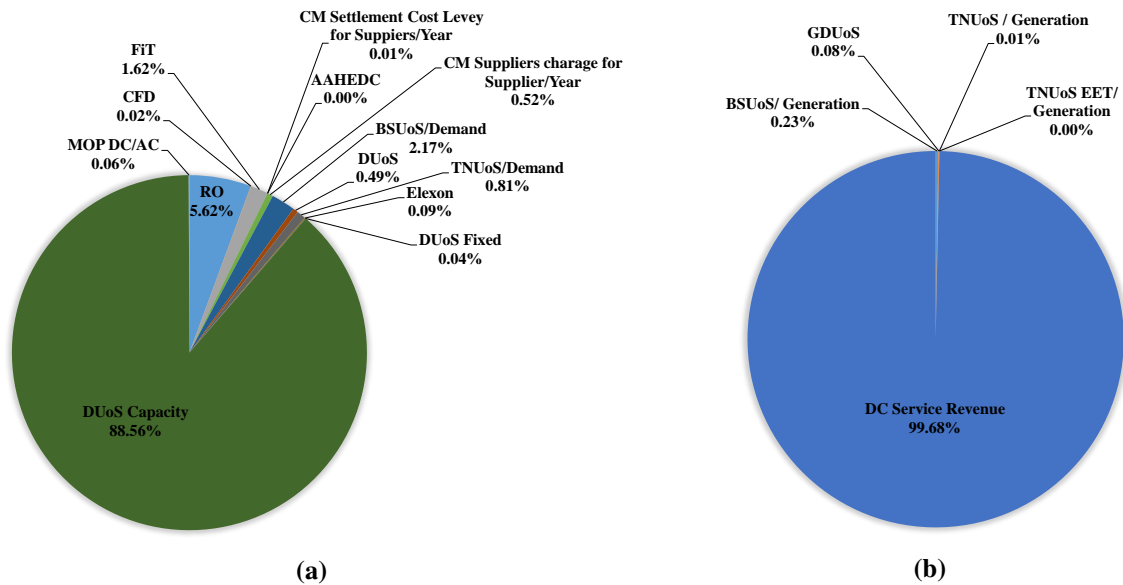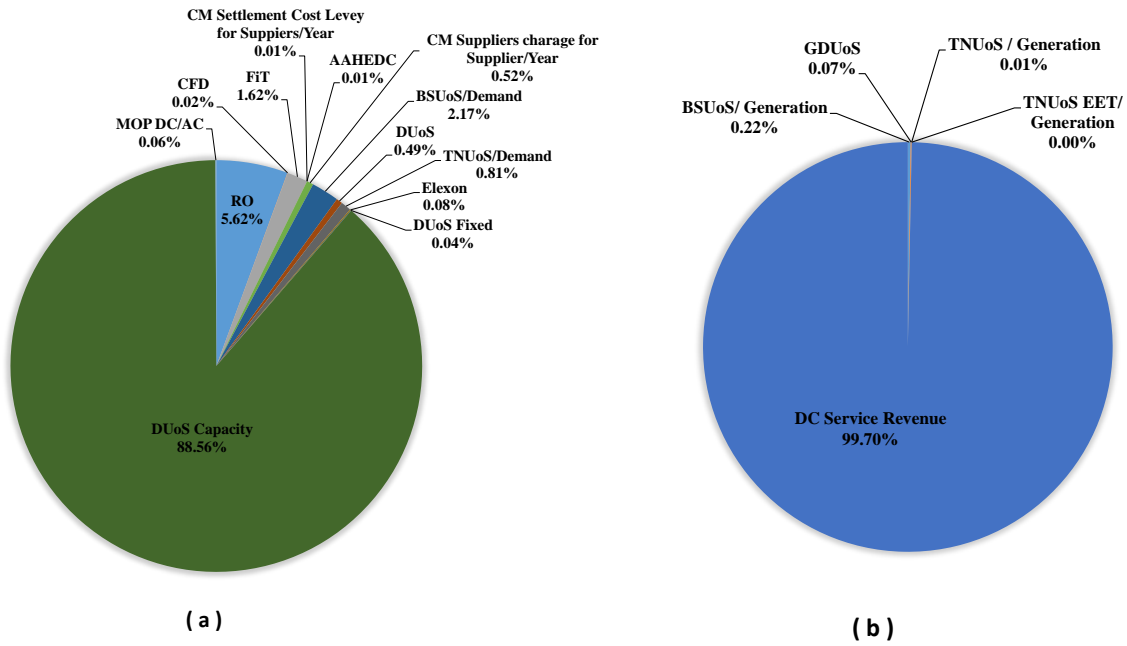
Figure. A15 Analysis findings of Cost (a), and Revenue (b) for BESS with 2C used to deliver DC service without submitting a P_{Base} for the whole year-2022, using frequency data of year-2019.
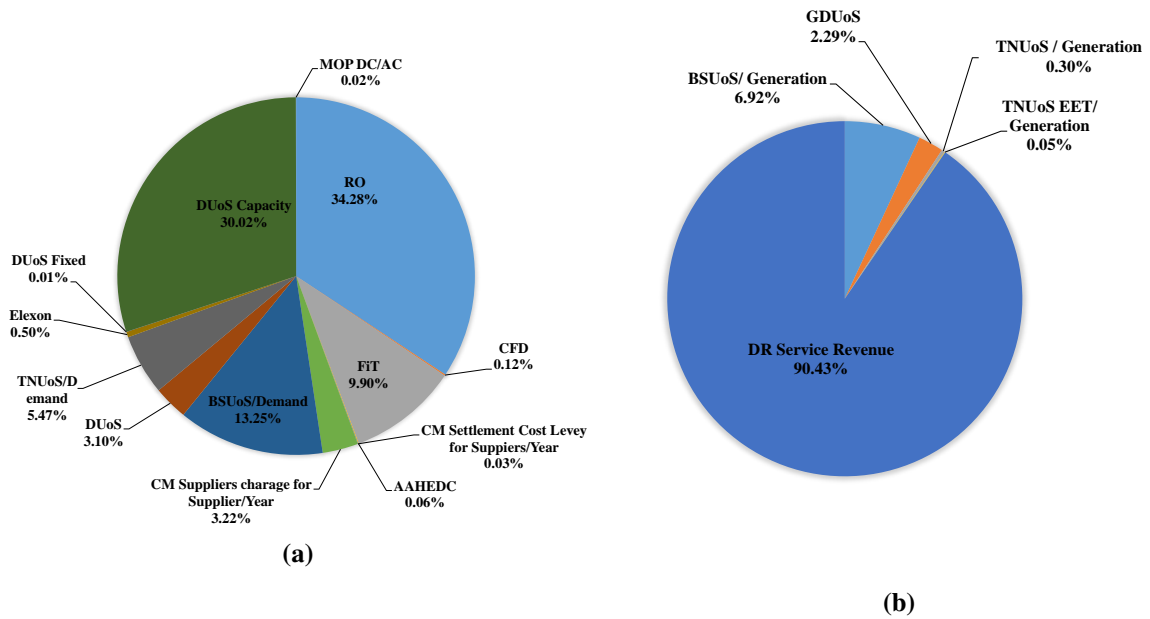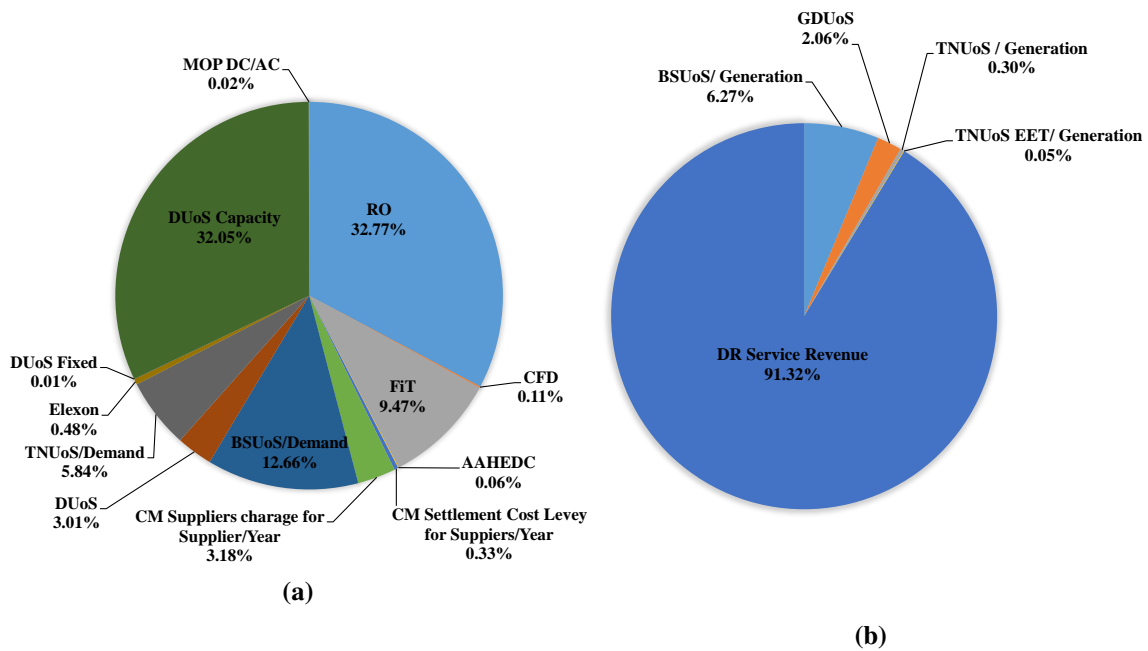

Figure. A16 Analysis findings of Cost (a), and Revenue (b) for BESS with 2C used to deliver DR service without implementing a dynamic control (S1) for the whole year-2022, using frequency data of year-2019.
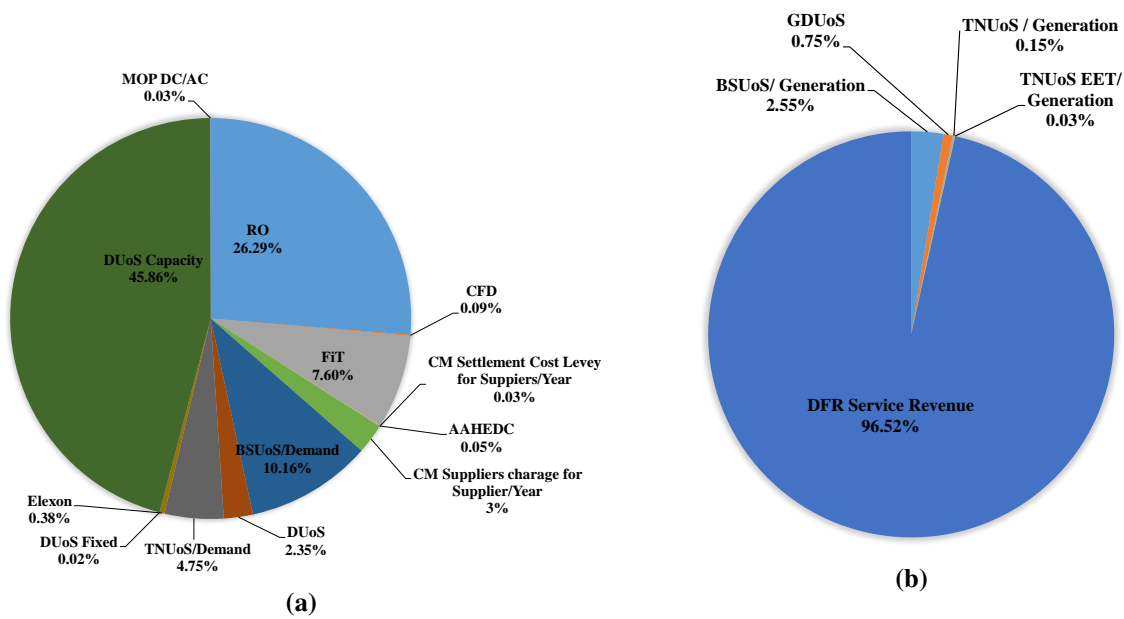
Appendix:E

Simulation Results of BESS with 1C used to deliver DC service with and without submitting a P_{Base} power for Jun-2019 frequency data

Table. A14 Simulation Results of BESS with 1C used to deliver DC service with and without submitting a P_{Base} power for Jun-2019 frequency data

Contracted Service Power (MW)	Baseline power (MW)	Total Import Energy (MWh)	Total Export Energy (MWh)	Avg.Availability (%)
±40	0	156.19	152.64	99.63
±39	±1	165.73	153.54	100

Table. A15 Energy supply invoice for Jun-2022, BESS with 1C-rate used to deliver DC services without and with submitting a baseline power for Jun-2019 frequency data

Cost Breakdown				
Cost		Charger Point	Cost/Revenue (without a baseline)	Cost/Revenue (with a baseline)
RO		MSP	£4,054.69	£4,302.35
CFD		NBP	£13.73	£14.57
FiT		MSP	£1,171.43	£1,242.98
AAHEDC		GSP	£1.44	£4.93
CM	Monthly Settlement Cost Levy for Supplier	NBP	£3.89	£3.88
	Monthly CM supplier charge for supplier	NBP	£291.89	£291.29
BSUoS	Generation	NBP	-£1,501.13	-£1,509.98
	Demand	NBP	£1,566.81	£1,662.51
DUoS		MSP	£320.14	£325.29
GDUoS		MSP	-£477.68	-£445.23
TNUoS	Demand	MSP	£6,896.07	£6,723.75
	Generation	MSP	-£631.67	-£615.85
Elexon		GSP	£61.77	£63.85
TNUoS EET	Generation	NBP	-£112.79	-£109.97
	Demand	NBP	0	0
DC Frequency Response Revenue		GSP	-£1,173,312	-£1,143,979.2
DUoS Fixed		Supply	£27.02	£27.02
DUoS Capacity		Site	£62,160	£62,160
MOP DC/AC		Supply	£45	£45
Total Cost		-	-£1,099,421.39	-£1,069,792.81

DUoS&GDUoS for BESS with different C-rates delivering DC service with and without submitting a P_{Base} power for the full year-2022

Table. A16 GDUoS for BESS with different C-rates delivering DC services for the full year-2022 (Export)

	DC (N-BL)			DC (BL)		
	Export			Export		
	Red	Orange	Green	Red	Orange	Green
Mon - Fri Energy (MWh)	204.15	651.20	595.98	201.49	643.84	585.56
Mon - Fri Cost (£)	3,674.70	2,038.26	101.32	3,626.82	2,015.22	99.55
Sat-Sun Energy (MWh)			497.56			496.78
Sat-Sun Cost (£)			84.59			84.45
Total unit charges (£)	5,898.87			5,826.04		

Table. A17 DUoS for BESS with different C-rates delivering DC service with and without submitting a P_{Base} for the full year-2022 (Import)

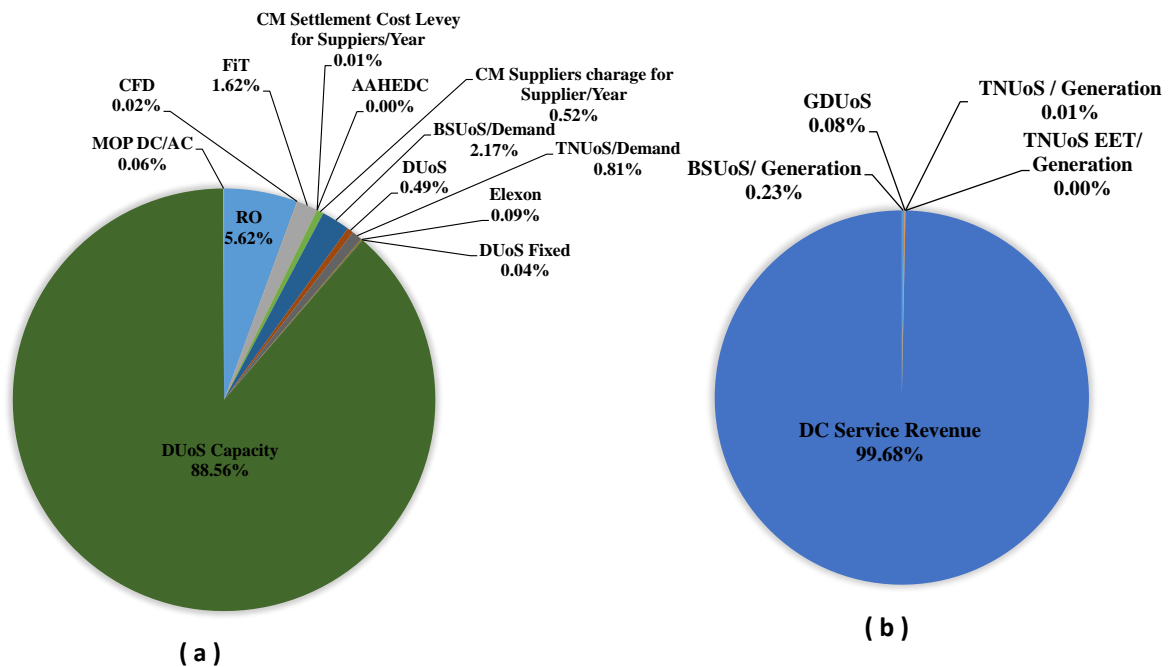|	DC (N-BL)			DC (BL)		
	Import			Import		
	Red	Orange	Green	Red	Orange	Green
Mon - Fri Energy (MWh)	201.79	656.79	593.25	211.77	680.90	609.46
Mon - Fri Cost (£)	2,590.98	1,471.21	53.39	2,719.13	1,525.22	54.85
Sat-Sun Energy (MWh)			507.05			541.14
Sat-Sun Cost (£)			45.63			48.70
Total unit charges (£)	4,161.21			4,347.90		

Figure. A17 Analysis findings of Cost (a), and Revenue (b) for BESS used to deliver DC service without P_{Base} for the whole year-2022, using frequency data of year-2019.

Simulation Results of BESS with 1C used to deliver DR service with and without applying a dynamic control for Jun-2019 frequency data

Table. A18 Simulation Results of BESS with 1C that is used to deliver DR service with a different scenarios (S1&S2) for Jun-2019 frequency data

Contracted Service Power (MW)	Total Import Energy (MWh)	Total Export Energy (MWh)	Avg.Availability (%)	Scenarios
±40	2,873.71	2,527.98	89.12	S1
±40	2,821.04	2,481.34	90.56	S2

Table. A19 Energy supply invoice for Jun-2022, BESS with 1C used to deliver DR Service with a different scenarios (S1 & S2) for Jun-2019 frequency data

Cost Breakdown				
Cost		Charger Point	Cost/Revenue DR/ (S1)	Cost/Revenue DR/ (S2)
RO		MSP	£74,601.51	£73,234.19
CFD		NBP	£252.59	£247.97
FiT		MSP	£21,552.83	£21,157.80
AAHEDC		GSP	£140.61	£138.16
CM	Monthly Settlement Cost Levy for Supplier	NBP	£70.82	£69.41
	Monthly CM supplier charge for supplier	NBP	£5,312.11	£5,206.66
BSUoS	Generation	NBP	-£24,861.28	-£24,402.26
	Demand	NBP	£28,827.44	£28,299.09
DUoS		MSP	£6,159.35	£6,022.36
GDUoS		MSP	-£7,684.40	-£7,471.22
TNUoS	Demand	MSP	£137,829.39	£137,105.77
	Generation	MSP	-£12,598.26	-£11,256.18
Elexon		GSP	£1,080.34	£1,060.48
TNUoS EET	Generation	NBP	-£2,249.58	-£2,009.94
	Demand	NBP	0	0
DR Frequency Response Revenue		GSP	-£557,856	-£557,856
DUoS Fixed		Supply	£27.02	£27.02
DUoS Capacity		Site	£62,160	£62,160
MOP DC/AC		Supply	£45	£45
Total Cost		-	-£267,190.51	-£268,221.69

DUoS & GDUoS for BESS with different C-rates delivering DR service with different scenarios for the full year-2022

Table. A20 GDUoS for BESS with different C-rates delivering DR service with different scenarios (S1 & S2) for the full year-2019 (Export)

	DR (S1)			DR (S2)		
	Export			Export		
	Red	Orange	Green	Red	Orange	Green
Mon - Fri Energy (MWh)	3,310.91	10,559.60	9,661.42	3,233.55	10,344.32	9,529.26
Mon - Fri Cost (£)	59,596.3	33,051.55	1,642.44	58,203.90	32,377.72	1,619.97
Sat-Sun Energy (MWh)			7,995.14			7,865.63
Sat-Sun Cost (£)			1,359.17			1,337.16
Total unit charges (£)	95,649.54			93,538.75		

Table. A21 DUoS charge for BESS with 1C delivering DR service for different scenarios for the full year-2022 frequency data

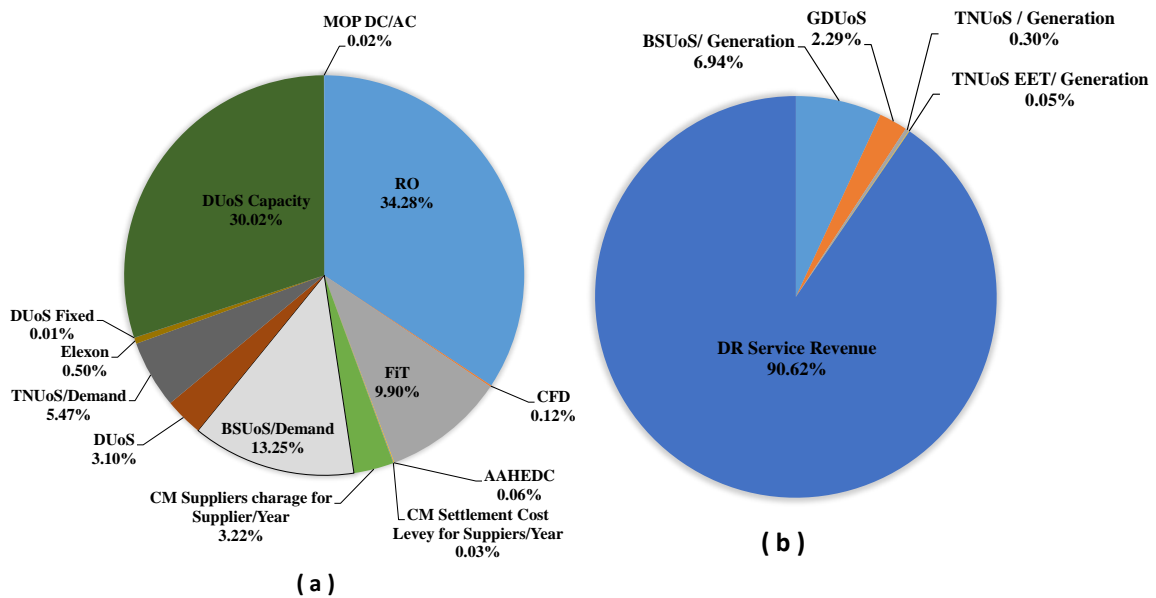|	DR (S1)			DR (S2)		
	Import			Import		
	Red	Orange	Green	Red	Orange	Green
Mon - Fri Energy (MWh)	3,832.39	12,162.32	10,187.19	3,754.76	11,934.77	10,012.19
Mon - Fri Cost (£)	49,207.8	27,243.59	916.85	48,211.12	26,733.89	901.09
Sat-Sun Energy (MWh)			9,126.44			8,993.36
Sat-Sun Cost (£)			821.38			809.40
Total unit charges (£)	78,189.71			76,655.50		

Figure. A18 Analysis findings of (a) Cost, and (b) Revenue for 1C BESS used to deliver DR service without a dynamic control (S1) for the whole year-2022, using frequency data of year-2019.